UNIVERSITÀ DEGLI STUDI DI NAPOLI "FEDERICO II"

in consorzio con
SECONDA UNIVERSITÀ DI NAPOLI
UNIVERSITÀ "PARTHENOPE" NAPOLI
in convenzione con
ISTITUTO PER L'AMBIENTE MARINO COSTIERO – C.N.R.
STAZIONE ZOOLOGICA "ANTON DOHRN"

Dottorato in Scienze ed Ingegneria del Mare
XVII ciclo

Tesi di Dottorato

Numerical Studies on Phytoplankton Responses in the Ocean Mixed Layer

Candidato:
Dott. ssa Serena Esposito

Tutor:
Prof. Maurizio Ribera d'Alcalà

Co-Tutor:
Prof. Enrico Zambianchi

Il Coordinatore del Dottorato: Prof. Bruno D'Argenio

ANNO 2006

A mia madre e a mio padre

Contents

Introduction

Phytoplankton play a major role in modulating the global cycles of several major elements such as silicon (Ragueneau et al., 2000, among the others), nitrogen (Altabet et al., 2002, among the others), sulfur (Simo, 2001, among the others), phosphorus (Baturin, 2003, among the others), iron (Archer and Johnson, 2000, among the others) and, obviously, carbon (Falkowski et al., 1998, among the others). The tight coupling among global biogeochemical cycles and plankton had been thoroughly analyzed since the seminal work by Broecker and Peng (1982) with a dominant view of plankton as basically responding to fluxes of energy, e.g., light, and matter, e.g., nutrients, oligoelements, etc., in a more or less linear way, i.e., more nutrients, more light, more plankton. While depicting one aspect of plankton dynamics, this view does not help in disclosing the classical, still unsolved, issue of plankton ecology, the so called *Paradox of Plankton* (Hutchinson, 1961).

Phytoplankton diversity is striking. Just looking at one of the most recent molecular phylogenetic tree it can be noted that, besides a large number of prokaryots, which dominate in several regions of the present ocean, phytoplankton species belong to widely different groups in the tree. This suggest a complex evolutionary history for what we consider an ecologically homogeneous group of organisms and differences in physiology, life cycle and responses which frequently elude present approaches to study their biology.

Indeed, even during blooms, when few key species may dominate, several other species coexists and are not outcompeted by the others. Other species may peak in a narrow time

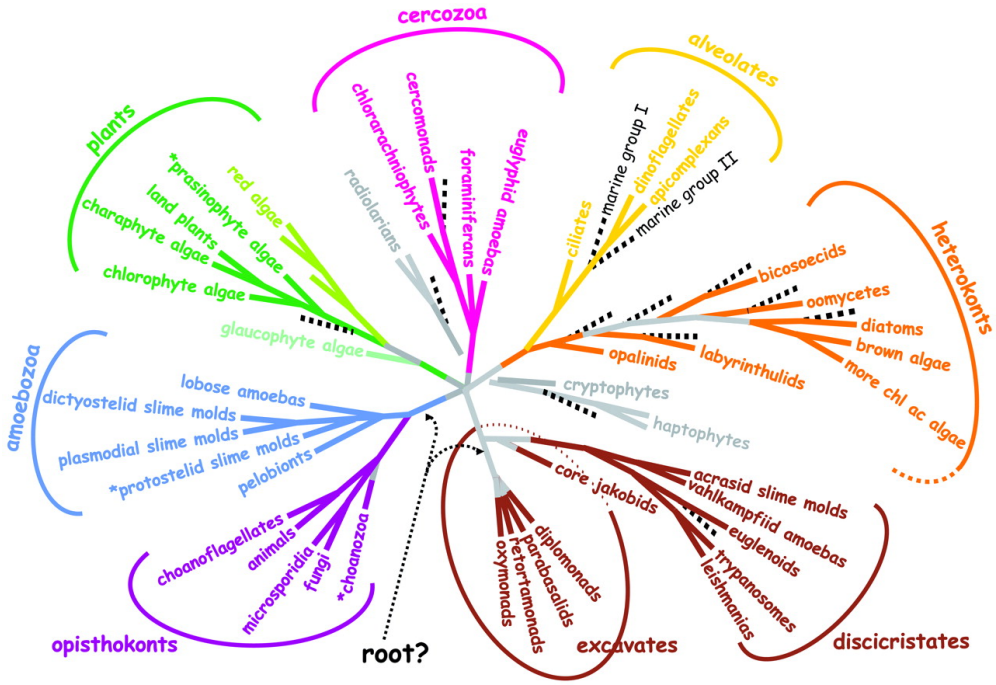

Figure 1: A consensus phylogeny of eukaryotes (redrawn from Baldauf, 2003)

window over the year, while being present in low abundance before and after (Zingone and Wyatt, 2004).

Along with the present view of phytoplankton ecology, the occurence of a species should correspond to a sort of optimum in its environmental, i.e., proximate conditions (temperature, light regime, nutrient concentrations, etc.) which should allow for the optimal growth rate pertaining to the species. This in turn would imply that variations in the proximate factors, mostly light and nutrients, should produce photophysiological responses that would account for the observed variations in growth and, eventually, dominance.

This assumption is implicit in most of the physical-biological coupled models currently used to reconstruct plankton dynamics at macroscopic scale, while different, mechanistic models, are used to analyze specific physiological responses to changes in, e.g., nutrients and light (Baklouti et al., 2006a, and refereneces therein).

Because light and nutrients are both modulated by the fluid motion, it could be inferred

that the variance spectra of nutrients and light, as well as other proximate factors, including shear at the scale of the organisms, may be the drivers of the variance in phytoplankton species spectra. This hypothesis that roots back in the pioneering work of Margalef (1978) has never been fully validated, mostly because laboratory experiments are run on cultured clones which certainly reflect the plasticity the species, but not necessarily, the dominant response in situ, while in situ experiment do not easily allow for a robust monitoring of organism's responses, especially in mixing regimes.

With the *caveat* just mentioned that physiological responses in the laboratory may differ from those occuring *in situ*, recent mechanistic models built on laboratory observations or theoretical studies are very suited tools to analyze dynamic responses in phytoplankton exposed to variable regimes (Baklouti et al., 2006b).

Variations can be either imposed as simple patterns, such as light shifts, or reproducing patterns which mimic those produced in a mixing water column. Also the latter can be generated by a modeling approach. Coupling both classes of models does allows for an in depth analysis of the emergent properties of a phytoplankton population living in a variable environment. In addition, it may shed light on the relevance of the observed responses in terms of fitness of the species, and therefore of their possible selective advantage.

The main scope of this work is an in depth analysis, through a modeling approach, of the photophysiological responses of a typical phytoplankton species in warying regimes and their consequences on the growth of the population. In particular the works is aimed at answering the questions that follow.

1. Which are the typical scales of photoacclimation as compared to the scales of possible variations in the natural environment;

2. which is the impact of mixing on the biomass accumulation of phytoplankton of known photophysiology;

3. what can be inferred from the above responses about key evolutionary constraints

on phytoplankton

The thesis is organized as follows.

In the first part the state of the art of the different aspects in phytoplankton photophysiology is briefly summarized. An exhaustive review of the subject would require a much larger space than the one available here and is certainly out of reach of a single person. Therefore in the first part are sketched only the processes that are considered relevant for the analysis conducted in this study. In the second part the methods used for the investigation and its main results are presented and discussed. In the third part a more general discussion on the anlysis is carried ou,t while in the last part supplementary material, such as the description of the differrent codes using for running the simulation, is added.

Part I

Background: Impact of Proximate Factors on Phytoplankton Dynamics and their representation in numerical models

Chapter 1

Growth Dependence on Light

Phytoplankton are phototrophic organisms, i.e., they use light as a source of energy to generate reducing power and chemical energy to perform biosyntesis. Therefore they have to capture light and transform it. As the potential energy input covaries with light intensity, they have to respond to light variations that occur regularly in their environment. To do so, they have specialized cellular structures, generically referred to as the *photosynthetic apparatus*, which adjust to changes in light intensity. In the next section, the structure of the photosynthetic apparatus and then its adjustments to a varying light field are described.

1.1 Overview of Photo-physiological Processes

Phytoplankton respond to light variations in nature either by changing the rates of biochemical processes related to light and by changing the organization, composition and functioning of the photosynthetic apparatus. The functional changes associated with the latter can be interspecific or intraspecific. Following the definition by Falkowski and LaRoche (1991) and recurrently used in the literature (Moore et al., 2006; MacIntyre et al., 2002), I will use the term *photo-acclimation* to refer to the phenotypic response of phytoplankton to changes in irradiance. The changes in components of the photosynthetic apparatus

involved in photo-acclimation can be assessed by measuring photosynthetic performance and biochemical composition of a genotype grown in different light conditions.

The term *photo-adaptation* will be used to refer to the response of a certain taxon on the evolutionary time scale. Different species exposed to the same growth irradiance will show different bio-chemical composition and photosynthetic performances. These characteristics derive from the adaptation occurred during evolution and are supposed to determine competitive traits of the species.

Photo-acclimation depends on changes of various components of the photosynthetic apparatus and displays different kinetics. It is an ontogenetic mechanism, whereas photo-adaptation is a phylogenetic trait. Photo-acclimation can act both on the light harvesting efficiency and the photosynthetic capacity.

In fact, the photosynthetic rate can be seen as regulated by two factors. The first is related to the ability of the photosynthetic apparatus to harvest light through pigments which absorb at different wavelengths and to channel the excitation toward the reaction center. The photosynthetic capacity, instead, is the amount of chemical products, typically organic carbon, that derive from the energy transported as electrons from the reaction center through the electron transport chain. Therefore, it represents the yield in the use of the captured energy, while the light harvesting efficiency represents the ability in capturing the available solar energy.

In order to highlight the modifications involved in the modulation of light harvesting and those related to the photosynthetic capacity, the structure of the photosynthetic apparatus and its functioning will be briefly summarized in section 1.1.1

1.1.1 The Photosynthetic Apparatus

The photosynthetic apparatus (fig. 1.1) is composed of photosynthetic units (PSUs). Each PSU is made up of a variable combination, often in the ratio of 1:1, of two photosystems

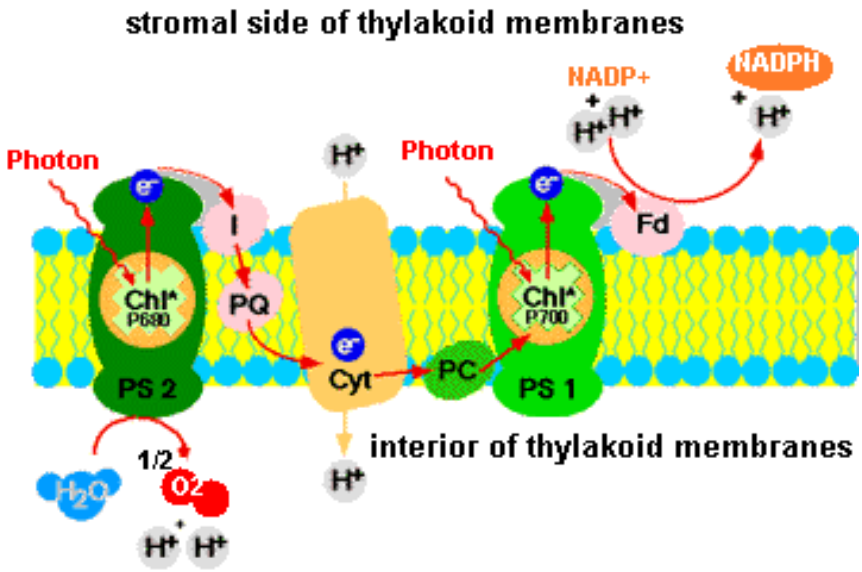

Figure 1.1: Main components of the photosynthetic apparatus and the electron transport chain.

embedded in the thylakoidal membrane and connected via the macromolecular complexes responsible for the electron transport chain. The two photosystems differ for the wavelength of the maximum absorption, with PSI centered at 700 nm and PSII at 680 nm. The light-dependent reactions of the photosynthetic process involve both photosystems through a series of reactions. The high-energy electrons generated by the charge separation at PSII move through PSI toward the final electron acceptor: NADP.

The overall process is called the Z-scheme of photosynthesis, because the energy of electrons drops from PSII to PSI, where the absorption of another photon generates a new energy input, to finally drop at the reduction site (Falkowski and Raven, 1997).

Each photosystem is made up of a reaction center and numerous antenna pigments and binding proteins. The pigments (predominantly chlorophylls and carotenoids) and the proteins that compose the light-harvesting antenna formed the so called "Light Harvesting Complex" (LHC). LHC directs through excitation transfer among neighbouring molecules the energy of the photons to the reaction center of the photosystems.

The PSII is composed of the LHC, the reaction center (P680), the D1 and D2 proteins and of a series of other molecules that participate to the electron transport chain, among them: 4 atoms of Mn, a tyrosine, a phaeophytin and two quinones (Q_A and Q_B).

Only the chlorophylls in the reaction centers do transfer electrons to the electron transport chain through charge separation. Once the excitation hits the pair of chlorophylls of the reaction center P680, they transfer the charge to the primary acceptor (a phaeophytin molecule). The deficit of electrons is replenished by taking electrons from a molecule of water, splitting it into O_2 and H^+. The electrons transfer from the primary acceptor to the quinones, while the four atoms of Mn and the tyrosine are involved in the replenishment of electrons from water.

The slower step in the electron transport chain between PSII and PSI is the transfer of electrons between the two quinones Q_A and Q_B (order of microseconds). For this reason, when the Q_A is reduced and is not able to take another electron, the reaction center of the PSII is said to be *closed*, whereas when the Q_A is in the oxidized state the reaction center is said to be *open*.

As soon as the Q_B is reduced, it moves and loses its charge picking up two protons and activating the Cytochrome b_6f, producing proton-motive force and driving ATP synthesis. The electron, then, passes to plastocyanin, as to end at PSI. There the electron is finally boosted to a higher energy level using a second solar photon. The highly excited electrons are transferred to the primary acceptor protein of the PSI to ferredoxin and then drives reduction of $NADP^+$ to NADPH.

This electron flow is the non-cyclic one, while the cyclic one involves the transfer from the primary acceptor of the PSI to ferredoxin, and then again to Cytochrome b_6f and plastocyanin before returning to chlorophyll. This cyclic transport chain produces a proton-motive force, pumping H^+ ions across the membrane, but produces neither O_2 nor NADPH and involves only the PSI.

This cascade of reactions takes place in a period of a few milliseconds, defined as the turnover time of the electron transport chain (τ). The ATP and NADPH produced are later involved in the carbon fixation through the Calvin-Benson Cycle, but alternative pathways in the photosynthetic organisms should exploit this reducing power [e.g nitrogen assimilation, photo-respiration, inorganic carbon accumulation, chloro-respiration, pseudo-cyclic electron transport (Mehler reaction), and respiratory phosphorylation (Behrenfeld et al., 2004)].

If a complex or molecule is already occupied in the reaction and its donor reach the excited state, the excitation is not directed from the donor to the acceptor but will be differently quenched. As an example, during the transfer the excited chlorophylls molecules can decay to the fundamental state, dissipating energy through heat and fluorescence. The different alternative sink of excitation that can be involved will be described in section 1.1.4, while in section 1.1.2 will be analyzed the light-driven modifications that can occur in the light-harvesting structures.

It is worth mentioning that the above description is very schematic. First of all, the ratio of PSI to PSII is not constant and equal to one in phytoplankton, in contrast with the 1:1 ratio found generally found in higher plants (Raven et al., 1999). In fact the ratio may vary significantly because of both phenotypic and genotypic adaptive traits, as it will be further analyzed in section 1.2.1.

1.1.2 Regulation of Light Harvesting

The increase in chlorophyll and light-harvesting accessory pigments content in cells grown at low irradiance and its decrease in cells grown in high light is an almost universal feature among microalgae. The pool of pigments and its internal quota change slowly during the photoacclimation. In cells exposed to step transition of irradiance the $chla$ quota reaches the stationary state corresponding to the new irradiance in a time of the order of days.

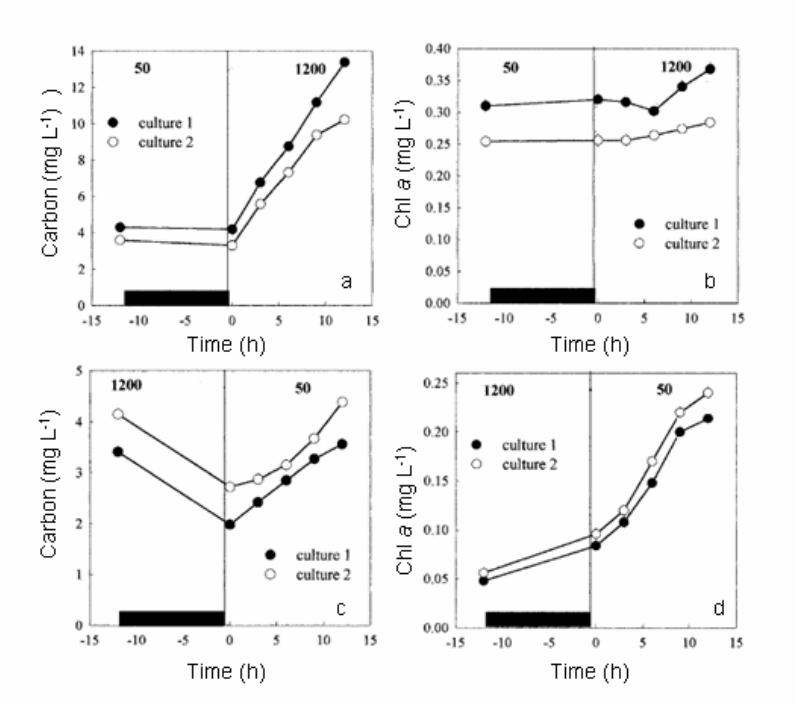

Figure 1.2: Initial changes in *chla* and carbon after a shift in irradiance from (a and b) 50 to 1200 µEinst $m^{-2}s^{-1}$ and from (c and d) 1200 to 50 µEinst $m^{-2}s^{-1}$ Redrawn from Anning et al. (2000)

The light-shift experiment described by Anning et al. (2000) on a marine diatom helps to understand and recognize the mechanisms and the kinetic of the adjustments in the *chla* cellular content, also if they cannot be generalized because performed on a single species.

In cells submitted to a shift from 50 to 1200 µEinst $m^{-2}s^{-1}$ and *viceversa* the cellular quota of *chla* decreased 2,5 fold in the shift from low light to high light, approaching a new steady state after 5 days, with a rate of *chla* synthesis of 0,077 h^{-1}. The reaction to the shift back to low light was quicker. The original level was reached in only 3 days and the average *chla* synthesis rate was estimated as 0,03 h^{-1}. The authors noticed that in shifts from low light to high light the rate of increase of the chlorophyll content in the suspension did not change significantly (fig. 1.2) and that the change in the increase of the carbon content mirrored the decrease in the cellular *chla* content. The authors suggested that the

change of cellular $chl\,a$ content after the shift to high light was not regulated by active rapid degradation of $chl\,a$ as previously supposed by Riper et al. (1979) but was a consequence of dilution due to higher rate of cell division and reduction in the rate of pigment synthesis, as found by Post et al. (1984). Instead, the symmetrical pattern observed in acclimation to lower irradiance is due to an acceleration in the rate of $chl\,a$ synthesis relative to that for net carbon assimilation or cellular division (Anning et al., 2000).

The implication of the asymmetry of this photo-acclimative response in fluctuating light and in the Ocean Mixed Layer are far to be negligible, because in an environment where shifts occur quickly and in both the directions this feature can produce remarkable consequences that will be analyzed in the section 1.2.2.

The transcription of genes coding for the synthesis of pigment-protein complexes, seems to be controlled by the redox state of the plastoquinone pool (Escoubas et al., 1995; Pfannschmidt et al., 1999). The redox state can thus be seen as a signal of the light-energy involved in carbon assimilation, given the amount of pigments invested in light harvesting.

Recently, Pfannschmidt et al. (1999) thoroughly reviewed the chloroplast redox signals that are known to regulate the expression of photosynthesis genes, but concluded that the regulation of the size and composition of photosynthetic complexes may depend not just on light intensity but also on several other processes that contribute to the life of the cell (e.g. respiration and interaction with other signaling pathways).

MacIntyre et al. (2002) reviewed 50 years of studies on photo-acclimation, manifested as modifications of photosynthetic pigment contents and changes in the photosynthesis *vs* irradiance curves (PE) occurring because of changes in growth irradiance.

The PE curves are plots that describe the relationship between light and photosynthesis normalized to an index of biomass (P^B) (generally $chl\,a$). The shape of these curves indicates that, at the lowest irradiance, photosynthesis is a linear function of irradiance

with a slope that is called the light limited initial slope or α^B. With further increases of light, photosynthetic yield per unit of available light decreases up to a steady level where photosynthesis becomes saturated and does not change any further. This is called the light-saturated maximum photosynthetic rate or (P^B_{max}). Indeed, a steady maximum is not always present because, beyond a certain threshold, the photosynthetic rate may decrease with a slope defined as β^B. This is the photoinhibited part of the PE curve and will be discussed in more detail in section 1.1.3.

A PE curve has in general two (without photoinhibition) and three (with photoinihibtion) degrees of freedom which completely characterize the curve, but other parameters may be used to highlight different photophysiological aspects. The light-saturated parameter E_k that is equal to the ratio P^B_{max}/α^B, for example, is frequently taken as an estimate of the irradiance level to which the cell is acclimated.

Shape and parameters of the PE curves of a certain algal suspension change with temperature, nutrient availability and growth irradiance; for this reason, historically, they are at the basis of the studies on photo-acclimation and then of the review by MacIntyre et al. (2002).

The authors analyzed the results occurred since Myers (1946a,b) papers focusing on the variability of the ratio of chlorophyll$a$ to carbon ($chla : C$) and of the PE curve. The $chla : C$ ratio is a key physiological variable because the light-limited photosynthesis rate is proportional to $chla$ content of the cells and the light-saturated rate to the carbon content. More in detail, PE curves can be normalized to different biomass index (B), and the shapes of the curves vary with the index of biomass chosen, generally $chla$, carbon or cell number. In particular light-limited region of the $P^{chl}E$ does not vary significantly with the growth irradiance, with the exclusion of photo-acclimative responses that will be described in sections 1.1.3 and 1.1.4. Therefore, the photosynthetic activity, in term of carbon assimilation or oxygen evolution, per chlorophyll does not change significantly at

light-limiting growth irradiances, while it strongly changes at light-saturated irradiances. On the contrary, the light-saturated rate per carbon, and in particular the P^C_{max}, does not change significantly with growth irradiances, while the α^C does. This is due to the fact that photosynthetic rates at light-limited irradiances depends on the light-harvesting efficency of the cell (and the cellular $chla$ content can be a good index for that), while the light-saturated photosynthetic rates does not. All these observations brought the authors to conclude that the assumption at the basis of various photo-acclimative models (Bannister and Laws, 1980; Kiefer and Mitchell, 1983; Geider et al., 1996, 1998b) that P^C_{max} and α^{chl} are, on a first approximation, independent of growth irradiance for the same species is confirmed from various data-sets.

For all the above, the $chla : C$ ratio is an indicator of the physiological state reflecting the proportion between the energy invested in the light harvesting apparatus and that invested in carbon growth. As already mentioned, the ratio increases with decreasing light so that the cells improve the light harvesting capacity. The opposite reaction at increasing irradiances occurs because cells submitted to high light invest more in somatic growth than in the light harvesting apparatus, decreasing the $chla$ synthesis and increasing the carbon cellular content.

Moreover, the review pointed out that, contrary to what could be thought, the decrease in the $chla : C$ starts at sub-saturating irradiances. In particular they showed that the $chla : C$ can be reduced to the 40% of its maximum value at an irradiance that supports half of the maximum growth rate (fig. 1.3).

It is evident (fig. 1.3) that the light limited slope normalized to carbon (α^C) decreases for increasing light also at sub-saturating irradiance as a consequence of the decrease in the $chla : C$. In fact $\alpha^C = chla : C \ \alpha^{chl}$, and since $P^C = \alpha^C \ E$ at light-limiting irradiances, as a secondary consequence cells do not maximize the carbon assimilation at all the sub-saturating irradiances.

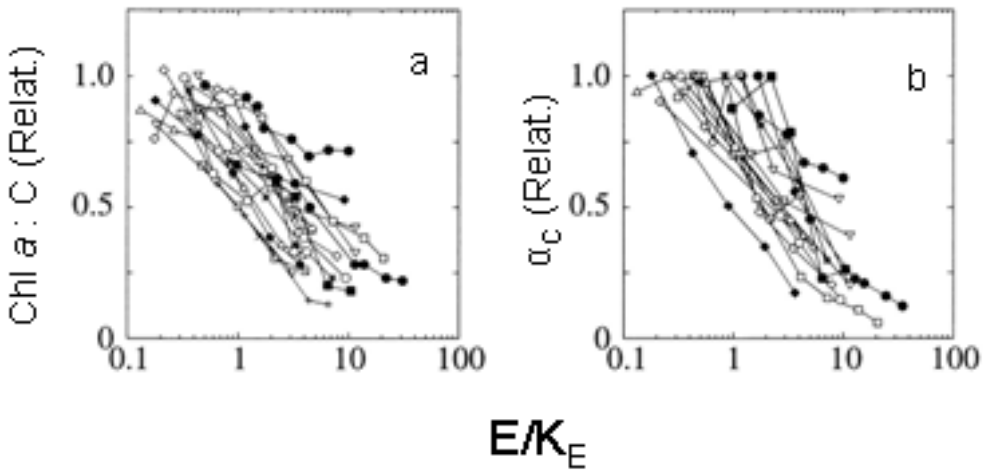

Figure 1.3: (a) Relationship between $chla : C$ and growth irradiance in nutrient-replete microalgae and cyanobacteria. Chl a : C is normalized for the maximum value and irradiance for the light saturation parameter for growth (K_E). (b) Relationship between the slope of the carbon specific photosynthesis irradiance curve, α^C, and growth irradiance. Both values are normalized. α^C is normalized for the maximum value. Redrawn from MacIntyre et al. (2002)

This pattern, that seems to be disadvantageous for the organisms, is common to all the eukaryotic species studied, while for the prokaryotic species $chla$ is not a good proxy for light absorption (MacIntyre et al., 2002). Why the cells start to decrease the $chla$ content at irradiances that are still sub-saturating for growth is still unclear, but it is clear that photo-acclimation occurs not only to maximize the carbon fixation (Pfannschmidt et al., 1999, see above). Current hypotheses are that photo-acclimation of pigment content at increasing light aims at decreasing the energy investment in other physiological adjustments that act to prevent damages from high irradiances, or acts as a sensitive redox regulator, or may respond to even low level of photo-oxidative stress (MacIntyre et al., 2002).

The hypothesis of a down-regulation as a way to minimize investment to repair damage due to light, has been proposed because over-excitation of the photosynthetic apparatus may reversibly or irreversibly damage pigments, proteins and lipids in the thylakoid membrane. Therefore, besides adjustments in light absorption, algae and plants developed

several ways to get rid of excess light energy that has already been absorbed. Those mechanisms will be described in the section 1.1.4.

Even if lacking mechanisms for such sophisticated responses, current models are still able to reproduce the decrease of $chla : C$ with increasing light. For example the dynamic model of Geider et al. (1998b) as reformulated by Flynn et al. (2001), reproduces the reduction of the $chla : C$ ratio at sub-saturating irradiances, just introducing a regulatory term whose impact covaries with the difference between realized and potential maximal carbon assimilation (but see section 1.3 for more details). However it is unclear whether the decrease of the $chla : C$ also at sub-saturating irradiances has to be considered as a sign of first damage or just reflects an *intentional* regulated decoupling of carbon and $chla$ synthesis.

The more general question about the adaptive benefit involved in acclimation to low light is open also for higher plants (Walters, 2005), but is reasonable to assume that it exist, otherwise all photosynthetic organisms would retain a high-light-acclimated state under all growth conditions.

It has been suggested that along with the increase of light intensity it is convenient for the cell to reduce the nitrogen investment involved in the synthesis of chloroplasts that make it available for other biosynthetic pathways (Walters, 2005). This leads to the relevance of protein turnover in different physiological conditions of the cells. Quigg and Beardall (2003) stressed this point after measuring the protein turnover rate of two unicellular eukaryotes grown a very low light intensity and concluded that:

> *Differences between protein turnover rates and maintenance metabolic costs may be one of the photo-acclimation strategies that determines which photon niches microalgae can successfully exploit.*

1.1.3 Photo-inhibition

Photo-inhibition is a broad term that describes the decline in photosynthetic viability of oxygen evolving photosynthetic organisms due to excessive illumination. Photo-inhibition is a phenomenon affecting specifically Photosystem II and is characterized by inactivation at high photon fluency of the electron flow and reduction of plastoquinone by PSII, both phenomena linearly related to the intensity of the absorbed light. On the other hand, the light-induced loss of PSII activity precedes the degradation of the D1 protein, another process associated to photoinhibition, which is the result of light induced damage to PS II and not the primary cause of the phenomenon (Adir et al., 2003). In combination with visible light UV light has a synergistic effect on the protein degradation (Jansen et al., 1996) also at relatively low light intensities. *In vitro* and *in vivo* experiments have been conducted to understand the molecular mechanisms at the basis of the loss of activity by PSII and the subsequent degradation of D1 protein. Two types of mechanisms of photo-inhibition, characterized *in vitro*, have been proposed: the acceptor-side and the donor-side photo-inhibition.

In acceptor-side photoinhibition, high light is considered to lead to an alteration of the acceptor side of the PSII reaction center which blocks electron flow from the reduced first quinone Q_A^- to the second one Q_B. This is considered to increase the possibility of charge recombination of the primary radical pair $P680^+$ (the chlorophyll of the reaction center that has lost the electron) and the primary acceptor phaeophytin that has gained the electron ($Phaeo^-$). The recombination is thought to produce a triplet chlorophyll $^3P680$, which then reacts with O^2 to generate a singlet oxygen with an extremely short life (Vass et al., 1992). The singlet oxygen is able to produce an oxidative damage to the PSII, targeting D1 protein for degradation (Ohad et al., 1994).

Donor-side photo-inhibition is considered to occur when the redox-active tyrosine is unable to replenish electron to the $P680^+$ at the rate in which the electrons are removed

from the $Phaeo^-$, causing the inactivation of the electron transport in the donor-side of the PSII. The persistence of the cations radicals derived form tyrosine and chlorophyll of the reaction center, may cause oxidative damage in the presence or absence of oxygen that triggers D1 protein degradation. It is important to note that the donor-side and acceptor-side mechanisms for PSII photo-inactivation are distinctly different. Both mechanisms form highly reactive but different oxidants that are assumed to cause damage to PSII reaction center leading to D1 protein degradation. It is not clear which of these mechanisms is dominating *in vivo*, or if other mechanisms are involved.

Anderson et al. (1998) have formulated a tentative unifying model for photo-inhibition *in vivo*, considering the radical $P680^+$ as the only cause of oxidative damage of PSII. They did not exclude that the charge recombination of the primary radical pair can occur and form damaging triplet chlorophyll $^3P680$. However, they suggest that the $^3P680$, rather than reacting with oxygen to form singlet oxygen, is probably quenched in the presence of the reduced first quinone Q_A^-.

Following this hypothesis, $P680^+$ being the only oxidative damaging species considered, PSII inactivation depends on the number of photons received, and not on the rate of delivery of photons, which would only determine the number of the damaging events. So Anderson et al. (1998) proposed that the photo-inactivation of PSII and the subsequent degradation of the D1 protein is a a light-dose process: it depends only on absorbed photons, and not on the irradiance rate *per se* (Park et al., 1996). For this reason they suggest that photo-inhibition can take place, with different impact on photosynthesis, over the entire irradiance range: limiting, sub-saturating, and saturating irradiances.

Even if the proposed mechanism would be able to unify photo-inhibition in a single mechanism, the theory is not entirely accepted and the involvement of different reactive oxygen species is still postulated.

However, whatever oxidative species is involved in damage of the D1 protein, photo-

inhibitory decrease of photosynthesis can be considered to occur when the rate of the repair fails to keep face with the rate of damage. The time required for the adjustment of this response to a new irradiance spans from tens of minutes to a couple of hours depending on the light intensity, on the previous conditions and on the intrinsic rate of damage and of repair.

The molecular basis of the process of damage and repair are outlined in the schema in figure 1.4. Functional PSII ($PSII_F$) is the pool of active centers that can be reversibly inactivated by over-excitation of the inactivated pool ($PSII_I$). These two pools can be transformed in PSII with a damaged D1 protein ($PSII_{NF}$). The repair of these non-functional centers requires migration in the stroma where they lose the damaged D1, becoming $PSII_{-D1}$. Here the D1 damaged can be substituted with a newly synthesized protein and migrate to the tylakoids re-gaining functionality. Photo-inhibition depends not only on the damage but also on the rate of degradation of the damaged protein, on the rate of the new synthesis and on the kinetic of the migration within the membrane. In addition, the loss of functionality by PSIIs and the consequent photo-inhibitory decrease in the photosynthetic rate can be done not only to the presence of damaged reaction centers but also on the number of PSII in the highly reversible inactivated stage (Long et al., 1994).

Finally, in their review of 2003, Adir et al. proposed an intriguing outlook about photo-inhibition. They suggested that the turnover of the D1 protein may be just another mechanism of PSII protection against light induced oxidative stress. The degradation of a protein that has an high turnover can be seen as another sink of over-excitation to avoid other unrepairable damages.

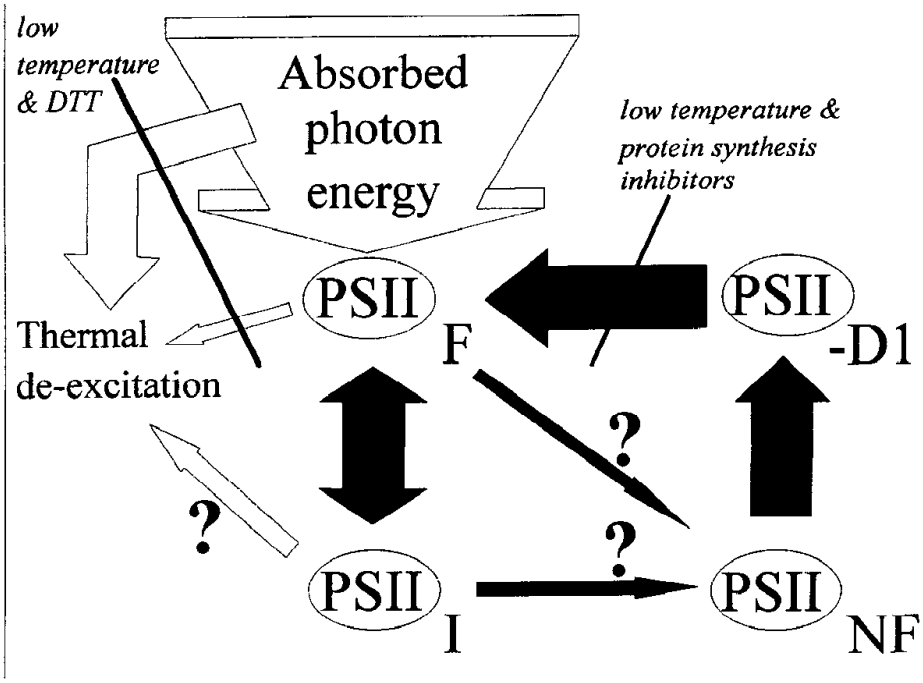

Figure 1.4: Simplified cycle of PSII inactivation and repair. The forms of PSII are functional ($PSII_F$), reversibly inactivated ($PSII_I$), irreversibly inactivated or non-functional ($PSII_{NF}$),and D1 removed ($PSII_{-D1}$). Synthesis of D1 could be blocked by inhibitors of chloroplast protein synthesis and by low temperature. Excitation of PSII is decreased by thermal de-excitation of both the PSII antenna and center. The component of de-excitation attributed to xanthophyll cycle activity may be inhibited by low temperatures and by the action of dithiothreitol (DTT). Redrawn from Long et al. (1994)

1.1.4 Photo-protection

The photo-acclimative responses that act to prevent the damage are known as photo-protective mechanisms. Photo-protection take place via different processes to decrease the absorption of light energy or provide alternative energy sinks when photosynthesis capacity is exceeded. First of all phytoplankton is able to dissipate the over-excitation as heat directly through the quenching of variable chlorophyll fluorescence, able to form and relax within seconds.

The so called non-photochemical quenching (NPQ) can be analysed in terms of three components: state transition (qT), photoinhibition (qI) and dissipation via xantophylls cycle (qE). The majority of NPQ is believed to occur through qE in the PSII antenna pigments (Demmig-Adams and Adams, 1992).

Xanthophylls are carotenoids able to dissipate excitation energy through heat by rapid internal conversion, occurring in tens of seconds. One photo-acclimative response with photo-protective role is the induction of *de-novo* synthesis of the energy-dissipating pigments (Lavaud et al., 2002), at a rate that is quite slow as typical for pigment synthesis (MacIntyre et al., 2002).

Chlorophytes and chromophytes differ in the carotenoids involved in the cycle. In the former, similarly to higher plants, the de-epoxidation reaction occurring at high irradiance involves violaxanthin, antheraxanthin and zeaxanthin in a two-step pathway; in the latter there is a one-step pathway which involves de-epoxidation from diadinoxanthin to diathoxanthin. The de-epoxidation reactions attend the dissipation of $chl\,a$ excitation. NPQ mechanism was intensively explored in higher plants (see for a recent review Müller et al., 2001). So far, it has been well established that non radiative excess energy dissipation occurs in light harvesting system of PSII, triggered by ΔpH and modulated by xanthophylls. A PSII protein called PsbS was found to be a key factor sensing ΔpH, binding zeaxanthin and probably triggering the conformational changes within PS II an-

tenna, which leads to its transition into the dissipative mode, but an ortholog has not yet been found in chromophytes (Lavaud et al., 2004; Bassi and Caffarri, 2000, and references therein).

The physical nature of this quenching is still under debate. Two major theories exist. One implies that zeaxanthin is a direct quencher of the chlorophyll excited state. The other theory suggests that the quencher is a chlorophyll dimer or excimer formed during the antenna conformational transition assisted by zeaxanthin.

NPQ is dependent on the build-up of a transthylakoid proton gradient and on xanthophyll cycle activity. The diatom cycle is different from violaxanthin cycle and involves, as mentioned above, a one-step process. Notwithstanding the de-epoxidation from diadinoxanthin to diathoxanthin parallels energetically one single step (antheraxanthin-zeaxanthin conversion) of the two-step pathway, diatoms possess the capacity for energy dissipation, which in some cases exceeds that of the higher plants (Ruban et al., 2004). This feature could originate from the unique organization and dynamic properties of light-harvesting antenna components, the high concentration of diathoxanthin in diatoms respect to zeaxanthin in higher plants and the structural properties of this xanthophyll (Guglielmi et al., 2005; Grouneva et al., 2006).

Even if green algae show similar light-harvesting and xanthophyll-cycle pigments as higher plants, the qE contribution to their non-photochemical quenching is not as significant as in higher plants and diatoms (Casper-Lindley and Björkman, 1998). It is hypothesized that they rely on other dissipation mechanisms, which operate along with xanthophyll cycle-dependent quenching. The most probable could be the state transition (Garcia-Mendoza et al., 2002).

The state transition takes place through phosphorylation and detachment of the light harvesting complexes (LHCII) from the PSII. This response acts on time-scales of the order of several minutes to hour, and until now have been documented only for chlorophyte.

Phosphorylation induces a transition between two possible states: state 1 is preferentially activated when a signal of under-excitation of the photosynthetic apparatus is present and brings up the relative magnitude of PSII. Alternatively, through phosphorylation of the LHCII the PSI is preferentially excited in order to avoid over-excitation of the PSII (state 2) (Campbell et al., 1998).

However, the dissipation of over-excitation can be achieved also through redirection of the electrons derived by the light reactions to different pathways not directly involved in the carbon fixation. For instance, it was observed that cells grown at 400 μEinst $m^{-2}s^{-1}$, could double the percentage of phosphorylation, occurring via cyclic electron flow, in comparison to cells grown at 100 μEinst $m^{-2}s^{-1}$ (Herzig and Dubinsky, 1993). Herzig and Dubinsky (1993) concluded that the cause of this phenomenon was the increase of the cross-section of PSI antenna in relation to that of PSII, even if at high light both decrease in absolute terms. In fact, the decrease of the light harvesting pigments and the increase of the photo-protective ones at high light, result in a decrease of the surface that can be hit by the photons and can transform via photochemistry the solar energy in energy available for the cell. As a result, a higher fraction of light energy reaches the reaction center of the PSI than that required to balance the electron flow to PS II. These excess photons provide the ATP needed by the increased metabolic demand of high-light adapted, fast-growing cells.

Therefore, the cyclic electron flow, as well as the oxidative pseudo-cyclic one via Mehler reaction, can be considered a way to dissipate excess energy from the electron transport chain when the maximum electron transport rate of the Z-scheme is reached (Raven, 1984).

The dependence of those and other sinks for electrons (e.g. nitrate reduction) on light intensity or physiological state is not easily determined and much remains to be learned about their regulation in microalgae.

Besides these adjustments involving modification in the amount of excitation transmitted to the electron transport chain, the photosynthetic carbon fixation can be highly regulated through changes down-stream of PSII (Behrenfeld et al., 2004).

Those of interest in this section are the light-mediated adjustments of the photosynthetic capacity: beside the change in the amount of components of the electron transport chain, the regulation of carbon fixation through the variation in Rubisco concentration and activity is the most efficient one.

Rubisco is an enzyme involved in the first major step of carbon fixation and, when light is not limiting, it is the primary rate-limiting enzyme of the Calvin cycle. High concentration or activity has been found to be strictly linked to an increase in the light-saturated rate of photosynthesis in phytoplankton through a decrease in the turnover time of the electron transport chain (τ).

Actually the situation is more complicated and a clear picture is not yet available. The concentration of this enzyme seems to be regulated by irradiance only during nutrient-limited growth and sensitive to the degree of nitrogen limitation in a chlorophyte (Sciandra et al., 1997; Geider et al., 1998a). In higher plants, nutrients-dependent regulation appears to reflect a secondary role for Rubisco as a nitrogen storage (Walters, 2005).

In any case, Rubisco activity is regulated rapidly in distinct species belonging to distinct groups. In fact, it can be activated or de-activated in several minutes, with re-activation proceeding faster than de-activation both in chlorophytes and chromophytes (MacIntyre et al., 1997). The overall simplified scenario is that Rubisco is de-activated in darkness and activated in the dark-light transition; its changes in activity due to light intensity shifts behave differently from those due to dark-light-dark transitions.

Until now, all phytoplanktonic species studied show the traits discussed above, though often regulated in different ways and with different kinetics. Those physiological adjust-

ments allow cells to reach a higher light-saturated photosynthetic rate under high irradiances (Fisher et al., 1989), without any disadvantageous consequence on the possibility of damage for the photosynthetic apparatus.

1.2 Photo-adaptation and Photo-acclimation

The tolerance of a species to high-light or to extremely variable irradiances depends on the kind of responses that this species is able to carry out. As mentioned in the previous section specific photo-physiological responses may or may not present inter-taxa variability.

Richardson et al. (1983) drew up a comprehensive data review regarding the variability between algal classes in photo-adaptation, that is still a reference in the field. Beside the difficulty to trace a conceptual scheme without over-simplifications, a first attempt was done and the fields of study requiring more investigations were detected. Studies conducted before and after, remarked the presence of high variability even between species belonging to the same class, but the scheme sketched below is still generally accepted.

Cyanobacteria, dinoflagellates and diatoms grow better than green-algae at very low photon flux. It is supposed that the type of the harvesting pigments (chl *c* and phycobilins), the differences in the structure of the thylakoids and a lower respiratory loss make the difference. Besides growing at low light, diatoms show lower photo-inhibition, probably for the presence of the diadinoxanthin-diatoxanthin cycle. This cycle is known to be more efficient in preventing photoinhibition. In addition, the greater pool of xanthophylls carried by diatoms, as compared to the other algae, may facilitate the NPQ (Lavaud et al., 2004).

Dinoflagellates are more affected by high light and are generally considered to grow better at low, possibly slowly varying, light (Blasco, 1978). Hasle (1950); Dodge and Hart-Jones (1977) have also noted that some dinoflagellate species avoid the surface waters during daylight hours.

On the opposite diatoms are thought to cope better with variable and intermittent

exposure to irradiances.

Green-algae, on the other hand, are reported to be tolerant to high irradiances, to the best of present knowledge, through state transitions.

Finally, Cyanobacteria are documented to show an intense Mehler activity (pseudo-cyclic electron transport via oxygen reaction) but does not show any xanthophylls cycle. Their ability to change buoyancy through gas vacuoles should help them to avoid extreme high light or low light conditions (Richardson et al., 1983).

In addition, Chlorophytes and Chromophytes seem to have an advantage over the Phycobiliphytes due to the lower cost their chormophores: the nitrogen cost of producing light-harvesting machinery is greater for phycobilins than for most chlorophyll or carotenoid-protein complexes (Raven, 1984).

This simplified scheme has to be taken with care, because it is known the existence of intra-classe, and inter-clonal (Mariella Ragni, University of Essex, personal communication) variability in this kind of generalized features. Furthermore, an estimate of the effective advantage that the photo-physiological responses sketched above can give to the survival of a species (or a clone) respect to another in the natural environment is still missing.

As previously described a widespread features of photoacclimation are the relative decrease of light-harvesting pigments versus carbon at high irradiances and the modification of the shapes of the P^C *vs* E curves with growth irradiance .

However, as already discussed in section 1.1.2, the change in the light-harvesting pigment quota seems to not maximise directly the carbon fixation. For this reason, it is important to focus the attention on the distribution of harvesting pigments in the photosynthetic functional structure. In fact, the adjustment of the chlorophyll content can occur in two ways which interfere differently with the other photo-physiological responses and have different coasts and benefits for the organisms.

In the next section the two strategies of adaptation to low light through increasing pigments that are assumed to occur in micro-algae, and the subsequent impact on their fitness in the ocean will be outlined.

1.2.1 Strategies of Different Groups to Irradiance Levels

In the late 60's Steemann Nielsen and Jørgensen (1968) and Jørgensen (1969) proposed the existence of two strategies of photo-acclimation to low and high irradiance. The two strategies were called *Cyclotella* and *Chlorella* types, from the algal genus from which they were retrieved. Jørgensen (1964) already observed that a number of unicellular algae, mostly diatoms, behave like *Cyclotella meneghiniana*. He exposed the putative mechanisms of this kind of acclimation in a study focused on the analysis of the different shape of photosynthesis normalized per cells *vs* Irradiance curves of cultures of *C. meneghiniana* grown at shade or high light and subjected to reciprocal shifts of irradiance (Jørgensen, 1964). *Cyclotella* type algae, after a shift from shade to high-light increased P_{max}^{cell}, while the α^{cell}kept almost constant value (fig. 1.5(a)). He also found that algae did not change significantly the chlorophyll content with the growth irradiances. Therefore, he concluded that the moderate change of the chlorophyll content at increasing (or decreasing) light was the cause of the constancy of the light harvesting efficiency with growth irradiance. The increased photosynthetic capacity of cells grown at high irradiances was thought to derive from an higher concentration of not better described photosynthetic enzymes. It is now possible to propose an increase of the activity or the concentration of the Rubisco enzyme as a possible explanation for this ability.

Cultures of the species *Chlorella vulgaris* behave dissimilarly and Jørgensen suggested that this strategy was very frequent in the group of green algae. The shapes of the *Chlorella* type cultures P_{cell} *vs* E curves subjected to a shift of irradiance from low to high light changed more clearly. Both parameters $\alpha^{cell}$and P_{max}^{cell}were significantly decreased by a

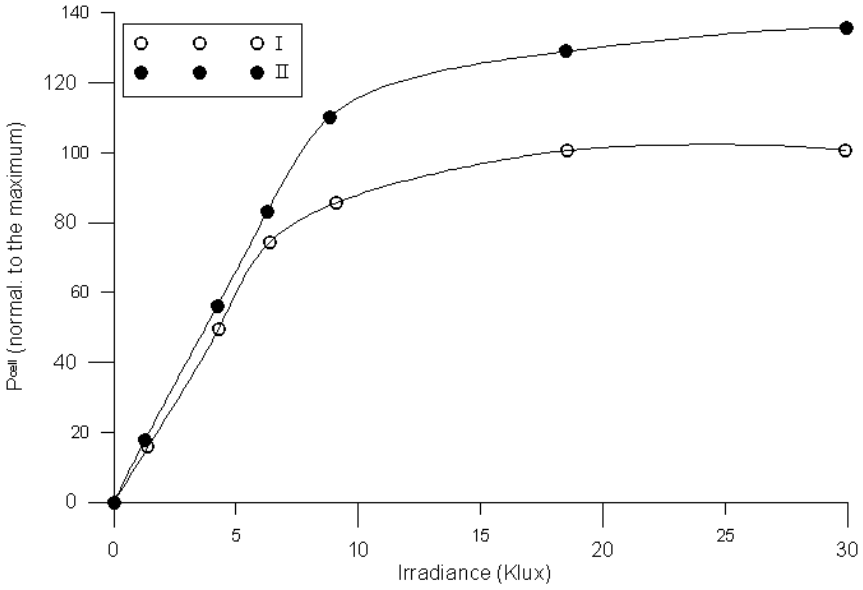

(a) The rate of photosynthesis normalized of *C. meneghiniana* grown at 3 Klux as a function of light intensity. I: directly from 3 Klux. II: After 3 hours at 100 Klux. Photosynthesis is normalized for the maximum photosynthetic rate at 100 Klux.

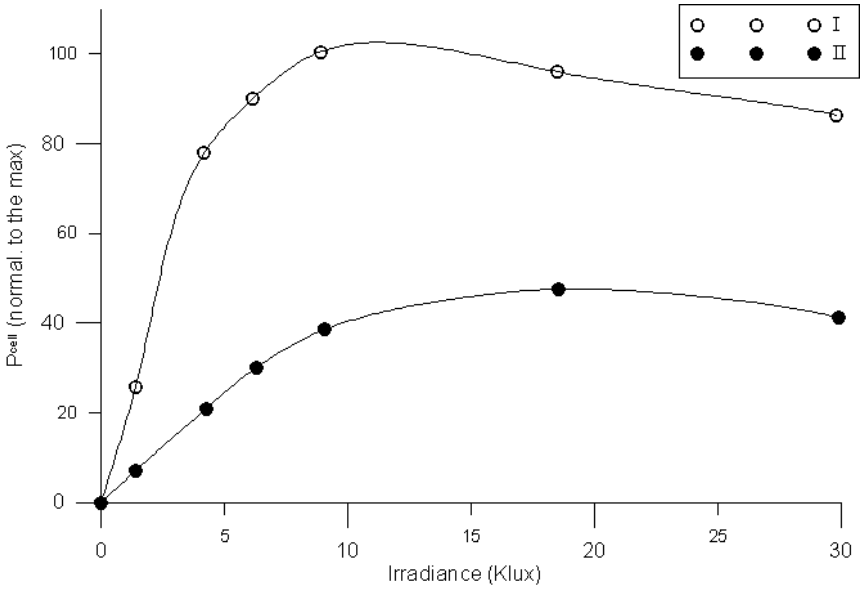

(b) The rate of photosynthesis normalized of *C. vulgaris* grown at 3 Klux as a function of light intensity. I: directly from 3 Klux. II: after 3 hours at 30 Klux. Photosynthesis is normalized for the maximum photosynthetic rate at 3 Klux.

Figure 1.5: The rate of photosynthesis as a function of light intensity for *Cyclotella* and *Chlorella* types. Redrawn from Jørgensen (1969)

shift of increasing irradiances. At the same time a large reduction in the cellular *chl a* content and in the cell size of *C. vulgaris* was observed. He suggested that the decrease of the *chl a* content at high irradiances was the reason for the decrease in the light harvesting efficiency and that a decrease in the enzymatic processes was the reason for the decrease of the photosynthetic capacity. He suggested that photo-inhibition was responsible for the second reduction in algae subjected to high irradiances after being grown at low light intensity. By contrast, photo-inhibition was not observed in cultures of *Cyclotella*, that indeed increased the P_{max}^{cell} after the same shift in irradiance.

Steemann Nielsen and Jørgensen (1968) finally outlined the idea of the two strategy: the *Cyclotella* type that gives to the organisms the possibility to well adapt to high-light, without *inactivating* chlorophyll, namely keeping the same chlorophyll content also at high light, and without suffering of abrupt exposure to high irradiances. They suggested the possibility of some still unknown mechanism of protection from photo-oxidation, that could be the NPQ through xanthophyll cycle. The *Chlorella* type was instead considered as a shade strategy, giving to the cells the ability of grow better at low light. In fact the *Chlorella* type algae can be considered as a better harvester of light in light limiting condition, while the great decrease in the *chl a* content when exposed to high irradiance do not completely prevent the photo-oxidative stress due to the large photons flux. This seems in contrast with the ability of green algae to well tolerate high growth irradiances, but first of all it is now evident that this kind of response can be species-specific and not group-specific. In addition, it seems that the phenotypic adaptation to high light in block type irradiances is significantly different from what can really happen in a variable environment (Garcia-Mendoza et al., 2002). The dynamic variation in the light perceived could trigger the induction of diverse and more efficient photo-protective responses as will be seen in section 1.2.2.

Afterwards, several papers in the early 80's have suggested that the increase in the

harvesting pigments at low irradiances can occur through two principal strategies that involve different modifications in the structure of the photosynthetic apparatus (Dubinsky et al., 1986; Falkowski and Owens, 1980; Perry et al., 1981).

The first involves the increase in the amount of pigments within the antenna (fig. 1.6a), the second involves the increase in the number of reaction centers (fig.1.6b).

Both strategies produce the common observed increase in the $chl\,a : C$ ratio and in the $chl\,a$ per cell (sec. 1.1.2) as light decrease, but the amount of chlorophyll increase and the way in which it is managed happen is different. Falkowski and Owens (1980) exposed these two strategies confronting the shape of the P^{chl} *vs* E curves and the biochemical composition of the photosynthetic apparatus of two algae: the diatom *Skeletonema costatum* and the green alga *Dunaliella tertiolecta*.

In the work of Falkowski and Owens (1980), the photosynthesis *vs* Irradiance curves was normalized to the chlorophyll rather then to the number of cells, as previously done by Steemann Nielsen and Jørgensen (1968). This different normalization could confuse, but the two strategies described by Falkowski and Owens (1980) can be reconnected to the *Cyclotella* type and the *Chlorella* type strategies.

In fact, the decrease in chlorophyll content with increasing irradiances of *S. costatum* is not great in comparison with the one observed in *D. tertiolecta*, similarly to what occurred in the *Cyclotella* type and in the *Chlorella* type. Looking at the structure of photosynthetic apparatus it is evident that diatom respond to a decrease of irradiance with an increase in the functional absorption cross section of the PSII (σ_{PSII}) and a decrease in the number of PSUs. The σ_{PSII} is a measure of the target size and efficiency of the pool of pigments that serves the reaction center and is measured from the photons channeled to the reaction center normalized for the surface of the photosystem that harvests the photons. More pigments in the antenna of the PSII would theoretically imply a more efficient harvesting of light in the PSII that would increase the functional absorption cross section of the PSII.

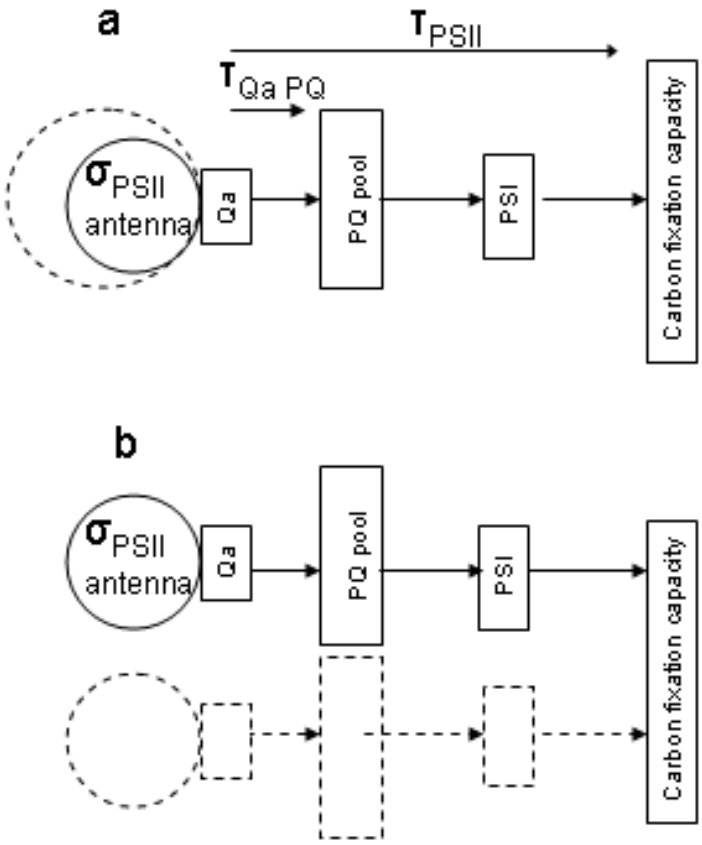

Figure 1.6: Simplified schematics of photosynthetic apparatus as related to two contrasting strategies of photoacclimation. (a) Acclimation to lower irradiance occurs via increases of the functional absorption cross-section of PSII (σ_{PSII}) at constant photosynthetic unit number per unit carbon fixation capacity. (b) Acclimation to decreased irradiance occurs by increasing the number of PSIIs of constant cross-section for a given carbon fixation capacity, leaving σ_{PSII} unchanged. Redrawn from Moore et al. (2006)

In reality, when the pigment content becomes too large, the chlorophyll molecules self-shade each other, decreasing the specific efficiency in the capture of the photons. This outcome is generally called the *packaging effect*.

Some of the equations summarized by Sakshaug et al. (1997) helps in understanding the relation between the σ_{PSII} , the number of reaction centers normalized to chlorophyll n^{chl} and the parameters regulating the shape of the PE curve normalized to chlorophyll:

$$\alpha^{chl} = \sigma_{PSII}\, n^{chl} \tag{1.1}$$

$$P_{max}^{chl} = \frac{n^{chl}}{\tau} \tag{1.2}$$

where n^{chl} indicates the number of reaction centers expressed as oxygen evolution or carbon fixation per unit of chlorophyll. The equations above show that the light harvesting efficiency indicated by α^{chl} is the product of two factors: the number of PSU involved in the harvesting normalized to the total $chla$ content and the size of the light harvesting antenna of the PSUs. On the other hand photosynthetic efficiency, indicated by P_{max}^{chl}, depends on the number of PSUs divided by the turnover time for the transport of the electrons and the formation of reducing power necessary for carbon fixation.

Cells that follow the *S. costatum* strategy exposed by Falkowski and Owens (1980) would theoretically increase the σ_{PSII} becoming shape adapted, while the absolute number of reaction centers n would remain constant, but because they will increase the $chla$ content, the n^{chl} expressed on the $chla$ basis will decrease. The σ_{PSII}would not increase linearly with the increase in the $chla$ content in the antennae, because a large amount of chlorophyll in the antennae would also produce the packaging effect. The $chla$ molecules

would start to self-shade each other in the thylakoids and the efficiency of the light harvesting would be decreased, also if the σ_{PSII} and the $chl\,a$ content will increase. Monoclonal cultures that follow the first strategy decrease the α^{chl} at decreasing irradiances. In addition, being $P^{chl}_{max} = n^{chl}/\tau$, the decrease in n^{chl} will also reduce the P^{chl}_{max}. The shapes of the $P^{chl}\,vs\,E$ curves of the diatom investigated by Falkowski and Owens grown at various light intensities (fig. 1.7) seem to suggest a different behavior than the *Cyclotella* type. Actually, the strategy is the same and the work of Falkowski and Owens elucidated the modification occurred in the photosynthetic apparatus.

On the contrary, the increase of the $chl\,a$ content takes place, in *D. tertiolecta*, through a raise in the absolute number of reaction centers n instead than through the change in the size of the antenna. For this reason the n^{chl} remains constant and the density of reaction centers per unit of chlorophyll does not change. As a consequence, since σ_{PSII} does not change, the α^{chl} remains constant as the culture experiences changes in growth irradiance. *D. tertiolecta* largely increases the $chl\,a$ content as well as the green alga investigated by Jørgensen.

Also in this case, it is evident an increase in the P^{chl}_{max} at increasing irradiances that is not explicable only looking at the light harvesting component. Then, it is reasonable to suppose that cells subjected to a high light increase τ through induction of Rubisco enzyme or that, in contrast, the new reaction centers synthesized at low light have a lower efficiency in the transport of the electrons.

These two forms of photoacclimation should produce different effects on cellular energetics. The increase of the size of the photosynthetic units would be a more appropriate response to low light exposure than the increase of the number of PSUs especially because the former strategy may also serve to reduce the costs of the production of PSUs at low photon flux densities (Richardson et al., 1983).

However, point must be reached when increasing the size of the light harvesting compo-

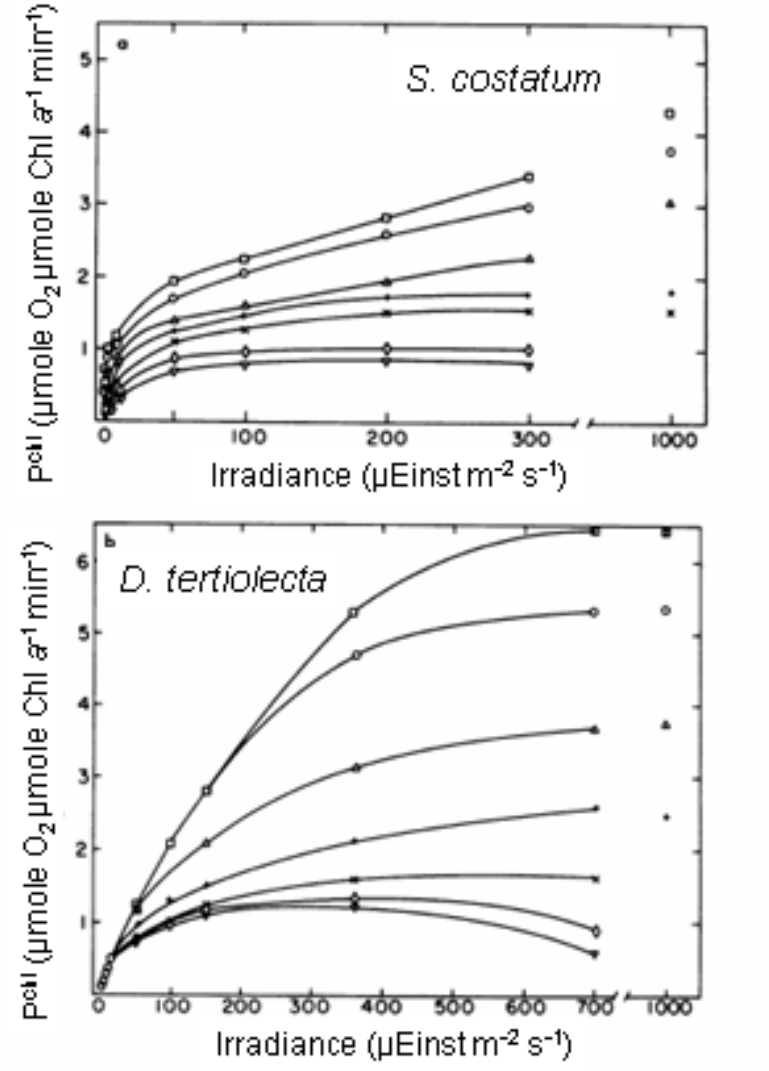

Figure 1.7: P^{chl}*vs* E curves for *S. costatum* and *D. tertiolecta* during steady-state growth. Cultures were adapted to 100% (squares), 50% (circles), 30% (triangles up), 15% (plus), 7% (crosses), 2% (diamonds), 0,5% (triangles down) of the maximum incident light intensity. Redrawn from Falkowski and Owens (1980)

nent of the PSU is no longer cost effective owing to the loss in efficiency of energy transfer within a large light harvesting apparatus. It has been postulated (Raven and Beardall, 1982) that this efficiency of energy transfer may be a controlling factor in determining the upper limit for the size of the photosynthetic unit.

The increase in the ratio of light harvesting pigments to energy transducing catalysts, even if likely favorable from an energetic point of view, has the secondary effect of increasing the probability of damage of the PSII at high photon flux. In fact, more pigments are present in the LHCII, more electrons are transferred to the same reaction center and more radicals with oxidative power will be produced in the photosystem. The NPQ that should prevent such damage decreases the functional cross section of the antenna, through an increase in the photons dissipated as heat. By contrast, increasing the number of reaction centers, the probability to damage one of them would not increase at the same fluence rate.

When such responses were firstly analyzed (Jørgensen, 1964), it was postulated that diatoms were able of increase the chlorophyll within the antenna, while green-algae were considered to increase the number of reaction centers as a consequence of a light-shade adaptation (Falkowski and LaRoche, 1991). This early idea of the green-algae specific strategy is now questioned and both strategies are now recognized as occurring within the same algal class and even between different clones of the same species.

Indeed, there is no evidence that such a mechanism is active in higher plants, and even the signals responsible for acclimation have not been yet unambiguously identified (Walters, 2005).

A general scheme can be outlined if one takes into account the most common responses observed in higher plants. It has been recognized the occurrence of a substantial reorganization of PSII ,and its associated antenna, which involves the increase in the number of PSIIs and a concomitant decrease in LHCII concentration in response to high light and an increase of the concentration of LHCII in low-light grown plants without an apprecia-

ble increase in the total amount of light-harvesting pigments, because of a compensating reduction in levels of PSII reaction centers.

The two strategies highlighted in unicellular organisms are not able to clarify the complex terms of low light phenotypic adaptation of phytoplankton, also because it is unclear the real advantage that this mechanism can produce (see section section 1.1.2). In addition, in 1983 Richardson et al. extended the concept of *strategies of acclimation* up to five different strategies including the two already exposed. They underlined the importance of differences in culture maintenance method and the differences in the P *vs* E curves normalized to the cells number or the chlorophyll. As an example, the role of the accessory pigments determining the α^{chl}, the role of photo-inhibition in the high-light response that had been previously neglected and the different responses of different cultures in terms of the change of cell size at different growth irradiances. In conclusion, the strategies of Richardson et al. do not consider other mechanisms of modification of the structure of the photosynthetic apparatus in respect to the two explained above .

By contrast, a new hypothesis on the evolution of different phenotypic adaptation of the structure of the photosynthetic apparatus has been recently proposed for coastal and oceanic diatoms (Strzepek and Harrison, 2004). Using laboratory cultures experiments, the authors found a difference between a coastal and an oceanic diatom in their photosynthetic architecture, that can explain the different iron requirement of the two species of diatoms. It was already noticed that oceanic diatom *Thalassiosira oceanica* was able to keep high growth rate also at low iron concentration and that the coastal *Thalassiosira weissflogii* was unable to keep the same growth rate at low iron concentration. Strzepek and Harrison (2004) demonstrated that the oceanic diatom had up to fivefold lower PSI and up to sevenfold lower Cytochrome b_6f complex concentrations than the coastal diatom. The PSI and the Cytochrome b_6f complex contain considerably more iron than PSII. The authors suggested that the oceanic species has adapted to the low iron concentration of the open

ocean through the development of a photosynthetic apparatus requiring low iron, but able of high photosynthetic rates typical of coastal diatoms. The hypothesis at the basis of this theory is that the few PSI present in the chloroplasts have a higher turnover rate in order to match with the larger relative pool of PSII, and the absence of a high signal of fluorescence respect to the coastal one is a good support to this hypotesis. The solar energy is effectively well channeled to the carbon fixation pathway even if the ratio between the PSII and the PSI that participate to the electron transport chain decreases. For this reason, the changes of the photosynthetic apparatus markedly decrease the cellular iron requirements of the oceanic diatom but not its photosynthetic rate. However, the authors suggested that this kind of *photosynthetic architecture* decreases the fitness of the oceanic diatoms to highly dynamic light regimes. *T. oceanica*, in fact, showed a limited ability to dissipate excess excitation energy through NPQ.

All the conclusions discussed so far were based on experiments conducted with abrupt changes in illumination, which for assessing the acclimation to a steady photon fluence rate and the kinetics of the acclimation. They are the base for mechanistic models of acclimation to changes in irradiance.

However the question on how the micro-algae react to fluctuating light regimes, which is what organisms experience in the ocean, arose since the beginning of the studies on photo-acclimation. With the improvement of technical facilities it became more feasible to simulate light transitions more similar to the natural ones. The topic of the next section will be to analyze the results derived by experiments conducted in fluctuating light regime.

1.2.2 Photo-acclimation under fluctuating irradiances

Irradiance field can vary *in situ* from seasonal to diurnal time scale because of the inclination of the sun and from hours to seconds for other reasons like changes in cloud coverage. In addition, plankton experience variations in the intensity and in the spectral quality of

the light because of its displacements due to vertical mixing.

For this reason, identifying photo-acclimative responses in a wide range of transitions, similarly to what phytoplankton experience in the real environment, is a crucial step for the assessment of the real advantage that the physiological adjustments can produce. To date, there are few studies which provide such information.

Among them, a pioneering attempt was conducted by Marra (1978a) that discussed the variation in the parameters of photosynthesis and growth for a marine diatom exposed to three different light regimes: constant light, periodic variation, and fluctuating light. The results of this work, even if demonstrated the existence of a different photosynthetic response in the three regimes, were not correlated to measurements able to clarify the biochemical and photo-chemical patterns at the basis of the variation of the photosynthetic parameters.

After a significant time lag, Ibelings et al. (1994) integrated the macroscopic results of differential growth rates in fluctuating or not-fluctuating regimes with a deep investigation of modifications occurred in the size and structure of the photosynthetic apparatus through variable fluorescence measurements together with analysis of pigment and biochemical composition and photosynthetic parameters.

The set-up of the experiments was planned to compare the responses of two microalgal species (a cyanobacterium: *Mycrocystis aeruginosa* and an eukaryotic green alga *Scenodesmum protuberans*) to three different gradual changes in irradiance. The three light regimes were chosen as representative of different mixing regimes. The first one represented a stable water column, while in the other two cases the cells experienced periodic fluctuating irradiances simulating two mixing type. In the first one, it was supposed that the cells reached a depth where the light was attenuated to 0,7% of the surface irradiance in one hour; in the second one algae spent half an hour in a completely dark environment because the base of the mixed layer (Z_m) was supposed to deepen to a depth that was twice the

depth of 1% surface irradiance (euphotic depth Z_{eu}).

The maximum irradiance perceived by the cells was very similar in the three light regimes (around 1100 µEinst $m^{-2}s^{-1}$), but the total daily light dose (TDLD) and subsequently the mean irradiance that the cells perceived during one photoperiod was different in the three simulations decreasing from the first ($Z_m = 0$) to the second ($Z_m = 0,7Z_{eu}$) to the third ($Z_m = 2Z_{eu}$). This experimental approach permitted to analyze the impact of different mixing regimes on the two species considered.

A clear pattern emerged: the diurnal average chlorophyll content of the green alga (as ratio of chlorophyll content on protein content) was independent on the light regime, while the cyanobacterium *M. aeruginosa* increased the $chla$ content from the first to the third light regime. It was possible to conclude that the green alga *S. protuberans* adapted its $chla$ content to the maximum light perceived, that was similar for all three regimes, while the cyanobacterium responded adapting its photosynthetic pigment content to an irradiance that was proportional to the average light. On the other hand, no kinetic parameters were derived because the TDLDs were different and it was not possible to properly assess whether the difference between the three light regimes were due to the difference in the mean light received.

In addition, the fluctuating light regime relieved algae from photo-inhibition. The quick and gradual passage from high to low light gave the cells the possibility of escaping from damaging irradiances. The green alga showed more plastic responses to exposure to high irradiance as well as to fluctuating one, decreasing the $chla$ content at midday of the sinusoidal regimes and decreasing the cross section of the PSII at fluctuating regimes. The impact of photo-inhibition on both the algae was generally low, but variable fluorescence showed that photo-inhibition was higher in cyanobacterium.

The dynamical adjustment of the photosynthetic apparatus found in *S. protuberans* was absent in *M. aeruginosa* that in addition showed a prompt NPQ in all light regimes,

even at low or moderate light intensity. Thus the cyanobacterium was unable to properly protect from or take advantage of the dynamic light regime and this was mirrored in the growth rate. Green alga grew always faster than the cyanobacterium at the same irradiance regime.

Moreover the experiment showed that growth rates of both the species was not proportional to the TDLD. This was because the cultures exposed to the sinusoidal regime experienced a mean irradiance that was saturating for photosynthesis. For this reason, the increase in the growth rates with the TDLD, even if present, did not show a linear relationship.

A complementary experiment was conducted by Flameling and Kromkamp (1997) on the same green alga of the previous study. Again three light regimes were imposed but keeping the TDLD constant. Therefore algae experienced a different peak irradiance and a different number of oscillations. Also the TDLD was lower, being less than the lowest tested by Ibelings et al. (1994).

Also in those regimes the chlorophyll content of the cells, corrected for the great variations of cell volume observed, did not vary significantly within the different regimes. By contrast, the absolute cellular $chl\,a$ content was lower in the fluctuating regime. The experimental setup, with different regimes, should have also clarified whether the chlorophyll content of the *S. protuberans* cultures was adapting to the highest irradiance experienced. The $chl\,a$ content not normalize to the cell volume was lower for the higher peak irradiance experienced.

The possible explanation came from the analysis of the sixe of the antenna. Apparently the acclimation of the green alga consisted in changes in the photosynthetic structure of the cells with little changes in the pigment content of the cell. In fact, they found that cells exposed to light fluctuations had a lower PSU size, but a larger number of reaction centers per chlorophyll (n^{chl}). The cultures exposed to fluctuating intensity showed also

an higher P^B_{max}, as a consequence of the increased number of reaction centers normalized to chlorophyll.

Those results confirmed that P^B_{max} and the photosynthetic pigment content in some algal strains were regulated by the maximal irradiance experienced by the algae and not by the TDLD. The authors concluded that the same response, even if previously observed in the diatom *S. costatum* (Kromkamp and Limbeek, 1993) and in the Prymnesiophycea *Phaeocystis globosa* kromkamp 1995, cannot be considered universal because they were unable to find it in two other diatoms (*T. weissflogii* and *Phaeodactylum tricornutum*). More generally, the results of Flameling and Kromkamp (1997) showed that the green alga optimized its photosynthesis in fluctuating light regime, through preventing photo-inhibition by down-regulating photosynthesis and by increasing the maximum photosynthetic rate normalized to chlorophyll, acclimating the cells more to the peak irradiance than to the TDLD.

A different pattern from the one recognized in *S. protuberans* and more similar to that of the cyanobacterium *M. aeruginosa* has been identified in the work of Havelková-Doušová et al. (2004) in another green alga: *D. tertiolecta*.

The experiments in the paper of Havelková-Doušová et al. have been conducted exposing twelve cultures to a range of six fixed and six simply sinusoidal irradiances to asses a *baseline* physiology. This baseline was then used to make comparisons with cultures grown in two fluctuating irradiances with a similar peak irradiance (around 1000 μEinst $m^{-2}s^{-1}$). The two fluctuating regimes simulated the light experienced by cells circulating within two hours in a mixed layer with the depth of the bottom Z_m near to the Z_{eu} superimposed on a sinusoidal light. These two regimes differed because in the first one the superimposed fluctuations followed a sinusoidal shape (as previously done in many studies), while in the second one the decrease and the increase followed an exponential equation that simulated the realistic attenuation of the light in the water. For this reason,

the two regimes slightly differed for the TDLD perceived.

The possibility to compare the results of these two growth conditions to a set of cultures grown at different irradiances that covered an high range of variability gives us a clear pattern for the acclimation of *D. tertiolecta* in more realistic light regimes.

The baseline regime shows a clear pattern of decrease of the average daily $chl\,a$ content at increasing irradiances (fig. 1.8(a)). The same parameter for the two fluctuating irradiances was higher than the $chl\,a$ content found in the single sinusoidal regime representative of no mixing condition, as already observed for *M. aeruginosa* by Ibelings et al. (1994). In addition, the average daily $chl\,a$ content of the *D. tertiolecta* cultures grown in fluctuating light was higher than the $chl\,a$ content of the baseline cultures with similar TDLD. Then, *D. tertiolecta* acclimated to an irradiance that was lower than the mean irradiance perceived by the cells during an oscillating regime, therefore responding differently than the other green alga *S. protuberans* that showed an acclimation to the peak light.

The possible mechanism at the basis of that pattern in *D. tertiolecta* is the induction of an '*hysteresis effect*'[1], i.e., the asimmetric light history dependence of a photo-physiological parameters. This effect is likely produced, in this specific case, by the kinetics of the reaction to increasing light, which proceeds with a slower velocity of acclimation in respect to the opposite shift in irradiance. Cells exposed to symmetrical variation of the irradiances over a time interval smaller than the time necessary for completing the acclimation to the new irradiance tend to values of acclimation closer to that of lower irradiances. The physiological effect is a larger light harvesting capacity as compared to cells grown at the same TDLD in non-fluctuating illumination. Obviously, the larger amount of harvesting pigment should cause an advantage in the capture of light but also an higher probability of over-excitation and damage of the reaction centers, if pigment were increased through an increase in the antenna of the PSU. That response was not observed by Falkowski and

[1]Hysteresis in physics represent the history dependence of a physical systems, in this case represent the light history dependence of a photo-physiological parameter.

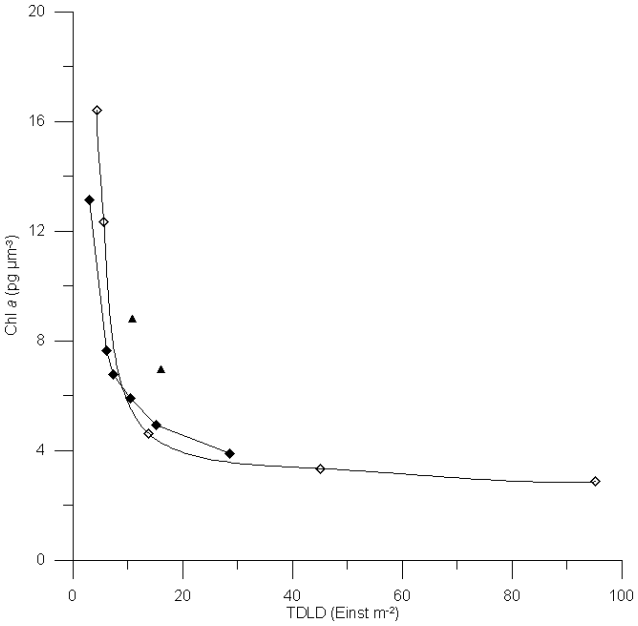

(a) Chlorophyll per cell volume of *D. tertiolecta* cultures as a function of growth irradiance (TDLD) for square wave grown cultures (open diamonds), for sinusoidal regimes grown cultures (black diamonds), for fluctuating regimes (black triangles).

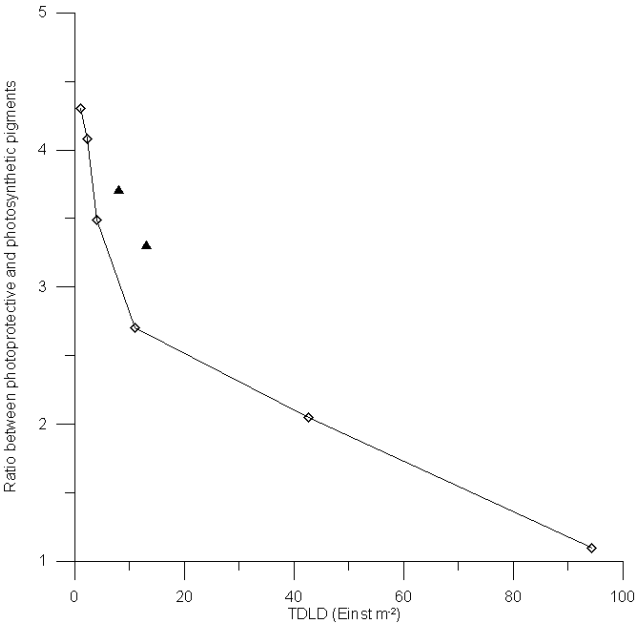

(b) As (a) but for the Ratio of photosynthetic to photoprotective pigments.

Figure 1.8: Pigment content as a function of light intensity and light variability. Redrawn from Havelková-Doušová et al. (2004)

Owens (1980) in *D. tertiolecta*.

The authors also showed that the ratio between photosynthetic and photo-protective pigments was larger than the one found in the baseline cultures and typical of lower mean irradiances (fig. 1.8(b)). The cells grown in fluctuating light regimes also showed a decrease in the σ_{PSII} not connected to a decrease in the chlorophyll content. The authors suggested that the more plausible mechanism implicated was a state transition, that, as it will be further analyzed, is an important response in dynamical light regimes.

The growth rates of the baseline cultures increased with TDLD until they reached the saturation point. It was unexpected that the cells grown at fluctuating regime would display growth rates comparable to those in sinusoidal irradiance, i.e., no mixing with higher TDLD. The authors suggested that the ability of protection to high irradiances through a mechanism of dissipation like state transitions, that quickly responds to the high irradiances, together with the increased light harvesting capability of cells grown at lower irradiances were the cause of this good adaptation in a highly dynamical simulated environment.

The presence of a double pattern of acclimation: to an irradiance related to the TDLD for the light harvesting (also if it was impossible to define through the baseline approach the characteristic of this irradiance) and to an irradiance closer to the peak irradiance for the photo-protection mechanism through the state transition strategy has been confirmed also in the work done on the green alga *Chlorella fusca* by Garcia-Mendoza et al. (2002). In this paper the great importance of the state transition respect to xanthophyll cycle related NPQ at highly dynamical regimes was demonstrated. The high variable light signal was not able to trigger the xanthophyll cycle pigment synthesis, while it triggered the dissipative mechanism of state transition. The existence of a slow acclimation process that shows up during experiments based on step transition in light in respect to fast acclimation reponses displayed in experiments with fluctuating light show that the responses are different. This

can possibly explain the inconsistency between the experimented high light tolerance of green algae respect to the opposite behavior documented in Falkowski and Owens (1980) and in Jørgensen (1969).

Similar experiments conducted on diatoms have shown not uniform responses, as already observed for *S. costatum* and the two *T. weissflogii* and *P. tricornutum*. An antarctic diatom *Chaetoceros brevis* was found to acclimate to an irradiance related to the TDLD received and to receive a net disadvantage in fluctuating light (van Leeuwe et al., 2005). The authors suggested that this effect was due to the high investment in repairing damage due to the high light and to an increased demand for energy consumed for maintenance at fluctuating light (van Leeuwe et al., 2005). They noticed, also, that this diatom did not respond to fluctuating light corresponding to a recirculating time in the euphothic layer of three hours with an increase in NPQ through xanthophyll cycle. This response was not observed in cultures of the same alga exposed to quicker oscillations, because of the relief from photo-inhibition mentioned above.

Opposite results on the ability of diatoms to increase the photo-protective pool pigments in fluctuating regimes have been presented by Lavaud et al. (2002). They found that culture of *P. tricornutum* grown in intermittent light regime were able to increase the xanthophyll content until a level able to down-regulate PSII by 90% and virtually eliminated photoinhibition by saturating light. The question of the real impact on biomass formation of this kind of acclimation was not answered in that work because it does not analyze the growth rates or the photosynthesis in term of carbon fixation or oxygen evolution and was unable to find out the impact of possible electron losses due to alternative pathways.

A recent paper have investigated the "balance of the energy flow from captured light into biomass " for *P. tricornutum* and the green alga *C. vulgaris*, accounting for the conversion of light harvested to biomass formation (Wagner et al., 2006). The authors estimated that the cultures of the diatom exposed to fluctuating light regime achieve a

very high conversion efficiency of photosynthesis and that almost all the energy that was reaching the electron transport chain was converted in biomass and not lose through other sinks of electrons. Instead, they noticed that, at excessive irradiances, other unknown form of sink of electrons were activated to prevent damage. On the contrary the green alga seemed to convert with a lower efficiency solar energy to biomass formation, because of the existence of the strategy of dissipation through state transition that seems to down-regulate the carbon fixation at fluctuating irradiances. In fact electrons seem to follow in this dynamical light regime cyclic transport around PSI, that decrease the energy source for biomass synthesis.

This paper underlined an important point: it is possible that different photo-physiological response can be considered highly dynamical and well coped with an intermittent regime, as the state transition seems to do, but the effective costs and the efficiency of the different physiological state on the real conversion of energy in biomass is the more important aspect that have to be considered also if often neglected.

As final message it seems that species-specific acclimation to fluctuating regimes exists. Some species seems to efficiently adapt to this kind of environment through a strategy that follows the peak irradiance experienced and is able to exploit it limiting the damages. Other species seem to adapt to an irradiance lower that the mean irradiance perceived increasing the light harvesting and protecting the photosynthetic apparatus from the highest light with different photo-protective pathways. However, it exists a certain number of species investigated that seems to possess a more static photosynthetic apparatus that does not give them the possibility to efficiently exploit neither the highest nor the lowest irradiances.

The unique analysis found of the effective efficiency of different strategies of acclimation to fluctuating light regimes underlined the importance to well connect the conversion in biomass with the physiological response in order to well define which strategy can be considered more efficient for the improvement of the fitness of an organism in a variable

condition.

1.3 Mechanistic Models of Phytoplankton Photo-Physiology

Numerous studies on phytoplankton photo-acclimation, partially summarized in the previous section, allowed to assemble a number of mechanistic models aimed at reproducing some of the key traits of photo-acclimation. The advantage of mechanistic models is that, reproducing the supposed underlying functional mechanisms of a process, allow for analyzing the relative importance of the different parameters and to test the consistency of the hypothesized mechanism.

It is quite obvious that, notwithstanding the continuous advances in modeling phytoplankton photophysiology, the existing models are far from reproducing the complexity of the processes discussed before. The usual approach is then to select and design a model according to the specific process under study.

In the next sections, some of the existing models of phytoplankton photoacclimation will be described, as an introductory tool to the presentation of the model assembled for the present study.

1.3.1 Mechanistic Models for the Regulation of Photo-capture

A number of models, reviewed by MacIntyre et al. (2002), describe the variability of $chla : C$ ratio under nutrient-replete and nutrient-limited balanced growth (Shuter, 1979; Kiefer and Mitchell, 1983; Laws et al., 1983). They all reproduce the observed trend in the $chla : C$ ratio along with the increase in growth irradiance in steady-state conditions. Some features are common to all these models, but they often invoke different mechanisms for the regulation of photo-capture. Some of them have a simple structure with a low and measurable number of variables like the models of Kiefer and Mitchell (1983) and Laws et al. (1983). Some others have a quite complex structure. There are also models like that

of Shuter (1979) which include variables that are not routinely measured in laboratory cultures, e.g., the RNA content, which makes their use more limited.

The first attempt for a dynamic model of phytoplankton growth and photo-acclimation under nutrient-replete conditions was presented in 1996 by Geider et al.. The paper provided a mechanistic basis for establishing the regulation of the biosynthesis of light-harvesting pigments and of the phytoplanktonic growth. In the following years the model has been extended to include nutrient limitation and temperature dependence (Geider et al., 1997) and an additional dynamic control linked to the nitrogen to carbon ratio (N:C) for the nitrogen assimilation (Geider et al., 1998b; Flynn et al., 2001).

The key feature of all the versions of the model is an explicit description of the regulation of the biosynthesis of light-harvesting pigments, in particular chlorophyll, by the ratio of photosynthesis to light harvesting. The implicit assumption is that the $chla : C$ ratio reflects the oxidative status of the photosynthetic electron transfer chain, that is supposed to be the crucial modulator of the rate of synthesis of chlorophyll (Escoubas et al., 1995; Pfannschmidt et al., 1999).

In previous models, photo-acclimation kinetics were modeled with empirically determined first-order rate constants, although expressions other than first-order rate equations may be more appropriate (Geider et al., 1996). In fact, it has been consistently reported that acclimation of light harvesting apparatus follows kinetic rates different than first order if cells are subjected to increasing or decreasing light shifts. A first-order kinetic is unable to reproduce those features (Cullen and Lewis, 1988). For this reason Cullen and Lewis suggested a logistic model instead of a simpler one based on first-order kinetics.

The model of Geider et al. reproduces the so called *hysteresis* effect (see also section 1.2.2) as an emergent result of mechanistic equations representing the underlying mechanisms that trigger and regulate it. In the model the carbon specific growth rate quickly decreases after a high to low light shift because of the lower energy available while the

synthesis of chlorophyll increases. On the other hand, during the transfer from low to high light the growth rate increases because of the higher energy flux. The $chla$ synthesis proceeds at a slower rate and no active degradation of $chla$ is assumed. Therefore, even if the $chla$ synthesis proceeds at a slower rate the $chla : C$ ratio decreases because $chla$ is diluted by the increased carbon content.

In brief, two mechanisms act synergistically in the high to low light shift, while only one is acting during the opposite light transition. This causes a quicker response of the $chla : C$ ratio to decreasing as compared to that displayed when irradiance increases.

The 1998 version of the model describes phytoplankton growth as a function of both environmental variables (external nitrogen concentration and irradiance) and cell chemical composition. External nitrogen concentration influences the nitrogen assimilation, that manifests in changes of the N:C ratio, that in turn modulates both assimilation and photosynthesis. Other growth controls related to nitrogen assimilation are due to the regulation of the respiration rate and of the chlorophyll synthesis. Light history, instead, is reflected in changes of $chla : C$. The $chla : C$ ratio, in turn, affects the instantaneous photosynthesis-light response.

The paper of Flynn et al. (2001), comparing the results of the model of Geider et al. (1998b) with those produced by different versions of the mechanistic model for nitrogen metabolism of Flynn et al. (1997), analyzed the environmental conditions for which each was better suited. In addition, the authors provided a revised version of both the original models and new hybrid versions of the two models. In particular, they found that both the original models had pitfalls: the Geider et al. model for what concerns the estimate of nitrogen cell quota and the Flynn et al. for what concerns the photo-physiological part. They concluded that the revised version of the Flynn et al. model was to recommend when both the interaction between light and nitrogen source and the interaction between nitrogen compounds (nitrate or ammonium) where the focus of the study.

On the contrary, they suggested the most simple revised version of the Geider et al. model for studies focused on the interaction between light and growth. The model, in fact, correctly reproduces the nitrogen metabolism when a single nitrogen source is considered. The additional hybrid models were formulated for intermediate conditions and for a direct control on the dark response of the phytoplankton. It is known, in fact, that the nitrogen metabolism and assimilation during dark differs from species to species. For this reason a direct explicit control on nitrogen assimilation was provided.

The model that will be presented in this section is the revised version of the Geider et al. model, called "GM3" in the paper of Flynn et al. (2001). This version of the model is the most suitable for studying photo-acclimation without any major pitfalls in modeling the growth of the phytoplankton, this without a too complex structure of the model.

The model was chosen also because it was able to simulate the dark-light change in biochemical composition of the cultures in the experiment by Anning et al. (2000). This was not at reach of the first version of the Geider et al. model. A better quantification of the costs due to biosynthesis and the ratio between the maximum carbon growth rate and the maximum nitrogen assimilation improved the results of this version of the model.

Because this model was fully included in mine I will describe them in more detail, briefly introducing the equations of the model. The cell carbon concentration changes following the equation 1.3:

$$\frac{1}{C}\frac{dC}{dt} = PS - resp \tag{1.3}$$

where PS is the photosynthetic rate and $resp$ is the respiration rate both expressed in terms of mg C mg C s^{-1}. The first one is:

$$PS = P^C_{max} \left[1 - \exp\left(\frac{-\alpha^{chl}\, \theta^C\, E}{P^C_{max}} \right) \right] \tag{1.4}$$

The photosynthetic rate normalized to carbon is expressed with a Poisson function to reproduce the classical photosynthesis irradiance curve. The variable θ^C represents the $chl\,a : C$ ratio expressed as mg Chl mg C^{-1}. The light limited initial slope of the $P^C vs$ E curve is the product of the given $\alpha^{chl}$and the θ^C. This is due simply to the different normalization of the parameter α^{chl} and the photosynthetic rate in the model, as already discussed in the section 1.1.2. In addition $P^C_{max}$is regulated by the nitrogen status of the simulated phytoplankton. In fact, it depends on a reference maximum value P^C_{ref} and on the N:C status that modulates it according to the equation:

$$P^C_{max} = P^C_{ref} \left(\frac{Q - Q_{min}}{Q_{max} - Q_{min}} \right) \tag{1.5}$$

where Q is the actual N:C ratio in terms of mg N mg $C^{-1}$and the Q_{max} and Q_{min} are respectively the maximum and minimum possible value for the N:C ratio expressed with the same unit. As a result of the equation 1.5, the maximum carbon growth rate will be equal to P^C_{ref} when the N:C ratio is equal to the maximum achievable, while the photosynthesis will stop if the internal N:C quota reaches the minimum possible value.

The net growth rate, therefore, is then equal to the difference of the photosynthetic rate expressed with a classical relationship of $P^C vs$ E curve that involves directly the $chl\,a : C$ ratio, minus the respiration (eq. 1.6):

$$resp = V_N\, N_{cost} \tag{1.6}$$

The respiration represents essentially the cost of biosynthesis through a direct dependence via a constant N_{cost} on the assimilation of nitrogen compounds V_N. The nitrogen assimi-

lation, in turn, follows this equation:

$$V_N = P^C_{ref}\, Q_{max}\, S\, \frac{1 - Q/Q_{max}}{1 - Q/Q_{max} + shape}\, \frac{N}{N + K_N} \tag{1.7}$$

The first part of this equation $P^C_{ref} Q_{max} S$ represents the maximum achievable assimilation rate, due to the reference carbon fixation rate multiplied for the maximum N:C ratio and for a constant S chosen to fit the model output carbon growth to the Anning et al. (2000) data. The second fraction is the control of the N:C quota to the assimilation: it stops the assimilation if the maximum quota is reached and allows the assimilation for reaching its maximum when the internal quota is at the lower limit. The *shape* constant has the effect to control and gradually decrease the assimilation when the nitrogen quota increases to the maximum possible value. The fraction on the right of the equation is, instead, the classical Michaelis and Menten kinetics proposed for enzymatic processes, that is generally used for the description of the kinetics of nutrients assimilation in phytoplankton.

The assimilation rate is expressed, as well as the other rates, in an absolute form: mg N mg N s^{-1}. It will increase the N:C ratio as it will be shown in the next equation:

$$\frac{1}{Q}\,\frac{dQ}{dt} = V_N - \frac{1}{C}\,\frac{dC}{dt} \tag{1.8}$$

The loss term on the right in this equation is the dilution term due to the carbon growth: the N:C ratio increases for the new nitrogen assimilated but decreases for the contemporary net growth in carbon. As it has been shown, the N:C ratio (Q in the equations) is a modulator for both the growth and the nitrogen assimilation, but also the chlorophyll synthesis is indirectly regulated by the nitrogen assimilation. The nitrogen metabolism and the chlorophyll synthesis are linked in the model. In fact, the $chla : C$ ratio changes

as expressed in the next equation:

$$\frac{1}{\theta^C}\frac{d\theta^C}{dt} = V_N\,\rho_{chl} - \frac{1}{C}\frac{dC}{dt} \tag{1.9}$$

The modification of the $chla:C$ ratio due to the $chla$ synthesis, depends on the nitrogen assimilation rate and on a regulation term for $chla$ synthesis ρ_{chl} (eq.1.10). In addition, similarly to the N:C ratio, the $chla:C$ ratio is regulated negatively by the carbon growth rate for dilution effect.

$$\rho_{chl} = \theta^N_{max}\,\frac{PS}{\alpha^{chl}\,\theta\,E} \tag{1.10}$$

The regulation term is a product of a constant that is the maximum $chla$ to nitrogen ratio (θ^N_{max}) and the ratio between the photosynthetic rate and the rate of photo-capture. This ratio is near to one when the simulated phytoplankton photosynthesizes at a rate similar to the rate of light-harvesting, while it is lower then one when the saturation of the electron transport chain is reached. This ratio indicates the oxidation state of the electron transport chain and down-regulates the synthesis of chlorophyll when the rate of light absorption exceeds the rate of utilization of photons for carbon fixation.

The pattern of N:C and $chla:C$ ratios produced when the model was forced with light and nutrients equal to that of the light shifts experiments of Anning et al. (2000) are reported in figure 1.9. The first five days in the simulation and in the experiments on cultures were exposed to and irradiance of 50 μEinst $m^{-2}s^{-1}$, that was the same at which algae were grown, the second five days to an irradiance of 1200 μEinst $m^{-2}s^{-1}$, and afterward they were kept for other five days under the low irradiance of the first period.

During all the experiment, the cultures were kept nutrient-repleted by daily manual dilution with fresh medium. For the simulation, that was only nitrate forced, the external nitrate concentration was taken equal to the fresh medium concentration: 500 μmol N $L^{-1}$of

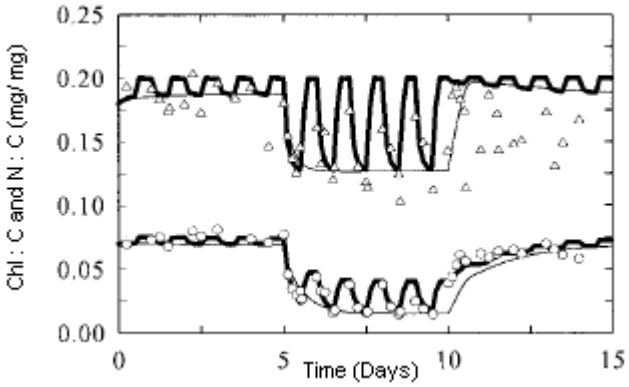

Figure 1.9: Comparisons of "GM3" model output with experimental data from Anning et al. (2000) [N:C(triangles) and $chla:C$(circles)]. The first half of each day was illuminated at 50 μEinst $m^{-2}s^{-1}$ until day 5 and after day 10 and at 1200 μEinst $m^{-2}s^{-1}$ between days 5 and 10. The latter half of each day was in darkness. Thin lines are for simulations where light was supplied continuously to attain the daily photon dose. Thick lines are for simulations where light was supplied in a 12 h : 12 h light : dark cycle, as used in the experiments. Redrawn from Flynn et al. (2001)

NO_3^-.

The N:C ratio, even in a constant nutrient replete conditions, changed during the shift irradiance experiment (fig. 1.9). The nitrogen-irradiance interaction had a consistent influence on the biochemical compositions also in nutrient-replete conditions. The uncoupling of the carbon assimilation and the nitrogen assimilation causes those results. At high light condition the carbon fixation proceeds faster than nitrate assimilation, for this reason the higher dilution of the carbon content decreases the N:C ratio, both in the laboratory experiment and in the numerical one. The timing of the recovery of the N:C ratio after the reverse shift to low irradiance is similar to that of the $chla:C$ ratio. This is an additional evidence of the central role of carbon fixation in determining the observed response. It is unlikely, indeed, that both the internal nitrogen and chlorophyll decrease at high light for the same mechanism of active degradation. It is most probable that the decoupling of the nitrogen assimilation and chlorophyll synthesis with the carbon fixation at high light is the cause of the pattern observed in the data. The model, that describes the variation of the

variables according to this hypothesis, is able to reproduce it and supports the hypothesis, reported also in the paper by Anning et al. (2000).

An alternative model developed for the study of the interactions between nitrogen source and irradiance is the BioLOV model (Pawlowski et al., 2002), builts on the observations of the response of cultures grown in a photo-bioreactor under light and nutrient limitation. The model has been also tested in realistic natural condition as a part of an hydrodynamical-biological model (Faugeras et al., 2004).

The innovative hypothesis at the basis of this model is about the existence of direct connection between the internal nitrogen pool and the light-harvesting pool. It considers, in fact, that chlorophyll complexes represent a large nitrogen reserve in phytoplankton cells that it can vary not only for the light intensity but also for the nitrogen status of the cell. The Geider et al. model does not consider explicitly the nitrogen content of the chlorophyll complexes as the BioLOV model does, but also in that model the chlorophyll synthesis is connected to nitrogen metabolism. In fact, as evident form equation 1.9, the rate of synthesis depends on the rate of assimilation of the nitrate. In the BioLOV model the conversion between non-chlorophyllian (N) and chlorophyllian (L) nitrogen pools is explicitly expressed and proceeds at a rate (r_2) given by this equation:

$$r_2(E) = \gamma(E)\,\frac{L}{C} \tag{1.11}$$

Where C is the carbon content. This rate depends on a function $\gamma(E)$ of the Irradiance, that follows a Monod type law at low irradiance and inhibits the synthesis of chlorophyll at high light levels. More in general, the amount of nitrogen internal pool that is converted in the chlorophyllian one is related to the ratio between the light harvesting pool and the carbon pool. The model has been validated and well reproduces the responses observed in condition of nitrate and light limitation.

The most important characteristic and advantage of BioLOV is that the structure is simple. This model, indeed, seems to be able to reproduce the features of the interaction between a double limitation due to light and to the nitrogenous nutrients maintaining relatively low the numbers of variables and necessary parameters.

In conclusion, the dynamic model of Geider et al. model as reviewed in the work of Flynn et al. (2001), can be considered a good compromise between simplicity and realism. The fact that this model uses a parameterization of the real mechanism that regulates the pigment content in phytoplanktonic cells gives the model the ability to properly analyze the photo-acclimative process and its impact on the phytoplanktonic growth in both theoretical process study and in realistic conditions.

1.3.2 Mechanistic Models for Photo-inhibition and Photo-protection

Several attempts have been made also to model processes of modification of the photosynthetic apparatus like photo-inhibition and photo-protection. Few models have been developed to specifically simulate photo-inhibition, that can regulate significantly the performance of phytoplanktonic organisms subjected to high irradiances or to highly dynamical light regimes (Eilers and Peeters, 1993; Duarte and Ferreira, 1997; Behrenfeld et al., 1998; Marshall et al., 2000; Han et al., 2000; Han, 2002). Even less attempts have been made to simulate the variation in variable fluorescence, focusing on the NPQ (Babin et al., 1996; Huot, 2004).

The dynamics of photo-inhibition can be modeled following two types of methods. One, used for example by Pahl-Wostl and Imboden (1990), is to extend an empirical static model to a dynamic model, introducing a time-dependent term. The incorporation of dynamic process of photo-inhibition into a mechanistic model is the alternative one. This second method has been explored in the past by Eilers and Peeters (1993) and Duarte and Ferreira (1997). However, they introduced the existence of idealized state transition without any

physiological evidence to support it. An early idea of Kok (1956) was exploited by Neale and Richerson in 1987 to express the UVB related changes in phtotosynthesis. Kok firstly developed a dynamic model of destruction and restore of light-sensitive component of the photosynthetic apparatus. He supposed that the concentration of a not yet individuated component was diminishing at high irradiance.

The first effort of a dynamical mechanistic model based on modern physiological and molecular evidences of the underlying mechanism of photo-inhibition was developed in 2000 by Han et al..

They were the first to include the mechanism of damage and repair of D1 protein in the regulation of the relative concentration of the functional D1, that, in turn, was considered as regulating the average turnover time of the electron transport chains τ in the cell. An increase in the fraction of damaged protein was supposed to increasing turnover time and, as a consequence, to decrease the photosynthestic capacity. Experimental evidence, on the contrary, shows that τ is modified by photo-inhibitory processes, only as a compensatory secondary effect and that the parameter affected directly by photo-inhibition is the number of reaction centers n (Behrenfeld et al., 1998). They, in fact have observed a significant decrease of n at photo-inhibitory irradiances without an initial contemporary decrease in the P_{max}^{cell}. They suggested that this feature was related to a compensatory decrease in the time necessary for the turnover of electrons in the electron transport chain τ.

In 2002, Han proposed a second version of the model. The author considers the existence of three states for the PSII, active, inactive and damaged or photo-inhibited, already presented in the schematic outline in section 1.1.3. In addition they postulated that the relative concentration of the damaged PSII should be related both to the average turnover time of the electron transport in the cell or to the number of reaction centers that participate to photosynthesis.

In detail, the model of Han (2002) is a PSU based model that consider a simple PSU

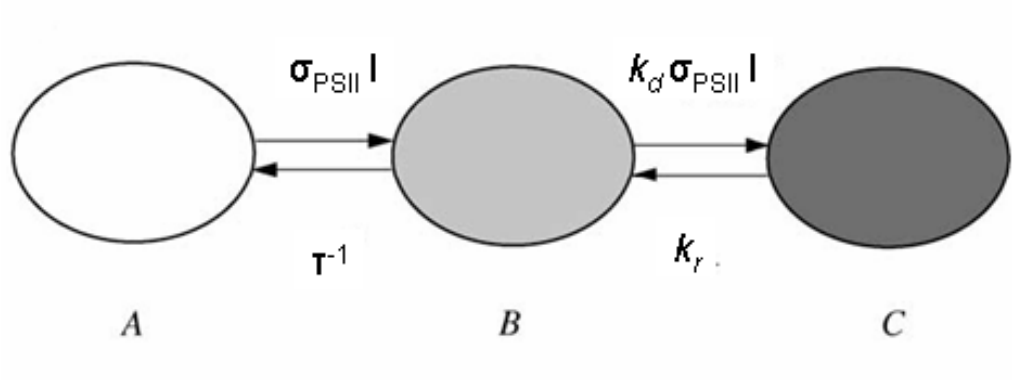

Figure 1.10: Transitions between three states of PSIIs: open, A; closed, B and inhibited, C. τ is the minimal turnover time of electron transfer chains, σ_{PSII} the effective cross-section of a PSII, k_d the damage constant for PSIIs, k_r the repairing rate of damaged PSIIs. Redrawn from Han (2002)

as constituted by a PSI and a PSII connected through the electron transport chain. After being hit by photons, the PSII transits from an open state to a closed one. Accordingly, the PSU becomes closed, while excessive absorption leads to the transformation in a photo-inhibited state. The probability of a PSU to be in the open, closed or photo-inhibited state are referred to as A, B and C in the Han paper. I will refer to them as to ϑ_a, $\vartheta_b$and ϑ_c. The transformation are reversible and the states and the rates of interconversion are indicated in figure 1.10.

The equations that regulate the probability at a given irradiance to have a PSU in a certain state, and so the equations that govern the interconversion between the three states are the following:

$$\frac{d\vartheta_a}{dt} = -E\,\sigma_{PSII}\,\vartheta_a + \frac{\vartheta_b}{\tau} \tag{1.12}$$

$$\frac{d\vartheta_b}{dt} = E\,\sigma_{PSII}\,\vartheta_a + k_r\,\vartheta_c - k_d\,\sigma_{PSII}\,E\,\vartheta_b \tag{1.13}$$

$$\frac{d\vartheta_c}{dt} = -k_r\,\vartheta_c + k_d\,\sigma_{PSII}\,E\,\vartheta_b \tag{1.14}$$

The probability of a PSU to pass from the open (ϑ_a) to the closed state (ϑ_b) depends on the light harvested that is expressed by the product of the irradiance and the σ_{PSII}, while the rate at which the PSU comes back to the open state depends on the velocity in electron transport: τ^{-1} (eq.1.12). The probability that a closed PSU becomes damaged is linked to the irradiance captured. The Han model follows the theory of the unifying model of photo-inhibition formulated by Anderson et al. (1998). In fact the damage rate is considered to depend on the dose of irradiance absorbed. Each photon harvested by the antenna of a closed PSII is considered to have a probability to damage it. This probability is expressed as a the constant k_d. It is not necessary to reach an excessive irradiance to have a damage of the D1 protein, each photon may cause such an effect, because a repeated over-excitation of the electron transport chain to create a reactive oxygen species is not required. The unifying model of Anderson et al. (1998) implies that the oxidative damage of the D1 is due directly to the $P680^+$, that is formed continuously at all the irradiances. The damage of the protein is proportional only to the absorbed photons, and not on the irradiance rate *per se*. For this reason the probability that a closed PSU becomes inhibited is expressed by the constant $k_d\,\sigma_{PSII}\,E$ in the equation 1.14, where $\sigma_{PSII}\,E$ is the irradiance absorbed. The occurrence of PSUs in the photo-inhibited state increases at high irradiances as the probability for the reaction center of the PSII (P680) to be in the radical form $P680^+$ increases.

The rate of repair of the D1 protein is considered to be constant and irradiance independent, and is given by k_r that is expressed in s^{-1}.

The author proposed the possibility to include the damage as a decreasing factor of the average turnover time for the electron transport chain or, and Han suggests this second

option, as a direct control of the active number of reaction centers. This model can be used dynamically, solving the previous equations, but he proposed the solution of a photosynthesis *vs* irradiance curve at the stationary state.

He used an hyperbolic fitting for the P^{chl}*vs* E curve expressed in this equation:

$$P^{chl} = P^{chl}_{max} \frac{E}{E_k + E} \tag{1.15}$$

with, in turn, E_k the light saturation irradiance expressed by this equation:

$$E_k = P^{chl}_{max}/\alpha^{chl} \tag{1.16}$$

It is important to mention that this model does not account for changes in the pigment content. Modifications in the absolute number of reaction centers n due to photo-inhibition will be mirrored in modification of the n^{chl}. In fact, following equations 1.1 and 1.2 for the α^{chl} and for the P^{chl}_{max}along with Sakshaug et al. (1997) and after some transformations the equation 1.15, becomes:

$$P^{chl} = n^{chl} \frac{\sigma_{PSII}\, E}{1 + \sigma_{PSII}\, E\, \tau} \tag{1.17}$$

The equation solved for the stationary state of the model of Han (2002) is similar but:

$$P^{chl} = n^{chl}_{*} \frac{\sigma_{PSII}\, E}{1 + \sigma_{PSII}\, E\, \tau} \tag{1.18}$$

where n^{chl}_{*} is the number of not damaged reaction centers normalized to chlorphyll at the

stationary state, that is governed by this equation:

$$n_*^{chl} = n^{chl} \frac{1 + \sigma_{PSII}\, E\, \tau}{1 + \sigma_{PSII}\, E\, \tau + K\, (\sigma_{PSII}\, E)^2\, \tau} \tag{1.19}$$

where $K = k_d/k_r$ is a constant that represents the ratio between damage and repair.

This model is the first mechanistic model that addressed photo-inhibition focusing on its bio-molecular mechanisms and on the unifying model that underlies the process. However, it is important to point out the limitations of this model, i.e., the absence of the changes in the effective cross section of the antenna due to NPQ or the compensatory changes in the turnover time of the electron transport rate. A model that tried to include both photo-inhibition and non photochemical quenching is the one formulated by Marshall et al. (2000).

Photo-inhibition is modeled as a time dependent decrease in α^{chl} because of D1 damage, The photo-inhibition model was incorporated within the ammonium-nitrate interaction model of Flynn et al. (1997) as reviewed by Flynn et al. (2001) to include the $chla$ synthesis term of Geider et al. (1998b).

The model is not fully mechanistic and some of the responses are reproduced empirically. For example, the decrease of the α^{chl} will start only at a threshold value for the damaged D1 relative concentration. Also the modelization of the NPQ, that is considered to decrease the damage rate of the D1 protein because of its photo-protective role, is parameterized to increase linearly with irradiance. Though, also the Marshall et al. (2000) model explicitly includes the damage and repair of the D1 with an interesting new feature: the decrease of the repair of the D1 protein in nitrogen stressed conditions, due to the requirement of nitrogen sources for the *de-novo* synthesis of proteins.

The rate of D1 damage is modelled as a linear function of the photon dose received in the previous hour and the repair rate is dependent on the nitrogen status of the cell.

The most complex attempt to model photo-inhibition and the photo-protective role of

NPQ has been recently made by Huot (2004).

This model is the first dynamic and mechanistic model that includes photosynthesis, heat dissipation and fluorescence in phytoplankton with photo-acclimation of the absorption cross-section of photosystem II and the capacity for energy dependent non-photochemical quenching. The author included in his model, the dynamical equations for the interconversion between the three PSU states of the model of Han (2002), but he considered the nitrogen-status dependent repair rate as expressed in Marshall et al. (2000). In addition, he considered explicitly the NADP and NADPH pools and he linked in this way, the light reactions with the bio-synthetic reductions in the Calvin cycle, considering also that a fraction of the electrons is involved in other sinks. Photo-acclimation through a decrease in the size of the antenna at high irradiances has been also included (eq. 1.20), as well as the parameterization of the xanthophyll cycle induction at high irradiances through an increase in the rate constant for the energy dependent quenching in these conditions (eq. 1.21).

Clarifying the methodology used in the above model is relevant to deal with a generally neglected feature: the acclimation of the antenna size of the PSII through two processes. The two processes considered are photo-acclimation of the pigment content and NPQ. For these reason, only the two equations that governs these responses will be described and discussed in detail, while the complete description, analysis and validation of the model are available in Huot (2004).

$$\frac{d\sigma^0_{PSII}}{dt} = K_{\sigma_{PSII}}\, \sigma^0_{PSII} \left[\frac{\vartheta_a}{\vartheta_a + \vartheta_b} \left(\sigma^0_{PSII} / \sigma^{opt}_{PSII} \right)^x - 0,3 \right] \tag{1.20}$$

$$\frac{d\gamma_{NPQ}}{dt} = \begin{cases} K_\gamma\, \gamma_{NPQ} \left[\vartheta_c \left(\gamma_{NPQ}/\gamma_{NPQ}^{opt}\right)^y - 0,05\right] & \text{if } \vartheta_c < 0{,}1, \\ \frac{0,1}{\vartheta_c}\, K_\gamma\, \gamma_{NPQ} \left[\vartheta_c \left(\gamma_{NPQ}/\gamma_{NPQ}^{opt}\right)^y - 0,05\right] & \text{if } \vartheta_c > 0{,}1. \end{cases} \tag{1.21}$$

The equation 1.20 is a semi-empirical expression for the modification of the optical cross section of PSII (σ^0_{PSII}). It depends on a rate constant $K_{\sigma_{PSII}}$, and it assumes that the regulation mechanism simulating the redox state of the electron transport chain is connected to the ratio between the relative open reaction centers in respect to the uninhibited ones. The 0,3 in the equation is an empirical expression to give the expected result that the cells acclimates to an extent that their photosynthetic capacity will be around the 70% of maximum. The optimal optical cross section (σ^{opt}_{PSII}) represents this reference condition. The exponent ($x \leq 0$) of the ratio between the actual and the optimal optical cross section is another empirical relation that decribe the biophysical limitation of photoacclimation. In fact, the photon capture and transfer efficiency to the reaction centers is expected to decrease as the size of the optical cross-section increases. The change obtained in the optical cross section of the PSII will affect, in turn, the functional cross section of the PSII and the light harvested and so photosynthesis.

Instead, the equation 1.21 describes the modification in the capacity for non-photochemical quenching (γ_{NPQ}), that affects the heat dissipation due to NPQ. This energy dissipation decreases at high irradiance the functional cross section of the PSII, similarly to the previous expression but with a different underlying mechanism. The author decided to model the regulation of this process using the relative concentration of photo-inhibited reaction centers as the trigger of the light-driven modification in NPQ. Photo-inhibition, indeed, is considered to be the process that is ultimately affected by photo-protection. The expression in equation 1.21 is similar to the one in equation 1.20. In this case, K_γ is the constant rate for the modification of the capacity for NPQ and the reference parameter

homologous of the σ_{PSII}^{opt} is the capacity for NPQ under optimal growth condition (γ_{NPQ}^{opt}). This equation requires two formulations, for higher and lower irradiances (higher or lower concentration on inhibited PSU), to prevent an unrealistic high rate of acclimation at high photo-inhibitory levels.

The model was able to reproduce most of the features recognized as a consequence of acclimation. The resulting maximal photosynthetic rates and initial slopes of chlorophyll normalized P*vs* E curves are constant over a wide range of irradiances, as found by MacIntyre et al. (2002) and discussed in section 1.1.2. In addition, an higher photo-inhibition is recognized in simulated phytoplankton adapted to low irradiance. It is a PSU based model, and for this reason, it would be able to include other parameterizations like an explicit inclusion of the other sinks of the electrons or the regulation of the Calvin cycle through changes in the concentration or activity of the Rubisco enzyme.

Up to now, the pitfalls in the complete understanding of complex responses, like the procesess leading to the non-photochemical quenching , do not allow for a complete mechanistic description of the photo-physiological phenotypic adaptations that occur in phytoplankton. Empirical relationships are the only solution to these gaps of knowledge, in order to include otherwise neglected processes that cannot be ignored in some environmental conditions.

Chapter 2

Turbulence in the Ocean Mixed Layer

In this chapter, I briefly present the mechanisms driving active mixing in the upper region of the Ocean, i.e. in the Ocean mixed layer (OML) (for a full description see Thorpe, 1985; Kantha and Clayson, 2000). A brief introduction to the modeling techniques for the simulation of the turbulence in this part of the Ocean is also given, while the reader is remanded to chapter 5 for the most detailed description of the OML models used in this thesis.

2.1 The Oceanic Mixed Layer

The OML is the ocean region adjacent to the air-sea interface, typically tens of meters deep (for a global climatology of the OML depth see,e.g., de Boyer Montégut et al., 2004). It mediates the exchange of mass, momentum, energy, and heat between the atmosphere and the ocean and hence plays a central role in long-term climate and weather regulation. For instance, because of the high heat capacity of water, and because the oceans cover over two-thirds of the surface of the globe, most of the solar heating on Earth passes through

the OML. Oceans are heat reservoirs, gaining heat during spring and summer and losing it slowly during fall and winter, and therefore act like a "flywheel" for what concerns weather on time scales of weeks and longer (Phillips, 1977).

More importantly, the OML plays an important role in the oceanic food chain. Primary production by phytoplankton is the first link in this chain. The need for an energy source in producing biomass restricts primary production to the upper few tens of meters (the euphotic or photic zone), in which the solar irradiance is strong enough to assist carbon fixation. A large part of the primary production in the Ocean is performed in the OML. As the analysis of the influence of mixing on biomass accumulation is still uncomplete, studies that estimate the interaction of mixing, small scale turbulence and phytoplankters are needed (see chapter 3).

An Oceanic Mixed Layer can be divided into four parts: the very thin but important molecular sublayer, a few millimeters thick; the wave sublayer, normally 2-6 m thick; the main bulk of the OML, 10-1000 m thick; and the entrainment sublayer of about 5-10 m thickness. In deep convective OMLs, where the mixed layer depth is a few hundred meters or more, the fractions of the wave and entrainment sublayers are small (e.g. Kantha and Clayson, 2000).

The OML is fairly uniform in temperature and salinity (and therefore density), because it is well mixed. The rapidly changing regions below these uniform regions of temperature, salinity, and density are called the thermocline, halocline, and pycnocline, respectively. The active turbulent mixed layer in the upper ocean is usually bounded below by a strong buoyancy interface, that can be related to an almost permanent thermal structure (seasonal thermocline) or a sharp increase in salinity (halocline), or both. In either case, this layer, called a pycnocline, is stably stratified, and here turbulence is damped by buoyancy forces.

An OML is mixed from both the top and the bottom. At the top, winds, waves, and convection driven by buoyancy fluxes stir the fluid. At the bottom, large turbulent eddies

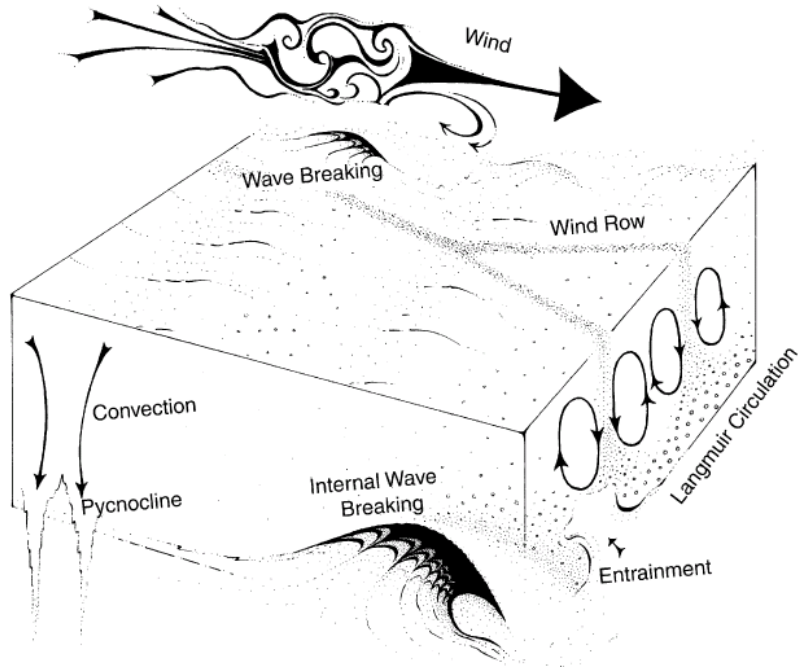

Figure 2.1: Schematic of the dominant forcing functions and energy-containing motions in the surface. Redrawn from Thorpe (1985)

entrain into the OML the denser fluid from below. Wind-driven current in the OML also causes strong shear at the base of the mixed layer; shear instability ensues, inducing Kelvin-Helmholtz billows, which thicken the buoyancy interface and hence decrease its resistance to erosion by turbulent eddies.

The dynamics of the upper ocean is, indeed, complex, not the least because of air-sea interaction processes (fig. 2.1). Winds cause various physical processes, which are not mutually independent: waves, currents, turbulence, and coherent flow structures such as Langmuir circulation. Convection further complicates the dynamics.

Especially at mid and high latitudes, the maximum OML depth is observed at the end of the winter. Thermal convection dominates the winter turbulence. In fact, in these convection regions, the stable stratification in the water column that normally isolates the abyss from the atmosphere is broken down violently by strong convective cooling at the

surface. Penetrative convection generally occurs on vertical scales larger than those usually associated with wind-driven turbulent mixing.

The focus of this study is to characterize the wind-driven turbulence occurring in a homogeneous water column. This situation characterize the OML at the end of the winter and early spring, when deep convection has homogenized the water column up to hundreds of meters and constant winds can easily generate active mixing in the upper ≈ 100 m of the Ocean. For this reason the next section is dedicated to the description of the wind-related turbulent mixing in the OML.

2.2 Wind-related Turbulence in the Ocean

Wind-driven mixing in the OML is primarily shear-driven. The classical picture of shear-driven mixing under neutral stratification is represented by the "law of the wall" theory. The law of the wall theory for turbulent boundary layer flow provides an analytic solution for the velocity profile and predictions of the shear stress. For OML subjected to a wind that produces a frictional velocity (the square root of the ratio of the wind stress to the water density) the law of the wall provides: $q \approx u_*$, $l \approx z$ and $\epsilon \approx z^{-1}$, where q is the turbulence velocity scale, l its length scale, ϵ the dissipation rate of turbulence kinetic energy and z the depth. The meaning of this approximation is that mean shear is proportional to u_*, but inversely proportional to the depth. Therefore the mean velocity is proportional to the logarithm of the distance from the free surface.

The extension of this simple theoretical approach to the Heart rotating case is the classical analytic velocity field for a turbulent flow generated near the ocean surface by a steady wind stress. Interest in this flow goes back to Ekman (1905) landmark work. Ekman assumed a balance between the Coriolis force, viscous friction and the pressure gradient, adopted the approximation of constant vertical eddy viscosity A_z, and derived a solution now known as the "Ekman spiral". In the case of a steady wind in the x-direction,

the steady-state Ekman velocity profile in the open ocean is (for the northern hemisphere) is:

$$u = V_0 \cos\left(\frac{\pi}{4} + \frac{\pi}{D}\, z^*\right) \exp\left(-\frac{\pi}{D}\, z^*\right), v = -V_0 \sin\left(\frac{\pi}{4} + \frac{\pi}{D}\, z^*\right) \exp\left(-\frac{\pi}{D}\, z^*\right) \quad (2.1)$$

where u and v are the components of the mean horizontal velocity, z^* is the vertical coordinate directed downward, $V_0 = \sqrt{2}\pi\tau_0/Df\rho_0$, is the amplitude of the surface velocity, $D = (2A_z/f)^{1/2}$ is the Ekman depth of exponential decay, τ_0 is the surface shear stress and $f = 2\Omega \sin\lambda$, the Coriolis parameter with Ω the Heart's rotation rate and λ the latitude.

According to the solution 2.1, mean horizontal current spirals clockwise and decays exponentially with depth. At the surface, the velocity is directed at 45^o to the right (northern hemisphere) or the left (southern hemisphere) of the wind direction.

The Ekman model is simple, elegant and clearly supported by laminar laboratory experiments, however, it is rather dissimilar to the actual turbulent flow near the ocean or lake surface. In fact, a persistent well-developed Ekman spiral has, probably, never been observed in field measurements (Price and Sundermeyer, 1999). The over-simplified character of the model, indeed, leads to significant inconsistencies between the predicted and actual flows.

The basic assumptions of Ekman's model of a steady-state wind and absence of any geostrophic currents are never completely realized in the open ocean. Particularly important is the effect of transient winds. Attempts have been made to sort out the Ekman layer component of measured data (Price and Sundermeyer, 1999, and references therein). In particular, the angle between the surface current and the wind was observed to be, typically, smaller than the 45^o angle predicted by the Ekman model. A high degree of uncertainty, however, still remains associated with field observations of the phenomenon. The assumption of a constant turbulent viscosity A_z is also a crude approximation. In real

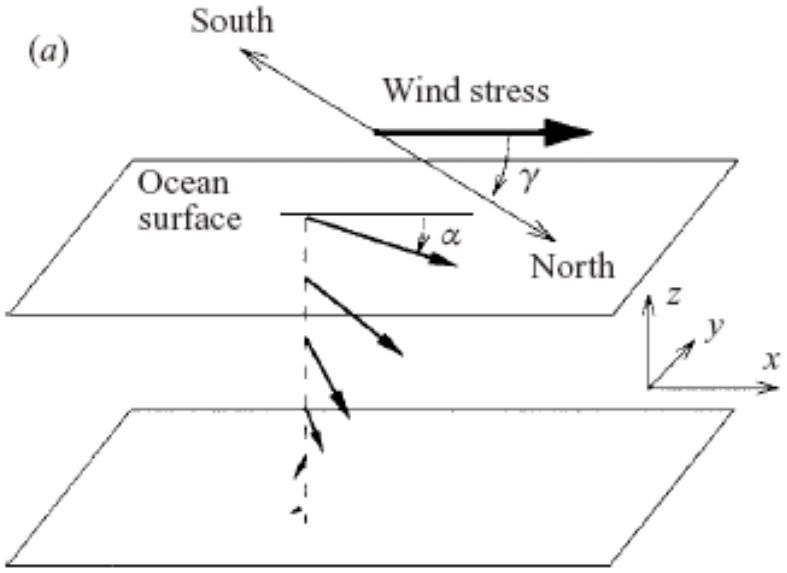

Figure 2.2: Model geometry of Ekman's spiral in the northern hemisphere. From Zikanov et al. (2003)

flows, the intensity of turbulent momentum transport expressed by A_z is expected to vary with depth and time. The mixing length l was assumed to decrease with depth in the bulk flow but to increase linearly in a thin boundary layer near the surface. Only few years ago a study that exploited Large Eddy Simulation (LES) confirm that these assumptions are not justified (Zikanov et al., 2003). The effective viscosity variability resulted in a mean flow profile that deviated significantly from the Ekman spiral. For example, the angle between the surface current and the wind was found by Zikanov et al. (2003) to be $28{,}5^o$, which is in clear disagreement with Ekman's prediction. A particularly strong difference was detected, also, in the rate of decay of the computed current amplitude in the subsurface region that was much higher than predicted by the Ekman model (Zikanov et al., 2003).

The Ekman model ignores the profound effects of density stratification and buoyancy. Stable stratification (e.g. in summer) can cause considerable reduction of the depth of the Ekman layer and the wind-driven transport becomes trapped in a relatively shallow surface layer. On the other hand, evaporative cooling during the night time can initiate turbulent thermal convection that leads to the growth of the surface mixed layer and to release of the constraint imposed by stratification. In this study, focused on early spring condition both these factors are neglected.

Another important flow mechanism is associated with surface gravity waves. It has been found that, under typical wave and wind conditions, increased turbulence intensity and coherent Langmuir circulation strongly affect the fundamental flow properties such as the mean velocity profiles and characteristics of turbulent momentum transport.

In fact, the combination of wind stress at the air-sea interface and the passage of surface wave trains generates a well-known feature of the ocean, called Langmuir circulation (Langmuir, 1938).

The impact of this particular process on the oceanic mixing has been supposed to be significant only in particular cases of strong wind in open Ocean. However, it has been

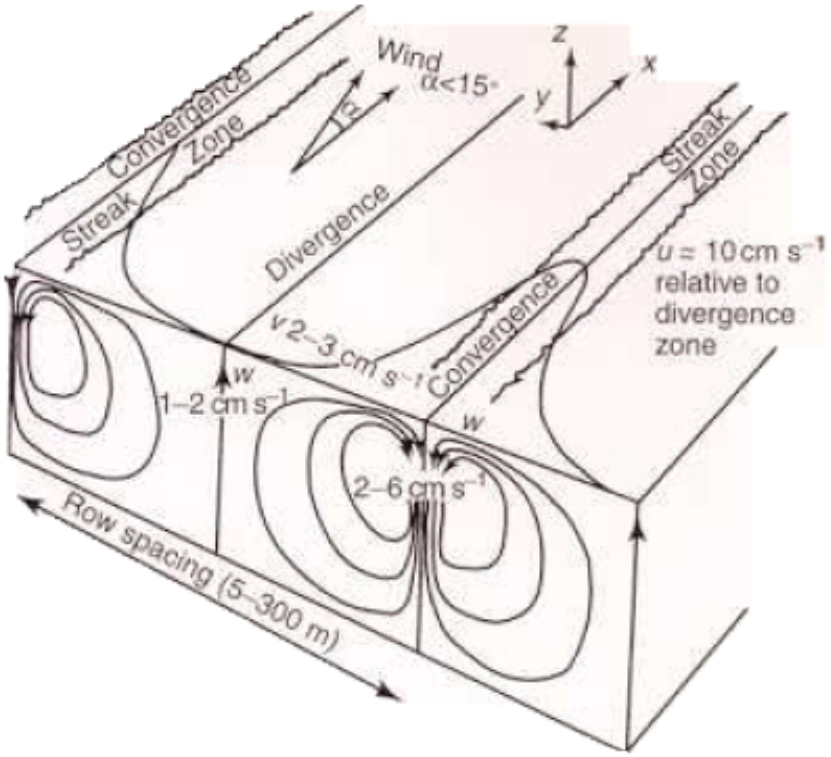

Figure 2.3: Langmuir cells and the associated velocities. Note the "windrows" and the strong near-surface vertical velocities associated with the convergence zones of a pair of counter rotating cells. α is the angle between the wind and the windrows, w is the vertical velocity, u and v are velocities in the x and y directions. Redrawn by Kantha and Clayson (2000).

recently suggested that the influence of this mixing process has been previously underestimated and that the Langmuir turbulence could dominate the mixing in the open OML (Li et al., 2005).

Langmuir cells are organized counter-rotating cells in the surface layer (fig. 2.2), with axes roughly aligned with the wind. Their presence is indicated by surface convergence at the boundary of counter-rotating cells, where seaweed and flotsam accumulate. The convergence region is also made visible by bubble entrainment due to breaking of small-scale waves, resulting in parallel white lines aligned roughly with the wind direction and almost uniformly spaced.

Organized motions in the OML such as those due to large eddies and Langmuir circulations are important to upper-ocean mixing and transport. Langmuir cells can be quite vigorous with downward vertical velocity immediately below the convergence zone as high as a few tens of centimeters per second.

This circulation is able not only to increase the mixing energy in the OML, but has been supposed to transport floating material and so also phytoplankton deep into the OML.

However, they are transient processes and its occurrence has been quantified, as already mentioned, only recently. Their existence depends on the presence of a surface wave field with the associated Stokes drift, a small residual current in the direction of surface wave propagation which decays exponentially with depth.

An instability due to the vortex force term that appears in the momentum equations due to the interaction of the Stokes drift with the mean shear in the upper layers leads to the formation of counter-rotating cells. Thus they are unique since they result from a subtle interaction of the wind-driven turbulence and the Stokes current drift produced by surface gravity waves. Observational programs and advanced computer models such as LES are increasing the understanding of such large-scale features of the OML (Li and Garrett, 1993; McWilliams et al., 1997).

Their effect on mixing in deep mixed layers can be significant, even though the Stokes drift decays rapidly with depth. The characteristic velocity scale for Langmuir circulation is:

$$V_L = \left[u_*^2 \; (k\, a)^2 \; C \; \cos\theta \right]^{1/3} \tag{2.2}$$

where u_* is the friction velocity, k the wavenumber, C the phase velocity, a the amplitude of the surface waves, and θ the angle between wind stress and the direction of wave propagation. Clearly, the strength of the Langmuir cells depends on both the Stokes drift

and wind stress, so that, in principle, strong winds and small waves can have an influence similar to that of weak winds and large waves.

Recently, McWilliams et al. (1997) showed how the simple view of regular cells is too elementary because of the turbulent nature of Langmuir circulation.

One of the peculiarity of this thesis is that the assumptions in the physics have been reduced as much as possible by using the state-of-the-art of physical modeling of the OML,i.e, the same approach of Zikanov et al. (2003) and McWilliams et al. (1997) has been used.

2.3 Modeling Turbulence in the Ocean Mixed Layer

Turbulence is usually defined as the irregular, random component of fluid motion. Its spatial scales are usually the smallest scales of the flow ($\approx$ 0,01 m). The complex nature of the flow makes deterministic analysis impossible and kinematic observations generally unsatisfying; therefore, the conceptual framework for understanding turbulence is largely statistical (for more details, see the comprehensive book of Tennekes and Lumley, 1972).

Although the statistical approach precludes detailed prediction of flow evolution, it does give access to the rates of mixing and property transport, which are of primary importance in most applications.

Statistical analysis focus on the various moments of the flow field, defined with respect to some averaging operation. The average may be taken over space and/or time, or it may be an ensemble average taken over many flows begun with similar initial conditions. Analysis are often simplified using three standard assumptions (Kolmogorov, 1941). The flow statistics are assumed to be

- stationary (invariant with respect to translations in time),
- homogeneous (invariant with respect to translations in space),

- isotropic (invariant with respect to rotations).

Much of the present understanding pertains to this highly idealized case. Spectral analysis however provide insight into the physical processes that govern motion and mixing at different spatial scales in more complex situations (e.g. Smyth and Moum, 2000).

Turbulent motions in a fluid mix fluid parcels from different parts of the flow, thereby enhancing mixing of tracers across concentration gradients created by molecular diffusion.

Since turbulent motions are rapidly dissipated in the absence of an energy source, it is critical to identify and quantify the sources of turbulence. Because of its complexity, even if understanding turbulence in the ocean is fundamental, its inclusion in numerical models is still critical (Yamazaki et al., 2002).

Most of the oceanic mixed layer models can be grouped into two categories: bulk models and diffusion or turbulence closure models. In addition new kind of models hybrids in their nature have been developed.

Bulk models attempt to model the OML in an integral sense (e.g. Kraus and Turner, 1967b). The governing equations are integrated over the entire mixed layer so that the momentum and heat balance of the OML, under the action of momentum and buoyancy fluxes at the ocean surface, can be considered. The major problem in bulk mixed layer modeling arises from the necessity to parameterize the advance and retreat of the OML under the action of surface forcings. The entrainment rate at the base of the OML, determined by turbulence processes, governs the deepening of the OML. For homology it is called detrainment, when waters that were part of the surface mixed layer become isolated from surface effects by formation of a lighter layer near the surface with a density gradient between the two layers greater than the density gradient within either of the layers. Bulk models parameterize the entrainment (OML deepening) and detrainment (OML retreat) in terms of surface fluxes of momentum and buoyancy, using well-known properties of turbulence in geophysical mixed layers and observational evidences.

Diffusion models, on the contrary, parameterize turbulent mixing in the OML. Those based on higher moments of governing equations close the governing equations for turbulence quantities at some level by modeling of the unknown higher moments and other terms. The so called turbulent closure models or K-theory models estimate at each time step and at each vertical grid point a vertical turbulent diffusion coefficient $K(z,t)$ from an analysis of Reynolds stresses, buoyancy fluxes, turbulent kinetic energy (TKE), stability expressions, and mixing lengths. The TKE equation is determined prognostically, but other gradients are determined diagnostically. The level of closure is determined by the highest-order moment that is calculated, not parameterized. The parameterizations result in diffusive transport, and only local, small-scale, gradients control the strength of the diffusive transports. The estimated $K(z,t)$ is used to mix temperature and salinity and can then be used to mix biological variables, such as phytoplankton.

Most models of this type originate from the set of formulations of Mellor and Yamada (1974, 1982). The development of these models applied to the surface ocean mixing layer can be traced through the widely used models of Mellor and Durbin (1975) and Kantha and Clayson (1994).

Attempts have therefore been made to simplify the set by once again utilizing certain aspects of turbulence such as its departure from the state of local isotropy. The result is a hierarchy of models, of which the most useful for geophysical applications is the model that consists of one conservation equation for TKE and a set of algebraic equations for turbulence second moment quantities. For the most part, TKE models do not parameterize the large vertical motions within the surface mixing layer, especially those associated with non local mixing such as convection or Langmuir circulation.

To deal with those limits hybrid models employ some nonlocal representations developed from LES modeling, whereby diffusive mixing within the mixed layer scales according to an initial estimate of its thickness. In addition, hybrid models represent some triple

products with parameterizations that result in counter-gradient fluxes, especially during convective conditions caused by surface buoyancy losses. They may also include parameterization of increased entrainment due to Langmuir circulations, resulting in more rapid or greater deepening of the mixing layer, especially when the layer is already deep and there is otherwise a small wind-driven shear at its base (Large et al., 1994).

Anyhow, the most reliable description of the turbulence and, specifically, energy cascade between larger and smaller eddies can be reproduced only with the use of 3D LES. An application of this turbulent model for an Oceanic Mixed Layer has been used in this study and for this reason, the description of this kind of models is remanded to section 5.2.

Chapter 3

Turbulence and Phytoplankton Responses

Physical processes are generally considered among the main drivers of the variance of phytoplankton species spectra both directly, by their influence on phytoplankton and indirectly, by affecting food web interactions. Light and nutrients are needed by phytoplankton for growth, but the light comes from above, while the source of nutrients is at depth. According to Sverdrup (1953), the physical motion and the density structure of the water column have a major role in controlling the ecology of phytoplankton, primarily through mechanisms that refuel the euphotic zone with inorganic nutrients.

These mechanisms act on a pelagic ecosystem that is, thanks to the particular physical processes acting on the given region, sufficiently defined in terms of seasonal biomass (Cullen et al., 2002).

From these factors may be derived the information to estimate the seasonality and possibly the phytoplankton production and the response of consumers.

However, almost all the research carried out to date within that framework generally involves comparison between average concentrations and physical processes characteristic

of the large scales. In comparing averages the researchers make many implicit assumptions about the behaviour of the individual plankters that make the specific community (Dower and Denman, 2001).

Moreover, these assumptions are made also on processes that are mostly unknown, such as the responses of the individual plankton to a specific physical stress.

A first step towards such an approach is possibly depicted by Margalef (1978) in considering the ecological succession in the plankton community in function of few relevant physical processes. Indeed, without denying the importance of ecologically relevant factors such as consumers or physiological adaptations to light, temperature, and nutrients, Margalef (1978) suggested that the most important factor in determining the prominent life forms of the phytoplankton in the pelagic ecosystems, is the mechanical energy of water column (fig.3.1).

He concluded that:

> *The combination of sedimentation with turbulence, or the variance in components of velocity, is believed to be the most important factor in the biology of phytoplankton.*

Following Cullen et al. (2002), if the euphotic zones were stably stratified and not perturbed by the physical forcing which could produce a variance in the mean velocity field, nutrients would be depleted by phytoplankton and bacteria, incorporated in the food web, and ultimately stripped from the surface layers by the sinking of particles. The small phytoplanktonic organisms with high ratios of surface area to volume, and hence low sinking rates and advantages in nutrients uptake, will dominate in these stable, nutrient depleted waters.

Turbulent mixing or upwelling brings nutrient to the upper ocean supporting the growth of larger cells, which are adapted to compete in a temporally variable, nutrient-rich environment. In some cases high nutrients concentration and weak mixing processes can support

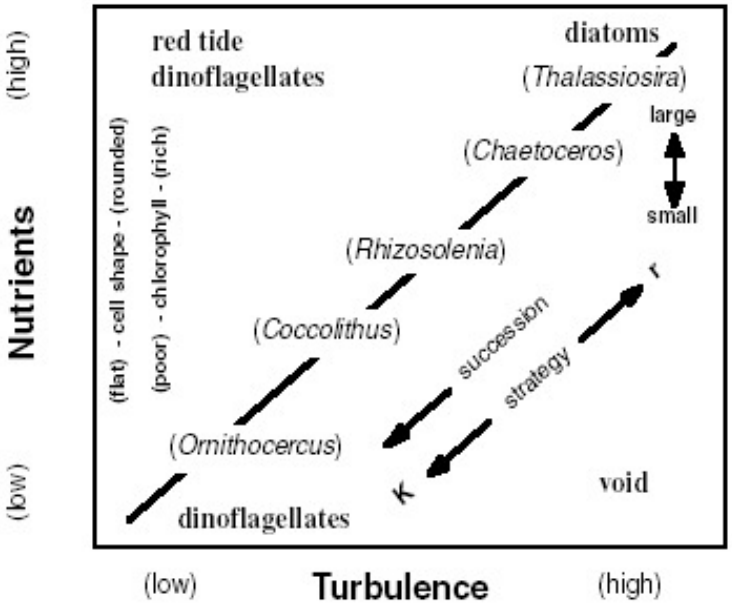

Figure 3.1: Life forms of phytoplankton in response to different regimes of turbulence and availability of nutrients. The trends in cell size, shape, pigment content, and ecological strategy are consistent with a strong influence of nutrient availability on selection. Redrawn from Cullen and MacIntyre (1998) after Margalef (1978).

specially adapted phytoplankton that form red tides. All the findings above support the idea that the physical processes, through the interaction at the organisms' scale, can act as a controlling factor in determining the community shape of the marine ecosystem.

Those hypotheses on the phytoplankton species succession in function of the environmental conditions are generally accepted, but the mechanisms have been never fully elucidated.

Anyhow, the effects of these physical processes at small spatio-temporal scales on the dynamics characterizing the life of a marine micro-organisms are a function of the time scale on which both processes occur.

The environmental grain perceived by living organisms is then of fundamental importance in determining its response. It is now extensively accepted that the small scale motion has a role in: influencing the uptake of nutrients in large phytoplankton cells, con-

trolling the aggregation of the smaller organisms, controlling the predator-prey relations through a regulation of the encounter, detection and capture processes, and regulating the fish ecology (Yamazaki et al., 2002). The first of these processes is the more "emphasized" small-scale effect on phytoplankton survival effort and is discussed in the following section.

In addition it is important to consider that, apart from the small scales interactions, motions at the scale of individual plankton influence the light supply that organisms perceive. In fact, plankton not only experiences small vertical displacements associated with diffusive motions within the mixed layer, but can experience displacements over many tens of meters vertically over time scales on the order of an hour. This second process is fully analyzed in this study and in section 3.2 are discussed the evidences until now collected.

3.1 Small-scale Turbulence and the Nutrient Uptake

All the activities performed by the plankton marine organisms take place in a surrounding environment dominated by the viscosity of the fluid.

A very low Reynolds number implies a dominance of viscous terms on the inertial terms in the Navier-Stokes equations, thus giving license to ignore the inertial forces. With this simplification, explicit solutions for many realistic biological physical interactions are possible and some of these are presented below. For example, a large diatom cell of a diameter of 100 μm, sinking at a speed of say $3\,10^{-4}$ m s^{-1}, exhibits a very low Reynolds number of about $3\,10^{-2}$. Obviously, the world of this phytoplankton microorganism is dominated by viscosity, and activities such as nutrient uptake or sinking prevention are influenced by the low Reynolds number (say viscous) forces. The sinking is regulated by a simple balance between the net body force (weight minus buoyancy) and the drag force. For $Re < 1$, the latter assumes a simple form given by Stokes' law and equal to $D = 6\pi\mu aU$, with a being the radius of the cell, μ the dynamic viscosity of the fluid and U the speed of the spherical object.

For a cell of density ρ falling in a medium of density ρ_0, the net body force is equal to $\frac{4}{3}\pi a^3 g(\rho - \rho_0)$, where g is the gravitational acceleration.

Equating the two forces and solving for U, we can derive the well known equation for the terminal velocity:

$$U = \frac{2a^2 g(\rho - \rho_0)}{9\mu} \tag{3.1}$$

This can be modified including to the denominator a shape factor, ϕ, to account for the reduced sinking velocity when the cell deviates from the spherical form (corresponding to $\phi \doteq 1$).

The density of the algal cells is always greater than the sea water density, but a distinction occurs between senescent cells and growing cells (Mann and Lazier, 1996), with the former sinking faster.

An active debate exists on the role of the sinking motion within the plankton community. A stationary phytoplankton cell cannot take up nutrients faster than they are transported towards it by diffusion. Relative movement between the water and the cell can be effective in enhancing the nutrient uptake only for large or fast moving (swimming) algae. In no case a sinking cell can overcome nutrient diffusion limitation with its relative slow motion within the sea water body (Mann and Lazier, 1996).

Swimming is the alternative to sinking, as a means to perform relative motion of a plankton organism within a body water. However, this activity is also strongly affected by the viscous forces and appears to be a good device to reduce the nutrient diffusion limitation only for the larger cells moving at the highest speed. Through the use of equation 3.11, it can be estimated that a small spherical organism of radius $a = 5$ μm, can increase by about 20 % the nutrient transfer towards its surface moving at a speed of $u = 300$ μm s^{-1}, i.e., 60 body lengths per second. In nature few organisms and for short time exist that can reach such high relative speed. In fact, a realistic value for the organisms' swimming

velocity lies generally 1 to 10 body lengths per second, which corresponds to a maximum increase in the nutrient transfer of about 5%.

A similar scenario is depicted in a much-admired reconstruction of the cell's motion through water done by Purcell (1977), which analyzing the role of the plankton swimming on the nutrient uptake, concluded:

> *But what (the cell) can do is find places where the food is better or more abundant. That is, it does not move like a cow that is grazing a pasture: it moves to find greener pastures.*

On the other hand, the only reason to swim for a small autotrophic cell is to seek a more concentrated patch of food.

Then, if the movement is assumed in some way related to the concentration gradient of the nutritive substances and, following Purcell (1977), it is supposed that the cell's movement follows the gradient, towards the greater concentrations, it could come as no surprise that the small scale motions can negatively affect the dinoflagellates.

The diffusion can limit the exchange of gas and nutrient molecules between the cell and the medium. This limitation may occur only if the cell's uptake rate V, in terms of μmol $cell^{-1}$ s^{-1}, is higher than the time needed to the transport process. Indeed, when V is lower the cell absorbs nutrients so slowly that transport has no influence.

Below, a perfect absorber is considered which represents a cell limited in the uptake of the nutrients by the molecular diffusion transport process.

For a spherical phytoplankton cell immersed in a uniform low nutrient concentration that is being absorbed at the same rate everywhere on the cell's surface, the rate of transport of the food to the a cell can be generalized as:

$$Q_a = A\, J_a \tag{3.2}$$

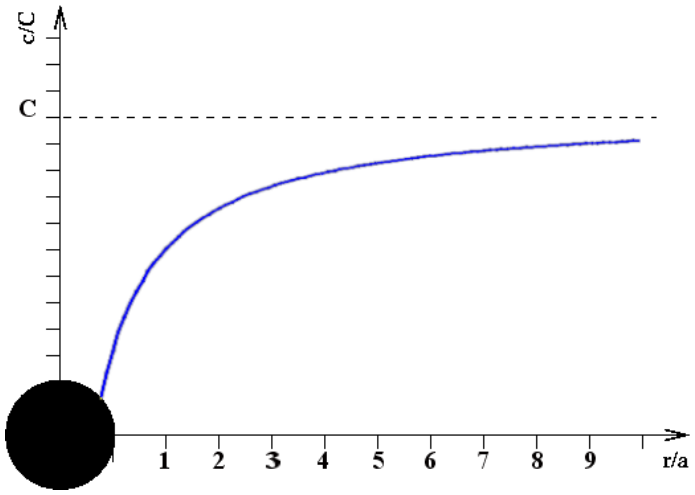

Figure 3.2: Schematic representation of the diffusive nutrient uptake for a spherical cell of radius R. Redrawn from Mariani (2004)

which has dimension μmol s^{-1}, with A being the surface area of the cell and, J_a the flux of nutrient measured as μmol m^{-2} s^{-1}.

The latter can be derived from the Fick's first law, that expressed in spherical coordinates is equal to:

$$J_a = D \left. \frac{dc}{dr} \right|_a \tag{3.3}$$

being D the diffusivity of the nutrient, expressed as m^2 s^{-1}, and c its environment concentration, expressed as μmol L^{-1}. The subscript a represents the cell radius while r is the distance from the center of the cell. At the steady state, the distribution around the cell is related to the Fick's second law, (see fig.3.2):

$$\frac{d}{dr}\left(r^2 \frac{dc}{dr}\right) = 0 \tag{3.4}$$

Integrating between $r = a$, where a surface cell concentration $c = C_a$ is assumed (for a

perfect absorber $C_a = 0$), and $r \to +\infty$, where an undisturbed environment concentration $c = C$ is prescribed, gives:

$$\frac{c - C}{C_a - C} = \frac{a}{r} \tag{3.5}$$

which corresponds to the nutrient distribution showed in figure 3.2.

The expression above can be used in the equation 3.3, and substituting it in equation 3.2, gives a transport rate for a spherical cell of $Q_a = 4\pi a^2 \left(D\frac{C-C_a}{a}\right)$, which, for a general cell's shape, and according to Pasciak and Gavis (1974) can be rearranged in:

$$Q_a = hA\left(C - C_a\right) \tag{3.6}$$

As before A is the cell's surface area while, the variable h, is a mass transfer coefficient expressed as m s^{-1} (Pasciak and Gavis, 1974). Its value is $h = \frac{D}{a}$, when the cell does not move, while when there is a relative motion between the sphere and the environment it is function of the "Sherwood number": Sh, which is defined as the ratio between the total flux of nutrient arriving to the cell surface in the presence of fluid motion and purely diffusional flux (Karp-Boss et al., 1996):

$$Sh = \frac{-D\int_A \mathbf{n} \bigtriangledown C}{4\pi a D(C - C_a)} \tag{3.7}$$

Therefore, h can be expressed as:

$$h = \frac{D}{a}Sh \tag{3.8}$$

being $Sh = 1$ when no relative motion is present between the fluid and the cell. Therefore any fractional increase in Sh traduces in the same fractional increase of nutrient flux towards the cell wall, all the other parameters staying constant.

In order to examine the effect of cell or fluid motion on nutrient flux a relationship between Sh and the "Peclet number" has to be found. The latter is the time to transport material by stirring for a distance L (that is L/v, where v is the fluid velocity) divided by the time to transport material by diffusion is L^2/D, where D is the diffusion constant. The ratio is equal to $\frac{L\,v}{D}$. It is a measure of the effectiveness of stirring versus that of diffusion for any given distance and diffusion constant (Purcell, 1977).

The Peclet number is, therefore, due by this relation:

$$Pe = \frac{u\,a}{D} \tag{3.9}$$

This issue was reviewed by Karp-Boss et al. (1996), who analysed the mass transfer in still water and in presence of fluid motion. Here the results concerning a moving cell in calm water and non-moving and moving cell in turbulent flow are considered and commented.

In case of stagnant (still) water and for a cell moving at a constant velocity u, they provided the following expression for $Sh(Pe)$:

$$Sh = 0,5\left(1 + (1 + 2Pe)^{\frac{1}{3}}\right) \tag{3.10}$$

As reported by Pasciak and Gavis (1974), this expression was originally derived by Kroning and Bruijesten (1951) and used also in the milestone work of Munk and Riley (1952).

Considering an average value of the molecular diffusion coefficient $D = 1,510^{-9}$ m^2 s^{-1}, a cell of radius $a = 5$ µm, can enhance the nutrient transport rate by 22% moving at a

speed of 60 bodylength per second, indeed:

$$\frac{1,22\,Q_a}{Q_a} \Rightarrow Sh = 1,22 \Rightarrow Pe \cong 1 \Rightarrow u \cong 300\mu\text{m s}^{-1} \tag{3.11}$$

As pointed out by Karp-Boss et al. (1996) the expression 3.10 is an approximation of the function $Sh(Pe)$, valid only for the so called creeping $Re < 0,1$ uniform flow.

However, besides the organism's motility, also the small scale turbulence driven motion can influence the transport rate of nutrient toward the cell. Indeed, the turbulence driven motion induces a shear whose magnitude depends on the level of the energy contained at the considered scale, which may affect the nutrient flux. The process can be taken into account through a modification of the Sherwood expression, which in that case is function of the Peclet number calculated with the characteristic velocity scale of the turbulent flow.

For a velocity scale $U = (\varepsilon/\nu)^{0,5}a$, the corresponding Peclet number is $Pe = \left(\frac{\varepsilon}{\nu}\right)^{0,5}\frac{a^2}{D}$.

If we take into account that the condition of low Reynolds number $Re <$ 0,1, limits all the results to cells of less than 100 μm large and that in ocean ε (the rate of injection of kinetic energy), varies between $10^{-6}$to 10^{-10} m^2s^{-3}, then the above Peclet number is in the range $0 < Pe < 2$.

Since all the results above are valid for neutrally-buoyant non motile cells immersed in a turbulent environment, for completeness also the behaviour of the Sherwood number when an organism swim or sink in a turbulent flow is analysed.

Assuming a value of $\varepsilon = 10^{-6}$ characteristic of the ocean surface layer, Karp-Boss et al. (1996) concluded that only the large organisms (cells, chains and colonies) with equivalent radius in the range 63-100 μm, have an enhancement of more than 50 % of the nutrient flux with a molecular diffusion coefficient of $D = 1,0\,10^{-9}$ $\text{m}^2\,\text{s}^{-1}$.

Then, only larger cells can derive a net increase of the nutrient flux when immersed in a turbulent environment (Karp-Boss et al., 1996). Clearly, for such cells turbulence represent a great advantage in the reduction of the nutrient diffusion limitation, also if the

lower limit case is considered.

It is important to underline that all the above does not consider the effects introduced by a different cell shape, which likely can introduce strong effects both on the nutrient uptake, and on the velocity of the cell motion.

In addition, such advantage have to be included in a more complete view of the nutrient assimilation metabolism, that shows internal regulation together with the process only related to diffusion in the cell's boundary layer. In fact, the uptake rate is dominated by the "mass transfer" of the molecules to the surface of the cell only when the concentration of the external nutrients is low, whereas the kinetic of transport and assimilation dominates it, if the external concentration is high enough to replenish quickly the cell's boundary layer (Sanford and Crawford, 2000).

However, the turbulence-related enhancement of nutrient uptake is one of the most stressed hypothesis for the dominance of larger cells under nutrient rich and highly turbulent conditions (Arin et al., 2002).

3.2 Mixing and Light Variability

Phytoplankton live in an highly dynamic environment; together with the small-scales effect that the dynamics of the fluid can produce on it, it exists an important larger-scale one. In fact, the light history of phytoplankton cells is directly affected by turbulence that moves them up and down through the light gradient. This mixing-related light variability, together with the diurnal variations and the one related to the passage of clouds or by focusing or defocusing of the sun light, generates the spectrum of variability that a phytoplankton cell during its life can perceive, excluding the seasonal related variation of irradiance. As already examined in chapter 1 phytoplankton react to these variations, the focus of this section is to sketch a scenario of the current knowledge on the interaction between turbulent mixing and phytoplankton photo-responses and growth.

In their seminal papers in the mid-eighties Lewis and co-workers showed by theoretical arguments via dimensional analysis (Lewis et al., 1984a), experiments (Cullen and Lewis, 1988) and observations (Lewis et al., 1984b) that the vertical distribution of phytoplankton photobiological descriptors as dependent on light variation due to turbulent mixing strongly reflects the relative time scale of photobiological responses *vs* the time scales of mixing. The theory that the recent light history of a cell could be used to derive information about the mixing intensity in the euphotic zone was already suggested (Marra, 1978b; Falkowski, 1983) and has been afterwards applied (Brunet et al., 2003).

However, the basical features of this process have been firstly recognized by the Lewis and co-workers studies. The relevant patterns observed by Lewis et al. (1984b) where, that at high turbulent kinetic energy (TKE) dissipation rates there was little variation in $P_{max}^{chl}$with depth. On days when TKE dissipation was low, surface samples showed higher values of P_{max}^{chl}which implies that these cells had enough time to adapt to the higher irradiance at the surface.

These observations where accompanied by a dimensional analysis of the rates of mixing and of photo-acclimation, which produced a criterion to quantify the rates of mixing by depth gradient of several photo-acclimative properties, each with a different time-scales (Lewis et al., 1984a).

Subsequently, Cullen and Lewis (1988) firstly introduced the concept of a kinetic of photo-acclimation different by a first-order kinetics. They recommended the logistic kinetic of adaptation, which produce different time of adaptation if the irradiance is increasing or decreasing. This new feature started the debate, until now open, about the irradiance which cells immersed in an actively mixed layer are adapted. The "histeresis effect" has been previously introduced in section 1.2.2, but in this section it is analyzed looking to the resulting properties of acclimation of phytoplanktonic population mixed by turbulent motions.

In fact, if the kinetic of logistic acclimation introduced by Cullen and Lewis (1988) predicts that phytoplankton subjected to continuous variation of irradiance acclimate to an irradiance that is lower than the mean irradiance perceived in the mixed layer, other findings suggest that the acclimation irradiance is equal to the mean one or higher than the mean one.

As shown in section 4.3.3, the dynamic model of Geider et al. (1998b), is able to reproduce, via mechanistic description of the modification in the light harvesting component, the data that follow logistic kinetics presented by Cullen and Lewis (1988). Also the experiments conducted by Havelková-Doušová et al. (2004), presented in section 1.2.2, produced results consistent with a tendency of mixed phytoplankton to adapt to irradiances lower than the mean one. As an observational confirmation Behrenfeld et al. (1998) suggested a photoacclimated state characteristic of relatively low light exposure for a phytoplanktonic assemblage immersed in a shallow mixed layer.

The logistic kinetic has been applied in a numerical photoacclimation-diffusion model to illustrate how rates of vertical mixing might affect phytoplankton physiology and growth (Dusenberry, 2000). The model used an hybrid structure, between a bulk model and an individual based one (see section 3.2.1), to represent the probability distribution function of the properties of single phytoplanktonic cells immersed in a diffusive mixed layer. Anyhow, the application of the model to both photosynthesis and carbon to chlorophyll ratios suggested that a combination of vertical mixing and hysteresis in acclimation kinetics can enhance specific growth rates of phytoplankton. The author showed that the enhanced growth occurred as a result of mixing-induced variation in carbon to chlorophyll ratios. The model were applied assuming the steady-state condition under a constant surface irradiance. The resulted reduced $C : chl\,a$ was found in contrast with the chlorophyll-specific productivity, which was maximal at low mixing rates.

However, the authors concluded that the decrease in the $C : chl\,a$ was able to increase

the P^C of the mixed population also if the P^{chl} was found lower at high mixing rates. This, although simplified, application suggested the importance of the differential rates of photoacclimation to upward or downward shifts in irradiance, to enable phytoplankton cells to better survive in a turbulent environment.

Even if the evidence of phytoplankton acclimated to light lower than the mean perceived has been found recurrently, the opposite tendency has been also observed *in situ* (Vincent et al., 1994; Moore et al., 2006). In addition, it can be predicted also by results of experiments conducted under fluctuating irradiance (Ibelings et al., 1994; Kromkamp and Limbeek, 1993). Moore et al. (2006) observed an acclimation to relatively high light at a station vigorously mixed in a shelf sea. This acclimation response was found dominated by changes in the number of reaction centers per cell rather than PSII antenna size. This kind of response has been suggested to be able to result in a larger excess PSII capacity, without a corresponding increase in the probability of photo-damage. It is noteworthy that the other occurrence of high light acclimated natural population has been observed in an estuary (Vincent et al., 1994). Shelf-seas and estuaries are environments where the high variability of the irradiance signal can be registered very often, and a phylogenetic trait of adaptation of their population can be interpreted together with a dependency from the high frequency signal that the population can perceive. In fact, as already concluded in section 1.2.2, photoacclimative responses to variable irradiance regimes should be species-specific but some of them seem also triggered by fluctuations of the irradiance.

The high irradiance acclimation has been connected to a form of hysteresis effect in two cases. In the first one, it was supposed a slower response to decreasing irradiance because of a delay due to the conversion of the redox signal in synthesis of $chla$ signal (Geider et al., 1996). The second case refers to a mechanistic model study of the photosynthetic rates and rubisco activation and de-activation under fluctuating irradiances (MacIntyre and Geider, 1996). As previously mentioned (see section 1.1.4), re-activation of Rubisco

enzyme proceeds faster than de-activation. The resulted hysteresis effect produced cells adapted to higher irradiance with an increased photosynthetic capacity. However, the advantage derived by this feature has been found in the study of MacIntyre and Geider (1996) as relatively small in estuarine systems.

The number of modeling study in the field of interaction between physical motion and biological responses of phytoplankton is large. In fact, this method allows to reproduce and control realistic processes without influencing the results. For this reason, it is important to briefly describe the possible approaches to modeling studies of physical-biological interaction in the Ocean.

3.2.1 Bulk and Individual Based Models

Until recently, modeling of the environmental processes has been treated statistically through ensemble averages, treating the organisms like a continuum property such as salinity or temperature. This method is generally coupled with Eulerian physical description of the ocean circulation and I will refer to this kind of biological or coupled bio-physical models as to bulk models. They have an inherent imprecision however, as Woods and Onken (1982) have noticed: averaging non-linear equations before integration does not give the same results as averaging them after integration. While only the second procedure is correct, the first is adopted, for example, in the bulk models for primary production.

Using this approach, the primary production of a mixed layer is computed applying the depth-averaged light intensity to the phytoplankton population immersed in the mixed layer and then calculating the growth over time.

It exists a second way of modeling a population in the environment: the Individual Based approach. Individual Based Models (IBM) refers in the following to simulation models that treat individuals as unique and discrete entities which have at least one property in addition to age that changes during the life cycle, e.g. weight, rank in a social hier-

archy, etc. These discrete simulations are generally coupled, in biological oceanographic application, with lagrangian trajectories, which describe the fluid properties following the position with time of a fluid particles.

The primary production of a mixed layer is computed differently by an IBM coupled with lagrangian trajectories of the particle motion. In fact, using the IBM approach, the light perceived by each individuals is calculated first, then the growth of each of them is integrated. The emergent property of the growth of the entire population produces the primary production estimate of the mixed layer, which can differ from the previous estimate. This second procedure, applied in the IBM developed in this study, would yield the correct results. However, the continuum bulk method has been used very successfully, because computationally less expensive and because more simple.

Processes like the light-related responses of phytoplanktonic cells, together with motility of phytoplankters or the interaction between them and predators at small scales, need to be studied with the second approach. The studies already conducted on photo-acclimation of "individual" phytoplankton are briefly summarized, in the next section, in order to clarify the scenario where the IBM here developed is placed.

3.2.2 Phytoplankton Lagrangian Photoacclimation Models

The lagrangian approach as a tool to modelize the behavior of planktonic organisms in the water column has been introduced in the late 70's (Marra, 1978b; Falkowski and Wirick, 1981). However, the utility of this approach has been fully recognized after the paper of Woods and Onken (1982). The authors used a Lagrangian ensemble biological model, embedded in a one-dimensional model of the upper ocean, to study how irradiance variations associated with diurnal cycling of upper layer turbulence can define the depth distribution and energy uptake of a group of multiplying cells. Such Lagrangian model also documents how the diurnal cycle affects the rate of loss of organic material from the upper ocean.

They found, indeed, that as the mixed layer deepens during the night, phytoplankton and particles produced in a shallow mixed layer during one day are mixed downward at rates far larger than their still-water settling rates. Particles settled in mixed water however can be reincorporated in the upper layer on the following day, on the contrary to the less mixed environment.

The study of Falkowski and Wirick (1981) explored the effects of variations in light regimes due to vertical mixing on primary productivity.

Cells were allowed to light-shade adapt on a fixed time scale by altering $chl\,a : C$ ratios in response to variations in light regimes. Photosynthetic response was adjusted according to variations in $chl\,a : C$ ratios by either varying the initial slopes of photosynthesis-irradiance curves, or varying photosynthetic capacities. The results suggested that despite physiological adaptation to light, vertical mixing may have little effect on the integrated water column primary productivity. They postulated also that, if photoinhibition does not have a pronounced effect, the average distribution of primary production in a water column is not related to variations in light regimes arising from turbulent diffusion processes.

It is noteworthy that Falkowski and Wirick (1981) considered that the $chl\,a : C$ ratio of individual cells adapts toward a target value according to a first-order acclimation equation. This kind of kinetic, produce an acclimation state for cells submitted to fluctuating irradiances equal to the state derived by an acclimation to the mean irradiance perceived by the individuals. The linear kinetic has been applied also in the paper of Denman and Marra (1986). Although, it was later on recognized that this kinetic does not corresponds to the one performed by phytoplankton cutures (Cullen and Lewis, 1988).

Subsequently the lagrangian phytoplankton photoresponse models have started to include photo-inhibition to analyze its effect on primary production estimates (Kamykowski et al., 1994; Franks and Marra, 1994; Farmer and McNeil, 1999; Nagai et al., 2003; Cianelli et al., 2004). The model of Kamykowski et al. (1994) included a temporally decaying de-

pendence on inhibitory light exposure. Its results, for the first time, clearly showed that vertical mixing regime, interacting with the time constants for photoresponse, strongly influences how the light history of the individual affects each population's statistical characteristics.

It has been frequently recognized the positive mixing-related effect of relief from photoinhibition: cells mixed downward from the inhibiting upper layer should decrease their photoinhibition at new non-inhibiting irradiances.

In fact, Nagai et al. (2003) found that stronger wind mixing in a lower-transparency water column contributes to greater phytoplankton production. According to their study, vertical mixing is insignificant for photoinhibition in relatively clear open ocean water, while it can be more important in relatively turbid coastal water. The relief from photoinhibitory irradiances has been, however, extended to an Oceanic Antarctic site (Cianelli et al., 2004), where the highest rate of cell accumulation was reached when the vertical mixing compensated for photoinhibition.

Concluding, Kamykowski et al. (1994) suggested that:

> *Standard approaches to primary production measurements applied in water columns that are mixing vertically can hide large differences among the individuals that occupy the same incubation bottle.*
> *Yamazaki et al. (1993) have shown that linear dynamics represent photosynthetic response of bulk populations with the same light history. Before the universal application of linear dynamics can be accepted, however, similar analysis are required to determine if population averaging is masking non-linear dynamics in individual cells or if non-linear dynamics characterize the bulk response of populations composed of several species with different light histories in spite of averaging. ...*
> *Statistical studies that compare the characteristics of individuals contributing*

> *to the population collected at the same depth . . . can provide a robust approach to the mean and the variance of photoresponse characteristics at that depth.*

Flow-citometry has demonstrated the capability to recognize the mixing related statistical properties of samples collected at the same depth (Olson et al., 1991). Dusenberry et al. (1999), indeed, showed that shoaling of the mixed layer, coupled with the diel cycle of solar irradiance, can drive the development of a depth gradient in mean red fluorescence of *Prochlorococcus*, due to photoacclimation, in the newly stratified layer.

Furthermore, they showed that the frequency distribution of single-cell fluorescence within field populations responds to changing mixing and photoacclimation dynamics, with photoacclimation in the absence of strong mixing generally resulting in a reduced variance in fluorescence within sample populations.

These results and the recent findings derived by Lagrangian models suggested the necessity to analyze quantitatively the influence of individuals variance and non linear photosynthetic dynamics on the growth of bulk phytoplankton population in the Ocean Mixed Layer.

The lagrangian model of Cianelli et al. (2004), firstly combined dynamic photoacclimation of the pigment content with a mechanistic description of photoinhibition, while previous applications used simplified description of single responses. As this fully mechanistic approach allows to recognize the overall effect of validated laws in a mixed population, it has been improved and applied in the Individual Based Model for phytoplankton responses for a mid-latitude Ocean Mixed Layer developed in this study, which is described and discussed in the the next part.

This IBM (described in chapter 6) is the first one using a sophisticated representation of mixing derived by the OML models, that are described in chapter 5. In addition, it couples these realistic simulations of the OML with an updated photophysiological phytoplankton model, described in chapter 4. The results derived by the IBM have been elucidated with an

integrated analysis of the biological responses under various fluctuating regimes, presented in chapter 7. The overall consequences of individual's responses on the bulk phytoplankton growth are discussed in chapter 8.

Part II

Methods and Results

Chapter 4

An Updated Model of Phytoplanktonic Light-regulated Growth

To analyze the impact of physiological plasticity of phytoplankton to the variations in radiance and nutrient concentrations on their growth in the upper layer of the ocean, which is the main scope of this study, I assembled a suite of models which could reproduce to a certain extent the key processes in plankton physiology and fluid motion.

In this chapter I describe the mechanistic photo-physiological model and show the results of the simulations carried out to analyze the responses to light-shifts simulated by the model.

4.1 Model Description

The model was firstly implemented in MATLAB. Afterward, the code was translated in FORTRAN90 to reduce the time of each run. All the simulations presented in the following

sections derive from the FORTRAN90 version. A forward Euler method was used to integrate the equations.

The photo-physiological model I assembled is based on the Geider et al. (1998b) model as modified by Flynn et al. (2001) in order to include a better reproduction of the nitrogen-irradiance interaction. The basic equations of this version of the model (GM3) have been already presented in section 1.3.1. The model has been coupled with the model by Han (2002) in order to include photo-inhibition. The coupling is significantly different from a previous version of an acclimation-inhibition model (Cianelli et al., 2004), because both constituting modules (photoclimation and photoinhibition) are different. While writing the thesis a coupled model, very similar to mine, came out in Progress in Oceanography (Baklouti et al., 2006a,b). There are some differences also with that model, that will be discussed later.

Being built on the Flynn et al. (2001) model, also my model is based on the hypothesis that *acclimation may include a tradeoff between maximizing growth at low irradiance vs minimizing the potential for photooxidative damage at high irradiance* (Raven, 1980, cited by Geider et al. (1998b)).

As already discussed in section 1.3.1 the Geider et al. model is based on the assumption that the decrease in the pigment content at high irradiances is due to an internal regulation of the biosynthetic process presumably aimed at decreasing the risk of photoinhibition effect at high light intensity. My model explicitly includes the compensatory effect of down-regulation of the pigment content through the Han (2002) photo-inhibition model.

Since the decrease of the pigment content at high irradiance may occur in two different ways, either decreasing the absolute number of reaction centers per cell or decreasing the pigment content of the antenna of the PSUs, keeping constant the number of reaction centers (see section 1.2.1), and the model by Geider et al. (1998b) does not include explicitly this trait, I modified their model to explicitly include this feature using the same approach

than Cianelli et al. (2004).

The strategy of decreasing in the absolute number of reaction centers per cell at low light would be reflected in a constancy in the number of reaction centers normalized to chlorophyll n^{chl}, because the increase or decrease in the absolute number of reaction per cell n would be accompanied by an increase or decrease in the chlorophyll content per cell. The constancy in the n^{chl} would be mirrored by the constancy in the α^{chl} of the P^{chl} *vs* E curve, because of the relation between n^{chl} and α^{chl} expressed in the equation 1.1. On the contrary, the increase in the absolute number of reaction centers per cell would affect the other parameter that in the Geider et al. model is considered independent by the growth irradiance, i.e., P^C_{max}.

As already discussed in section 1.3.1, the Geider et al. model has two parameter that define the P *vs* E response: the constant α^{chl} and the constant P^C_{ref}. The P^C_{max} of the modeled P^C *vs* E curve of the Geider et al. model is unaffected by irradiance while it depends from the P^C_{ref} modified to consider the N-status of the modeled phytoplankton.

In the case of this first strategy the P^C_{max}would be affected by photo-acclimation of the pigment content.

This becomes explicit substituting the expression for the P^{chl}_{max}in equation 1.2 $P^C_{max} = P^{chl}_{max}\, chl\, a : C$ which becomes $P^C_{max} = \frac{n^{chl}\, chl a}{\tau\, C}$. With a simple transformation due to the fact that $n = n^{chl}\, chl\, a$, the new relationship is: $P^C_{max} = \frac{n}{tau\, C}$. This means that the light driven pigment adjustments that involve the absolute number of the reaction centers will affect the parameter P^C_{max} that in the Geider et al. model is independent on the light history.

This strategy, however, does not interfere with the photo-inhibition process. The light harvested per PSU does not change and the interaction between acclimation of the pigment content and photo-inhibitory damage does not change along with the growth irradiance.

In order to include in a photo-physiological model explicitly the beneficial effect of the

decrease in the pigment content, it is necessary to modify the Geider et al. to explicitly include the effect of the other strategy. Changes in the antenna size will cause a change in the functional cross section for the PSII (σ_{PSII}). It is worth reminding that the assumption that only changes in PSII are to be considered is based on the evidence that these adjustments are the most important in determining the adjustment of photosynthetic rates.

If we consider a change in the σ_{PSII} accompanying the adjustment in the pigment content, the Geider et al. model was modified as follows. The parameter α^{chl} changes with σ_{PSII} because of the equation 1.1, while the P^C_{max} remains constant. This change, on the contrary of the previous one, affects the photo-inhibition term because the light harvested by each PSU changes and,with it, the probability of damage.

The dynamical mechanistic description of photo-inhibition proposed by Han (2002) has been included in the model considering that the number of photosynthetically active reaction centers was reduced by damage of the D1 protein. For this reason, both α^{chl} and P^C_{max} would decrease as the damage proceeds increasing the number of photo-inhibited reaction centers, along with the equations 1.1 and 1.2.

In table 4.1 are resumed all the equations that are solved in the model, including those already presented above.

The first two equations are derived from the equations 1.2 and 1.1 for the new photo-acclimation and photo-inhibition traits. The decrease in the P^C_{ref} due to the increase in the relative concentration of damaged reaction centers ϑ_c, modifies the photosynthetic capacity. The expression $(1 - \vartheta_c)$ in both the equation expresses the relative concentration of the undamaged reaction centers that participate to the photosynthetic process. In the equation 1.2, n^C represents the number of reaction centers normalized to carbon that, in this case, is expressed as gC fixed $\mathrm{gC}^{-}1$ and is the variable directly affected by photo-inhibition.

Instead, the α^{chl} decreases at high irradiance, both because photo-inhibition decreases the number of reaction centers participating to photo-capture and because of the decrease

Equations	**Equation number**
$P^C_{ref} = \frac{n^C}{\tau}\ (1 - \vartheta_c)$	(4.1)
$\alpha^{chl} = \sigma_{PSII}\, n^{chl}\ (1 - \vartheta_c)$	(4.2)
$P^C_{max} = P^C_{ref}\ \left(\frac{Q - Q_{min}}{Q_{max} - Q_{min}}\right)$	(1.5)
$PS = P^C_{max}\left[1 - \exp\left(\frac{-\alpha^{chl}\,\theta^C\,E}{P^C_{max}}\right)\right]$	(1.4)
$V_N = P^C_{ref}\, Q_{max}\, S\, \frac{1 - Q/Q_{max}}{1 - Q/Q_{max} + shape}\, \frac{N}{N + K_N}$	(1.7)
$resp = V_N\, N_{cost}$	(1.6)
$\rho_{chl} = \theta^N_{max}\, \frac{PS}{\alpha^{chl}\,\theta\,E}$	(1.10)
$\frac{dQ}{dt} = Q\, V_N - Q\, \frac{1}{C}\, \frac{dC}{dt}$	(1.8)
$\frac{d\theta^C}{dt} = \theta^C\, V_N\, \rho_{chl} - \theta^C\, \frac{1}{C}\, \frac{dC}{dt}$	(1.9)
$\frac{dC}{dt} = C\ (PS - resp)$	(1.3)
$\vartheta_b = \frac{\sigma_{PSII}\, E\, \tau}{1 + \sigma_{PSII}\, E\, \tau + k_d/k_r\, \tau\, (\sigma_{PSII}\, E)^2}$	(4.3)
$\frac{d\vartheta_c}{dt} = -k_r\, \vartheta_c + k_d\, \sigma_{PSII}\, E\, \vartheta_b$	(1.14)
$\sigma_{PSII} = \sigma_{PSIIref}\ \left(\theta^C/\theta^C_{ref}\right)^a$	(4.4)

Table 4.1: Equations of the updated photo-physiological model, if the equations have already been presented they keep their original numbers.

in the functional cross section of the PSII.

The equation that governs the modification in the cross section of the PSII (eq4.4) considers the dependence of the σ_{PSII} from the number of pigments involved in photo-capture in the antenna of the PSII. The σ_{PSII} changes in the same direction of the θ^C, but the relationship is not linear. At low irradiances, the increase in the $chl\,a$ content increases the pigment in each antenna, and as a general effect this increases the σ_{PSII}. However, the packaging effect, due to the self-shading of the $chl\,a$ molecules in the antenna decreases the benefit due to the increase in the light-harvesting pigments. For this reason, in equation 4.4 the σ_{PSII} at the current acclimative state θ^C depends on a $\sigma_{PSII_{ref}}$, that is the σ_{PSII} at a certain θ^C_{ref}, following the rule $\left(\theta^C/\theta^C_{ref}\right)^a$, where $0 < a < 1$ is an empirical exponent to parameterize the packaging effect.

Because of the above relationship, α^{chl} changes along with photo-inhibition as it is evident form eq 4.2. Photoinhibition, in turn, acts on the relative number of undamaged reaction centers that concur to the photo-capture $(1 - \vartheta_c)$.

The relative number of damaged reaction centers ϑ_c is then calculated integrating the two equations: 4.3 and 1.14. The equation 4.3 represent the steady-state solution derived in Han (2002) from the equation for the relative concentration of the closed reaction centers (eq 1.13). The closed ones are the reaction centers that can be photo-inhibited if the rate of damage is greater that the rate of repair.

In this work, I chose to do not solve dynamically ϑ_b equation (as also suggested by Mark Moore and Oliver Ross, University of Essex, personal communication) because the integration time step used in the simulations is significantly longer than the time required to a PSU to pass from the open to the closed state and *viceversa*. For this reason, the number of closed reaction centers ϑ_b is calculated as at the equilibrium with the actual irradiance following equation 4.3. The ϑ_b so calculated is then used in equation 1.14, so that the change in the relative concentration of D1 damaged reaction centers is accounted

for dynamically. As already illustrated in section 1.3.2, the closed reaction centers are converted in the photo-inhibited state with a rate that depends on the damage constant k_d and on the light harvested by the antenna: $\sigma_{PSII}\, E$, while the rate of repair proceeds independently from the perceived or harvested irradiance at a rate k_r. The σ_{PSII} in this equation are changed because of the modification in the pigment content. This constitutes the feedback of down-regulation of the damage at high irradiances.

The other equations solved by the model are the equation for the $chla : C$ and the N:C ratio, the photosynthetic rate, the nitrogen assimilation and the growth rate of the Geider et al. model. Those equations are modified, because the parameters that regulate them, in the original model considered constant, are changed by the two processes here considered. In general, the formulation of the equations, and the theory at their basis, are the same and have been already discussed in section 1.3.1. The inclusion of the new equations includes processes neglected before.

In order to clarify the consequences of these modifications on the results, a set of simulations in simple simulated conditions has been performed. They are presented in the next section in order to test the model responses and to better understand the final outcome of the inclusion of new photo-physiological processes.

4.2 Testing the model Response

The set of simulations that is presented here, has been performed on the simple bulk architecture of the model. The simple architecture considers the state variable C in terms of mgL^{-1}, and describes the evolution of this state variable in response to the environmental forcing, as if a homogeneous phytoplanktonic culture was subjected to a dynamical regime of irradiance and nutrient concentrations. The photo-physiological variables, N:C ratio Q, the $chla : C$ ratio θ^C and the fraction of damaged reaction centers ϑ_c change during the simulations and their modification is then analyzed in term of the changes occurred to the

other variables of the system, such as P^C_{max} and σ_{PSII}.

The general aim of the analysis is the characterization of the responses of this new model with those derived from the previous models.

First of all, I analyze the response of the new model to a simple shift of irradiance. The results shown in section 4.3.1, derive from a simulation in which a simulated phytoplanktonic suspension was subjected to an irradiance of 50 μEinst $m^{-2}s^{-1}$ for 72 hours, 1000 μEinst $m^{-2}s^{-1}$ for the second 72 hours and again to 50 μEinst $m^{-2}s^{-1}$ for other 72 hours.

In order to obtain a simpler and a more perceptible response, the model was forced with continuous irradiance. This simplification, also if representative of a less realistic conditions, allows for highlighting the irradiance shift modifications, without the changes due to the interaction between the light-dark and the light shift adjustments, which could mislead the analysis.

Afterward, a comparison between the steady state solutions of the model here presented with that of the Geider et al. model, derived from the final conditions of long simulations performed over a wide range of irradiances, is presented. The model have been forced for five days of simulation at a fixed irradiance. After a few tests a five day time interval has been found sufficiently long for the system to reach the steady state with all the irradiance (results not shown). Therefore, in section 4.3.2, the steady state solutions of the photophysiological variables over a wide range of irradiances will be analyzed and compared with the ones derived by the Geider et al. model. The two simulations were performed with the same common parameters, while the photoinhibition part, in the new model, was parameterized with damage and repair rate so as to obtain an evident photoinhibitory effect at high irradiances.

In Section 4.3.3, the responses of three models subjected to reciprocal shift of irradiance, from 100 to 2200 μEinst $m^{-2}s^{-1}$ and *viceversa* are then analyzed. This experiment has

been performed in order to compare the model responses to the same shift used to study the kinetic of acclimation by Cullen and Lewis (1988). In Geider et al. (1998b), a reproduction of the Cullen and Lewis (1988) experiment has been already performed.

It is not my scope to perfectly reproduce this experiment. The intent of this set of simulations is to test the impact of processes not considered before on the differential response to increasing or decreasing light shift. It is in fact plausible that the hysteresis observed in the Cullen and Lewis experiment could also be connected to a photo-inhibitory response in cells grown or abruptly subjected to high irradiance, and 2200 μEinst $m^{-2}s^{-1}$ should be considered as a high irradiance. More in general, it is important for the purpose of this set of simulations, to understand to what extent the modifications introduced to produce a new photo-acclimation model induced different results and how the performance of the model were modified in already studied conditions. In particular I was interested in finding out whether the inclusion of a photo-inhibition model and of a strategy of acclimation related to the antenna-size would amplify or depress the hysteresis reproduced with the Geider et al. model. For this reason, 20 hours of reciprocal shift from 100 to 2200 μEinst $m^{-2}s^{-1}$ and *viceversa* were simulated with three configuration of the model: the original Geider et al. model, the new model presented here and an hybrid of the two, a model modified as the previous one for the modification in the antenna size, but not including modelization of photo-inhibition ($\vartheta_c = 0$ during all the simulation).

Another test has been carried out on the impact of illumination regime. Two regimes where compared: a sinusoidal and a square wave one. The results are reported in section 4.3.4.

The whole set of simulations have been performed in nutrient-replete conditions, with an external concentration of nitrogen of 100 μgN L^{-1}. The values of the parameters used in the simulations are summarized in table 4.2. To parameters in common among the different models were assigned the same value, which implies that the observed differences

Constant	Value	source
n_{chls}	1,33e^{-5} mg C mg $chla^{-1}$	
τ	5,80e^{-3} s	
θ_s^C	0,0254 mg $chla$ mg C^{-1}	
n_{cs}	3,39e^{-7} mg C mg C^{-1}	
σ_{PSIIs}	1,78 m^{2}µEinst^{-1}	
k_d	8,00e^{-7} d.l.	
k_r	1,33e^{-3} s^{-1}	
Q_{max}	0,05 mg N mg C^{-1}	(Flynn et al., 2001)
Q_{min}	0,2 mg N mg C^{-1}	”
S	0,236 d.l.	”
$shape$	0,01 d.l.	”
N_{cost}	3,21 d.l.	”
θ_{max}^N	0,389 mg N mg $chla^{-1}$	”
a	0,627 d.l.	(Bricaud et al., 1998)

Table 4.2: Table of the constants used for the tests, here presented, effected on the updated photo-physiological model

derive only from the new processes included in the new model.

4.3 Results and Discussion

A preliminary qualitative analysis of the response of cells exposed to a double shift of irradiance from 50 to 1000 µEinst m^{-2}s^{-1} and back is reported in section 4.3.1. A comparison of the output of the two model when cells reach the steady state over a wide range of irradiance are discussed in section 4.3.2, whereas an analysis of the impact of the new processes introduced in the new model on the time scales of adaptation is presented in section 4.3.3. There the diagnostic variable is $C : chla$ ($\theta^{C^{-1}}$).

It will be analyzed this variable and not the $chla : C$ ratio, because the response in the former is more evident and allows a comparison with the results of Cullen and Lewis (1988).

A quantitative comparison then follows to derive the time scale of adaptation emerging

from the different simulations. The time scale of adaptations was calculated as in Cullen and Lewis (1988). In this case the chosen diagnostic variable is the time required to attain the 50% of the full response of the $C : chla$ variable after the irradiance shift in either direction.

Finally the time course of acclimation to sinusoidal and square wave irradiance is presented in section 4.3.4. The diagnostic variable used is again $C : chla$ ($\theta^{C^{-1}}$).

4.3.1 Simulation of Irradiance Shift

The unique forcing of the photophysiological response is in this case the shift in irradiance which is plotted in figure 4.1(a). The simulation were over 216 hours divided in three periods of 72 hour for each of the irradiance levels according to the pattern low - high - low.

θ^C reached the stationary state at low irradiance from any arbitrary initial condition of $chla : C$ ratio in 48 hours (fig. 4.1(b)). Moving to low irradiance the synthesis of $chla$ increased reaching a values of almost 50% of the maximum value attainable with the model. Imposing a shift to high irradiance, the ratio decreased to approximately one third of the value at low light. At the end of the second period the variable reached the steady state corresponding to high irradiance. Again, after about 48 hours of the shift back to low irradiance the model reproduced the values found at the end of the first 72 hours.

The kinetic of the change of θ^C because of the shifts will be analyzed in detail in section 4.3.3. For the time being it is important to note the pattern in the change of the functional cross section of the PSII (fig. 4.1(d)). As expected, the decrease in the pigment ratio at high irradiance, from hour 72 to 144 of the simulation, corresponded to a decrease of the σ_{PSII} which followed a similar kinetics which, similarly to the synthesis of the pigment, was slow if compared with the time scale of response to photo-inhibition or the photo-protective activation of NPQ. On the other hand, the decrease of σ_{PSII} produced the same

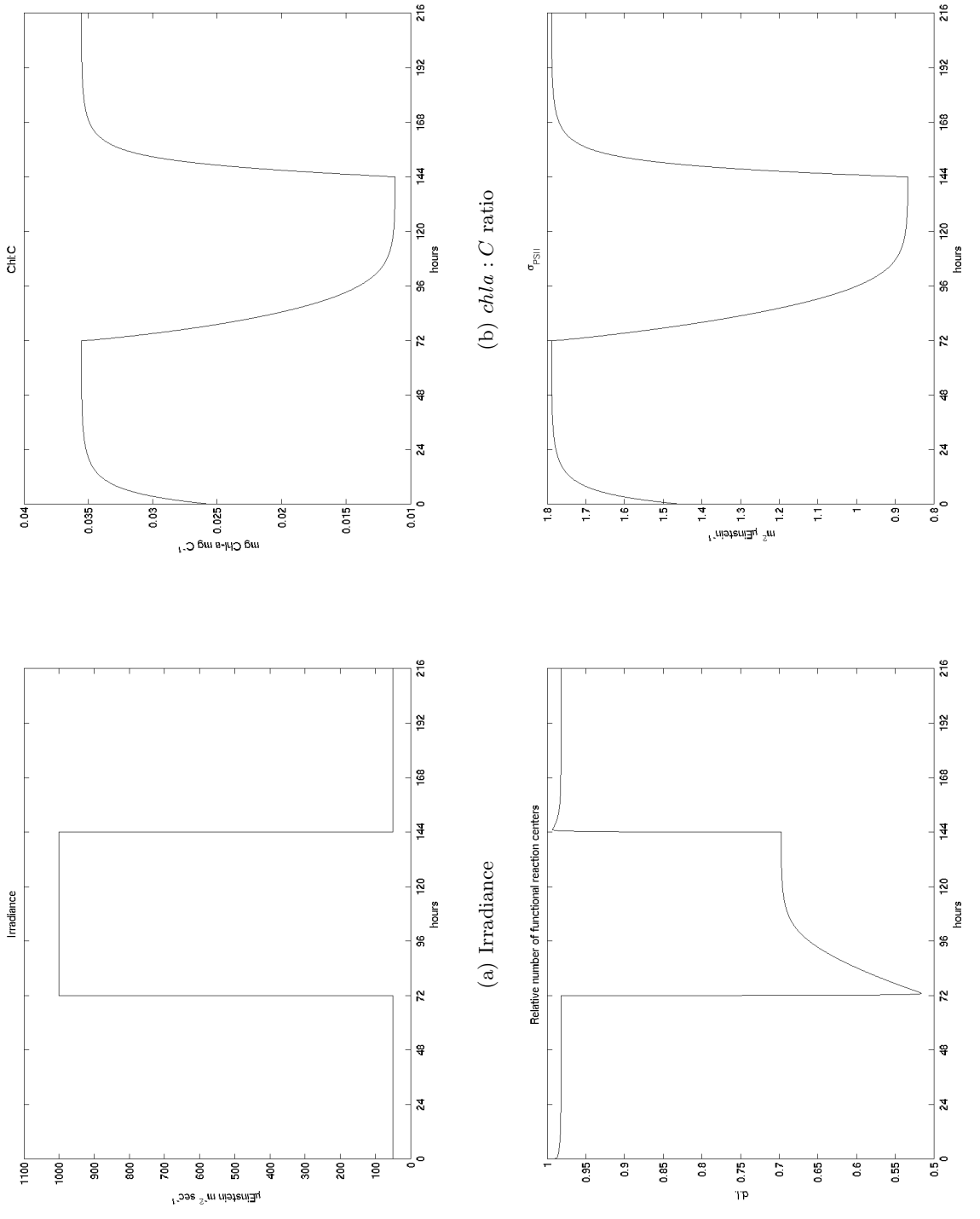

(a) Irradiance (b) $chla : C$ ratio

(c) Relative number of not-damaged reaction centers (d) Functional cross section of PSII

Figure 4.1: Temporal evolution of the properties of the irradiance shift simulation effected with the updated photo physiological model.

effect that NPQ would have had on the photosynthetic performance of the virtual algae. For this reason acted as a photo-protective mechanism. It is also visible in figure 4.1(c) that the increase in the irradiance to which the virtual algae were exposed immediately affected the relative number of functional (because not damaged) reaction centers. In one hour the number of PSUs carrying on photosynthesis were reduced by almost one half. Afterwards the fraction of functional reaction centers increase again, reaching the 70% at the end of the shift, because the damage rate decreased along with the decrease of σ_{PSII} due to the reduction of pigment content (fig. 4.1(d)).

The latter increase (about 20%) in the number of active reaction centers was a consequence of the protective mechanism which depended on the decrease of light harvested by the PSUs. An opposite response occurred after shifting back to low irradiance. The inhibition was lower immediately after the shift, but it was slightly increased because of the increase in pigment content and in the functional cross section at low irradiance. Though, this effect was not relevant.

By contrast, the effect of the higher susceptibility to reversible damage of the PSUs adapted to an irradiance of 50 µEinst $m^{-2}s^{-1}$ and exposed to an abrupt shift to 1000 µEinst $m^{-2}s^{-1}$ was reflected in the increase of 20% of damaged reaction centers notwithstanding their σ_{PSII} were halved in comparison to those typical of low irradiance.

The connection between cross section of the PSII and of the number of reaction centers active in the photo-capture modified the response in term of photosynthetic performance and therefore in terms of growth, because the two variables controlling the photosynthetic rate α^{chl} (fig. 4.2(b)) and P^C_{max} (fig. 4.2(a)) changed. The light-limited slope of the $P^{chl}vs$ E curve decreased in the central period and increased at low light conditions, because of the decrease at high irradiance of both the relative number of active PSUs and the size of the antennae.

As a consequence, the harvesting efficiency of the culture subjected to the lower irra-

diance was almost three times larger than the one fully adapted to high irradiance. The first sharp decrease of the 50% in the α^{chl} after the first shift of irradiance is due to the decrease by 50% of the number of PSUs involved in photo-capture.

Afterward, there was a tradeoff between the continuous decrease of the σ_{PSII} and the recovery of functionality of reaction centers affected by this decrease. The decrease of α^{chl} due to the decrease of the σ_{PSII} was lower than expected because the decrease in σ_{PSII} produced an increase in the number of active PSUs.

As for P^C_{max}, it is evident from figure 4.2(a) that it was modified during the simulation because of the change in the number of reaction centers contributing to photosynthesis and because of the nitrogen status. The comparison between the black and the red line in the figure shows that the N-status of the cell and the inhibition acted both in the direction of decreasing the P^C_{max} at high irradiance. The dilution effect that was the responsible for decreasing $chl\,a : C$ ratio at high light, had a similar impact on the N:C ratio, thus lowering the maximum photosynthetic rate (see section 1.3.1 above). Therefore the Geider et al. model predicts that at high irradiance the photosynthetic capacity will depressed in any case even without photo-inhibition. The overall outcome is that virtual algae exposed to 1000 µEinst $m^{-2}s^{-1}$ have a photosynthetic efficiency equal to one half of that found in those acclimated to 50 µEinst $m^{-2}s^{-1}$

In figure 4.2(c) is reported the evolution of the instantaneous carbon growth rate during the simulation. The carbon growth rate had a positive peak immediately after the shift from 50 to 1000 µEinst $m^{-2}s^{-1}$ The light became no more limiting and the high light harvesting efficiency, due to the low light adaptation, gave the possibility to capture light effectively, thus allowing to grow at high rate. After less than one hour the damage of half of the reaction centers participating to photosynthesis affected the growth rate, even if photo-inhibition was mitigated because of the mechanisms discussed above which took place during the second half of the period. The effect of this down-regulation, because of

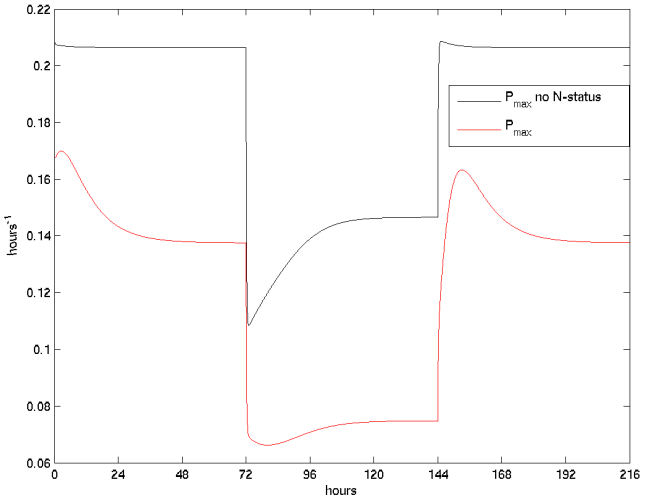

(a) Maximum Photosynthetic rate. The red line refers refers to the normal value, while the black one represents the value if is not considered the dependence on the Nitrogen status.

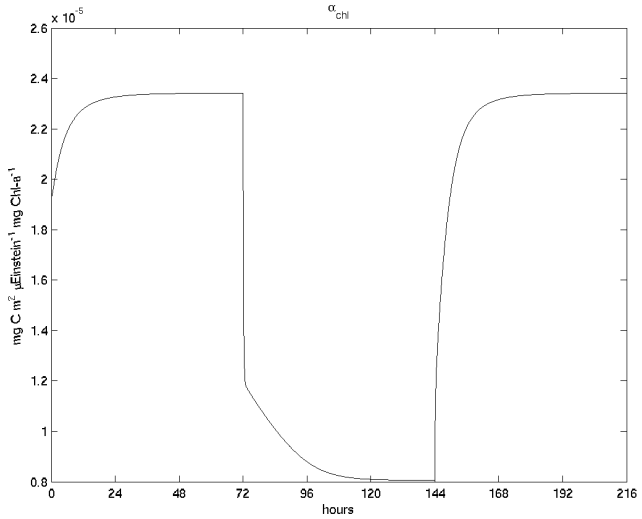

(b) Light-limited slope of the P^{chl} *vs* E curve

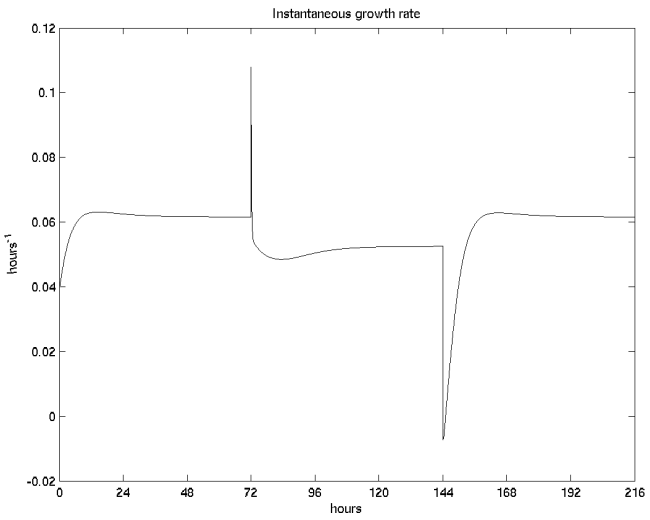

(c) Carbon growth rate

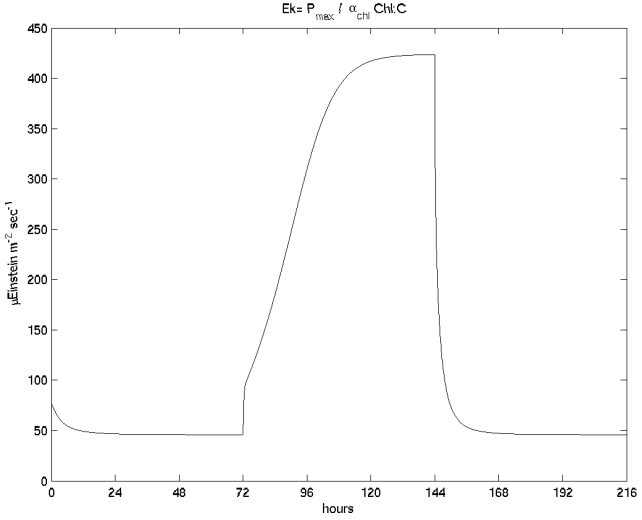

(d) Light saturation irradiance

Figure 4.2: Temporal evolution of the properties of the irradiance shift simulation effected with the updated photo physiological model.

the decrease in the light-harvesting and mainly because of the photo-inhibitory process, resulted in a growth rate about 15% higher at a 50 μEinst $m^{-2}s^{-1}$ in respect to that at 1000 μEinst $m^{-2}s^{-1}$

The recovery of the growth rate returning to low irradiance proceeded at slower rate. The recovery from photo-inhibition, as noted above proceeded fast, but the changes in the light harvesting apparatus dependent on pigment content were relatively slow. At low irradiance, the growth rate was dominated by the light-harvesting efficiency, because the change in irradiance brought the cells in the linear part of the $P^C vs$ E curve. By contrast the photo-inhibition induced decrease of the photosynthetic efficiency at high irradiances modified the growth rate very quickly, because at saturating irradiances the growth rate is determined by the photosynthetic efficiency.

Finally it is worth showing the time course of the light saturation irradiance E_k during the simulation (figure 4.2(d)). The E_k was modified by all those responses. This means that the model produces an E_k-dependent change in the $P^C vs$ E curve. During the first and the third period the light saturation irradiance was slightly lower than the growth irradiance. In the second period the E_k reached 400 μEinst $m^{-2}s^{-1}$, showing the high flexibility of the system.

4.3.2 Comparison with Geider Model

After the analysis of the instantaneous response of the virtual algae exposed to a shift of irradiance, I compare the results of the steady state solutions of the new model with those of the photo-acclimation model of Geider et al.. The steady state solutions of the carbon growth rate versus irradiance are reported in figure 4.3(a).

The figure shows that the $P^C vs$ E curves of the two models differ because my model at high irradiance decrease the photosynthesis while the $P^C vs$ E curve generated with the Geider et al. model saturates at almost 200 μEinst $m^{-2}s^{-1}$, and keeps that maximum

growth rate for all higher irradiance values. The new model, does not reach the same high values at the corresponding irradiances because the model of photo-inhibition modifies the original $P^C vs$ E curve. This is a well known feature of the Pvs E curves with and without photoinhibition. With photoinhibition the effective maximum photosynthetic rate is lower than the P^C_{max} and it is generally indicated as P^C_s.

It is also evident that the steady state carbon growth rate at 100 µEinst $m^{-2}s^{-1}$ is higher than the one obtained at 1000 µEinst $m^{-2}s^{-1}$ At the low irradiance of the shift experiment presented in the previous section the carbon growth rate is almost at the maximum, while at the second one the carbon growth rate is really affected by photo-inhibition.

The time course of the maximum carbon growth rate is reported in figure 4.3(b). When photoinhibition is not included it is affected only by the N-status whereas it is affected also by the inhibition in the second case. Both decrease increasing the irradiance, because of the depression of the N:C ratio in cells grown at high light. However the distance between the two curves increases because of the decrease in the number of functional reaction centers that determine the photosynthetic efficiency.

The modifications of the parameters that regulate the light harvesting efficiency are more subtle, because the only differences are related to the explicit modification of the architecture of the antenna. The $chla : C$ ratio that the new model displays at high irradiance is higher than that shown by the Geider et al. model, because the lower growth rate due to photo-inhibition decreases the effect of the dilution (synthesized chlorophyll vs. fixed carbon).

The effect of a higher $chla : C$ instead, is not mirrored in a higher α^C (fig. 4.3(c)). The light limited slope of the $P^C vs$ E curve is in fact the product of the α^{chl} and the $chla : C$ ratio. α^{chl}, in turn, is the product of the number of reaction centers that participate to photo-capture and their σ_{PSII}. Therefore, the new feature present in the model of a lower

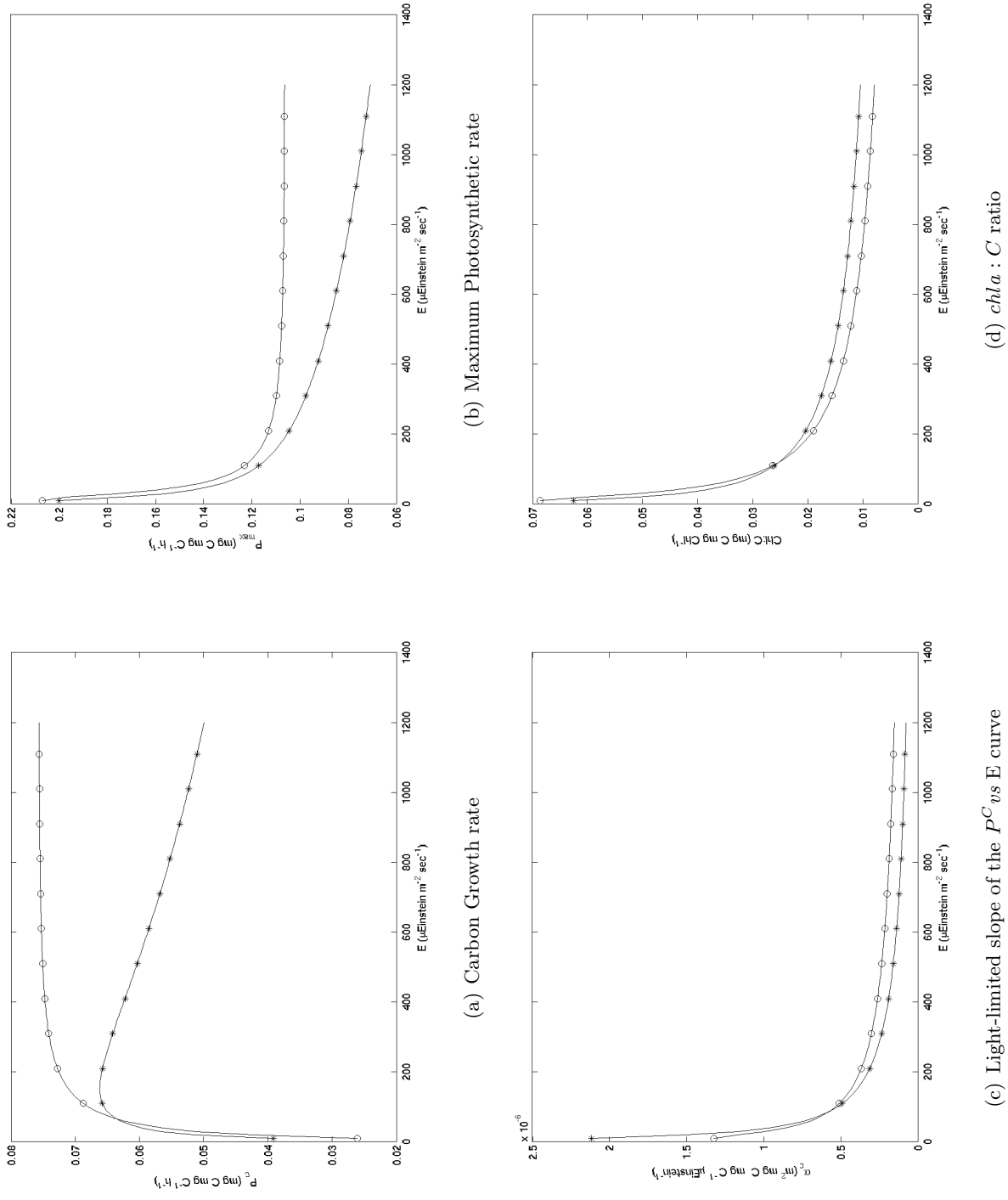

(a) Carbon Growth rate

(b) Maximum Photosynthetic rate

(c) Light-limited slope of the $P^C vs$ E curve

(d) $chla : C$ ratio

Figure 4.3: Comparison between the steady state properties of the Geider Model (open circles) and the updated one (asterisks) *vs* the acclimation irradiance

functional cross-section together with the damage that decreases the number of active reaction centers at high irradiance, overcomes the effect of the increases $chl\,a : C$.

It is also evident that at irradiances lower than 100 μEinst $m^{-2}s^{-1}$, the light harvesting efficiency is increased significantly by the same factor. It is worth noting that the σ_{PSII} and the α^{chl} chosen as a fixed parameter in the simulation performed with the Geider et al. model, correspond to the value that the dynamical new model shows for 100 μEinst $m^{-2}s^{-1}$ This is the reason why the values shown by the two models at this irradiance for the light harvesting components are the same and the curves cross.

From all the above I conclude that the inclusion of the photo-inhibition component decreases the photosynthetic efficiency of the virtual algae, while the modification of the architecture of the pigments in the PSUs increases the light harvesting efficiency at low irradiance. In addition, the decrease at high irradiance of the light harvesting efficiency protects significantly the photosynthetic apparatus from damage.

The steady state E_k versus irradiance is reported in figure 4.4. Both models predict that the light saturation irradiance increases with the increase in the growth light intensity, but the slope among the two is not one. The new model reaches higher values at saturating irradiances because of the decrease in the σ_{PSII} at high irradiance, while its increase at low irradiance decreases it. The plasticity in the σ_{PSII} is reflected in a higher flexibility in the E_k. In the new model, respect to the other one, the E_k is closer to the growth irradiances, both at the high and at the low irradiance.

So far I analyzed the steady state solutions over a wide range of irradiance. The next feature I want to compare is time scale of the the responses for the two opposite transitions for cells exposed to more realistic values of irradiance.

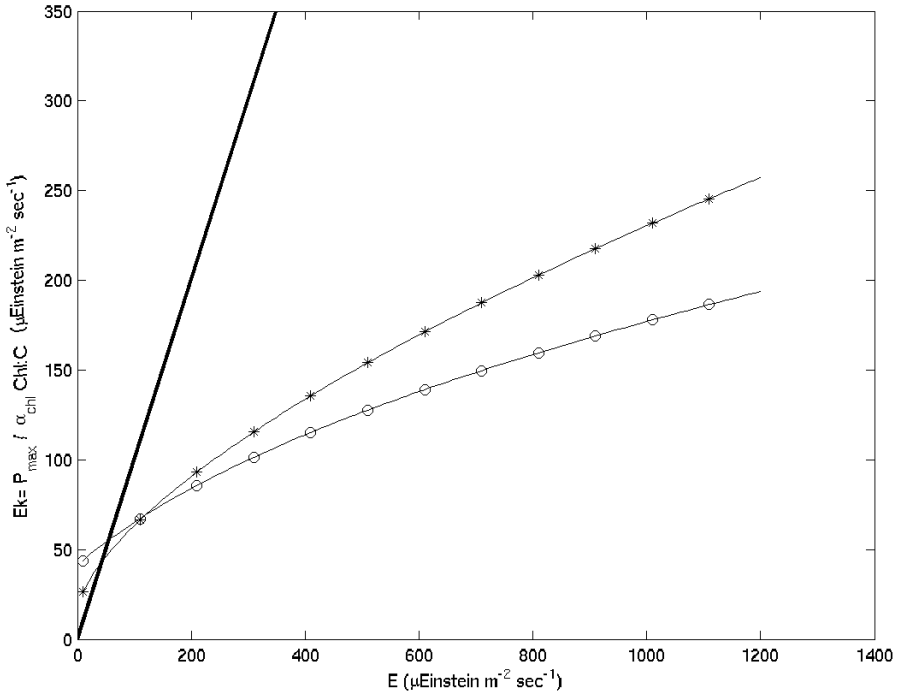

Figure 4.4: Comparison between the E_k of the Geider Model (open circles) and the E_k of the updated one (asterisks) *vs* the acclimation irradiance. Bold line is the 1:1 relationship

4.3.3 Hysteresis in biological response

In this section I analyze the time scale of responses for $C : chla$ ratio to reciprocal shift of irradiance for three configurations of the model: the model of Geider et al. (described in section 1.3.1), the new model modified only for the description of photo-capture and the new model including photo-inhibition.

The time course of $C : chla$ ratio, scaled to the high light value, of the three models during the 20 hours following a shift of irradiance from 100 to 2200 μEinst $m^{-2}s^{-1}$ (line with open circles) and from 2200 to 100 μEinst $m^{-2}s^{-1}$ (line with crosses) are reported in figure 4.5. The red dots mark the time required to reach 50% of the change from the initial condition to the fully acclimated state $T_{0,50}$. The Geider et al. model with the parameters selected for these simulations led to the acclimation of the ratio for the transition from high to low light in less than one hour, while seven hours were required to adapt to the opposite shift. The reason behind this response was already mentioned in section 1.3.1: the increase of the $chla$ synthesis acted sinergistically with the decrease in the growth rate at high intensity passing from high to low irradiances. For this reason, the $C : chla$ of the simulation presented in figure 4.5(a) reached $T_{0,50}$ in less than one hour, while the $T_{0,50}$ of the transition between low to high light was significantly longer.

When the model was modified in order to decrease also the cross section of the PSUs together with the decrease of the pigment content at high light, the time required to attain $T_{0,50}$ of the $C : chla$ ratio was, also in this case, less than one hour. However, the response to the opposite shift was faster than that produced by Geider et al. model (fig. 4.5(b)). The $T_{0,50}$ of the $C : chla$ of virtual algae subjected to the shift from 100 to 2200 μEinst $m^{-2}s^{-1}$ were less than five hours. The inclusion of the new flexibility of the photosynthetic apparatus increased the velocity of the response of the $C : chla$ ratio to increasing irradiances.

By contrast, the inclusion of the photo-inhibition delayed the modification of the ratio

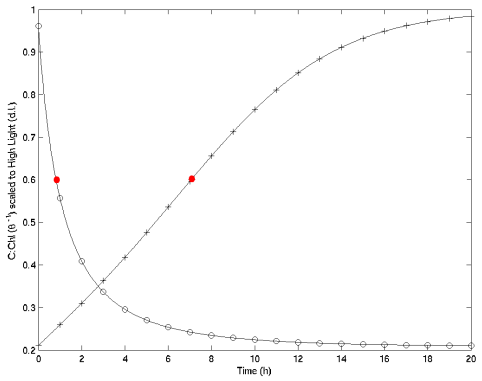

(a) Geider model

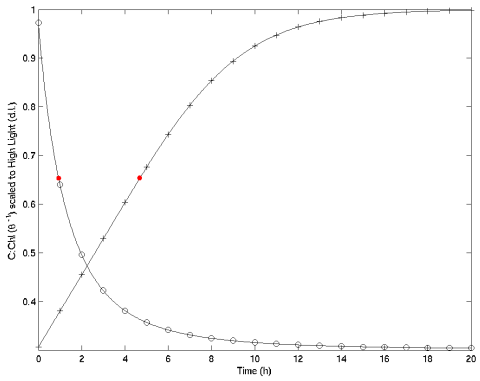

(b) Updated model without photo-inhibition

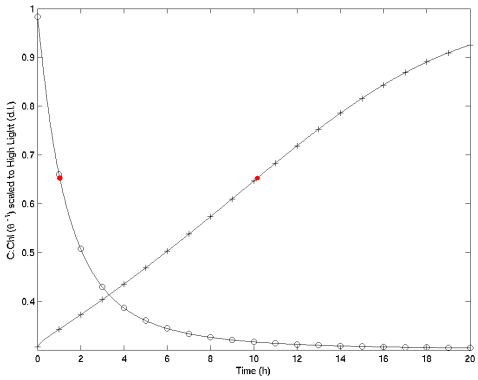

(c) Updated model

Figure 4.5: Comparison between the temporal evolution of the C : $chla$of simulated phytoplankton subjected to the 2200 - 100 µEinst $m^{-2}s^{-1}$ shift (open circles) and the 100 - 2200 µEinst $m^{-2}s^{-1}$ shift (crosses), the red dots mark the 50% completion of the change from the inizial to the fully acclimated condition.

in the simulation from 100 to 2200 μEinst $m^{-2}s^{-1}$ The $T_{0,50}$ of this shift was around ten hours, while the response to the decreasing shift was very similar to the others with a time scale of more than one hour.

Photo-inhibition, due to the abrupt change of irradiance hitting cells with a higher cross section, slowed the organic carbon synthesis. In some cases the increase could not happen at all, because algae exposed to photo-inhibitory irradiance would grow slower than those exposed to a sub-saturating one, as evident in figure 4.3(a). For this reason, the dilution effect was based only on the decrease in $chla$ synthesis. Photo-inhibition due the the abrupt shift from low to high irradiance, reproduced with the model, amplified the hysteresis effect shown in the experiments conducted in laboratory with the same irradiance shift.

It is noteworthy that during supplementary simulations performed with a shift from 100 to 1000 μEinst $m^{-2}s^{-1}$, the timing of the response from the high light to low light regime was slightly increased in all the three simulations (fig. 4.6). On the contrary, the responses to the increasing shift have been found significantly faster than those obtained with the shift to 2200 μEinst $m^{-2}s^{-1}$ for all the three models. The faster response was, as in previous simulations, that produced by the model modified for the light-harvesting component without photo-inhibition. The $T_{0,50}$ was longer than three hours (fig. 4.6(b)). However the Geider et al. model and the new one had both a $T_{0,50}$ for the low-high shift of more then five hours (fig. 4.6(a) and fig. 4.6(c)). The delay of the response due to photo-inhibition compensated the acceleration of the response due to the modification of the σ_{PSII}. As a result, the final outcome was similar for the two models.

Thus the model is be able to reproduce the principal features presented in the Cullen and Lewis (1988) paper:

It shows that more time is required if cells are exposed to an increase of irradiance as compared to a decrease.

Likewise it shows that more time is required to adjust to a large increase of irradiance

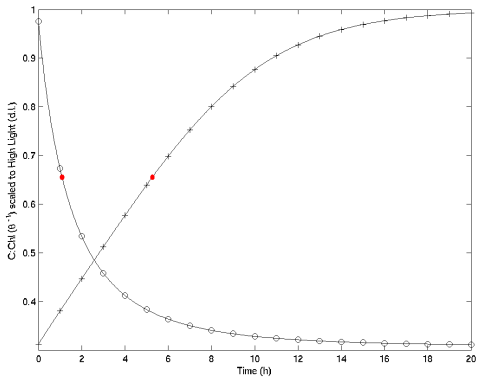

(a) Geider model

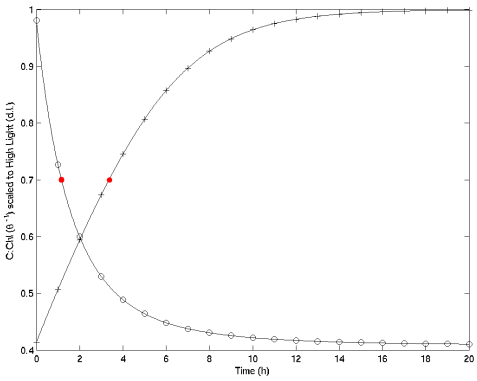

(b) Updated model without photo-inhibition

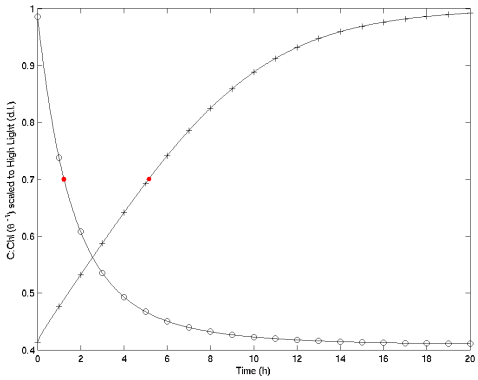

(c) Updated model

Figure 4.6: Comparison between the temporal evolution of the C : $chla$of simulated phytoplankton subjected to the 1000 - 100 µEinst $m^{-2}s^{-1}$ shift (open circles) and the 100 - 1000 µEinst $m^{-2}s^{-1}$ shift (crosses), the red dots mark the 50% completion of the change from the inizial to the fully acclimated condition.

in respect to a smaller increase.

Photoinhibition increases the time needed to acclimate during larger increase of irradiance.

4.3.4 Sinusoidal *vs* Square Wave Illumination

A final test was conducted on the updated model. The laws on which the model is based, have been derived from observations of experiments with irradiance shifts conducted on cultures grown under square wave or continuous illumination.

In nature, the cycle of illumination, or photoperiod, which the phytoplankton experience changes continuously because of the change in the inclination of the sun.

As it was already discussed in Flynn et al. (2001), the version of the Geider model that is at the basis of the updated model, is able to reproduce the nocturnal and diurnal pattern of square wave grown cultures. The test, then, consisted in a a comparison of the response produced by the model to a sinusoidal and to a square wave illumination with the same total daily photons flux (TDPF).

As reported before, the model reacts to positive or negative abrupt changes of irradiance with different kinetics. The model should then reproduce an hysteresis effect, just because the irradiance is increasing or decreasing with time.

It can be supposed that, because the diurnal oscillation of the irradiance due to the diel cycle is a pattern that exists since the appearance of phytoplankton on the Hearth, the organisms should be able to cope with this pattern, maybe, having some internal control. Circadian clocks exist in cyanobacteria (Kondo et al., 1993) and there are several evidences that suggest that a circadian clock might exist also in eukaryotic phytoplankton, especially diatoms (among the others Ragni, 2005). Therefore the possibility that an endogenous control helps the organisms to cope with sinusoidal illumination might not be so remote.

The mechanistic models presented so far do not accommodate for such a feature be-

cause they do not discriminate between the diurnal modification of the irradiance and the modification of irradiance occurring if a cloud is passing or if cells are displaced at different depths in the water column.

The time course of the $C : chla$ ratio during two different cycles of illumination are reported in figure 4.7. The time course that the model produces under square wave irradiance is the same as the one presented in Flynn et al. (2001)(fig. 4.7(a)). During the light period, the increase in the carbon content because of the irradiance perceived lets the $C : chla$ ratio to increase, because of the relatively high irradiance. This increase lasts until the light is on. Afterwards it immediately start decreasing, reaching a minimum value, that lasts until the light is on again, almost four hours later than the beginning of the dark period.

The $C : chla$ ratio under the sinusoidal illumination shows a shifted sinusoidal shape respect to the irradiance (fig. 4.7(b)). The model reproduces the increasing pattern produced under the square wave illumination until almost four hours after the occurrence of the peak irradiance. Subsequently the $C : chla$ ratio starts to decrease anticipating the time when it reaches the ratio for the dark, two hours after the end of the illumination period, as compared to the previous four hours of the square wave illumination.

The memory of the gradually increasing irradiance in the sinusoidal light regime, is prolonged, because of the biological hysteresis effect, which lasts longer than the effective duration of the increasing signal. On the contrary, the response to decreasing irradiance, even if postponed by the memory of the previous signal, is faster.

Experimental data reports on the pigment content under sinusoidal irradiance are rare, but a complete analysis of the diel pattern under this kind of illumination has been found in Claustre et al. (2002).

The irradiance experienced by the *Prochlorococcus* strain studied is similar to the simulated irradiance, the peak irradiance in the experiment is about 1000 μEinst $m^{-2}s^{-1}$

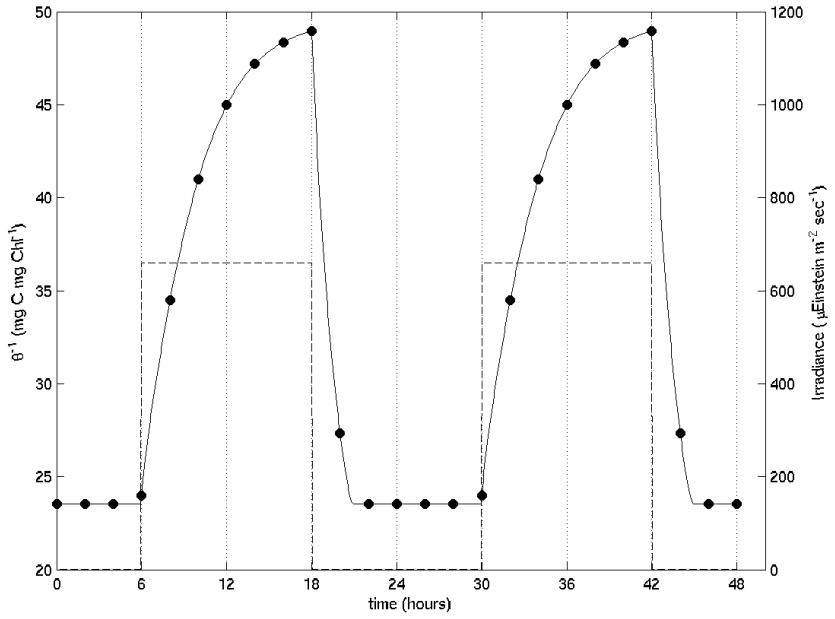

(a) Square wave illumination

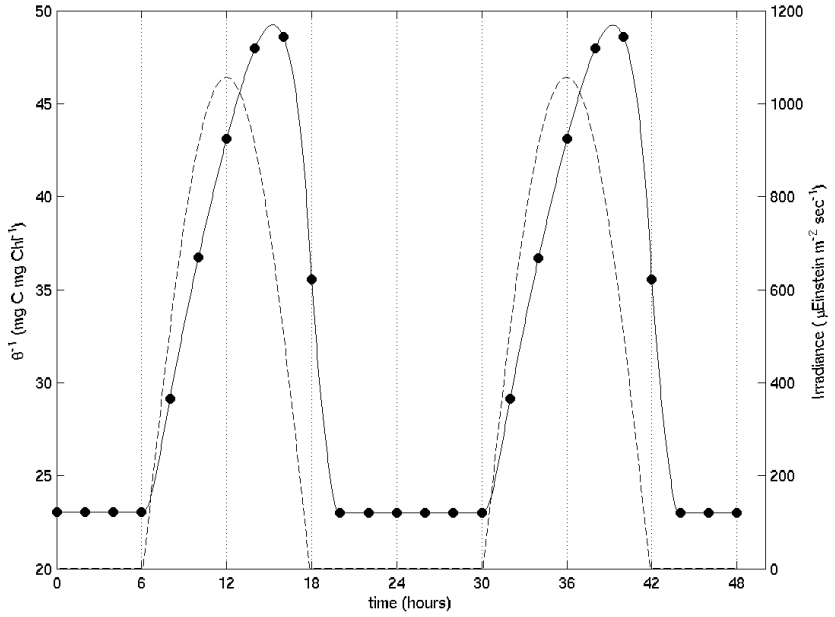

(b) Sinusoidal illumination

Figure 4.7: Temporal evolution during two days of the $C : chl\,a$ ratio (continuous line), under two kind of illumination (the temporal evolution of the irradiance is represented by the dashed line). The TDPF is equal in both the simulations. Black circles corresponds to a sub-sampling of the continuous values effected every two hours of simulated time. This sub-samples time corresponds with the sampling time of the experiments of Claustre et al. (2002)

The authors noted a clear pattern in the $C : Dv - chla$ ratio: it increased during the day and decreased just after the light-dark transition.

The data shows a slower decrease of the ratio during the night, whose reduction is prolonged until the next dawn. The daily increase is similar to the one reproduced by the model, even if the time when it starts decreasing is closer to the beginning of the dark.

On the other hand it is important to note that a comparison between continuous and discrete samples could be misleading. The black dots in the plot, correspond to the timing of the discrete data of the Claustre et al. (2002) experiment. It is evident that the continuous data, produced by the model, if examined as discrete samples show the same diurnal pattern of the *in situ* data. The ratio increases during the day and decreases just after the light-dark transition.

The control of the nocturnal responses of the virtual phytoplankton is simple in the version of the model applied, but as already mentioned in section 1.3.1, additional control have been considered for the models of nitrogen-irradiance interaction by Flynn and Geider.

Whether the nocturnal metabolism of individual plankters, besides photosynthesis, is different from the diurnal one is still an open question.

The regulation of the diel cycle in phytoplankton is an active area of study, which produced contrasting results and explanations.

If any circadian regulation exists, it should affect primarily the cell cycle. The regulation of the cell cycle could be related to environmental factors such as irradiance or nutrient concentration or be endogenously controlled, or both (Vaulot et al., 1987, 1986).

To date, very few studies exist that relate biochemical and photosynthetic characteristics of a cell to the stage of the cell cycle in which it is (Kaftan et al., 1999; Claquin et al., 2004).

For this reason the model developed in this study does not incorporate this kind of regulation, that should be at the basis of the regulation of the diurnal behavior of the

organisms.

The updated model presented here, seems to amplify the hysteresis effect, that in the experimental data available seems to miss.

Inter-specificity of this kind of response should be considered. In addition, the pattern of increase in the ratio during the illumination cycle and its decrease during the dark period is reproduced by the model, but the timing is different. It can be supposed that the response to that signal, even if similar, is regulated in a different way, in respect to the one addressed until now. The nature and the kinetic of this kind of regulation are still unknown.

The possible limits evidenced by this photo-physiological part of the model under this kind of signal will be considered during the analysis of the results presented in section 6.4.1, but to date no experimental evidence is which allows to introduce the trait in the model.

Chapter 5

Models for Turbulent Mixed Layer

The mayor challenge in setting up a numerical simulation of ocean turbulence is the necessity of describing a very wide range of length scales. The ideal solution would be to use a spatial resolution capable of describing directly all the scales of turbulence, without any model assumption, that is a so called Direct Numerical Simulation (DNS) of motion. This is realistically possible only in few cases, and becomes rapidly unfeasible, due to the huge amount of computing power that would be necessary, for most applications. As an alternative, several researchers have started to investigate the potentiality of Large Eddy Simulation (LES), where only some of the scales of motions are resolved directly and the computational cost required is much smaller than the one required by a DNS, in simulating ocean turbulence. An excellent introduction to the LES approach can be found in the book of Sagaut (2001), while some tipical applications of LES to ocean turbulence are presented in Wang et al. (1998) and Skillingstad et al. (1999).

The scope of the physical models here used and presented, is to be capable of describing the turbulent environment in the OML, in order to analyse its effects on the organisms there immersed.

The models that will be presented here have been used to derive vertical lagrangian

trajectories as a part of Individual Based Model simulations of the phytoplankton photo-acclimative response. Two strategies have been adopted: the first, more classical one, is based on a random walk approach and will be described in section 5.1. The second strategy for obtaining lagrangian trajectories has been to use passively buoyant particles released in LES simulations that will be presented in section 5.2. The LES model here presented has been developed in C++ language by Vincenzo Botte and Daniele Iudicone at Stazione Zoologica 'A. Dohrn' in Napoli, while to the lagrangian statistical analysis has involved also Guglielmo Lacorata at ISAC-CNR in Lecce. My personal contribution to this part of the work has been related to the application of the transilient turbulence methods for the analysis of the outputs of the model and to its coupling with the Individual Based Model, while the development of the random walk approach is completely due to my own contribution.

5.1 The Random Walk Approach

In most of the existing models trying to reproduce phytoplankton moving in a mixed layer, cell displacement due to mixing is mimicked through a random walk. This approach albeit simplistic is generally considered sufficiently reliable in representing some statistical properties of turbulence, mainly the mean ones, especially if the eddy diffusivity is not considered spatially uniform.

The eddy diffusivity coefficient is used in place of the diffusion coefficient and generally derives from modeling related estimates or more rarely from direct measurements.

The random walk models that are usually adopted are simple stochastic approaches. They are Markovian in terms of displacement: the particle position is a process whose conditional probability density at a certain time depends solely on its value at the previous time-step.

Visser (1997) showed that the choice of the model can lead to misinterpretations. In

fact trajectories show a tendency to concentrate in regions of relatively low diffusivity. This violates continuity and leads to physically impossible situations.

For this reason, he developed a "corrected" model suitable for environments with diffusivity spatially non uniform.

The "corrected" displacement equation formulated by Visser (1997) is the following:

$$z_{n+1} - z_n = K'(z_n)\,\Delta t + R\sqrt{\frac{2\,K_z\,\Delta t}{r}} \tag{5.1}$$

where z_n and z_{n+1} are respectively the position at time t and $t+\Delta t$, R is a random process of zero mean and variance r (e.g $r = 1/3$ for $R \in [-1, 1]$),

$$K_z = K(z + 1/2K'(z_n)\,\Delta t) \tag{5.2}$$

and

$$K' = \frac{\delta K}{\delta t} \tag{5.3}$$

Equation 5.1 consists of a deterministic component and a diffusive random component. The first term after the equal sign on the right-hand side is the deterministic component, which causes a net displacement of the centre of mass of the suspended particles toward increasing diffusivity at a rate K'.

The second term, the diffusive random component, is obtained by a random process multiplied for a non-random part (defined in eq.5.2), which has been introduced on the basis of the "well-mixed" condition of the particles according to criteria stated by Thomson (1987).

This non-random component, in practice, moves particles from areas of low diffusivity to areas of high diffusivity to produce a realistic spatial particle distribution.

It has, however, been found that additional precautions have to be taken to avoid unrealistic accumulation (Ross and Sharples, 2004).

The unrealistic accumulation pointed out by Ross and Sharples (2004), is very important when the study subject is photo-acclimation in phytoplankters immersed in an OML. Generally the diffusivity profiles for this environmental conditions show an upper layer with a higher diffusivity and a lower one with a lower diffusivity. The presence of this steep gradient between upper highly mixed layer and a lower less turbulent layer should produce a "trap" effect on the particles in the upper part of the water column. Obviously, this unrealistic effect, that is due only to the numerical approach adopted, could have a profound impact on the results of studies focused on the light perceived by the organisms. Also unrealistic accumulation on the boundaries should affect negatively the results. For these reasons, Ross and Sharples (2004) gave a simple recipe to reproduce realistically trajectories for phytoplankters.

As for the first problem, because any discontinuity can lead to artificial particle accumulation, the diffusivity profile has to be well approximated, locally, by the first-order Taylor expansion. To ensure this approximation, a constraint has to be applied to the determination of the Δt, i.e.:

$$\Delta t << \frac{1}{K''} \tag{5.4}$$

where K'' is the second derivative of the eddy diffusivity profiles with respect to z.

As for the second problem, the authors suggest to force at the boundary $K' = 0$. To prevent loss of particles from the domain, the boundaries are reflecting. That means that the particles are forced to stay in the domain $0 \leq z \leq H$ according to:

$$z_{n+1} \rightarrow \begin{cases} -z_{n+1} & \text{if } z_{n+1} < 0, \\ 2\,H - z_{n+1} & \text{if } z_{n+1} > H \end{cases} \tag{5.5}$$

The authors showed that a reflecting boundary, in combination with an inhomogeneous diffusivity, will produce artificial particle accumulations at the boundary. They suggested that this error is systematic and that it is caused by the fact that $K' \neq 0$ at the boundaries. In fact, if K and K' have to be both continuous and differentiable within all the domain, they have to keep these characteristics also at the boundaries. If $K' \neq 0$ at the boundaries, K will have a spike there and K' will be discontinuous.

For this reasons, they suggested to use a cubic spline forced to reproduce $K' = 0$ at the boundaries to interpolate the raw data of eddy diffusivity. In fact, cubic spline have continuous first and second derivative.

All these rules have been followed for the implementation of the random walk used to mimic the displacement of the virtual phytoplankton in the Individual Based Model, that will be the focus of chapter 6. In the next section are presented the other approaches used to determine the trajectories of the individuals immersed in the mixed layer.

5.2 Large Eddy Simulation

The idea behind Large Eddy Simulation (LES) is to simulate directly the largest and most energetic turbulent eddies and to parameterize motions smaller than the model grid spacing. Because LES models resolve the largest turbulent motions, they can provide useful information on mixing processes such as convection or Langmuir circulations, provided that the scale of the process is adequately bracketed by the model grid spacing and the domain size. A key requirement in the use of LES models is that the spatial resolution includes the scales of the energy-containing eddies so that the smallest resolved motions lie within an inertial subrange.

Direct calculation of the largest turbulent eddies in LES is what sets these models apart from more simplified turbulence modeling approaches, such as bulk mixed layer models (e.g. Kraus and Turner, 1967a; Garwood, 1977; Price et al., 1986), high-order turbulence closure

models (e.g. Mellor and Yamada, 1982), or eddy diffusion models (e.g. Large et al., 1994). In comparison to those approaches, assumptions regarding the formation of turbulence and the transport of momentum and scalars by turbulent eddies are minimized in LES, although parameterization of unresolved turbulent motions is still required. Because LES has fewer assumptions, the technique should provide a more accurate simulation of turbulence in comparison to typical parameterizations of the ocean boundary layer.

5.2.1 Model Description

The numerical approach used here is based on a Finite Volume solution of the incompressible Navier-Stokes equations, using a regular Cartesian grid and a staggered positioning of the variables. The equations that are solved are identical to the set used by Skillingstad et al. (1999), where density variations from the reference value are neglected everywhere except than in the buoyancy term, and an additional source term is introduced to take into account the interaction between the surface waves and the boundary layer turbulence. The effect of surface waves is parameterized using the Craik and Leibovich (1976) Stokes drift vortex force, as explained in detail in McWilliams et al. (1997). The momentum equations are given by:

$$\frac{\partial \underline{u}}{\partial t} = -\underline{\nabla} \cdot \underline{u}\ \underline{u} + \underline{\nabla} \cdot \left[\left(\frac{\mu}{\rho_0} + K_m \right) \underline{\nabla}\ \underline{u} \right] - \frac{1}{\rho_0} \underline{\nabla} P + \underbrace{2\left(\underline{u} + \underline{u}^S\right) \times \underline{\Omega}}_{CORIOLIS} - \underbrace{g \frac{\rho - \rho_0}{\rho_0} \underline{k}}_{BUOYANCY} + \underbrace{\underline{u}^S \times (\underline{\nabla} \times \underline{u})}_{STOKESDRIFT} \tag{5.6}$$

where:

K_m = sub-grid scale eddy viscosity;

$\underline{\Omega}$ = earth rotational velocity;

$\underline{u}^S$ = Stokes drift velocity;

$\underline{k}$ = versor of vertical direction.

The Stokes drift velocity is parametrized following Li and Garrett (1993), using:

$$\underline{u}^S = 11,5u_* \frac{\underline{\tau}}{|\underline{\tau}|} \exp\left[\frac{4\pi d}{\lambda}\right] \tag{5.7}$$

where:

$\underline{\tau}$ = surface wind stress;

$u_* = \sqrt{|\underline{\tau}|/\rho}$ = friction velocity;

d = depth;

λ = surface wave wavelength.

In the initial tests we assumed a constant surface wavelength of 30 m as in Skillingstad et al. (1999). The sub-grid stress model adopted here is based on an eddy viscosity assumption. As in the most commonly used model developed by Smagorinsky (1963), the eddy viscosity is obtained by assuming that the small scales are in equilibrium, so that energy production and dissipation are in balance. This yields an expression of the eddy viscosity as a function of the large-scale strain-rate tensor:

$$K_m = c\Delta^2 \sqrt{S_{ij}S_{ij}} \tag{5.8}$$

where:

c = modeling constant;

$\Delta = \sqrt{h_x h_y}$;

$S_{ij} = \frac{1}{2}\left(\frac{\partial u_i}{\partial x_j} + \frac{\partial u_j}{\partial x_i}\right)$.

In the tests presented here the constant c has been set equal to $0,01$. The three

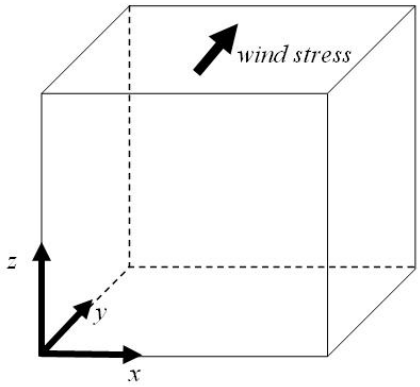

Figure 5.1: Schematic representation of the imposition of the wind stress as an upper boundary condition to a hypothetical domain.

components of the earth velocity are given by:

$$\begin{aligned} \Omega_x &= \Omega \cos(\phi) \cos(\alpha) \\ \Omega_y &= \Omega \cos(\phi) \sin(\alpha) \\ \Omega_z &= \Omega \sin(\phi) \end{aligned} \tag{5.9}$$

where:

$\Omega = 2\pi/86400$ rad s^{-1};

$\phi =$ latitude;

$\alpha =$ angle between the x axis and the North direction.

The code adopts a Marker-and-Cell (MAC) projection method for the enforcement of continuity (Harlow and Welch, 1965). The grid used is uniform in the horizontal direction and can be non-uniform in the vertical direction, with a clustering at the surface. Each one of the systems of linear equations obtained by the discretisation of the transport equations is treated explicitly, while the system of equations for the pressure is solved with a sparse-matrix QMR procedure (Barrett et al., 1994). Convection is evaluated with a two-dimensional third-order QUICK scheme (Leonard, 1988). A flux-limiter is used to avoid unphysical values (overshoots/undershoots) due to the third-order scheme (Leonard

and Mokhtari, 1990). Periodic conditions are applied to the horizontal boundary, while the bottom is treated as a solid wall and the top boundary as a rigid lid. The wind stress is imposed as boundary condition at the top boundary (fig. 5.1).

The set-up of the simulations performed will be explained in section 5.4, In the next section the tools adopted for the diagnostic analysis of the results are presented.

5.3 Diagnostic Tools

The analysis of the lagrangian nature of the turbulence simulated with the LES has been performed with two different diagnostic tools, described in the following sections.

5.3.1 Lagrangian Statistics

The analysis has been restricted to the principal features of turbulence derived by the model, in order to use this information for the analysis of the results of the coupled Individual Based Model. And the statistical properties have been selected accordingly. A detailed analysis will be part of a manuscript in preparation on the lagrangian properties of Ekman and Langmuir turbulence.

The characteristics of the dispersion of the particles released in the LES has been analyzed via a Finite Size Lyapunov Exponent analysis.

The Maximum Lyapunov Exponent (MLE) is:

$$\lambda = \lim_{t\to\infty} \lim_{\delta_0\to 0} \frac{1}{t} \ln \frac{\delta(t)}{\delta(0)} \tag{5.10}$$

It measures the typical exponential growth of the distance $\delta(t)$ between two trajectories arbitrarily close at the initial time, that is, $\delta(t)$ is assumed of infinitesimal value. In practise, it is difficult to calculate the MLE in realistic conditions. Moreover it is of limited interest in case the focus is the large scale behaviour. By contrast, the other parameter often used

in dispersion studies, the effective diffusion coefficient:

$$D = \lim_{t\to\infty} \frac{1}{4t} < A^2(t) > \tag{5.11}$$

where $A(t)$ is the relative dispersion, requires the knowledge of the system at large scales and infinite times. It is is thus not well suited for geophysical cases, in which the physical domain is often limited, i.e., it has spatial scales only one or two order of magnitudes larger than the smallest resolved scale.

By defining $\tau(\delta)$ as the time interval after which the perturbation is amplified by a factor $r > 1$, the Exponent of Lyapunov at Finite Size (FSLE) is instead defined as

$$\lambda(\delta, r) = \frac{1}{< \tau_r(\delta) >} \ln r. \tag{5.12}$$

The FSLE is thus suitable for describing the dispersion between particles over finite spatial scales in non asymptotic conditions, that is, when a diffusive regime has still not clearly established. It is characterized by the following remarkable properties: for $\delta << l_0$, where l_0 is the smallest characteristic scale of the system, we have that the FSLE tends to the MLE; for $\delta << l_M$, where l_M is the largest scale, we have that the standard diffusion can be assumed to be valid and $\lambda \approx D\delta^{-2}$. A plateau over a certain range of scales indicates an exponential separation of the trajectories (Lagrangian chaos). The shear dispersion is shown as $\lambda \approx < dV > \delta^{-1}$, where dV is the typical scale of the relative velocity.

For this reason the FSLE is a well suited method to understand the mixing structures and to distinguish between shear due mixing or diffusive mixing.

The relative dispersion of the particles is also useful to evaluate the vertical diffusivity profiles corresponding to the pure diffusive nature of turbulence, that have been used to assign a value to the random walk parameters.

5.3.2 The Transilient Turbulence Theory

The Transilient turbulence theory, named after a latin word *transilire*, that means "jump over" or "leap across", is a framework born to analyze the average effect of many eddies of different sizes on the net non-local vertical mixing in the atmosphere (Stull, 1984, 1993).

It produces a method for parameterizing turbulence that allows non-local vertical mixing between every pair of grid points in a vertical column, even between non-neighboring points.

This method can account for the advective-like turbulent transport within large and coherent turbulence structures. The method also parameterizes the mixing effects of medium and small size eddies, so it gives a physical-space representation of a spectrum of turbulence wavelengths.

The method has been used as a tool to parameterize a non-local first-order closure for turbulence and has been extended to derive mixing parameters from oceanic *in situ* micro-structure turbulent profiles (Stull, 1993; Piera, 2002).

The framework for this parameterization is a matrix, called transilient matrix.

The basis of the transilient turbulence theory resides on the discretization of the column of water in n layers or boxes that are stacked one on top of each other. The state of the fluid within each box is characterized by the specific concentration of some property s. Turbulent eddies of different sizes transport fluid mass between these boxes. As a result, the concentration of s_i in a particular box i at time $t+\Delta t$ is a function of the concentration in the other boxes at an earlier time t.

The following assumptions were initially made: internal sources or sinks of any kind were not considered and the property s was considered a non reactive tracer. It means that the property s was conserved during the transport from one box to another. This simplification, as we will see in section 6.3 has not been allowed in some cases.

However these assumptions are valid for most of the typical properties of the ocean,

and, for this reason, this is an optimal tool to parameterize and study the nature of vertical mixing in the ocean.

In this case, it can be considered that:

$$\begin{aligned} s_i(t+\Delta t) &= c_{i1}\, s_1(t) + c_{i2}\, s_2(t) + c_{i3}\, s_3(t) + \ldots + c_{in}\, s_n(t) \\ &= \sum_{j=1}^{n} cij(t,\Delta t) s_j(t) \end{aligned} \tag{5.13}$$

where $s_i(t+\Delta t)$ is the final value of any scalar such as temperature, salinity, after time step Δt at destination grid point i, $s_j(t)$ is the initial value at time t at any source grid point j and n are the number of layers (grid cells) in the gridded domain. This equation describes synthetically the effect of exchange of the properties s from all the layer of the fluid to the selected layer during an interval of time Δt. The dimensionless coefficient c_{ij} represents the portion of fluid, which is mixed from box j to box i during this interval.

Equation 5.13 can be redrawn in matrix notation to represent the simultaneous mixing exchange between all the boxes:

$$\mathbf{S}(t+\Delta t) = \mathbf{C}(t,\Delta t)\, \mathbf{S}(t) \tag{5.14}$$

where $\mathbf{S}$ is an n-element column vector, that represents the distribution of s and $\mathbf{C}$ is the n x n transilient matrix.

Each transilient coefficient c_{ij} in the n x n matrix represent the portion of fluid that has been mixed during the time Δt from the ith box to the jth box, so the diagonal coefficient of the matrix c_{ii} represent the portion of fluid that remains in each box during the period between t and $t+\Delta t$ (main diagonal on figure 5.2b).

The matrices have some physical constraint:

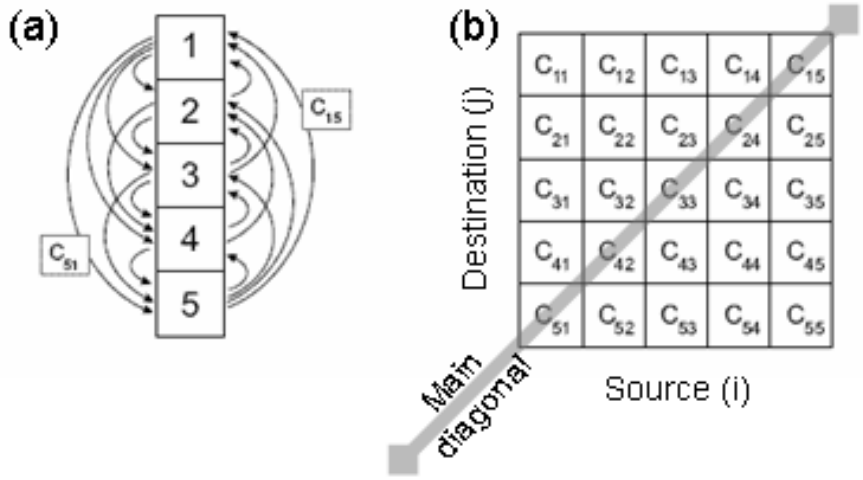

Figure 5.2: Schematic representations of a turbulent field and the associated transilient matrix: (a) Mixing between all the possible pairs of $n = 5$ cells, the exchange between cell 1 and 5 is highlighted, (b) the transilient matrix associated. The main diagonal, which coefficients represent the amount of water entrained in the same cell after Δt is highlighted. Redrawn from Stull (1993).

$$\sum_{j=1}^{n} c_{ij} = 1, \quad \sum_{i=1}^{n} c_{ij} = 1, \quad 0 \leq c_{ij} \leq 1 \tag{5.15}$$

These equations mean that: the total amount of water at each destination must have come from somewhere and, consequently, the sum of each row must be equal to 1. For similar reasons, each column must sum to 1 because the total amount of water initially within each cell must go somewhere. These rules are necessary to satisfy the conservation of mass and state. In addition, each element must be less or equal to 1,0, because each coefficient represents the fraction of the water arriving at the destination layer from some source layer. Numbers greater than 1,0 would represent a percentage greater than 100% and it is obviously impossible that the destination water is more than 100%. Even if it is mathematically possible to obtain coefficients that do not obey the rules in equation 5.15, physically such coefficients would have no meaning. For this reason it is necessary to

constrain the matrices to obey to these rules during their calculation.

It is possible to derive transilient matrices from LES simulations, by releasing passive tracers in the simulated velocity field. Knowing the position of each tracer during time, it is possible to parameterize the percentage of water that moved from a box to another.

A tracer matrix TR is constructed in order to evaluate the dispersion of the tracers. Each coefficient of the tracer matrix tr_{ij} corresponds to the mean fraction of tracer that at time zero were in the ith layer and after Δt have been detected in the layer j. At time zero, with $\Delta t = 0$ the tracer matrix should have 1 in the main diagonal and 0 at the rest. The tracers matrix corresponds to the transilient matrix.

By monitoring the tracer positions during the LES simulations it is possible to evaluate the transilient matrices for different time intervals Δt. This set of matrices differ from one another for the time required for a transfer from a box to another.

As already said, if Δt is zero or small, the main diagonal will have numbers near to one and in the upper and lower triangles the values will be zeros or very low. In fact, with small Δt turbulence has no time for mixing water parcels from their starting points. On the contrary, for very long time steps, turbulence can cause a significant mixing across large distances. In this case, isotropic turbulence is associated with a full matrix of nearly equal elements.

Sets of transilient matrices, calculated with different Δt, are, indeed, useful to study the evolution with time of the mixing processes. In fact, from these sets of transilient matrices it is possible to evaluate visually or through calculations that involve their coefficients, the length and the time scales of the mixing process studied.

In order to highlight the underlying physics, transilient matrices are generally displayed as a contour plot of element values (Ebert et al., 1989). The coefficient of the matrices tell how much water has been potentially interchanged between water parcels and the contour plot shows the relative locations where the coefficients reach the highest values 5.3.

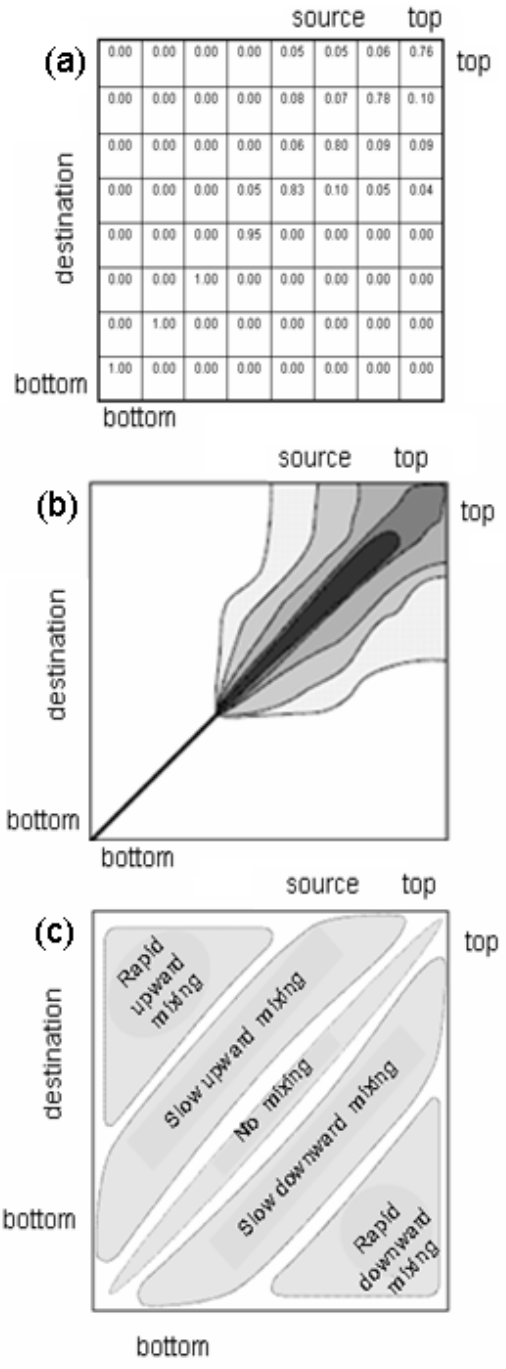

Figure 5.3: A transilient matrix (a) and its contoured way of visualization (b). The type of mixing that the transilient matrix represents, can be obtained comparing the zone of high coefficient detected in (b), with the schematic representation in (c), that highlights the kind of mixing involved for the zones contoured. As an example, the transilient matrix (a) shows a symmetric mixing in the upper part of the domain and no mixing at the bottom. Redrawn from Piera (2002) after Stull, 1993.

In figure 5.3c is redrawn a scheme that shows the type of mixing process, as related to high value coefficients in the zones highlighted. As an example the elements of the lower left corner of the matrix are associated to the shallow-parcel sources and deep-parcel destinations.

During the Δt specified for the matrix, a certain amount of water transfers between these sources and destinations. High values of these elements are interpreted as rapid downward mixing. Elements closer to the main diagonal are transported to relative shorter distance during the same time interval, and indicate the intensity of slower mixing processes.

Both the physics and the time step selected determine the magnitudes of elements in a transilient matrix. For a very short time steps, turbulence has no time for mixing water parcels from their starting points, leading to a diagonally-dominated matrix with zeros in the upper and lower triangles. For very long time steps, turbulence can cause a significant mixing across large distances and, in the case of isotropic turbulence, is associated with a full matrix of nearly equal elements.

The transilent matrices are used in section 5.4.2 to analyze the type of mixing associated with the lagrangian simulations performed.

5.4 Results and Discussion

The numerical code has been implemented using a uniform grid of $1,5\ m$ as spatial resolution and a $150 \times 150 \times 120\ m$ domain, corresponding to $100 \times 100 \times 80$ grid points. The boundary conditions are periodic on the horizontal and a non-penetrative slip condition is applied at the bottom. Density is assumed as constant and buoyancy fluxes are nil at surface. The reference latitude for the Coriolis parameters is $45°N$. At surface, a steady wind stress is applied directed at 45° with respect to the North.

The wind intensity is such that the corresponding typical scale for the turbulent velocity

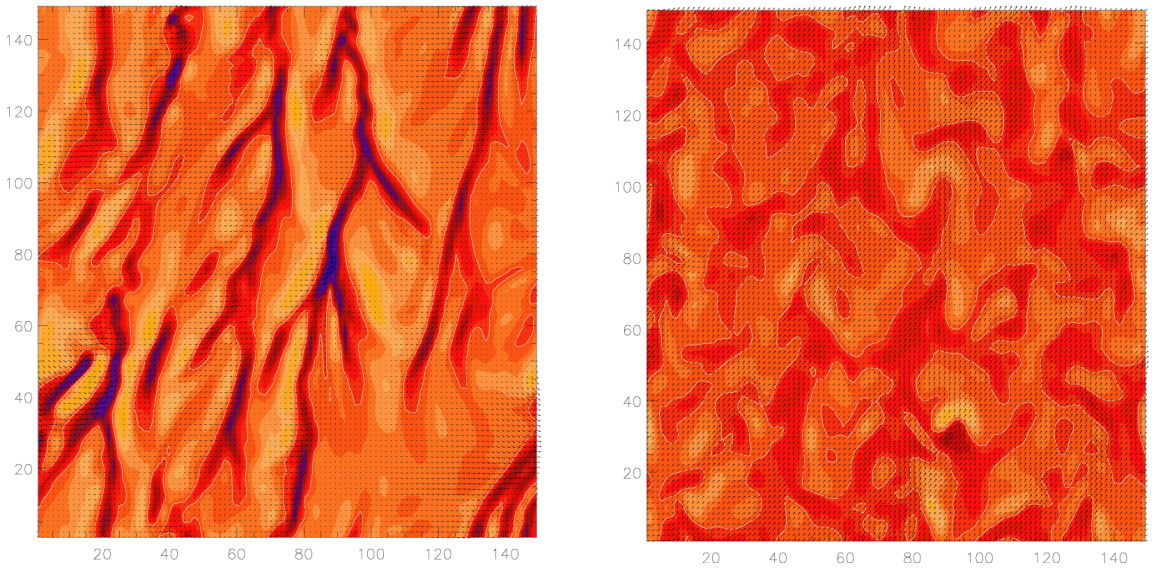

Figure 5.4: Istantaneous vertical velocity field at surface in LES model. Simulation with Stokes drift on the left panel and standard turbulence shear simulation on the rigth. In both cases wind direction is the Y direction.

is $u* = 0,008\ ms^{-1}$, a value typical of the response to moderate atmospheric events. As a consequence we have $Z* = 80\ m$ as a priori estimate of the vertical scale for the turbulent Ekman layer and $\tau* = 1.10^4\ s$ as temporal time scale for the largest eddies.

Here the outputs of two simulations have been used, a reference simulation without Stokes drift ($La = \infty$, i.e. no surface waves and thus no Langmuir cells, that will be called Ekman) and a simulation with a Stokes drift that gives $La = 0,3$, typical of a Langmuir-dominated turbulent regime, that will be called Langmuir (McWilliams et al. 1997).

The two simulations have a physical time duration of 24 h (that is about 3-4 times the time scale of the largest eddies) and were both preceded by a spin-up of 8 h. As an initial condition, the analytical solution for the Ekman spiral was used, superimposed to a random noise (Zikanov et al. 2003). At the end of the spin-up phase, 100000 couples of purely passive particles have been released randomly in the model domain; their Lagrangian trajectories have then been integrated online over the following 24 h.

As shown in figure 5.4, the vertical motions appear to be organized with different patterns, with the appearance of regions of large convergence and the presence of Y-junctions directed downwind, both features typical of Langmuir circulation (in the case of $La = 0,3$). It is to note that this circulation is highly unstable and the classical view of Langmuir cells as regular and steady cylinders does not apply when the non-linearity of the dynamics is taken into account, as it is the case here (see discussion in McWilliams et al. 1997).

It is also to note that in both cases the mean motion of the particles is close to that of the classic Ekman spiral but, as clearly visible, the effect of the "noise" due to turbulence on the trajectories is significant (fig. 5.5).

5.4.1 Lagrangian Statistics of Ekman and Langmuir Turbulence in an OML

The analysis of the trajectories shows that in both physical conditions the presence of coherent turbulent structures (3D eddies) increases the mixing efficiency with respect to a $1D$ stochastic model for vertical dispersion, generally used in dispersion studies (see Zikanov et al. 2003).

In figure 5.5 is reported the horizontal dispersion of the particles released in the Ekman case simulation: it is evident the formation of the spiral of Ekman, that dominates the mean flow of the horizontal pattern.

The most important features for the current analysis, however, are the vertical features of the dispersion that modulate the vertical position of the particles and so the light history of the individuals.

It is evident from the top panel in figure 5.6, that for the Langmuir simulation the dispersion has typical time scales that regularly increase with depth, whereas for Ekman simulation the first 50 m of the water column show the same typical time scale. Taking into

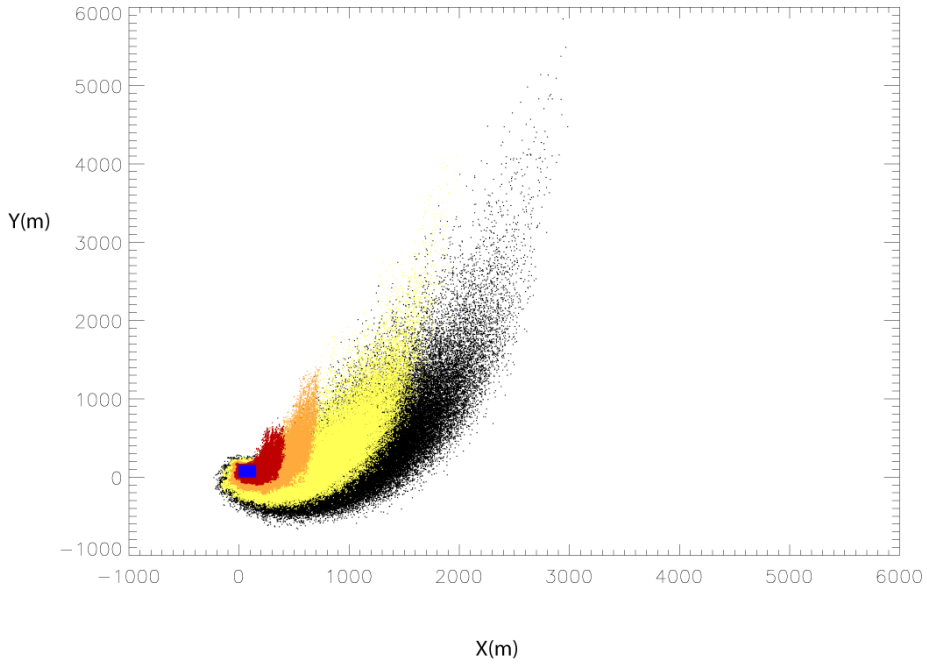

Figure 5.5: Horizontal dispersion of the particles at given times (blu indicates the initial position, colors refer to the position every 6 h) for the reference case, i.e. without Langmuir cells. The dispersion is dominated by the mean flow, i.e., the Ekman spiral, with superimposed the effect of turbulence.

account the dynamics of surface waves (Stokes drift) various changes in the fluid response are observed.

The main of these effects is that the value of *equivalent* vertical diffusivity is double with respect to the no-wave condition ($\approx \ 0,06\ m^2/s$ instead of $0,03\ m^2/s$). Also, the resulting mixing is efficient up to a depth that is about 40 m deeper than the case without Langmuir cells (fig. 5.6)

It is commonly assumed that the motion of suspended particles in a turbulent environment is purely random, that is, the probability distribution function (PDF) of a single movement at a given time follows a gaussian distribution. This approximation is coherent with a diffusivity approach, in which the motion is given by small diffusers having scales smaller than the mean motion. This approximation, indeed, is at the base of the formulation of the random walk approach for the reproduction of the trajectories of particle

immersed in turbulent fluids.

The latter assumption is not valid if the scale of the diffusers (eddies) is comparable to that of the considered domain, as for our case study. In fact, from a first analysis of the vertical movements of particles on a given time interval, we observe that the distribution of vertical movements at finite times is not gaussian shaped (fig. 5.7). In fact the larger excursions are more probable than if having a gaussian distribution. In addition, it is over-estimated the frequency of the smaller ones. It is important to note that the right side of the PDF has a higher frequency, that means an higher probability of downward movement respect to the upward one. This feature, here less evident, will be fully highlighted by the application of the transilient matrices to the outputs of the simulations, presented in the next section. That tool is, in fact, able to show the non-local or asymmetric nature of the dispersion of particles, as mentioned in section 5.3.2.

To conclude the analysis, it is important to note that the relative dispersion in terms of the FSLE pointed out the presence of Langmuir cells of about 30 m of diameter which generated an isotropization of the dispersion for scales up to 30–40 m. At larger scales, in both cases the horizontal dispersion induced by the vertical shear of the mean current (Ekman current) dominates, even if it is less efficient in presence of Langmuir cells. The vertical displacements of the Langmuir case behave more like a shear dispersion case, while the Ekman case is more similar to a standard diffusive case.

It is, indeed, impossible try to reproduce the patterns presented by the LES Langmuir case with a random walk. For this reason the random walk technique used to compare this more classical approach with the innovative LES derived trajectories in the IBM has been based on the diffusive reproduction of the Ekman case.

The vertical eddy diffusivity profiles derived by the averaged analysis of the relative dispersion of the particle released in the LES are shown in figure 5.9. It is evident by the noise of the signal that the Langmuir case produces a more chaotic and less diffusive

turbulent mixing, while the Ekman case produces an eddy diffusivity decreasing with depth that is similar to a more diffusive turbulent nature. This last profile has been used, with the modality that has been described in section 5.1 and that will be detailed at the end of section 6.2 to reproduce the vertical displacements of individuals in the Individual Based photophysiological model.

In the next section the transilient matrices derived by the random walk displacements are compared with the Ekman and Langmuir LES cases, in order to highlight the non-local nature of the simulated turbulent mixing processes.

5.4.2 Local *vs* Non-local Mixing

The transilient turbulent theory has produced an additional powerful tool to distinguish the features of the mixing. In particular it was useful for the determination of the importance of the non-local mixing events, respect to the more local diffusive ones.

The transilient matrices have been computed for different Δt associated with the corresponding displacements. The Δt considered go from fifteen minutes to three hours and are able to keep all the time scales of the processes considered.

The contour plots of the transilient matrices for the LES simulation in the Langmuir case, for the chosen Δt are reported in figure 5.10. Comparing the shapes of this contour with the schematic diagram in figure 5.3, it is possible to highlight that the mixing reproduced by the LES Ekman simulation, dominated by the main diagonal coefficients, shows a local slow upward and downward components. The mixing is increased in the upper part of the domain, and decreases with the depth. No coherent structures are evident nor the formation of patterns suggesting changes in the time for displacements. The mixing is dominated by a local and diffusive nature, that decrease with depth, feature typical of the diffusive nature of wind mixing.

In figure 5.11 are reported the homologous contour plots of the transilient matrices

computed with the random walk derived trajectories. The two family of contour plot are quite similar, suggesting that the random wolk is correctly reproducing the pattern and nature of the mixing. However, a general increased mixing is evident, concentrated in particular in the zones of gradient in the vertical profile of the eddy diffusivity. The shape of the contours seems to show a barrier to the cascade of energy in the domain. The random walk approach can only try to parameterize the cascade of energy between larger and smaller eddies, that the LES Ekman simulation directly reproduce until a certain scale. The influence of these differences on the results of the IBM will be further discussed.

It is, however, important to note that this comparison is focused on the mean nature of the mixing process: exceptional displacements are not represented if not enough frequent. For this reason, a possible inability of the random walk approach to describe the extra-gaussian behaviour of the LES Ekman simulations cannot be evidenced by this comparison and they can only been supposed on the basis of the results shown in figure 5.7.

The influence of the missed reproduction of large excursions of organisms over the entire mixed layer due to the random walk approach on the performances of lagrangian phytoplanktonic models was already highlighted by Yamazaki and Kamykowski (1991). The comparison of the results of the IBM with trajectories derived from the LES Ekman simulation with the random walk approach results, will allow to quantify its influence on the performance of the model.

Finally, in figure 5.12 are plotted the contours of the transilient matrices derived by the LES Langmuir case. It is possible to detect an asymmetrical nature of the mixing even for displacements realized in fifteen minutes. In the matrix relative to two hours displacements it is possible to notice, from the second contour (Δt = 30 minutes), the presence of a coherent structure due to the Langmuir cells in the first 30 meters. However, this structure increases the downward mixing from the surface to almost 80 meters, until after three hours the pattern is no more recognizable. In addition it is also visible, a high

frequency zone correspondent to the upward mixing from about 30 meters to the surface. This is the evidence of the upward mixing due to the continuity law, that corresponds to the zones of larger upward mixing typical of the Langmuir cells.

The powerful tool of the transilient matrices will be extended in section 6.3 in order to couple this analysis with the photophysiological characteristics and growth performances of the individuals subjected to this mixing. The Individual Based Model that used those three reproductions of the mixing to mimic the movement of phytoplankters in the water column is presented in the next chapter.

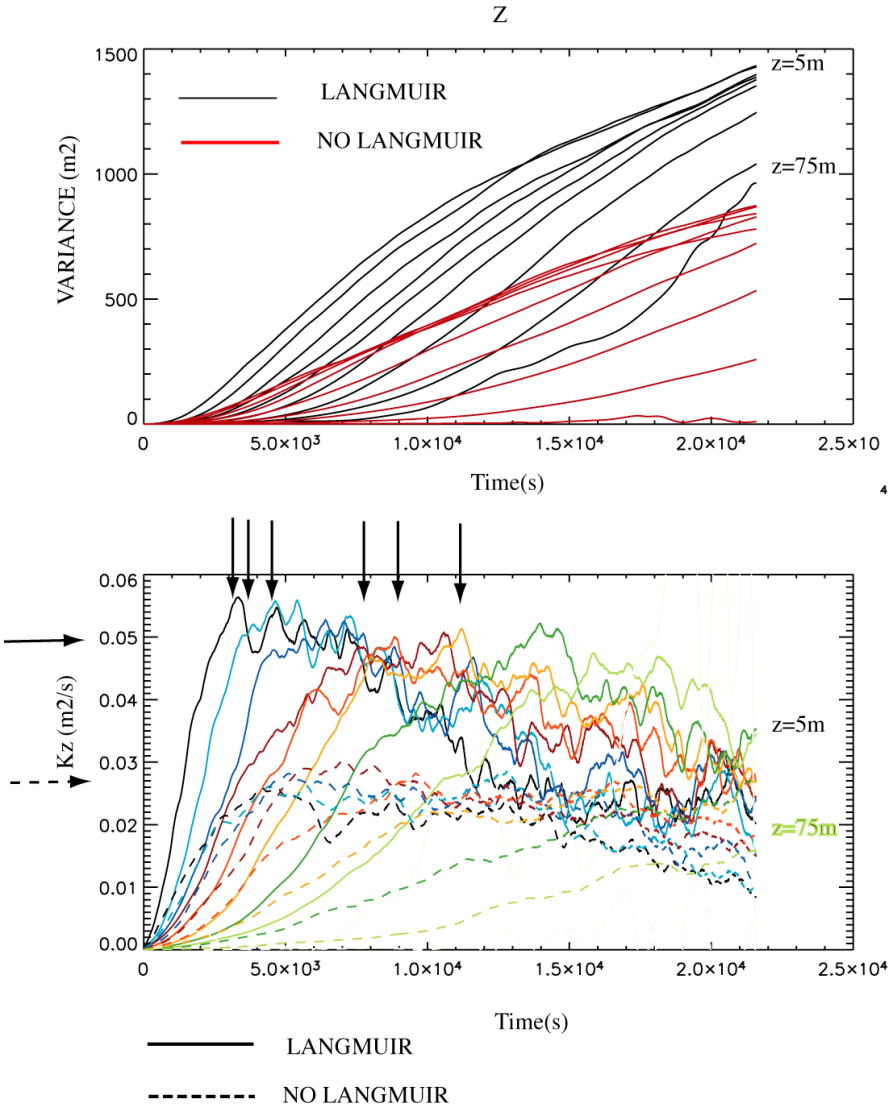

Figure 5.6: The top panel reports the relative dispersion of the particles as a function of time for various depth classes (of 10 m each). The cases with and without Langmuir circulation are drawn in black and red respectively. Bottom panel reports the equivalent vertical diffusivity. The major dispersion efficiency together with significant values at greater depths for Langmuir case in respect to no-Langmuir case is evident.

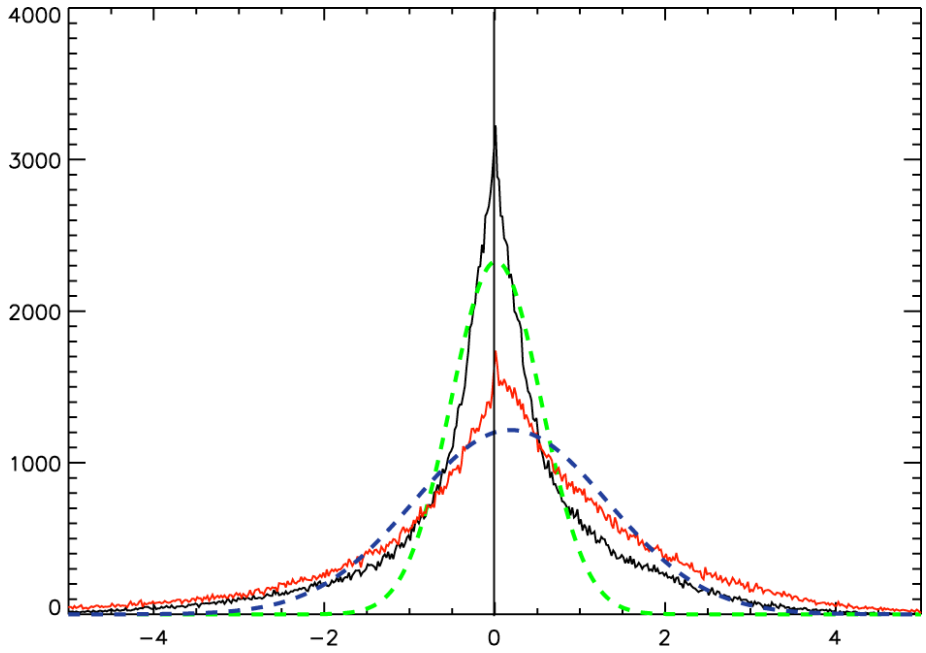

Figure 5.7: Hystogram of the difference of vertical position (m) at a given time interval ($2\ h$). In both cases the distribution cannot be approximated with a gaussian function, as the probability to have greater values is higher than for the gaussian case. The simulation with Langmuir circulation shows a standard deviation double than the case without Langmuir and a major deviation from a gaussian shape.

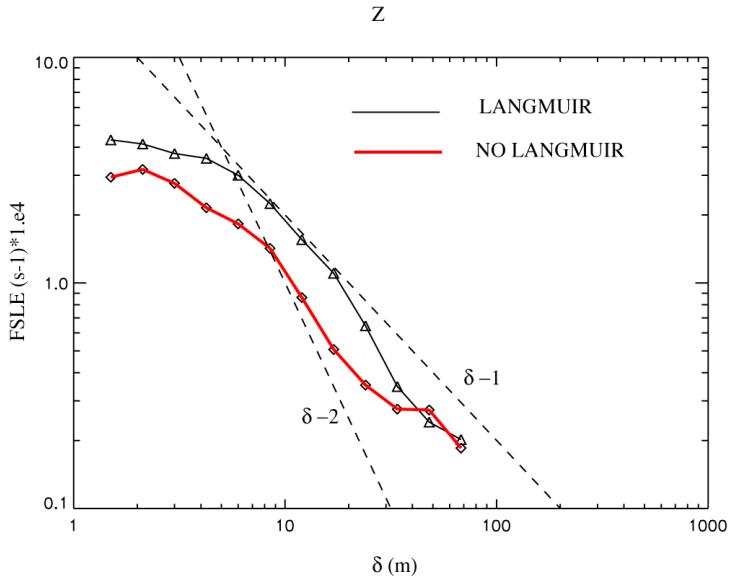

Figure 5.8: FSLE of vertical movements. The Langmuir case displays vertical displacements that are closer to the shear dispersion case, whereas the dispersion in the Ekman case is closer to the standard diffusive case.

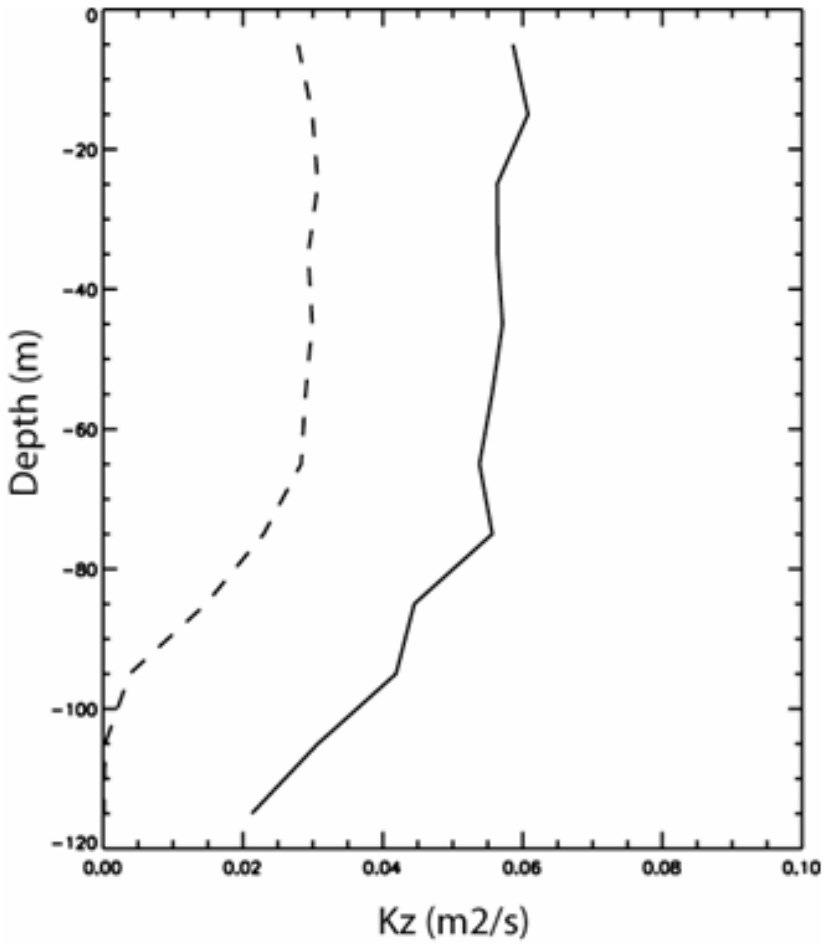

Figure 5.9: Eddy diffusivity profiles derived by the FSLE analysis of the particles dispersion in the LES simulations: continuous line for the Langmuir and dashed one for the Ekman case.

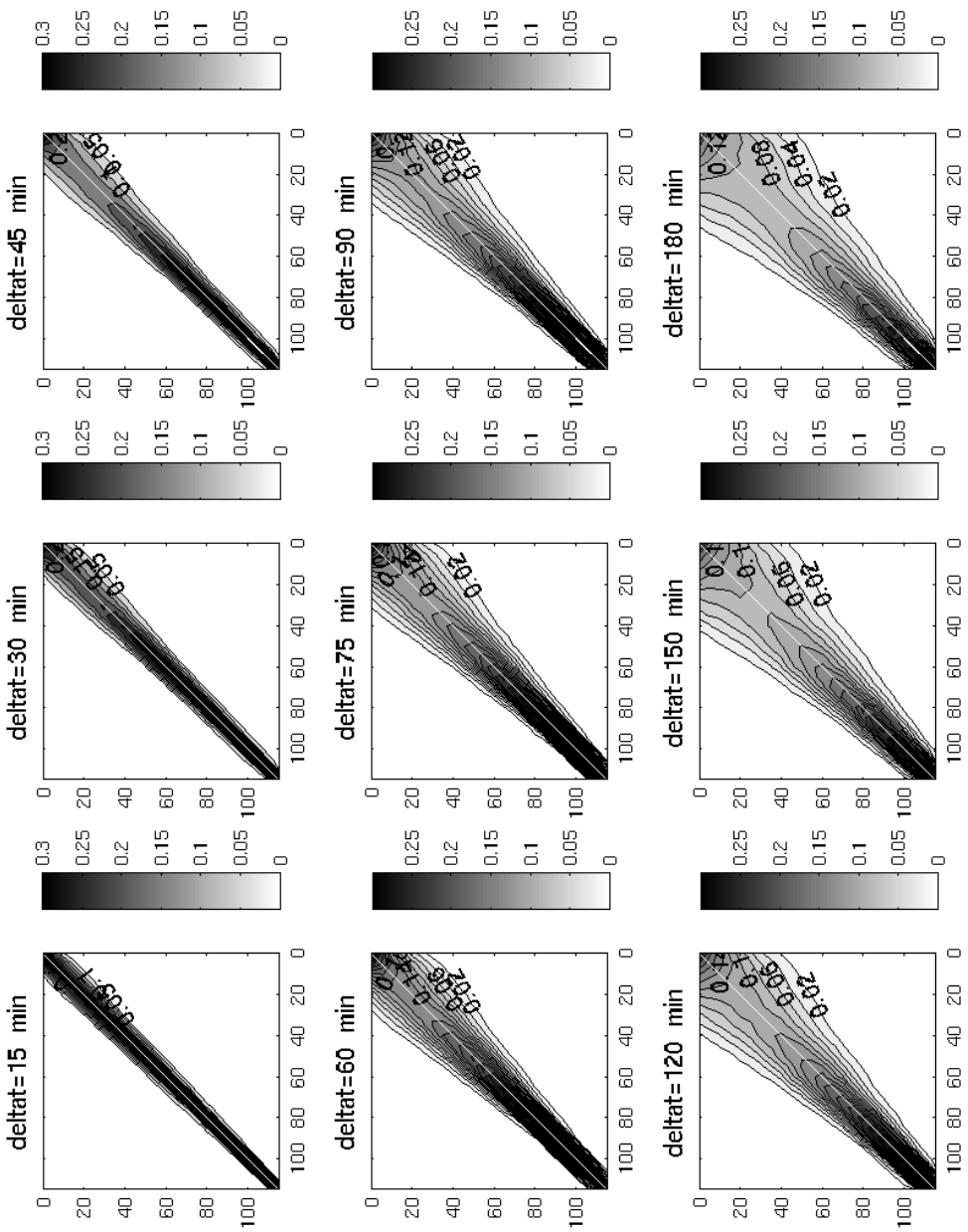

Figure 5.10: Contour plots of a family of transilient matrices computed for the LES Ekman case, with increasing Δt.

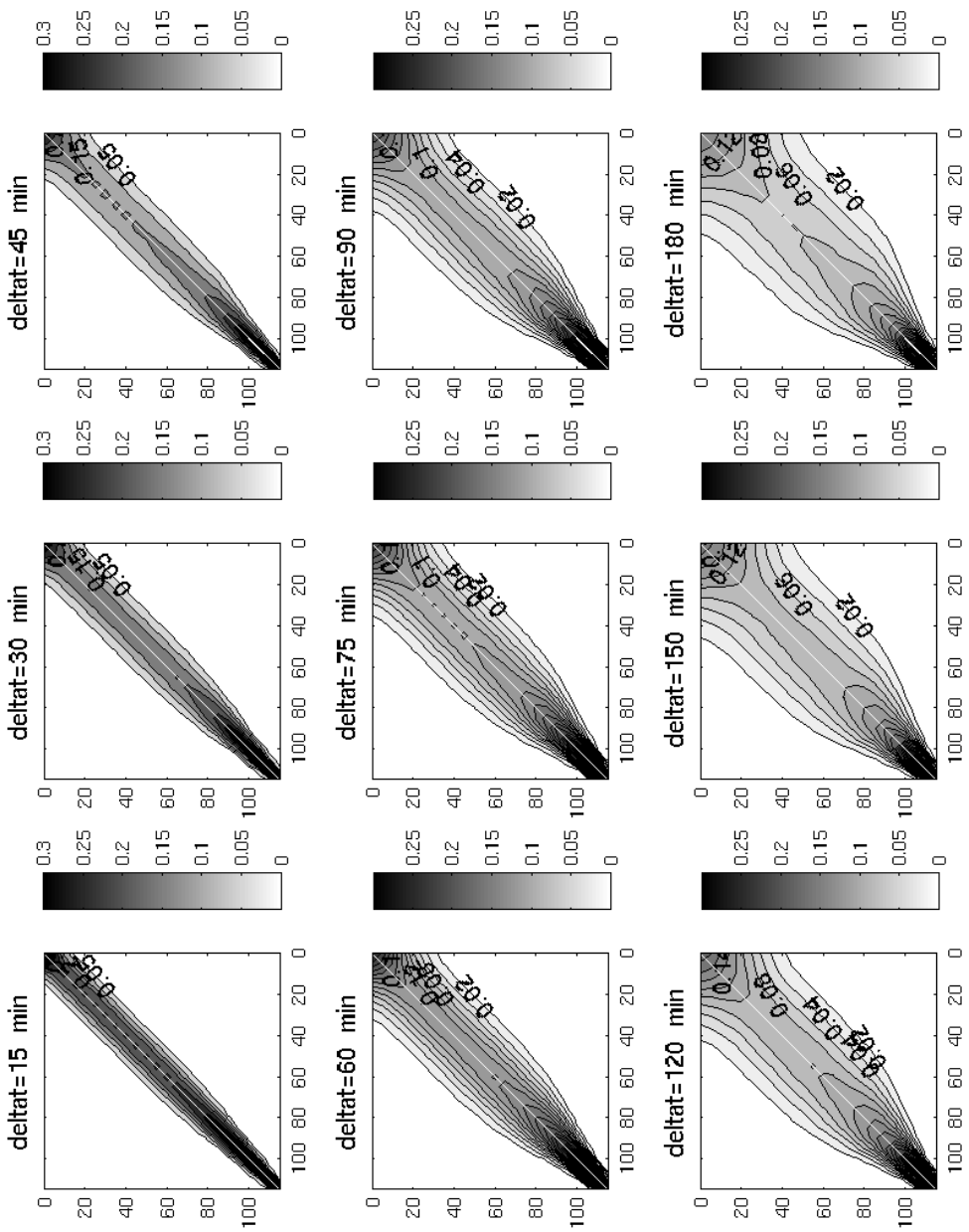

Figure 5.11: Contour plots of a family of transilient matrices computed for the random walk reproduction of the mixing due to the LES Ekam case, with increasing Δt.

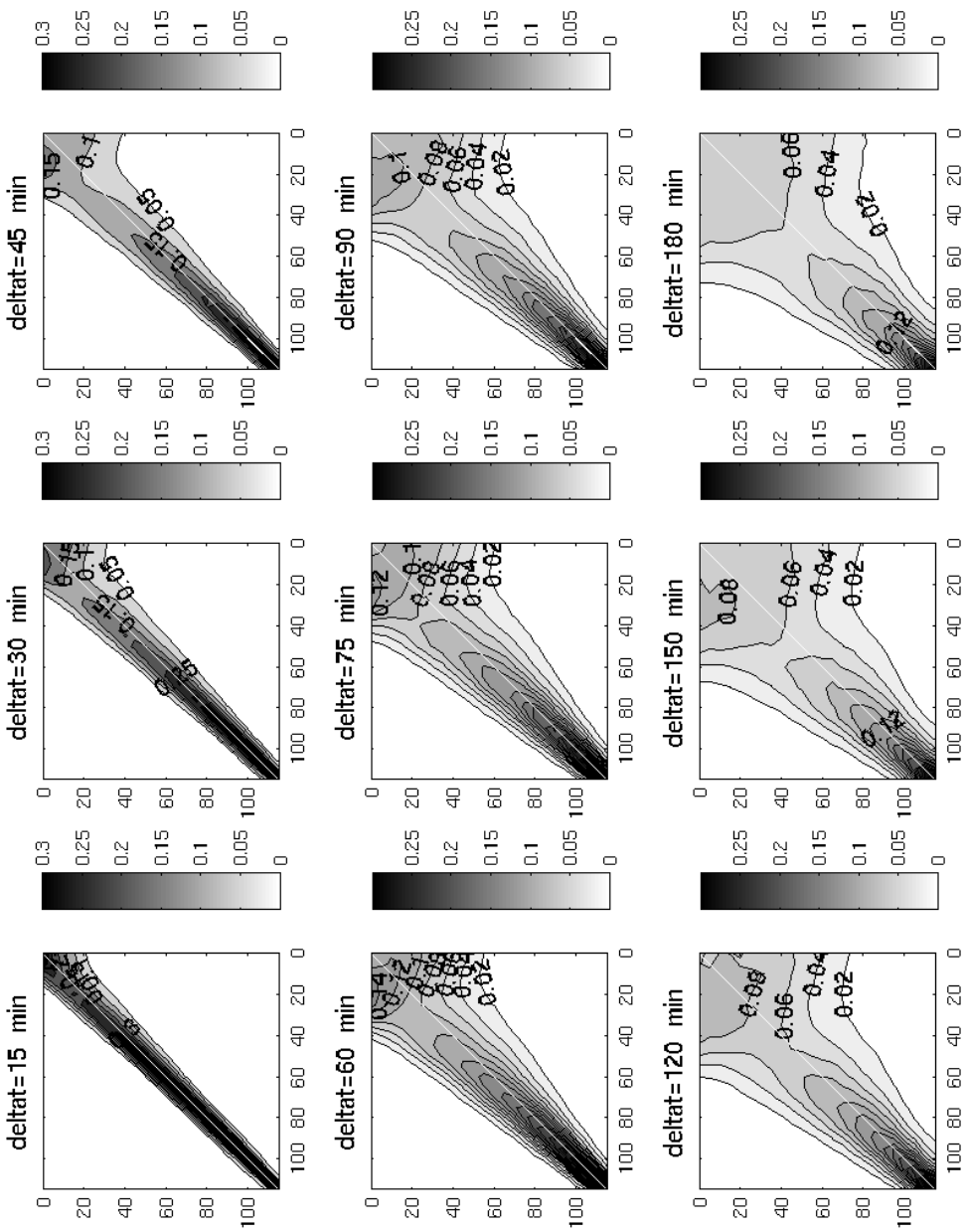

Figure 5.12: Contour plots of a family of transilient matrices computed for the LES Langmuir case, with increasing Δt.

Chapter 6

Photo-physiological Individual Based Model for Phytoplankton Moving in the Ocean Mixed Layer

In this chapter a coupled model of interaction between the dynamics of the Ocean Mixed Layer (OML) and the photo-physiological responses of phytoplankton is described together with the analysis of the results. The model has an Individual Based architecture: the phytoplankters are considered as single entities that react to the perceived irradiance with the adjustments simulated by the updated model presented in chapter 4. The light perceived by the individuals derives from simulated trajectories of passively buoyant particles released in the two LES simulation of the OML presented in section 5.2. An additional simulation is performed with trajectories mimicked with a random walk technique (described in details in section 5.1). This supplementary simulation is conducted to compare the results of the two innovative numerical experiment with a more "classical" approach.

The scope of this study is to analyze the emerging properties of a complex system, simulated with mechanistic equations that reproduce the most important responses of phy-

toplankton when subjected to a dynamical irradiance regime. The question that is at the basis of this work is: how much the photo-physiological flexibility can modify the growth rate in the natural environment? This is a first attempt to quantify the impact of physiological plasticity on the survival effort of a phytoplankton community in realistic mixing conditions. For this reason a mechanistic photo-physiological model able to simulate the major responses that are considered the most important in determining the growth performances of marine phytoplankters have been developed. This advanced photo-physiological model has been coupled with a representation of the dynamics of an oceanic water column that is, currently, the best possible.

The results of the simulations are analyzed in terms of mean properties and distribution of probability inside the individuals. The individuals, in fact, are subjected to different light histories and this modifies the photo-physiological properties of each individual. The probability distribution functions of the characteristics of the individuals are analyzed, together with the average emerging results. These results are linked to results obtained from the lagrangian statistical analysis of the LES simulation (see section 5.4).

6.1 Model Description

In section 6.1.1, the adaptation of the photo-physiological model to the IBM *phylosophy* is described together with the coupling techniques developed to mimic the motion of individuals in the LES model. The parameters chosen for the description of the physiological state of a phytoplankton population, have been derived from *in situ* primary production measurements performed in the North-western Mediterranean Sea during a spring Cruise in 2003 (the technique is described in section 6.1.2). In section 6.3 a new diagnostic tool, developed to study the interaction between the turbulent motion and the phytoplankton response, will be presented. In fact, the transilient turbulent theory (see section 5.3.2), has been extended to cope with the photo-physiological "reaction" connected to the turbulent

motion. A powerful method to study the mixing properties of a fluid has been extended to map and analyze the photo-physiological characteristics of individuals subjected to similar displacements.

6.1.1 Individual Based Model Description

The photo-physiological model (described in chapter 4) has been adapted to the simulation of the responses of individual cells. The IBM simulations are structured in a way that each individual represents a group of cells. Since it is not computationally feasible to have an IBM with as many individuals as phytoplankters in the mixed layer, each entity is considered representative of a certain number of phytoplankters. It is important to find a good balance between the time required for the simulations and the representativity of the system, so that the individuals are enough (order $10^3 - -10^4$) to be statistically significant.

All the individuals simulated in the IBM modify their photo-physiological and biochemical properties following the same equations and the same parameters. Therefore, the differences observed between them only depend on the different light history. For this reason the model can be considered an *hybrid* IBM. Generally, in IBMs the individuals are differentiated in some way, whereas, in this case, they are all identical and respond to the same mechanistic laws.

In the IBM architecture, the equations are modified so that the state variable C represents the carbon content of the individuals in terms of pgC cell^{-1}, thus substituting the concentration of phytoplankton carbon in a homogeneous solution (mgC L^{-1}) for the bulk architecture. In addition, each individual is characterized by a $chla : C$ ratio (θ^C), a N:C ratio (Q), a number of damaged reaction centers (ϑ_c), and a functional cross section of the PSIIs (σ_{PSII}) that react to the perceived irradiance such as in the bulk model, but they have to be intended in an individual form.

The individual variables together with the irradiance define the photosynthetic rate and,

then, the carbon growth rate of the virtual cells by integrating the equations expressed in table 4.1, section 4.1. The properties of each entity are tracked and memorized each time-step into a matrix. The code has been structured so that each physiological variable is an element of a matrix with n_{cells} columns and t_{end} rows.

n_{cells} is the number of individuals in the simulation and t_{end} is the number of time steps of the simulation. A subroutine solving the equations with the forward Euler method is called each time step t for each individual i. Inputs of the subroutine are the values of the variables saved in the ith row and in the column $t-1$, together with the irradiance perceived by the ith individual at the time step t and the nitrogen external concentration. The outputs of the subroutine, that are the solutions of the equations for all variables, are then saved in the ith row and in the column t of the corresponding matrix.

With this structure it is possible to follow each variable of the individuals during the simulation.

The IBM considers also the possibility for the cells to divide or die, as time goes by. The division process is governed by the carbon content of the individuals: if an individual passes a threshold value for the carbon content the division process takes place. The threshold has been chosen to be the double of the starting carbon content for all cells at the beginning of the simulation. In all the simulations the cells start with 10 pgC cell^{-1} so they divide when they overcome the threshold of 20 pgC cell^{-1}. This approach is quite innovative and has been previously used in the lagrangian IBM presented in Cianelli et al. (2004). Previous IBMs for phytoplankton the division was never considered to act at the level of individuals (see section 3.2.2). In practice, the technique commonly adopted is to increase the number of cells, and therefore the amount of carbon, that each individual represents, thus ignoring the different phate of the daughter cells. However, in the turbulent nature of the real ocean, if two particles splits when the distance between them exceeds the Kolmogorov scale, the intrinsic chaotic nature of the system produces two distinct trajectories. This behaviour

has been confirmed by the lagrangian statistical analysis performed on the LES trajectories (section 5.4.1). If a constant number of individuals is used, this process is totally neglected. Using LES derived trajectories, as for this study, it is important to consider the effect of the separation of the trajectories derived from the direct solution of the eddies containing the large part of the energy. The distance between individuals which start close to each other increases with time.

For this reason an individual that passes the threshold of carbon content splits into two individuals separating on different trajectories. The two new individuals will keep the physiological properties of the *mother*, but they will possess half of the carbon content of the mother. In the matrices of each variable a new row is occupied by one of the new entities, while the other one occupies the row of the mother.

The simulations begin with the particles uniformly distributed in the water column. Each particle has assigned its own trajectory. The latter is selected among the trajectories of the passively buoyant particles released in the LES. The vertical position in the water column affects the light intensity perceived each time step by the individuals, as will be explained below. The Large Eddy Simulations covered one day, but the IBM simulations covered ten days of spin-up of the IBM followed by two days of realistic simulation with division and death of the individuals. The initial ten days were aimed at acclimating the cells to the dynamic environment.

To obtain trajectories over 12 days with just one day of simulations I did the following: at the end of each day of simulation each particle was relocated to the closest starting point of the ensemble of trajectories generated by the LES. Therefore the trajectory k was chosen when the *distance* (D) between the initial point k $(x_1(k), y_1(k), z_1(k))$ of the trajectory and the the position of the ith particle at the end of the day $(x_{24}(i), y_{24}(i), z_{24}(i))$ was at minimum, with D defined as:

$$D = \sqrt{(x_{24}(i) - x_1(k))^2 + (y_{24}(i) - y_1(k))^2 + 33\ (z_{24}(i) - z_1(k))^2} \tag{6.1}$$

Eq. 6.1 is similar to the euclidean distance between two points, but a larger weight is given to the vertical dimension in order to avoid an unrealistic abrupt change of light intensity.

The same rule was adopted to choose the trajectory for one of the daughter cells. In fact, one daughter keeps the trajectory of the mother, the other follows the trajectory (not already used by another individual) that occupies the nearest position during the same time of the day.

During the simulation the individuals died at random. A fixed mortality rate was used. It represents the percentage of cells dying during one day. In practice, the control parameter was the time interval between two death events (t_d). As the number of cells changed due to division and mortality, t_d changed accordingly. The calculation of t_d was made only after each death, because it slowed down the simulation, without any specific advantage. When the number of cells overcame a certain threshold, indeed, for each time step an individual or more died so that the number of alive cells was updated only when a death occurred.

The time course of the proximate factors (light and nitrates) affecting phytoplankton growth was simulated as follows.

The nutrient concentration in the water column, was considered constant and equal to 100 μgN L^{-1}. This value is representative of the nutrient concentration observed during the cruise, when the data used to fit the parameters of the model were collected. The simplification of considering nutrient replete conditions is motivated by the need of distinguishing among the responses due to the dynamical regime of irradiance from those due to nutrient availability. In addition, a condition of high mixing, as that simulated in the physical model, is hardly nutrient limited, because the turbulent motion refuels the upper layer.

The variation of irradiance perceived by the virtual cells, is determined by two factors:

the changes of surface irradiance due to the varying inclination of the sun (diel cycle) and its attenuation along the water column.

The irradiance reaching the surface of the sea follows the equation:

$$E_0 = E_{max}\ (\sin\phi\ \sin\delta - \cos\phi\ \cos\delta\ \cos\omega) \tag{6.2}$$

where E_{max} is the maximum incident irradiance, ϕ is the latitude, δ is the sun declination and ω is the hour angle. δ and ω change respectively for the day of the year considered and for the time of the day. The variations due to meteorological conditions such as clouds were not considered.

The surface irradiance was attenuated along the water column from the medium itself and from dissolved and suspended matter. The irradiance that ith particle was perceiving at the time t is given by the following equation:

$$E_z(i,t) = E_0(t)\ \exp\left(-k_w\ z(i,t) - k_{Chl}(t)\right) \tag{6.3}$$

where $E_0(t)$ is the solution at time t of equation 6.2, k_w is the diffuse attenuation coefficient for the water, $z(i,t)$ is the vertical position at time t of the ith particle expressed in metres from the surface and k_{Chl} represents the attenuation due to the biogenic content absorbing light from the surface to the depth of the particle, that, in turn, follows the equation:

$$k_{Chl}(t) = k_c \sum_{\zeta=0}^{z(i,t)} Chl(\zeta,t)^b \tag{6.4}$$

with k_c the attenuation coefficient due to the $chl\,a$ alone. The other member on the right represents all the chlorophyll that overlie the individual. $0 < b < 1$ is an empirical coefficient due to the non-linear relationship between absorption and chlorophyll content. The $chl\,a$ content in the water column was calculated each time step, taking into account the number of cells represented by the individuals per each layer multiplied by the $chl\,a$ content of each particle. The equations and the values of the parameters for the calculation of the attenuation of irradiance in the water column, have been derived from Morel (1988).

In the next section the procedure followed for the derivation of the initial photophysiological parameters is described.

6.1.2 Photo-physiological Model Setup

The parameters for the photo-physiological equations, have been derived by two $P^{chl}vs$ E curves. The experiments were conducted during a cruise in the North-western Mediterranean Sea in March (Imma Santarpia, Stazione Zoologica 'A. Dohrn', personal communication). Primary Production measurements were carried out with the ^{14}C-labeled carbonate technique. The incubations lasted one hour and a half. The $P^{chl}vs$ E curves chosen for the parameterization, correspond to the samples taken at surface and at 20 min a station located along the North Balearic front, where $chl\,a$ and nutrient rich water meets less productive water (Daniele Iudicone, Stazione Zoologica 'A. Dohrn', personal communication). Those curves were chosen because they had the same coefficients at the two depths, suggesting that the photo-physiological status was the same. This, in turn, makes me hypothesyzing that the water column was actively mixed or was recently mixed. The physiology of this community, acclimated to a mixing regime, was used as the starting point for the parameterization of the individuals in the IBM. The derivation was carried out as follows.

First of all, the classical formulation of the $P^{chl}vs$ E equation, not considering photo-

inhibition of Platt et al. (1980):

$$P^{chl} = P^{chl}_{max} \left[1 - \exp\left(\frac{-\alpha^{chl}\, E}{P^{chl}_{max}}\right)\right] \tag{6.5}$$

was rewritten in terms of the parameters considered in the model for the steady state solution:

$$P^{chl} = \frac{n_{chls}}{\tau} \left[1 - \exp\left(-\sigma_{PSIIs}\, \tau\right)\right] \tag{6.6}$$

where the subscript s indicates the steady state values.

The steady state solution for the fraction of functional reaction centers $\vartheta^a_s + \vartheta^b$ (eq.6.7, as derived by Han (2002)) was then added to eq.6.6 as a multiplicative factor of the number of reaction centers (n_{chls}).

This because the P^{chl} *vs* E data are affected by photo-inhibition and the real number of reaction centers that participate to photosynthesis is given by the sum of the opened and closed ones in the Han (2002) model.

$$\vartheta_{as} + \vartheta_{bs} = \frac{1 + \sigma_{PSIIs}\, E\, \tau}{1 + \sigma_{PSIIs}\, E\, \tau + K \left(\sigma_{PSIIs}\, E\right)^2\, \tau} \tag{6.7}$$

where K is the ratio between the constants of damage and repair of the D1 protein.

For similarity with the classical solution for P^{chl} *vs* E curves considering photo-inhibition by Platt et al. (1980):

$$P^{chl} = P^{chl}_{max} \left[1 - \exp\left(\frac{-\alpha^{chl}\, E}{P^{chl}_{max}}\right)\right] \exp\left(\frac{\beta\, E}{P^{chl}_{max}}\right) \tag{6.8}$$

The equation 6.5 was rewritten, after some transformations and the addition of the multiplicative factor that indicates photo-inhibition (eq. 6.7), in the following form, with the photo-inhibition to the right:

$$P^{chl} = \frac{n_{chls}}{\tau} \left[1 - \exp\left(-\sigma_{PSIIs}\, \tau\, E\right)\right] \left[\frac{1 + \sigma_{PSIIs}\, E\, \tau}{1 + \sigma_{PSIIs}\, E\, \tau + K \left(\sigma_{PSIIs}\, E\right)^2 \tau}\right] \tag{6.9}$$

The final equation has 4 parameters to be determined: σ_{PSIIs}, τ, n_{chls} and the constant K.

They were derived through a non-linear fitting computed with the MATLAB build-in function *fitfun*, that execute optimal fitting of non-linear functions to a set of data. '*fitfun* uses an implementation of the Nelder and Mead simplex (direct search) algorithm, to minimize a nonlinear function of several variables (Lagarias et al., 1998).

The parameters estimated correspond to the steady state solution of the equations used in the model, though redrawn for the solution of the P^{chl}*vs* E curves instead of the P^{C}*vs* E curve represented in the model. The assumption behind the estimates is that phytoplankton had reached the steady state during the incubation time. It means that, for what photo-inhibition concerns, they were fully adapted to the irradiance perceived at the end of the incubation. In other words the prerequisites for the procedure were that the incubation was not too long to modify the pigment-related properties, but was long enough to reach the steady state with the incubation irradiance for what photo-inhibition concerned.

The extrapolation of the parameters necessary for the simulations required other operations.

First of all it is was necessary to derive the k_d and k_r constants from its ratio K. This operation was carried out by looking at the proper couple of constants that reached, in dynamical simulations, the steady state with all the incubation irradiances within one

hour and half from the start of the incubation, using the other parameters derived by the non-linear fitting (not shown).

The results of all the operations were the parameters for the proper fitting of the $P^{chl}vs$ E curves: σ_{PSIIs}, τ, n_{chls} and the constants for the damage and repair k_d and k_r.

The last parameter to derive was the value for the the steady state of θ_s^C to transform from n_{chls} in n_{cs} and to find out the value for the pigment quota $chla : C$ associated with the estimated σ_{PSIIs}. Those two parameters were respectively involved in the equations 4.1 and 4.4 reported in table 4.1 at page 113.

The value for the θ_s^C was derived through iterative simulations of the IBM. In practice, a first simulation was performed using a first θ^C as θ_s^C to complete the estimate of the parameter for the simulations. This θ^C was the steady state solution of a simulation performed with the bulk architecture of the model at the mean daily irradiance in the simulated mixed layer. The depth of the mixed layer was estimated from the eddy diffusivity profiles derived from the lagrangian statistic analysis of the LES Langmuir simulation (see section 5.4.1).

The value was taken as a starting point for the definition of the θ_s^C. With that value, a first simulation with the IBM with the trajectories derived by the LES LANG simulation, was carried out. In such simulations mortality and division were not considered. The individuals moved in the water column and were let to adapt to the dynamic light regime. Iteratively, the daily average $chla : C$ ratio of the individuals at the end of the simulation θ^C was used to recompute the n_{cs} and the initial value for the θ^C to be coupled with the initial value for the $\sigma_{PSII} = \sigma_{PSIIs}$. The iteration was repeated until the daily average $chla : C$ ratio derived at the end of the simulation converged with the θ_s^C. The final value θ_s^C was then used as initial condition for the variable θ^C and to calculate the n_{cs}, necessary to derive the P_{ref}^c in equation 4.1. In equation 4.4, the value of $\sigma_{PSII}$and θ^C, used as the reference value $\sigma_{PSIIref}$ and θ_{ref}^C were, for each integration step, the value of the previous

time step.

The value of the above parameters depend on the irradiance field that the individuals perceive during the simulation. Experiments conducted in this study, whose setup will be described in section 6.2, belong to two set of simulations, differentiated for the initial chlorophyll concentration. The second set, via the modification of the attenuation of light in the water column, changed the irradiance field perceived by the organisms. Moreover, each set of simulations required an extrapolation of parameters through the technique explained above. In fact, the physiology represented in the IBM was chosen in order to reproduce the primary production of organisms subjected to an irradiance field.

6.2 Simulations Description

As already mentioned two sets of simulations were performed with the photo-physiological Individual Based Model. The two sets are different for the initial concentration of chlorophyll in the mixed layer. The first set of simulations had an initial homogeneous concentration of chlorophyll of nearly 0,01 mg $chla$ m^{-3}. The amount of chlorophyll was calculated by dividing the domain in bins one meter thick and counting for the sum of the $chla$ content of the phytoplankters represented by the individuals in each layer. The second set of simulations was performed by modifying the initial number of individuals and the number of phytoplankter that each individual represented so that the initial homogeneous chlorophyll concentration was ten times higher than for the previous set of simulations (about 0,1 mg $chla$ m^{-3}). This dual set of simulations was performed in order to test the responses to different light profiles in the mixed layer. In fact, an higher concentration of chlorophyll, as for the second set of simulations, produces a greater variability of irradiance for the individuals, in respect to the first set, even if they are subjected to the same mixing. The more realistic simulation is that with a lower concentration of chlorophyll, considering that the oceanic scenario that we were simulating was, in general, not eutrophic.

For the two simulated conditions, the parameters were derived and reported in table 6.1 and 6.2 at page 184.

The last iterative simulations, performed to estimate the average θ^C to use as initial condition, can also be considered as the spin up for the IBM that used the trajectories derived by the LES simulation in the Langmuir case.

The spin up was performed in this way: for 10 days the initial individuals were moved in the water column and their photo-physiological and biochemical characteristics were modified to let them adapt to the dynamical condition. The carbon growth was considered equal to zero as well as the mortality rate, so that the individuals were not growing and die in those days. During that period the average of the variable θ^C changed during the day, but at the end of the period, the trend of the variable was stable.

At the end of the 10 days of stable condition, a control was performed to ensure that the simulated conditions corresponded to the reference $P^{chl}vs$ E curves. This control as well as the simulations to define the θ^C_s as initial and stationary condition to determine the n_{cs}, were computed for both the $chla$ concentration for the simulation that uses the trajectories derived by the LES that reproduce also the Langmuir circulation. This simulation of the mixed layer is considered the more realistic and the reference simulation for the extrapolation of the parameters.

The control was performed in this way: the individuals present at 10:00 in the first five meters and between 20 and 25 meters of the water column were selected. Those individuals were virtually incubated under 161 irradiances, between 0 and 1600 µEinst $m^{-2}s^{-1}$ After the simulation of the photosynthesis *vs* irradiance incubation, the bulk growth in carbon performed at each irradiance was calculated. The fixed carbon was normalized by the $chla$ concentration from the sum of the $chla$ content of the cells represented by the selected individuals.

After these operations, the simulated $P^{chl}vs$ E curves were compared with *in situ* data

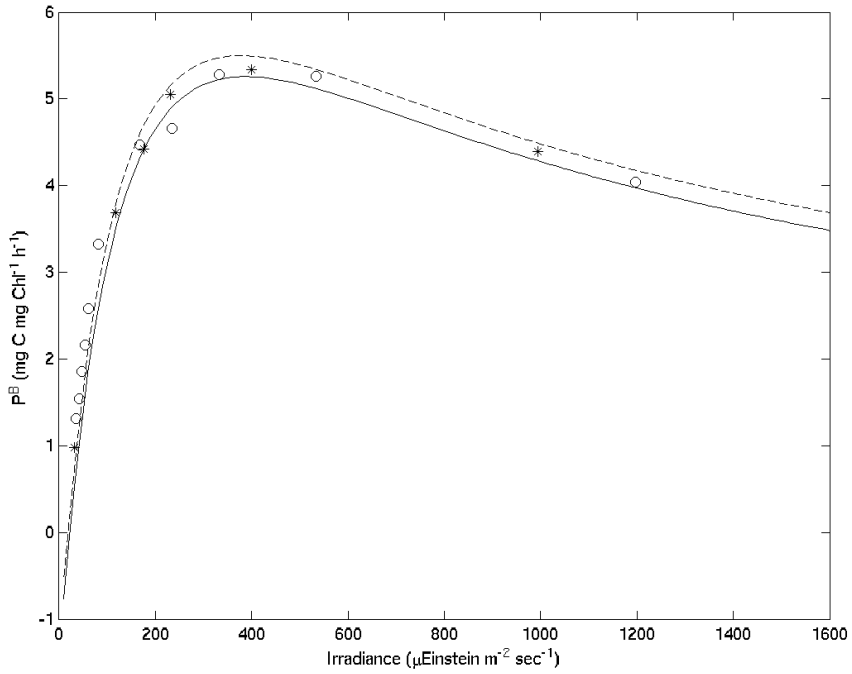

Figure 6.1: The P^{chl} *vs* E curves derived from simulations of incubation in comparison with the data used to parameterize the IBM: the continuous line represents the 0 m simulated incubation, the dashed line the 20 m incubation; the asterisks correspond to the data of incubations performed on the 0 m water sample, the open circles to the data of incubations performed on the 20 m sample. Data show a higher homogeneity respect to the two curves, but the trend of increasing α^{chl} in the deeper sample is confirmed by the simulations. The difference of the simulated curves will be clarified with the discussion of the results that will be carried out in section 6.4.1. However the trend was confirmed and the simulated P^{chl} *vs* E curves produced results comparable with real data.

selected for the extrapolation. The results (fig. 6.2), show that simulations are consistent with *in situ* data and the realistic simulation can be considered as a starting condition as near as possible to the observations.

The 10 days spin-up simulation, with the parameters derived from the iterative LANG simulations, was the starting point for all the realistic simulations, conducted with division and mortality enabled. The realistic simulations, whose results will be discussed and analyzed in section 6.4, lasted two days. Most of the results here presented correspond to

the last of this two days of realistic simulation.

It is important to summarize the simulations that are discussed and to give each of them an acronym to refer to them in order to make clear the analysis that follows.

Two set of simulation were performed, with two initial conditions for the homogeneous $chla$ initial condition.

The simulations performed starting from about 0,01 mg $chla$ $m^{-3}$are called:

- LANG1: the simulation that conducted with the movement of the individuals simulated with trajectories derived from the simulation with LES that reproduces the Langmuir circulation,
- EKM1: the simulation where individuals move with trajectories derived from the simulation with LES that reproduces only the wind-driven Ekman turbulence,
- RW1: the simulation which uses a random walk approach, that uses the eddy diffusivity profiles derived from the LES without Langmuir cells parameterization, to mimic the movement of the individuals in the water column.

The simulations that use the same representation of movement for the simulated phytoplankters, but immersed in more turbid water with an initial concentration of chlorophyll ten times higher, are called respectively LANG2, EKM2 and RW2.

The RW1 and RW2 were both implemented with the characteristics presented in section 5.1: the eddy diffusivity profile derived from the LES EKM simulation was smoothed with a cubic spline, forced to produce first derivative of the profile equal to zero at boundaries. This operation was made using a MATLAB library for setting up and evaluating splines [1], based on the methods found in De Boor (2002).

The simulations were performed with the forcings and the technical details explained above, with the parameters derived by the fitting method presented in section 6.1.2, using

[1]developed by John Burkardt and available at `http://www.scs.fsu.edu/~burkardt/m_src/spline/spline.html`

Constant	Value	source
n_{chls}	1,66e^{-5} mg C mg $chla^{-1}$	non-linear fitting
τ	5,80e^{-3} s	”
θ_s^C	0,0421 mg $chla$ mg C^{-1}	iterative simulations
n_{cs}	6,97e^{-7} mg C mg C^{-1}	non-linear fitting and iterative simulations
σ_{PSIIs}	1,60 m^{2}µEinst^{-1}	”
k_d	6,00e^{-7} d.l.	non-linear fitting and simulation control
k_r	9,23e^{-4} s^{-1}	”
Q_{max}	0,05 mg N mg C^{-1}	(Flynn et al., 2001)
Q_{min}	0,2 mg N mg C^{-1}	”
S	0,236 d.l.	”
$shape$	0,01 d.l.	”
N_{cost}	3,21 d.l.	”
θ_{max}^N	0,389 mg N mg $chla^{-1}$	”
a	0,627 d.ll	(Bricaud et al., 1998)
k_w	0,027 m^{-1}	(Morel, 1988)
k_c	0,0518 mg $chla^{-1}$	”
b	0,428d d.l.	”

Table 6.1: Constants for the LANG1, EKM1 and RW1 set of simulations.

Constant	Value	source
n_{chls}	1,66e^{-5} mg C mg $chla^{-1}$	non-linear fitting
τ	5,80e^{-3} s	”
θ_s^C	0,0517 mg $chla$ mg C^{-1}	iterative simulations
n_{cs}	8,56e^{-7} mg C mg C^{-1}	non-linear fitting and iterative simulations
σ_{PSIIs}	1,50 m^{2}µEinst^{-1}	”
k_d	8,00e^{-7} d.l.	non-linear fitting and simulation control
k_r	1,11e^{-3} s^{-1}	”
Q_{max}	0,05 mg N mg C^{-1}	(Flynn et al., 2001)
Q_{min}	0,2 mg N mg C^{-1}	”
S	0,236 d.l.	”
$shape$	0,01 d.l.	”
N_{cost}	3,21 d.l.	”
θ_{max}^N	0,389 mg N mg $chla^{-1}$	”
a	0,627 d.l.	(Bricaud et al., 1998)
k_w	0,027 m^{-1}	(Morel, 1988)
k_c	0,0518 mg $chla^{-1}$	”
b	0,428d d.l.	”

Table 6.2: Constants for the LANG2, EKM2 and RW2 set of simulations.

FORTRAN90 codes. The preliminary work for the fitting of the parameters and the tools for the analysis of the outputs of the models (the matrices of the variables and of the forcings described above), were performed with scripts written in MATLAB language.

Before presenting the results of the simulations, the work made to extend the utilization of the transilient matrices, presented in section 5.3.2, to the reactive tracers considered in this lagrangian numerical study, is introduced in the following section.

6.3 Extending Transilient Matrices to Reactive Tracers

In section 5.3.2 the powerful framework of the transilient turbulence theory has been presented and applied in its classical form. In this section a new method based on transilient turbulence theory is presented. Here the method is developed to map the physiological properties of the individuals simulated in the IBM specularly respect to the associated transilient matrix.

The transilient matrix represent the amount of water that has been mixed from a source to a destination. The new transilient matrices, named biological transilient matrices, represent the photo-physiological averaged features of the individuals associated with a selected transfer. In practice, with this method it is possible to recognize the photo-physiological characteristics associated with a certain type of mixing.

These matrices were calculated, for each considered Δt, from dawn to sunset: the coefficients were calculated accounting for all the *jumps* occurred during the period of illumination. The biological transilient matrices, represent the mean daily effect of a certain type of mixing on a determined photo-physiological property.

Being R the biological transilient matrix, r_{ij} the reactive transilient coefficient, z the number of individuals passed from the initial layer j to the destination layer i during a Δt from dawn to sunset, and $\rho(k)$ the property of the kth individual of the z that performed during the day the same jump'. The equation for the biological transilient coefficient r_{ij}

is:

$$r_{ij} = \frac{\sum_{k=1}^{z} \overline{\rho}(k)}{z} \tag{6.10}$$

where $\overline{\rho}$ represents the mean values of the properties ρ during the period between t_0 and $t_0 + \Delta t$ associated with the transfer between the layers j and i. In practice, during a certain Δt, were selected the individuals that were transferred from box j to box i. Then the mean properties of the individuals during the transfer were summed for all the individuals that were supposed to have undergone the same transfer. The average properties of the individuals subjected to the same jump was calculated dividing that value by the number of selected individuals. In addition, to represent the daily averaged properties associated with the transfer from a layer to another, the transilient matrices have to consider all the time steps from dawn to sunset, so the equation 6.10 was applied iteratively and the daily average had to be calculated. The biological transilient matrix gives information about the physiological characteristics of the individuals subjected to the same displacement.

This method is a useful tool to interpret the impact of a certain mixing pattern on the individuals. A further analysis was carried out through the comparison of the biotic response tansilient matrix and the kinematic transilient matrix.

6.4 Results and Discussion

The outputs of the simulations performed with the IBM are analyzed under different aspects. The analysis are conducted comparing the responses of the individuals under the three type of simulated mixing starting from a more detailed comparison of the responses, going to a more synthetical analysis that try to correlate the emergent properties of the simulations to the detailed ones.

The depth dependent averaged properties of the individuals subjected to the three mixing modes are compared for the two sets of simulations for different times of the last simulated day.

Then a more synthetical analysis is presented, comparing the probability distribution functions (PDFs) of the daily averaged properties of the individuals. In fact, the impact of the variability of the light history on the individuals can be synthetically described by the PDFs of the daily averaged properties of the individuals within the actively mixed layer of the water column.

Subsequently the daily averaged properties of the individuals belonging to the upper mixed layer between LANG1 EKM1 and RW1 are compared, these latter and LANG2 EKM2 RW2 are compared too. By this way, the differences originated among different mixing modes in a similar light regime and between different light regimes can be evidenced.

This quantitative comparison of the responses governed by the same physiological mechanistic rules should help us to determine the effect and the impact of photo-physiological adaptations on the average growth performances of the simulated population.

Finally, the application of the biological transilient matrices is presented. This innovative tool is helpful to evidence the mixing mode that can give a growth advantage to the physiologically plastic simulated individuals respect to a theoretical condition of full adaptation to the perceived irradiance.

The results derived from the analysis of such a complex environment represent the basis for the development of more theoretical numerical experiments. These experiments, that will be presented in the next chapter, are necessary to clarify the impact of the phenomenon that the IBM simulations show to be important to determine the performances of the organisms. In other words, in more controlled and comparable conditions, the correlation between mixing and photo-physiological adaptation and their overall impact on the growth performances should come out better.

6.4.1 Photo-physiology in Ekman and Langmuir Turbulence

As already mentioned in chapter 3 mixing in the OML influences the depth-dependence of photo-physiological features of phytoplankton. In fact, the interaction between the kinetic of the photo-physiological adaptations and the rate of mixing occurring in the water column, produce well defined patterns (Lewis et al., 1984a). At the start it could be assumed that, if the rate of mixing is quicker than the kinetic of photo-physiological adaptations, the vertical profile of a certain photo-acclimative character should be flat. On the contrary, if the rate of mixing is slower than photo-acclimation, organisms would adapt to the light intensity perceived at each depth and the vertical profile of a photo-physiological indicator should follow the irradiance profile.

In order to analyze this aspect, the average values of the indicators of the pigment-acclimation and of the photo-inhibitory response for the LANG1, EKM1 and RW1, are plotted against the depth (fig. 6.2 and fig. 6.3). It is important to underline that in this simulation, during the last day, the euphotic depth was similar to the depth of the mixed layer (data not shown).

The profiles of the $C : chla$ ratio for the last day of the simulations (upper part of fig. 6.2) correspond to different times, from 8:00 (two hours after sunrise) to 20:00 (two hours after sunset), with a time interval of two hours. It is evident that during the day, the inital approximately flat profiles, produced by the nocturnal mixing, changed their shape forced by the light intensity. The upper part of the water column, subjected to increasing irradiance, displays a modified $C : chla$ ratio, reaching the highest values at 16:00, i.e., almost two times higher than in the lower part. The last two profiles show that, when irradiance decreased, the discontinuity between the first 30 metres of the water column and the lower part was less pronounced.

It is important to note that, the LANG1 simulation always shows a more homogeneous distribution of the $C : chla$ ratio with depth. The high rate of mixing due to the Langmuir

circulation quickly changed the depth of the individuals and they were not able to adapt to the new irradiance regime, in respect to the individuals subjected to the other mixing. This typical pattern is confirmed, but it is important to note that, during the high irradiance period of the day, the complete homogeneous condition due to mixing is never reached, even if the type of mixing simulated is very high.

Another important evidence, found in intensely mixed layer, is the increased variance among the photo-physiological characteristics of individuals belonging to the same water sample (Dusenberry et al., 1999). If turbulence is high, cells coming from different depths are mixed together at a certain depth increasing the variance between individuals of the same sample.

In the simulations with the IBM, the normalized standard deviation of the $C : chla$ ratio between the individuals at the same depth (lower part of the fig. 6.2) is alway greater for the LANG1 simulations, confirming that higher mixing increases the variance. It is noticeable, indeed, that in the upper part the normalized standard deviation is lower: the individuals in the first 30 meters are more homogeneous during all the day. The layer where the variance increases is just below the euphotic zone ($Z_{eu} \approx 65$ m). This is due to the fact that the limit for the euphotic zone and for the mixed layer (Z_m) are coincident. So this layer can be considered as the convergence zone between the upper individuals with the others trapped in the lower part.

The lower variance in the upper layer, together with the timing of the maximum values found at surface, unravel the reasons for the inconsistency between the expected more homogeneous profiles and the simulated ones. The higher $C : chla$ ratio is found at 16:00 and, as already mentioned, the timing of the maximum response in cells subjected to sinusoidal irradiance regime is around 3-4 hours after the maximum irradiance (section 4.3.4). In addition, the low variability of the upper individuals (expressed by the standard error in the lower part of fig. 6.2), shows that they are all forced by the same trigger.

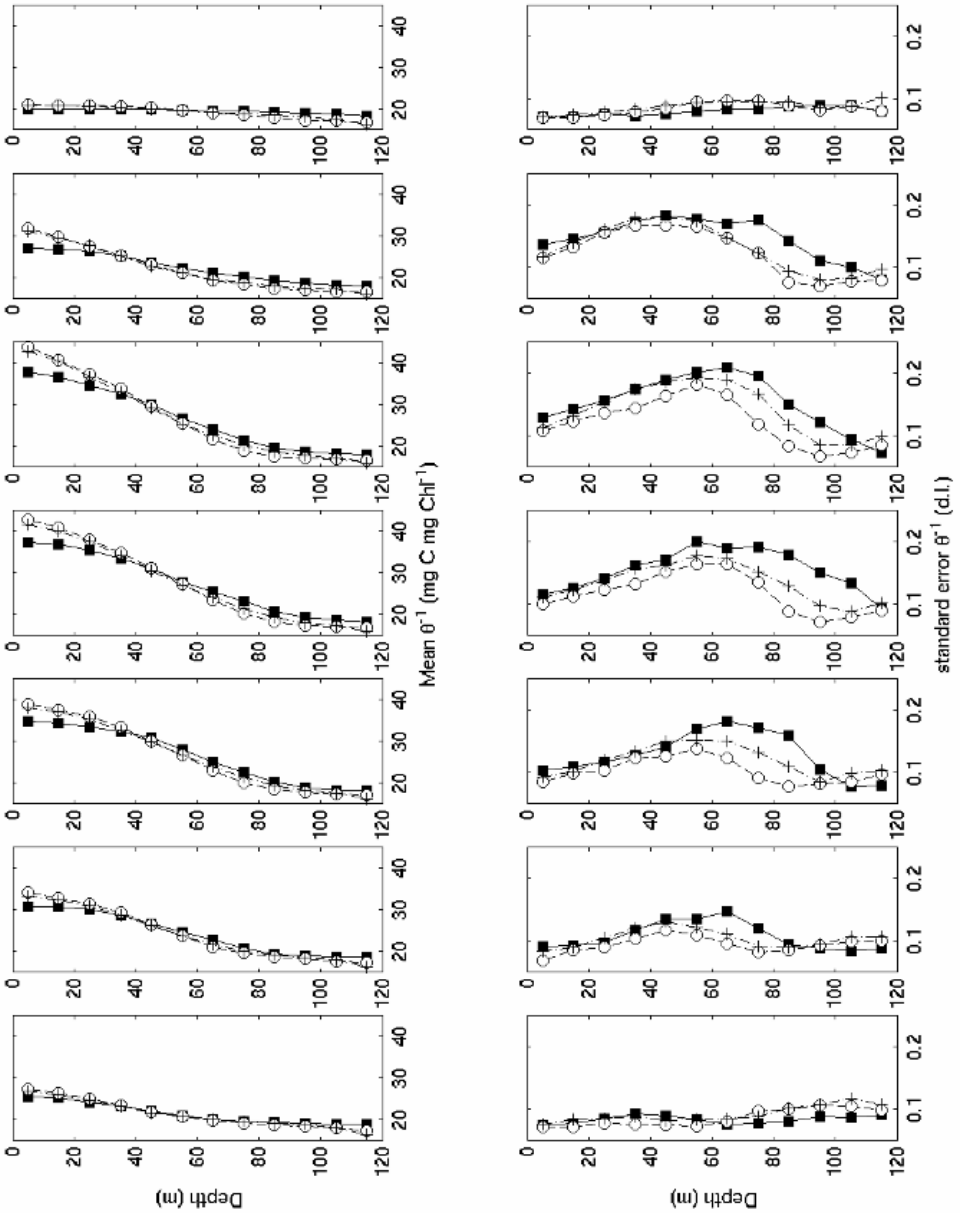

Figure 6.2: Averaged $C : chla$ ratio as a function of the depth upper panels, Standard error of $C : chla$ ratio between individuals lower panels. From left to right the 7 panels correspond to time: 8:00, 10:00, 12:00, 14:00, 16:00, 18:00 and 20:00. Black squares correspond to LANG1, open circles to EKM1, plus to RW1.

For this reason, it is possible to consider the visible photo-acclimative responses in the $C : chl\,a$ ratio in the upper layer as a response to the sinusoidal illumination. It has been already discussed the possibility for the organisms to react to irradiance by increasing or decreasing on a daily base differently from the reaction to increasing or decreasing irradiances because of the depth were they are located. The model used, however, in absence of supplementary evidences, does not discriminate the processes that cause light modification. This phenomenon is at the basis of the results now presented. Its influences on the overall results of the simulations will be analyzed and discussed with supplementary simulations in the next chapter.

The features of the photo-inhibitory response with depth, for the same set of simulations, show no remarkable differences (fig. 6.3). The fraction of photo-inhibited reaction centers mirrors the irradiance profile. The kinetic of the response is quicker than the rate of mixing and cells are fully adapted to irradiance, for what concerns photo-inhibition. The standard error between the individuals is maximum at the base of the mixed layer, and can reach 20 %. The greater variance is again shown by the LANG1 simulation, confirming the influence of the mixing intensity, though limited. The profiles refer to the period between 10:00 and 18:00 and they were calculated with an interval of two simulated hours. The intensity of photo-inhibition is significant, and the greater amount of damage is recognizable after the maximum peak of irradiance. Also photo-inhibition shows a biological hysteresis: the effect of the peak irradiance is prolonged for the later hours. It is important to note that the low values encountered at the deeper layer at 18:00 make noisy the values of the correlated relative standard deviations.

The profiles of the $C : chl\,a$ ratio during LES2, EKM2 and RW2 were homogeneous with depth if compared to the previous set of simulations (fig. 6.4). The less transparent water lets the euphotic zone to reach the 35 meters horizon. The photo-acclimative response is less evident than in the more transparent scenario presented before. In fact the effect

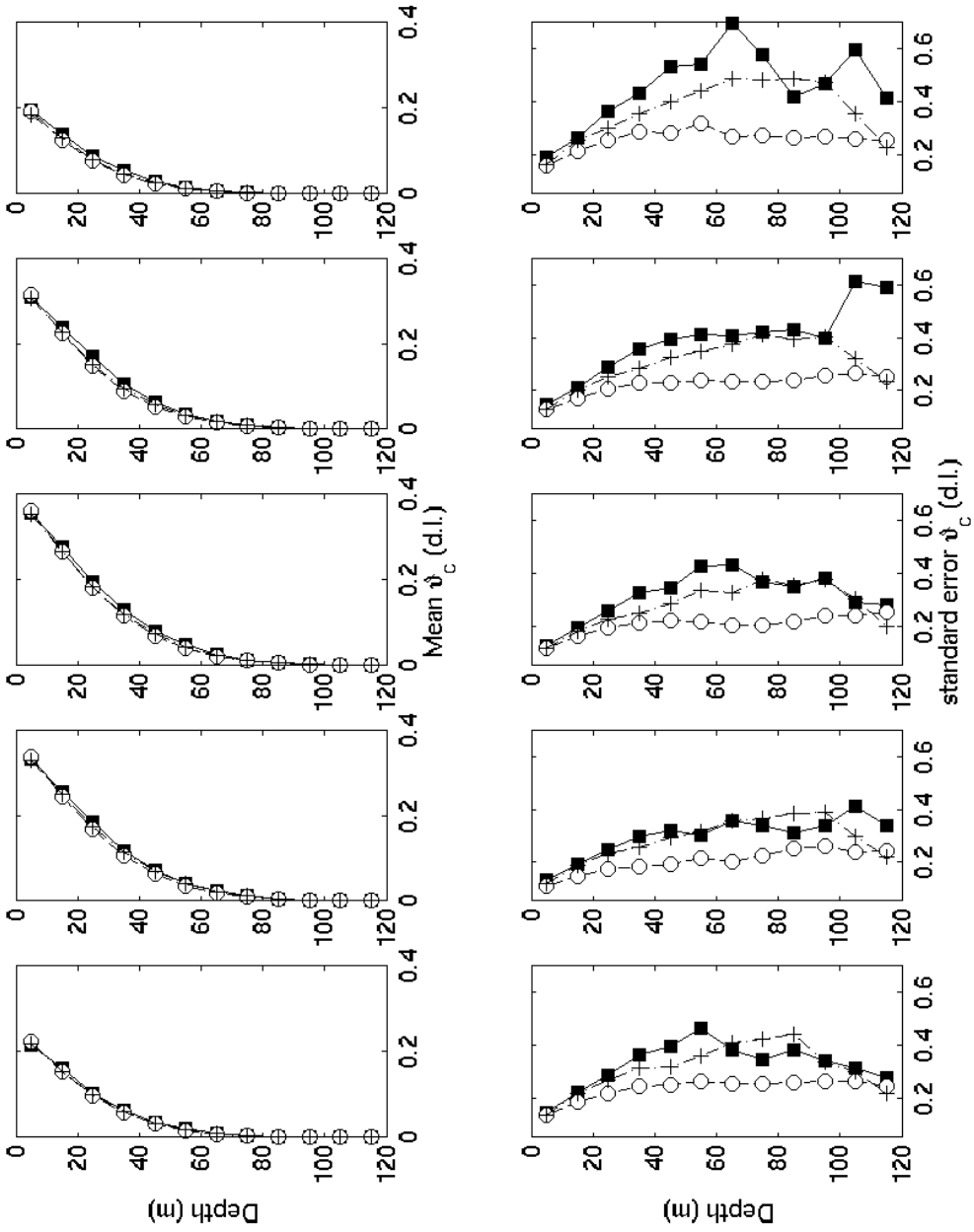

Figure 6.3: Averaged relative number of damaged reaction centers as a function of the depth upper panels, Standard error of the relative number of damaged reaction centers between individuals lower panels. From left to right the 5 panels correspond to time: 10:00, 12:00, 14:00, 16:00 and 18:00. Black squares correspond to LANG1, open circles to EKM1, plus to RW1.

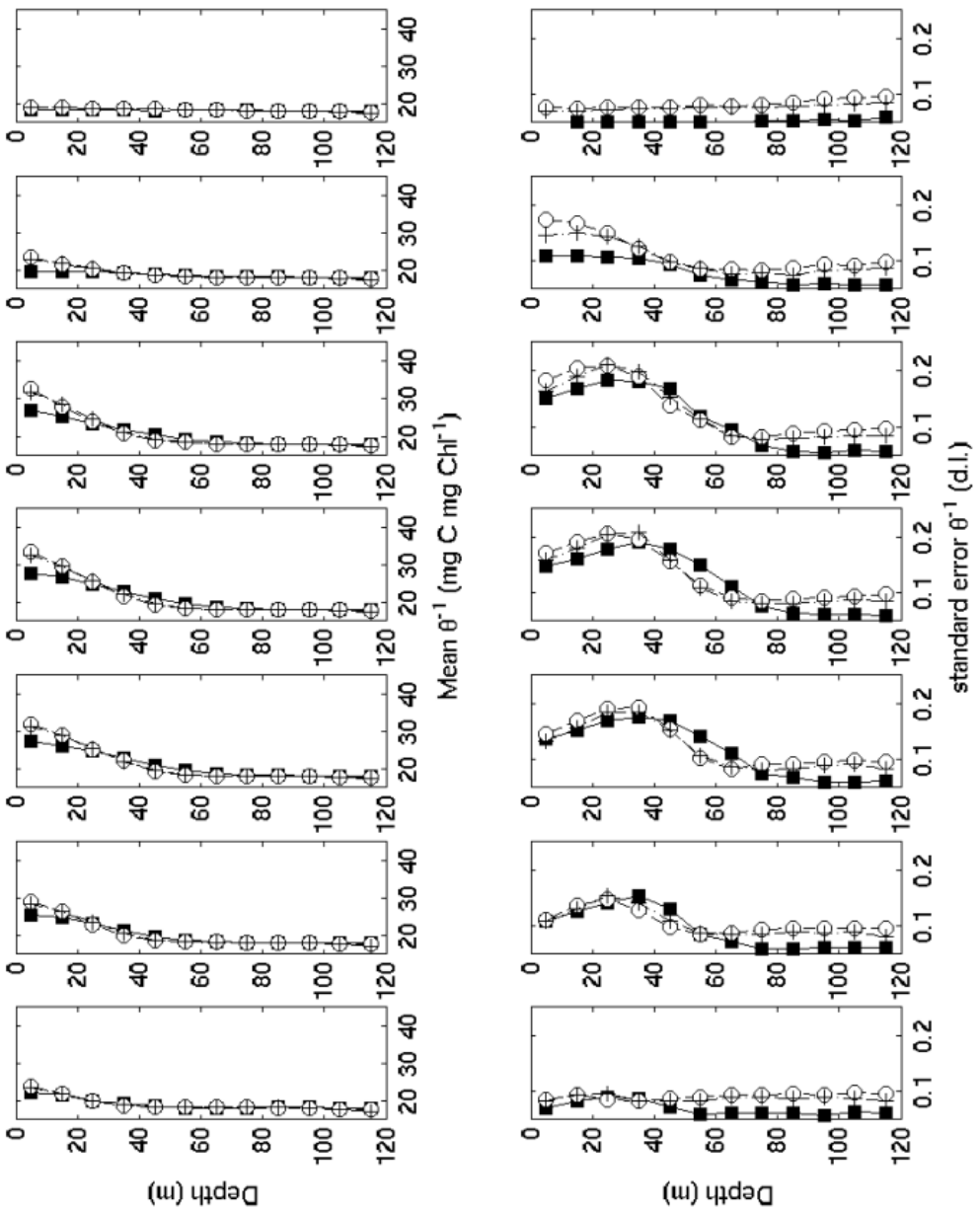

Figure 6.4: As fig. 6.2, but black squares correspond to LANG2, open circles to EKM2, plus to RW2.

connected to the sinusoidal light regime, is less evident and the shape of the LANG2 simulation is practically flat. The kinetic of acclimation, in fact, depends on the irradiance gradient and the sinusoidal gradient is diminished because chlorophyll absorbs light.

As the *sinusoid-related* effect is not important, the effect strictly related to the interaction between the kinetic of response and the rate of mixing is more clear. The high intensity of the mixing homogenizes the pigment related characteristics of the individuals transported, especially if the wind-driven mixing produces the Langmuir circulation.

Unexpectedly the standard error of the LES2 simulation is lower respect to the RW2 and EKM2 irradiance (lower part of fig. 6.4). A hypothesis can be made: the intensity of mixing decreases the light exposure for the cells and their adjustment, so that the individuals have a lower and convergent acclimation kinetic.

In this second set of simulations, the effect of the photo-inhibition decreases together with the light intensity (upper part of fig. 6.5). It is again possible to recognize the euphotic depth from these profiles because they follow the irradiance profiles. It will be shown later, that this instantaneous similar profiles of the photo-inhibitory indicator, is just an aspect of the phenomenon, that on an averaged daily basis behaves differently from one simulation to another.

In this case the noise on the standard error due to the low values of the variable becomes evident only deeper in the water column (lower part of fig. 6.5).

It is important to note, that, by looking at these features of the physiology of the individuals simulated with the three different approaches, no remarkable differences are found between the simulations performed with the random walk approach respect to the LES simulation (EKM1), both in the more transparent and more turbid waters (RW2 respect to EKM2). However, the random walk approach increases the variance of the properties with depth, probably because the fully diffusive and random displacement should overcome the variance due to coherent structures simulated by the LES. It is also possible

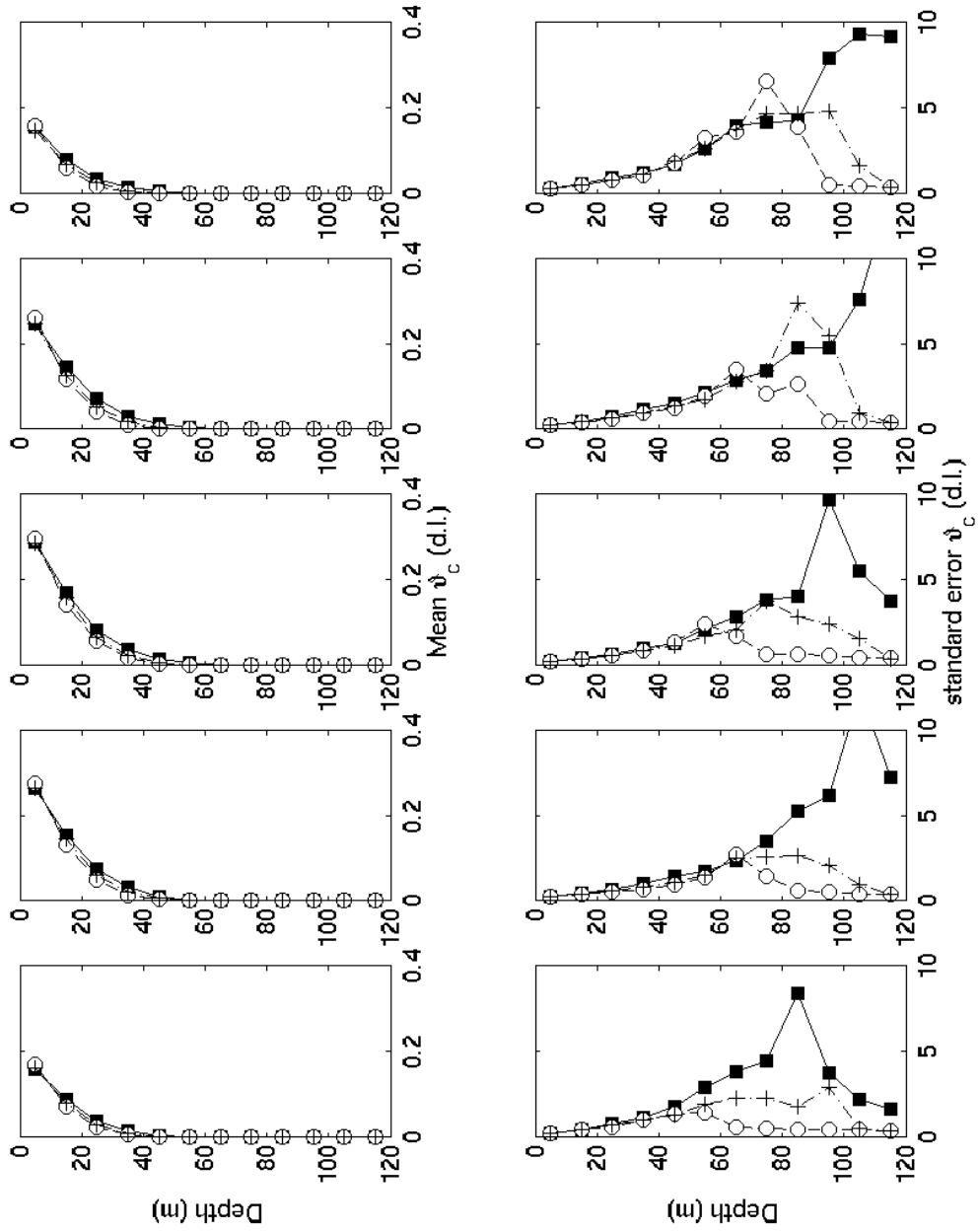

Figure 6.5: As fig. 6.3 but black squares correspond to LANG2, open circles to EKM2, plus to RW2.

that these results are due to the boundaries parameterization or to the gradient of the eddy diffusivity with depth, though all possible expedients to decrease their influence were adopted.

As already mentioned above, the instantaneous vertical profiles of the photo-physiological features of the individuals is just an aspect of the phenomenon. In fact, the variability of the irradiance perceived by each individual during the day may have an effect, that is not visible in the profiles shown before. In order to recognize the variability of the irradiance between the individuals, the mean properties of each individual during the illuminated hours of the last day are calculated for the simulated cells within the upper mixed layer. The PDFs of these averaged properties were then calculated. The PDF shows how much each kind of mixing affects the inter-individual spreading of the properties. So it helps us to recognize the synthetical patterns produced by the different mixing on the individuals.

In figure 6.6 the PDFs of the average irradiance perceived by the individuals during the last day of simulation under the three mixing mode is shown for the set of simulations performed with more transparent water. It is evident that the highest percentage of the individuals perceives a mean irradiance lower than 100 μEinst $m^{-2}s^{-1}$, in all cases. The LANG1 simulation shows a PDF flatter than EKM1 and RW1: there is a higher variability between the mean irradiance perceived by the individuals prone to this kind of non-local mixing. On the contrary, the EKM1 and RW1 PDFs reflect a less variable environment, where the individuals are, on average, subjected to the light vertical profile: the zones at high irradiance are confined within the first meters and are less probable in the spatial domain. Therefore, if the individuals are locally more mixed they likely undergo a mean daily irradiance representative of the zone where they are, because their position during the illumination cycle will vary less than before.

The PDF of the mean daily $chla : C$ ratio of the individuals does not reflect the PDF of the mean daily irradiance (fig. 6.7). In fact, even if the mean daily irradiance of the

individuals of the LANG1 is characterized by higher irradiance, the PDF of the $chla:C$ ratio is shifted towards higher values of the $chla:C$ ratio. Higher values of the $chla$ content are representative of a phenotypic adaptation to a lower irradiance. It is evident that in these dynamical simulations, the impact of the fluctuating irradiance perceived by the individuals, produces a mean result on the acclimation of photo-capture that does not have a direct reference to the mean irradiance experienceded. For what pertains to photo-capture regulation, the time course of the perceived irradiance is more important than its total dose. This pattern maybe related to the effect under fluctuating irradiance of the biological hysteresis of this response. In the next chapter, numerical controlled experiment with a similar irradiance patterns will be discussed to clarify the impact and the nature of that feature.

The mean daily number of damaged reaction centers PDFs of EKM1 and RW1, follows the mean irradiance profile. This means that, if the individuals are subjected to a higher irradiance, they stay at this irradiance enough to be damaged.

On the contrary, the PDF of this variable for the LANG1 does not follow the PDF of the mean irradiance. Again the mode of mixing overcomes the effect due to the mean intensity perceived. In particular, high damage is avoided because of the effect of the relief from photo-inhibition due to the intermittent displacement towards darker depths. An intermediate damage is most likely to occur ($\vartheta_c \approx 0{,}1$) probably due to this intermittent exposure to high irradiances. The interaction between the σ_{PSII} low light acclimated, because of the adaptation of the pigment content to the fluctuating light, and the photo-inhibitory damage is another point that needs further investigation. Looking only at the overall results of those realistic forcings, the influence of that phenomenon can only be hypothesized. The numerical experiments, conducted under fluctuating irradiance (chapter 7), also reveal the impact of the increased cross section on the photo-inhibitive response, due to the light time course.

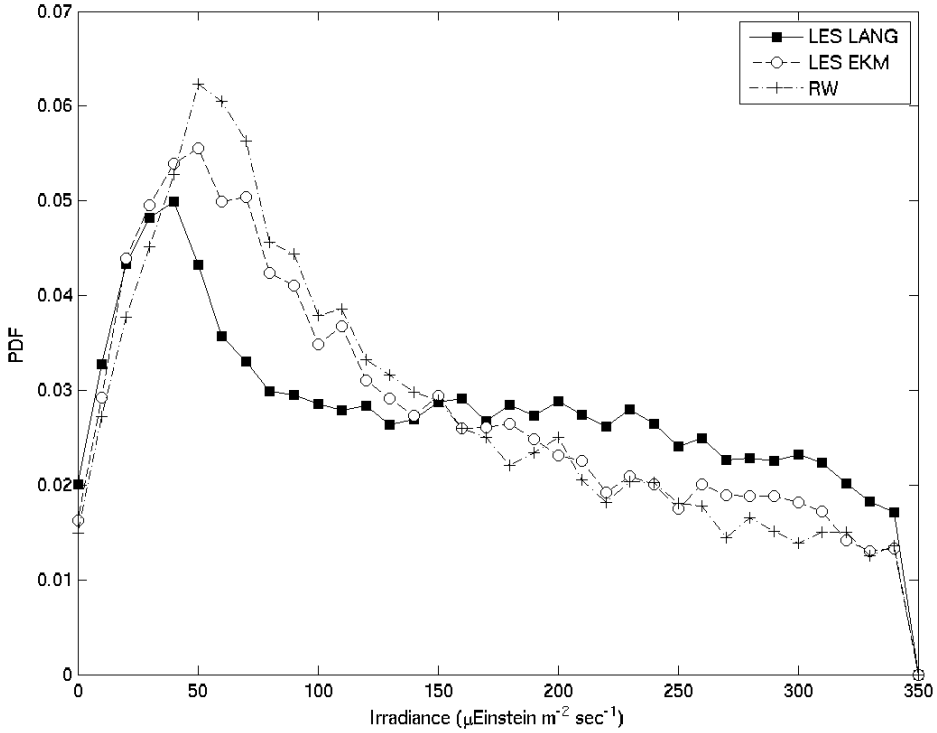

Figure 6.6: PDFs of the daily mean irradiance of the Individuals, black squares correspond to LANG1, open circles to EKM1, plus to RW1.

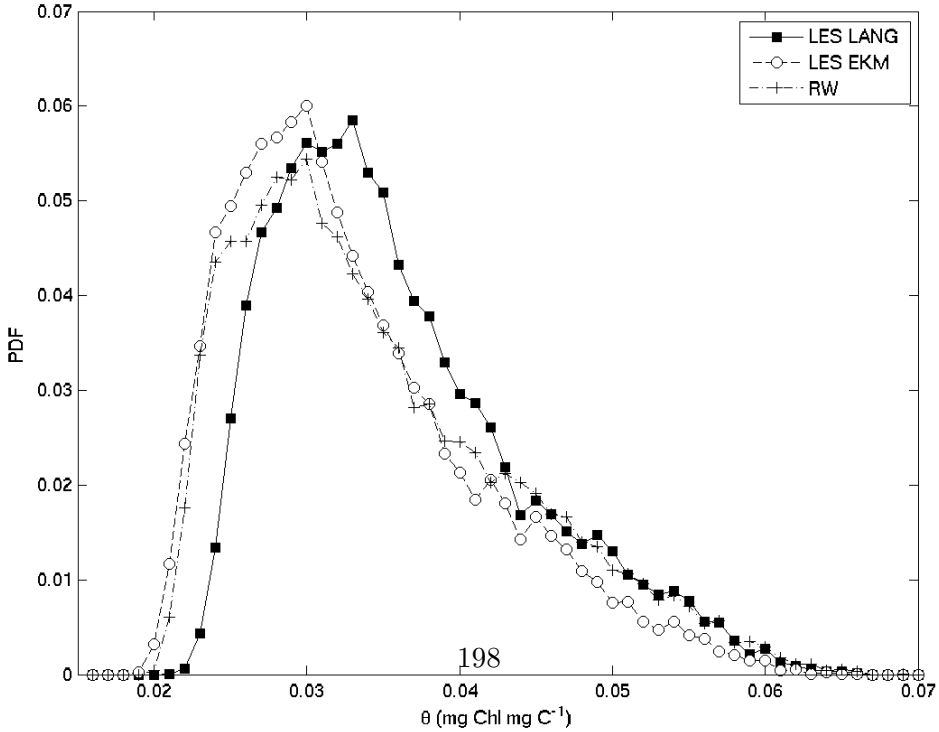

Figure 6.7: PDF of the daily mean $chla : C$ of the Individuals, black squares correspond to LANG1, open circles to EKM1, plus to RW1.

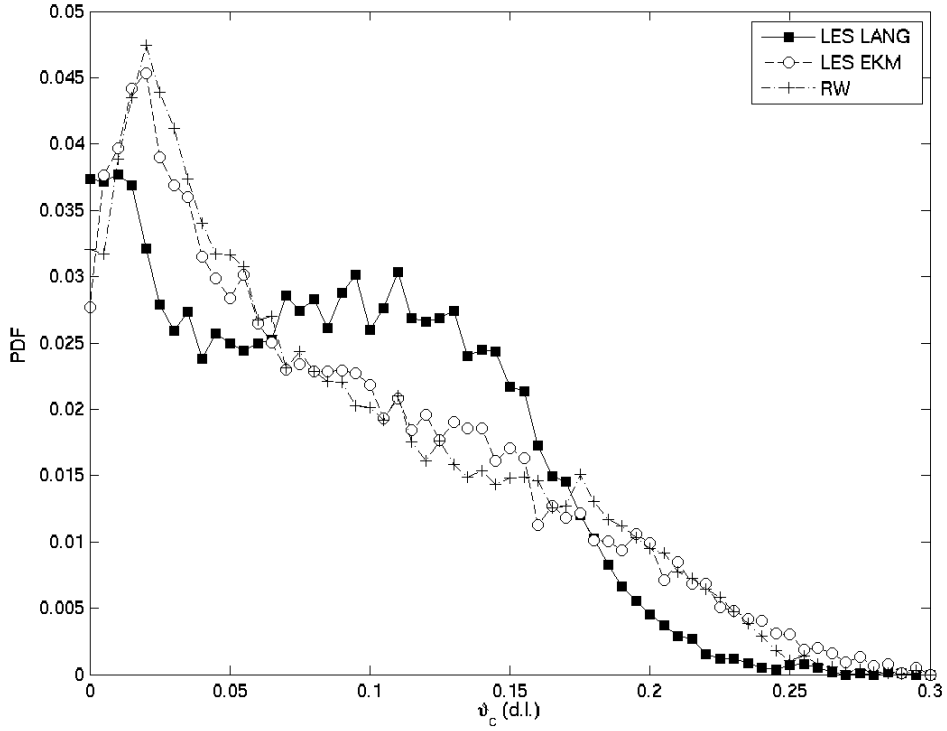

Figure 6.8: PDF of the daily mean relative number of damaged reaction centers of the Individuals, black squares correspond to LANG1, open circles to EKM1, plus to RW1.

The general impact of these environmental conditions, in terms of space-time variability, on the growth performance of the individuals, can be highlighted by analyzing the PDFs of the mean daily carbon growth rate of the individuals for the three mixing modes (fig. 6.9). Surprisingly, no remarkable differences come out. The three mixing modes produce very similar PDFs. Though the mean daily irradiance PDFs of LANG1, EKM1 and RW1 were different, as well as the photo-capture, the markers for photo-acclimation and photo-inhibition, the distribution of the mean daily carbon growth rate for the three simulations are very similar. This result can be interpreted in two ways. First, the photo-physiological adaptation does not influence the growth response at all, with the PDF connected to the mean irradiance. Second, the impact of the photo-physiological adaptations on the growth rate is not nihil. The latter hypothesis is that the photo-physiological responses, in a highly dynamical light regime compensate for the less favorable irradiance perceived by the individuals in LANG1. In fact, the increase in the LANG1 photo-capture and the lower photo-inhibitive effect due to the escape form the photo-inhibitory irradiances should favour the individuals subjected to the Langmuir circulation.

6.4.2 Phytoplanktonic growth in Ekman and Langmuir Turbulence

The impact of the photo-physiological adjustments on growth performance of the individuals subjected to different turbulent environments can be quantified by comparing the mean properties of the mixed layer population of the IBMs (table 6.4.2).

These mean values are calculated computing a first mean on the individuals belonging to the upper mixed layer at each time step of the illuminated period of the last day, thus obtaining a temporal dependent value of the mean properties between all the individuals. Then, a second mean is computed on those values to obtain the averaged value of the selected property for the entire population of individuals immersed in the OML.

From the comparison between the mean properties of the simulations with the same

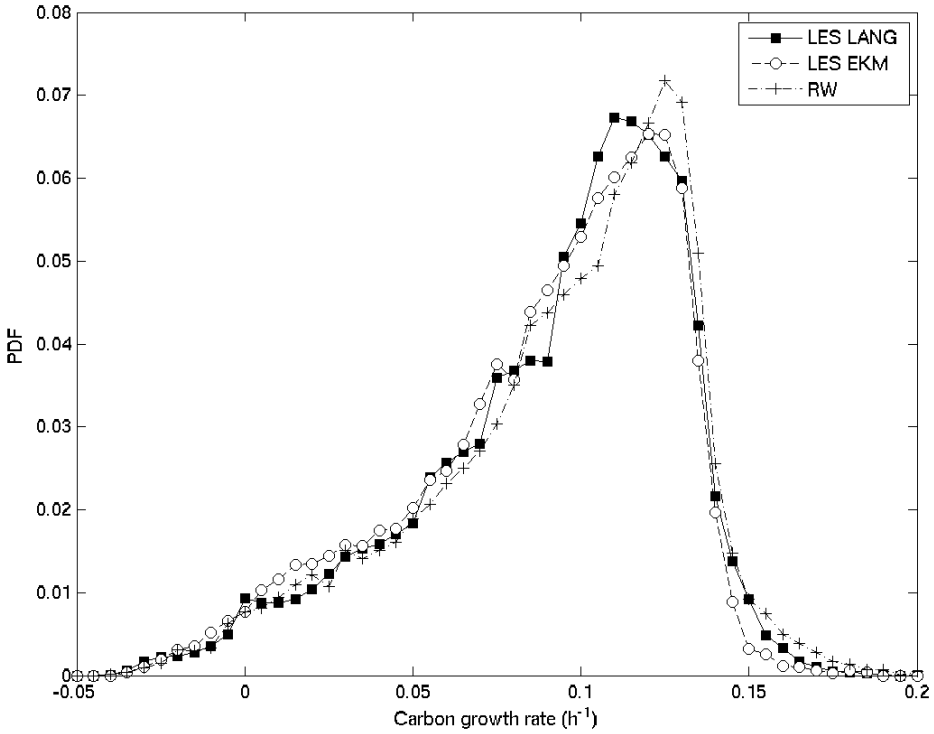

Figure 6.9: PDF of the daily mean Carbon growth rate of the Individuals, black squares correspond to LANG1, open circles to EKM1, plus to RW1.

Averaged daily property	**LANG1**	**EKM1**	**RW1**
Irradiance (µEinst $m^{-2}s^{-1}$)	213,140	238,354	240,187
$\boldsymbol{\vartheta_c}$ (d.l.)	0,051	0,054	0,055
$\boldsymbol{chla : C}$ (mg $chla$ mg C $^{-1}$)	0,044	0,042	0,042
Carbon growth rate (h^{-1})	0,112	0,114	0,117
Static carbon growth rate (h^{-1})	0,085	0,144	0,096

	LANG2	**EKM2**	**RW2**
Irradiance (µEinst $m^{-2}s^{-1}$)	123,969	147,345	148,612
$\boldsymbol{\vartheta_c}$ (d.l.)	0,029	0,032	0,033
$\boldsymbol{chla : C}$ (mg $chla$ mg C $^{-1}$)	0,051	0,049	0,049
Carbon growth rate (h^{-1})	0,077	0,081	0,084
Static carbon growth rate (h^{-1})	0,032	0,043	0,046

Table 6.3: Averaged daily properties of the population of the IBM in the different simulations. Static carbon growth rate have been computed without considering photoacclimation.

irradiance profiles, it is evident that the percent difference between the mean irradiance perceived by EKM1 OML population during the last day of simulation and the mean irradiance perceived by the LANG1 one is about 11%. This 11% difference in irradiance corresponds to a growth rate able to produce, during one day, a carbon accumulation 2,4% lower than the carbon accumulation obtained by EKM1. It is clearly a compensatory effect that makes the mean carbon growth rate similar to that of a population submitted to an irradiance 11% higher. That compensation could be due not stricly related to the dynamic pattern of photo-acclimation, but to the non linearity of the $P^C vs$ E irradiance curve, even if static. In fact, the efficiency in carbon fixation is higher in the linear part of the curve than at light saturated irradiances. The compensation in the carbon growth in the LANG1 simulation, in respect to the carbon growth in the EKM1, should be thought to be only related to the higher persistency of the individuals of the LANG1 simulation at irradiances where the efficiency in the conversion of light to carbon fixed is higher.

In order to find out if the compensation was only a static response of the organisms to the time variations of the perceived light, the theoretical carbon growth rates of the individuals subjected to the identical light history in the LANG1 and EKM1 simulations, but without any form of dynamical photo-acclimative response, was calculated. This *static* growth rate is calculated by integrating the carbon fixed if the individuals subjected to the dynamic light regimes grew following the static initial condition (the $P^C vs$ E curve correspondent to the 20 m $P^{chl} vs$ E curve in figure 6.2).

This can be intended as the growth rate that the individuals should perform if any pigment content modification and photo-inhibitive dynamic response were absent. Photo-inhibition is only statically derived by the $P^C vs$ E curve, but no damage and repair occur shifting form 1200 to 10 μEinst $m^{-2}s^{-1}$ The only change in the growth rate is the one due to the movement on the determined $P^C vs$ E curve and no memory of the previous light history exists. This value can help us to discriminate and quantify the real impact of the

photo-physiological adjustment on the carbon fixation and growth of the phytoplankters.

The carbon that the individuals fix, during one day of static simulation in the LANG1 condition, is almost double than the carbon fixed in the EKM1 condition. In the EKM1 static condition, the individuals accumulate 72% carbon more than for LANG1 (in one day). In fact the static growth rate found in LANG1 is the 60% of the static carbon growth rate of EKM1, whereas the dynamic carbon growth rate of the LANG1 simulation is 98% of EKM1. These differences produce a theoretical carbon accumulation greater of 72%, whereas the dynamic simulations differs only by 2,4%.

The dynamic acclimation, in fact, produced a growth rate for the EKM1 that was 21% less than the static growth rate (from 0,144 to 0,114 h^{-1}), whereas it produced an increase of 24% in the carbon growth rate for the LANG1 (from 0,085 to 0,112 h^{-1}).

In practice, the dynamic acclimation favours the individuals in the LANG1 while it sfavours those in the EKM1.

Probably, the pigment content at low light acclimative state increased the photo-capture of the LANG1 individuals, that, in addition, could escape from high irradiances before being damaged. The longer persistency at the same irradiance of the EKM1 individuals increased the photo-inhibitive response and did not give them the possibility to reach the higher part of the water column, with an increased light-harvesting capacity due to the intermittent regime or to low light intensity.

Looking at the mean profiles of the instantaneous carbon growth rate of each cell respect to the depth where they are located (fig. 6.12), it is evident that instantaneously, the mean cells mixed by the Langmuir circulation grow better than the other two simulations, when they are located in the upper part of the water column, because they are mixed before being fully inhibited and before decreasing the light-harvesting capacity because of the higher irradiance.

On the contrary, they probably keep with them the high light properties when they are

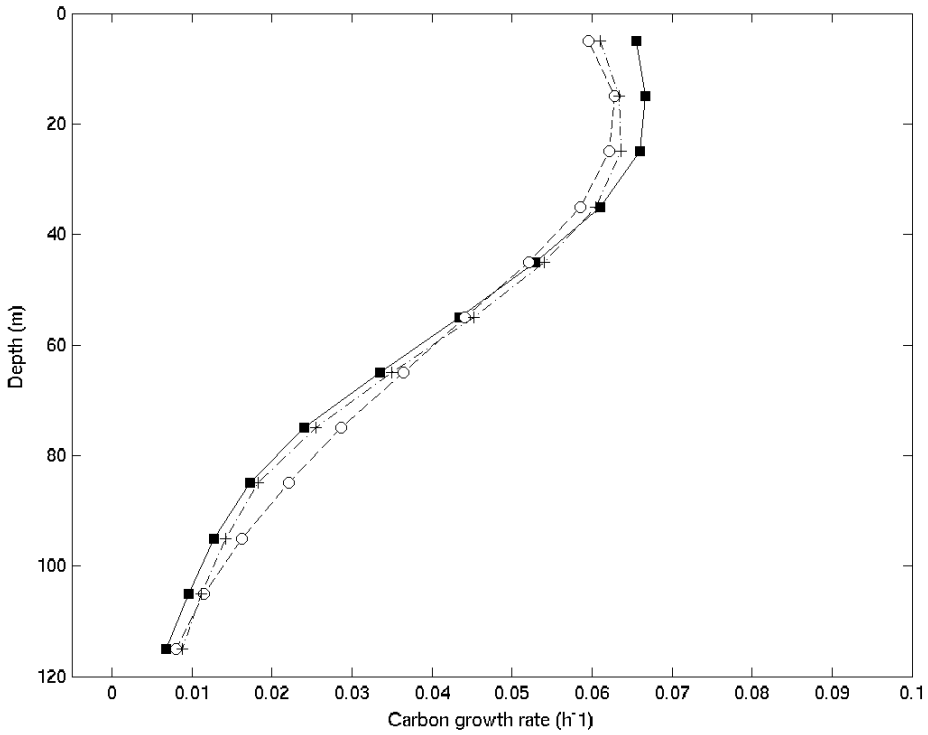

Figure 6.10: Mean daily Carbon growth rate as a function of depth, black squares correspond to LANG1, open circles to EKM1, plus to RW1.

quickly transferred down, showing a growth rate lower respect to the other two simulations. The intense vertical downward mixing due to the Langmuir circulation let them reach the lower part of the water column, when they are still relatively acclimated to high irradiances, with a lower pigment content (the most probable values in fig. 6.7) and an higher percentage of damaged reaction centers (the probable $\vartheta_c \approx 0{,}1$ values in fig. 6.8).

In general the photo-acclimative responses, in this set of simulations, down-regulated the growth performances in the higher irradiance life of the EKM1 individuals while increase the growth performances in the highly variable life of the LANG1 individuals.

The same pattern of growth, is evident also in the LANG2 simulation (fig. 6.11). The irradiance distribution changes the shapes of the profiles, and it is not evident a saturated or inhibited flat part in the upper layer as it was present in the LANG1, EKM1 and RW1 simulations (see fig. 6.10). The maximum growth rate occurs in the first meters and the LANG2 individuals are able to take advantage deeply of the high irradiance when they can perceive it. For the rest, the typical features can be confirmed and a similar role of high irradiance life down-regulation for EKM2 and high variable life encouragement for LANG2 can be suggested on the part of the dynamic photo-acclimative responses.

More in general, the pattern recognized comparing the static and dynamic growth responses in LANG2, EKM2 and RW2, is different from that recognized in the more transparent water set of simulations. In fact the dynamic of the photo-acclimative response favour all the three simulations.

The dynamic LANG2 had a growth rate 58% higher than the static LANG2 (passing from 0,032 to 0,077 h^{-1}). The dynamic EKM2 had a growth rate 47% higher than the static simulation (passing from 0,043 to 0,081 h^{-1}) and the dynamic photo-acclimative responses increased the growth rate of the RW2 of the 45% (passing from 0,046 to 0,086 h^{-1}). The dynamic growth rates are always greater than the correspondent static ones. The same types of mixing, in fact, produce always a greater variability in the irradiance perceived by

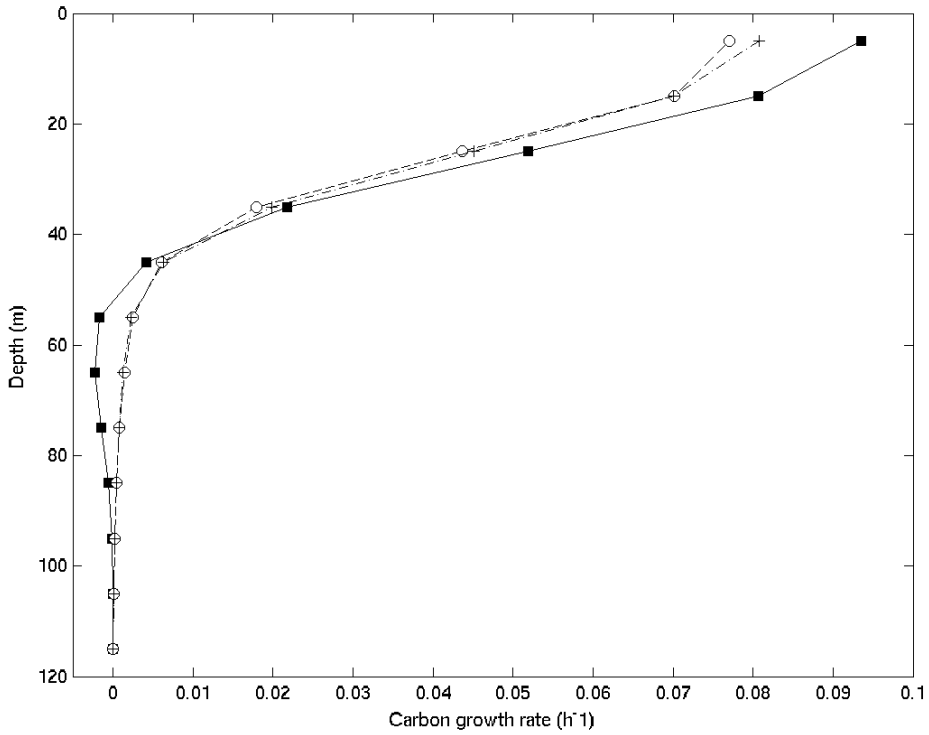

Figure 6.11: Mean daily Carbon growth rate as a function of the depth, black squares correspond to LANG2, open circles to EKM2, plus to RW2.

the organisms immersed in a more turbid water. In addition, the dynamic acclimation to lower mean irradiances, giving the individuals a higher light-harvesting capacity, in general increases the photosynthetic rates, both at high and low irradiances. For these reasons, the favourable effects of the photo-physiological plasticity in a highly variable light regime are evident in all the three mixing modes.

However, also in this case the individuals subjected to the high Langmuir turbulence are the most favoured by photo-acclimation.

In fact, the difference in the mean irradiance perceived by the population between LANG2 and EKM2 is of the 18% (almost twice the difference between LANG1 and EKM1), whereas the difference between the daily carbon accumulation due to the dynamic carbon growth rates is of the 4,8 % (two times the difference between LANG1 and EKM1). The compensating effect is, indeed, evident also in this case, with an influence similar to the more transparent case.

The photo-physiological plasticity always favours the individuals in the highly variable light regime, in particular when cells are subjected to Langmuir circulation.

This growth produces the chlorophyll profiles represented in figures 6.12 and 6.13 for the two set of simulations.

The amount of chlorophyll is clearly different between the two sets of simulations, but the shape of the profiles is conserved between the two sets: the LANG1 and LANG2 have a more homogeneous $chla$ concentration at all depths, while the RW and EKM simulations accumulate more chlorophyll in the upper layer. The RW1 and EKM1 simulations have a concentration of chlorophyll comparable with that at the surface down to 65 metres (the Z_{eu} and Z_m depth), while in the RW2 and EKM2 those high values are found until approximately 45 metres (with $Z_m \approx 65$m and $Z_{eu} \approx 35$m).

An other question is still on the stage: does a population living in a mixed dynamic environment grow better if it is always fully acclimated to the actual irradiances or if

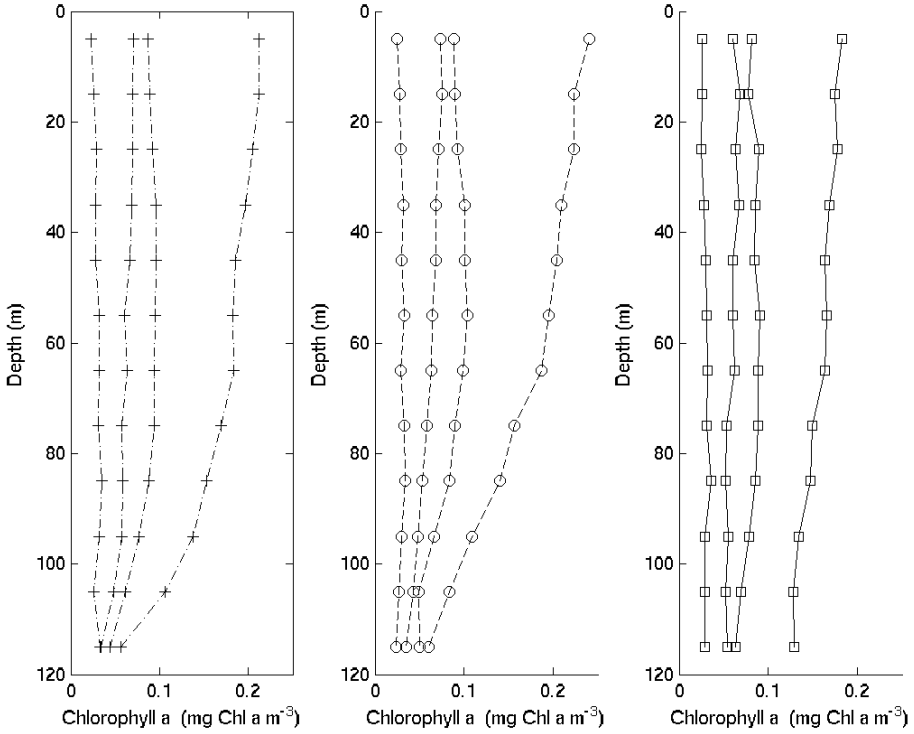

Figure 6.12: Temporal evolution of the mean *chla* concentration as a function of the depth during the two days of simulation: the lines correspond to midday and midnight of the 2 days. *chla* concentration increases with time. Left panel plots with plus corresponds to RW1, central panel with circles to EKM1 and right panel with squares to LANG1.

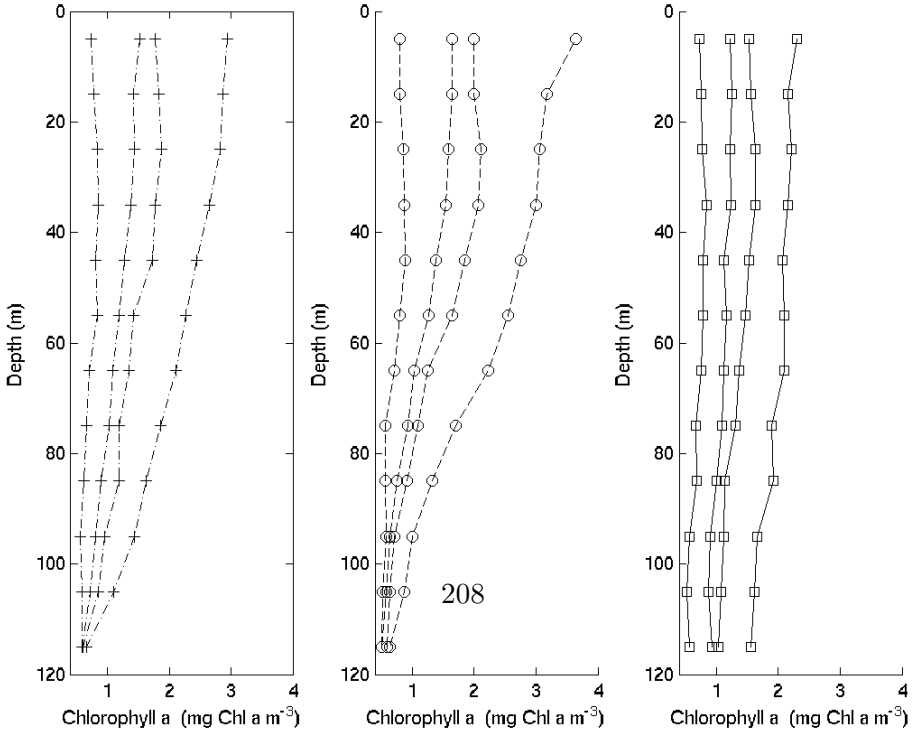

continuously acclimates to the irradiances perceived?

To answer this question and to recognize which kind of displacements favour a phytoplankter respect to another fully adapted to the irradiance where it is located, the biological transilient matrices are applied. They are calculated for an indicator of photosynthetic efficiency ϵ:

$$\epsilon(i,t) = \frac{PS(i,t) - PS_a(i,t)}{PS_a(i,t)} \tag{6.11}$$

where $PS(i,t)$ is the photosynthetic rate, as dynamically calculated in the model, of the ith individual at the time step t and $PS_a(i,t)$ is the photosynthetic rate that the individual i would have at time t, if it was fully acclimated to the irradiance $E_z(i,t)$, perceived at that moment.

In practice ϵ is the normalized difference between the fully acclimated state (an individual immersed in a stable water column), and the real photosynthetic rate that at time t depends on the previous light history as much as on the actual irradiance perceived. As the light history is strictly dependent on the displacements, the biological transilient matrices, calculated for the normalized difference of the dynamic photosynthetic rate respect to the fully acclimated one, are very informative.

It is important to stress the difference between the *static condition*, used to investigate the impact of the photo-physiological plasticity on growth performances, and the *fully acclimated* one. The static condition refers to individuals completely un-acclimated to the irradiance perceived, whereas the fully acclimated condition refers to individuals that reach the steady state with the instantaneous irradiance perceived. For this reason, the first state can corresponds to the state that the individuals would have if they would not have any physiological adaptation, whereas the second one to the state that the individuals would have if they were always placed under the irradiance that they were actually perceiving.

Therefore the fully acclimated state can be compared to the state of the individuals immersed in a stable water column, and the ϵ can be related to the advantage or disadvantage to be moved along the water column.

The biological transilient matrices of the ϵ for the LANG1 simulation, calculated with different Δt for the diplacements are reported in figure 6.14. As a general pattern, the individuals that are upward mixed have, on average, an advantage up to 50% respect to the photosynthetic performances of the individuals that are already there. The opposite occurs for individuals that are downward mixed. The individuals that are subjected to quick downward asymmetric mixing, as for Langmuir turbulence, are the most disadvantaged. They photosynthetize at a rate that is lower than the fully acclimated individuals of more than 50%.

All the individuals that are moved upward or downward in the first 40 meters of the water column display a net advantage respect to the fully acclimated ones. By increasing the time necessary for the displacements, the zone of intense disadvantage decreases, because the individuals begin to adapt to the lower irradiance while falling down. The intensity of the advantage decreases too, but the advantage is still present if the individuals take three hours to reach the upper layer. It is important to note that the fully acclimated state is also fully photo-inhibited if irradiance is high, so that cells moving upward are generally always advantaged if they reach the upper layer before they photo-inhibit at the same level. In addition (as already analyzed in section 4.3.3) the response to increasing irradiance is always slower than the response to decreasing irradiance. For this reason, the state of the individuals moved downward become more quickly close to the fully acclimated state than the individuals moved upward. As a consequence the ϵ of the individuals moved downward will lean towards zero more quickly by increasing the time necessary to move, respecto to the the ϵ of individuals displaced upward.

Looking at the mean values of the ϵ for all the individuals subjected to displacements

(title of the transilient matrices in fig. 6.14) it is evident that, even if the benefit zone is large enough, it is always negative. This means that, on average, the individuals, not fully acclimated to the irradiance perceived, perform photosynthesis less efficiently. In fact the average is not only due to the mean properties of the individuals that have been equally displaced, but also to the frequency of the displacements. As already shown (see section 5.4.2), in Langmuir turbulence the downward displacements are more frequent than the upward. Moreover, the individuals staying on the lower part of the main diagonal, and whose frequency is still high, show lower photosynthetic efficiency respect to the fully adapted individuals.

In general, displacements towards low irradiance gives the individuals a disadvantage respect to the fully acclimated ones, whereas the movement towards high irradiance favours them. This can be correlated to the mean profiles of the Carbon growth rate of the LANG1 simulation respect to the less mixed EKM1 (fig. 6.12). The lower part of the domain is disadvantaged, while the upper part is advantaged.

Finally, a movement towards low irradiance generates a disadvantage greater than the advantage due to a displacements to high light. This pattern is displayed even if increasing the time for the displacement, the advantage is more stable than the disadvantage. As a consequence the mean percentage difference decreases from 6,6%, for a 15 minutes displacements, to 4,4% for displacements occurred in three hours.

A similar pattern is also shown in the EKM1 biological transilient matrices, though the highly disadvantageous downward displacements are absent as well as the low ϵ (fig. 6.17). The net disadvantage never reaches 50%, that is instead exceeded by the individuals subjected to the large vertical excursion due to Langmuir cells. For this reason, increasing the displacement and acclimation time from fifteen minutes to three hours, the mean percentage difference of the photosynthetic rate of the dynamical individuals is lower than for the fully acclimate state, decreasing from 3,6% to 1,2%. This is also due to the displacements

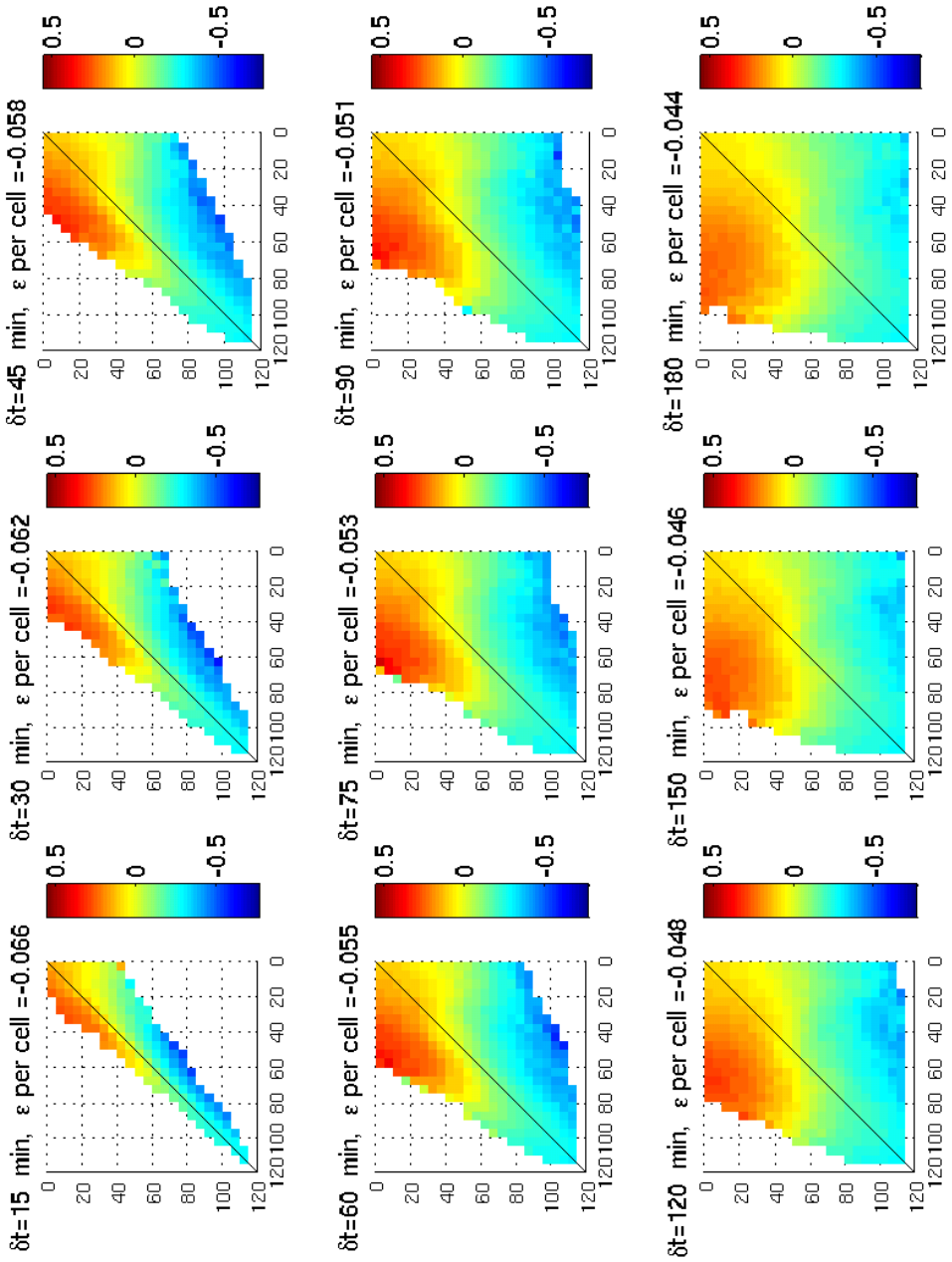

Figure 6.14: Biological transilient matrix for ϵ of the LANG1 simulation. Red colors are associated with mean growth rate higher than the one shown in the fully acclimated state, blue colors with mean growth rate lower than the one shown in the fully acclimated state.

frequency, that is always more symmetrical in the EKM1 simulation (see section 5.4.2). The RW1 shows a behavior similar to EKM1, and it is not shown.

The biological transilient matrices for the LANG2 simulation are presented in figure 6.16. The high frequency of very low photosynthetic rates, caused by the low light experienced by the individuals, produces $\epsilon(i,t) \geq 1$ and $\epsilon(i,t) \leq -1$. These values have been ignored because they are due to the small $PS(i,t)$ and $PS_a(i,t)$, so they have no meaning but should negatively affect the overall nature of the transilient matrices. This is why blank zones are present in the biological matrices, that correspond to possible displacements (e.g. the lower 40 meters in almost all matrices).

More in general, the shallower euphotic depth decreases the advantageous surface zone, together with a low impact of photo-inhibition on the dynamical organisms, able to repair damages as soon as they reach low irradiance zones, also present in the upper part of the domain.

These features yield the mean individual percentage difference of the photosynthetic rate more negative than the fully acclimated one. The photosynthetic rate, for individuals dynamically acclimated and displaced in fifteen minutes, is 14% lower than for fully acclimated individuals. This difference increases with increasing time displacements, reaching 16% for a period of three hours. In fact the increase in time for movement only increases time for the displacements towards zones never reached before. These new zones are all disadvantageous for the individuals, both for the upward and downward movements. The advantage obtained by individuals moving upward decreases by increasing the rising time. The reason behind this behaviour, different respect to the LANG1 individuals, should be connected to the different parameters, mainly the damage and repair rate. Another possibility is that the low irradiance adapted individuals should be more quickly damaged because of the larger cross section, before they photo-protected by down-regulating the pigment content. These features will be analyzed in more details with the numerical

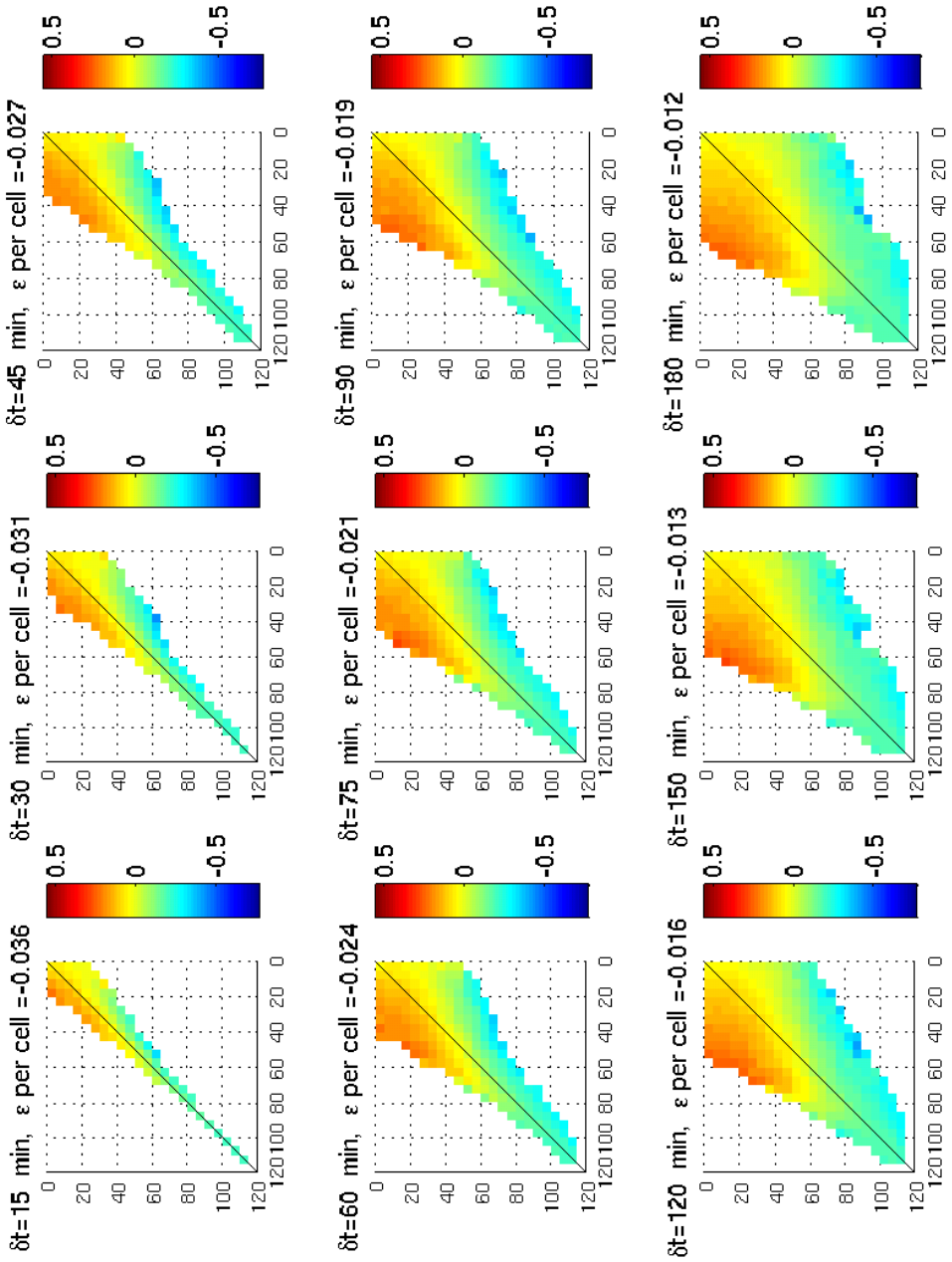

Figure 6.15: Biological transilient matrix for ϵ of the EKM1 simulation. Red colors are associated with mean growth rate higher than the one shown in the fully acclimated state, blue colors with mean growth rate lower than the one shown in the fully acclimated state.

experiments that will be presented in the next chapter.

The EKM2 individuals show a more constant mean ϵ by changing the displacements time, even if a slow trend towards more negative values still exists. On average the photosynthetic rate of the acclimating individuals is 16% lower than the fully acclimated ones. The fact that new zones of lower normalized difference do not appear by increasing the displacements time, should give these more constant values, respect to LANG2.

In conclusion, the individuals displaced in the water column photosynthetize always worse than the fully acclimated encountered during the displacements. This is not the same as saying that a stable water column would be more productive. In fact, the individuals in that mixing mode are always moved towards new zones. I can conclude that the final result of photo-acclimation is the improvement of photosynthetic performances. However, cells moving up benefit of the low light harvesting efficiency, until they are photo-inhibited, whereas cells moving down are disadvantaged until they do not increase the light-harvesting capacity because they can still have some damage signal due to light encountered at surface.

6.4.3 Summary

It is important to summarize the results obtained by the analysis that was carried out, to better introduce the experiments presented in the next chapter and their rationale.

The sinusoidal light signal due to the diel cycle produces a photo-acclimative response of the $C : chl\,a$ ratio in the individuals placed in the upper meters of the water column in simulations performed in a more transparent water case. This effect is less pronounced in the turbid water case simulations. The profiles with depth of this variable show, however, a mixing dependent shape: Langmuir turbulence produce always more homogeneous profiles respect the other kind of simulations differentiated for the mixing reproduction. In the simulations performed under the more turbid conditions, the mixing related decrease of the difference between the value of the mean surface $C : chl\,a$ and the deep value is more

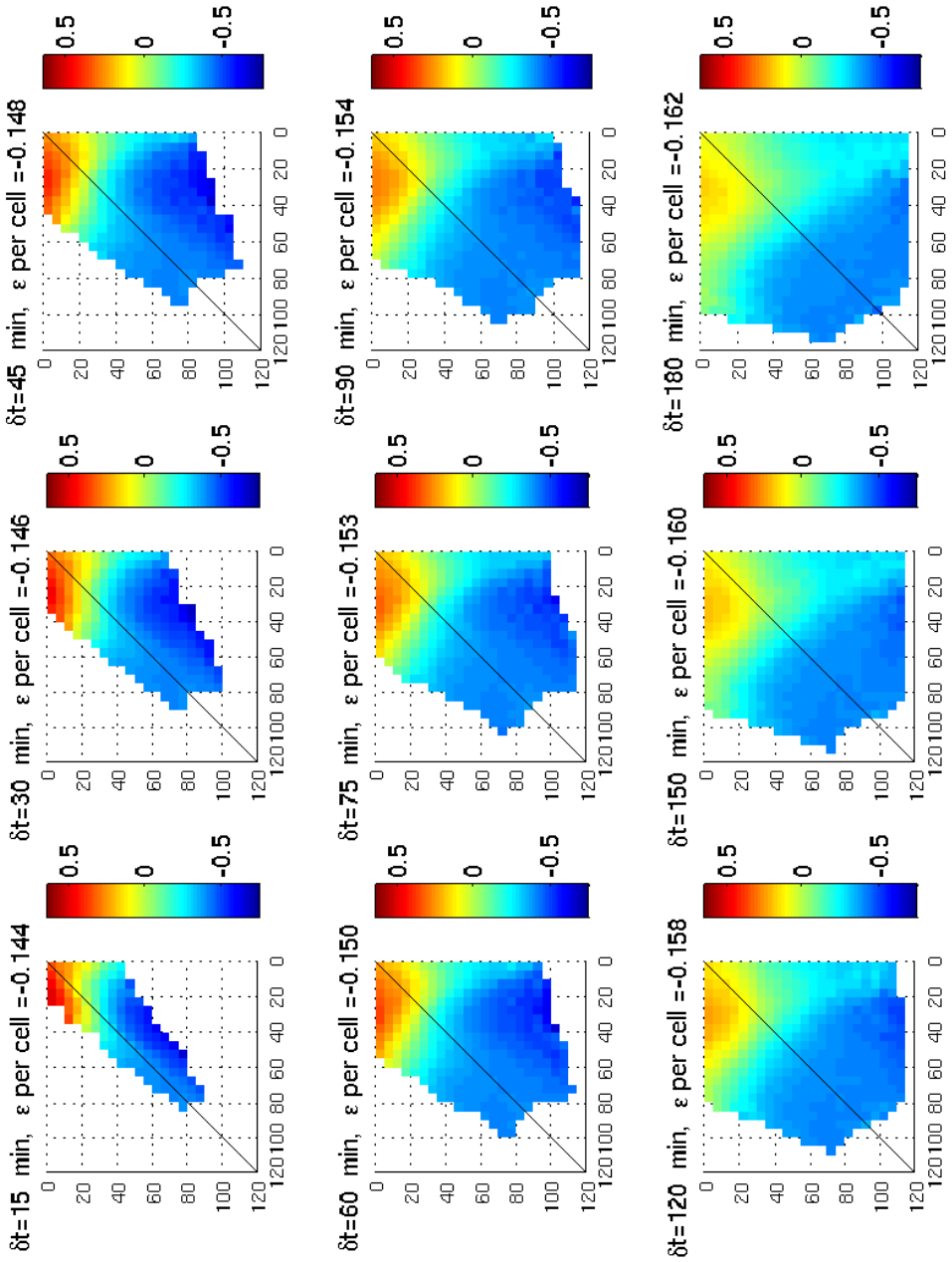

Figure 6.16: Biological transilient matrix for ϵ of the LANG2 simulation. Red colors are associated with mean growth rate higher than the one shown in the fully acclimated state, blue colors with mean growth rate lower than the one shown in the fully acclimated state.

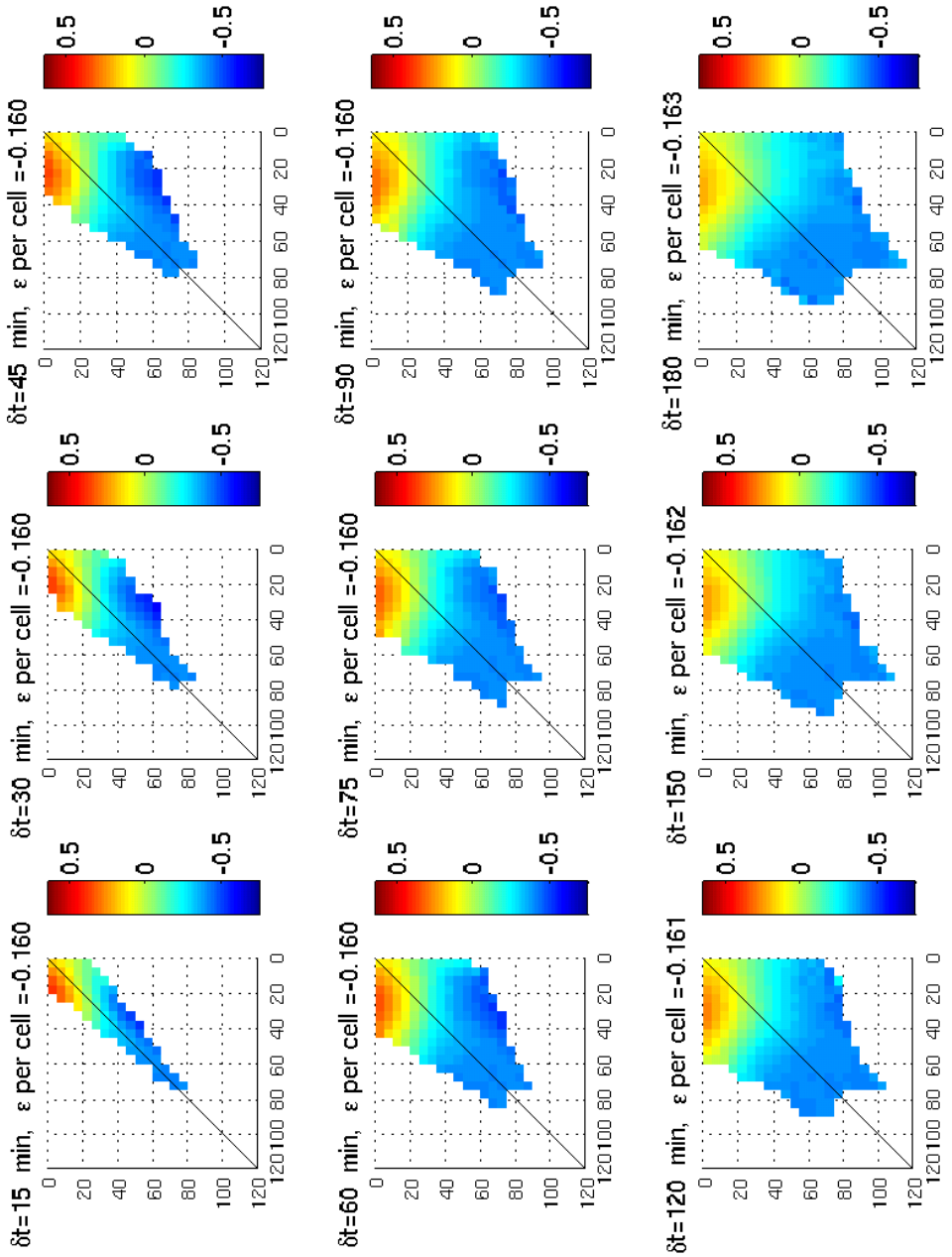

Figure 6.17: Biological transilient matrix for ϵ of the EKM2 simulation. Red colors are associated with mean growth rate higher than the one shown in the fully acclimated state, blue colors with mean growth rate lower than the one shown in the fully acclimated state.

evident. In fact, being the sinusoidal signal more attenuated by the first meters, its effect is less visible. The sinusoidal signal produce also a decrease of the variability between the individuals collected at the same depth subjected to its trigger, that is in contrast with other evidences (Dusenberry et al., 1999).

The photo-inhibition property, instead, show mean values that change with depth. The kinetic is so quick, that the individuals, on average, seems almost acclimated to the instantaneous irradiance. The variance of this property in the individuals collected at the same depth is increased by the Langmuir turbulence.

The PDFs of the daily mean properties of the individuals immersed in the OML have shown that the high time variability of the daily irradiance of individuals subjected to Langmuir turbulence produces effect on their photo-physiology not related to the mean irradiance.

The PDF of the pigment content of the individuals immersed in an OML interested by Langmuir circulation is shifted to a lower light acclimative state, respect to the individuals mixed with wind-driven Ekman turbulence. The PDFs of the photoinhibitory variable show, for the first, absence of intense damage and more frequent moderate damage, while the latter turbulence produces an effect related to the mean irradiance received.

Surprisingly, the difference in the PDFs of the photo-physiological properties between the three mixing modes simulated is not mirrored in a difference on the PDFs of the Carbon growth rate in the three simulations.

The photo-physiological adjustment has been considered to have a compensatory effect for the individuals subjected to large and non local displacements, while the impact of the photo-physiological adaptations determining the growth performances of the individuals has been quantified.

In more transparent water case, photophysiological adaptations increase the growth rates of the individuals immersed in the Langmuir interested OML up to 24% of its “static”

growth rates. On the contrary, the mean growth rate of individuals immersed in the OMLs interested by Ekman turbulence, is decreased of the 21% by the photophysiological plasticity. For this reason individuals immersed in two OMLs where the mean irradiance differs for the 11% produce daily carbon accumulations that differ only for 2,4%.

In the more turbid case, for the same reason, individuals immersed in two OMLs where the mean irradiance differs for the 18% perform daily carbon accumulations different just for the 4,8%. The differences computed without considering photo-physiological adaptations are far larger. However in the more turbid water case, the ability to acclimate increases significantly the growth rate of the individuals subjected to all the three mixing types.

The transilient matrices have underlined the displacements that favour the individuals. The upper mixing transport individuals with an increased harvesting efficiency to highest irradiance. These displacements produce high photosynthetic rates. On the contrary downward mixing, as the mixing increased in the Langmuir circulation, take individuals damaged or with a decreased light-harvesting efficiency where light is far limiting. These displacements produce a net disadvantage.

In the Langmuir circulation the light-harvesting efficiency of the individuals displaced upward is higher than the one of the individuals immersed in the Ekman turbulent OML. The advantage of these individuals is larger and cause the compensatory effect.

The advantage to be moved from the lower part of the domain to the highest part is bigger in the more transparent case as well as the disadvantage to be moved from the upper to the lower part of the domain. It has been suggested that, in more turbid water, the individuals subjected to a displacement towards high intensity, are less advantaged because of the increased possibility to be damaged because of the increased cross section for the PSII.

All the phenomena observed in the set of simulation just discussed are clarified com-

paring their features with the results derived by more simple simulations conducted under representative fluctuating irradiances, that are presented in the next chapter.

Chapter 7

Photo-physiology under Simulated Periodically Fluctuating Irradiances

In the previous chapter were presented simulations conducted using an Individual Based Model (IBM), with movement in the water column prescribed using the most plausible reproduction of the OML. The main responses of the model to a series of simple shifts in irradiance have been analyzed in section 4.2. In this chapter I describe the peculiar features that emerge when the model simulates phytoplankton response to assigned patterns of fluctuating illumination.

In section 1.2.2 I showed the dependence on time variability of the irradiance of the photo-acclimative responses and highlighted the difficulty of recognizing a species-specific pattern. The simulations described in the following were aimed at clarifying whether non-linear interactions of the simulated photoresponses did reproduce the observed dependence on the time variations of illumination without any additional stimulus.

This, in turn, should shed light on the results discussed in the previous chapter, in

particular the link between mixing, photo-physiological responses and growth rate.

The numerical experiments have been organized following the laboratory experimental set-up used by Havelková-Doušová et al. (2004) (section 1.2.2). First of all, the baselines of the mean daily photo-physiological properties under simple square wave and sinusoidal light regimes have been derived and plotted as a function of diverse mean daily irradiance perceived. Then, the results obtained superimposing fluctuations on the square wave and sinusoidal light regimes have been compared with these baselines.

An additional comparison has been conducted with the mean properties of the mixed layer population derived by the IBM simulations. This analysis highlights the impact of time variability of the irradiance on populations simulated under realistic mixing intensities.

Finally, the influence of the photo-physiological plasticity on the phytoplankton survival under simple fluctuating irradiances is summarized and extended to realistic environmental scenarios.

7.1 Model Description

Simulations and analysis were carried out using MATLAB.

The photo-physiological model (section 4.1) has been used to investigate on the response of a bulk population, i.e., not in the IBM mode to a combination of square wave or sinusoidal irradiance with superimposed fluctuations representing the vertical movement in the water column. These simulations were run to cover eighteen days of model time. The virtual phytoplankton did not acclimate to the variable irradiance until the last days of the simulations. Although six initial condition for the $chla : C$ ratio were used, those ratios were identical at the end of the simulations.

Since the $chla : C$ ratio is the slowest photo-physiological response considered, the phytoplankton were fully adapted, by that time, to the irradiance regime independently from the chosen initial conditions.

Two sets of simulations were conducted, each related the two sets of IBM simulations.

The first set used the constants derived from the IBM simulations for the more transparent water case (see table 6.1). In this case, the $chla$ concentration has been set to an homogeneous concentration of 0,1 mg $chla$ m^{-3}over the 80 meters depth water column. This concentration is based on the concentration reached by the IBM simulations in the last simulation day (see fig. 6.12).

The second set of simulations used the constants derived from the IBM simulation of the more turbid water case (see table 6.1). The $chla$ concentration is higher in order to reproduce steeper fluctuations, with 1 mg $chla$ m^{-3}. This concentration is comparable with the $chla$ concentration found in the LANG2, EKM2 and RW2 last simulated day (see fig. 6.13).

A typical simulation consists of a patch of phytoplankton with a size less then the model resolution (1 m) oscillating in the water column with three different velocities (slow, medium and fast in the following) in a light field generated by periodic background illumination (square wave or sinusoidal). Because of the oscillatory movement the light field is perceived by phytoplankton as a regularly oscillating light field with different periods. I refer to the simulations performed in the more transparent water case as follows:

- LD1: simulations conducted with square wave irradiances.
- LD1a: simulations with fluctuations due to the slow velocity have been superimposed on different amplitude square wave irradiances.
- LD1b: simulations with fluctuations due to the medium velocity have been superimposed on different amplitude square wave irradiances.
- LD1c: simulations with fluctuations due to the fast velocity have been superimposed on different amplitude square wave irradiances.
- SIN1: simulations conducted with sinusoidal illuminations.

- SIN1a: simulations with fluctuations due to the slow velocity have been superimposed on different sinusoidal illuminations.
- SIN1b: simulations with fluctuations due to the medium velocity have been superimposed on different sinusoidal illuminations.
- SIN1c: simulations with fluctuations due to the fast velocity have been superimposed on different sinusoidal illuminations.

Likewise, the turbid water case simulations are named:

- LD2: simulations conducted with square wave irradiances.
- LD2a: simulations with fluctuations due to the slow velocity have been superimposed on different amplitude square wave irradiances.
- LD2b: simulations with fluctuations due to the medium velocity have been superimposed on different amplitude square wave irradiances.
- LD2c: simulations with fluctuations due to the fast velocity have been superimposed on different amplitude square wave irradiances.
- SIN2: simulations conducted with sinusoidal illuminations.
- SIN2a: simulations with fluctuations due to the slow velocity have been superimposed on different sinusoidal illuminations.
- SIN2b: simulations with fluctuations due to the medium velocity have been superimposed on different sinusoidal illuminations.
- SIN2c: simulations with fluctuations due to the fast velocity have been superimposed on different sinusoidal illuminations.

The periods of the fluctuations is associated to three vertical velocities, that are 0,001 m s^{-1}(LD1a and LD2a), 0,005 m s^{-1} (LD1b and LD2b) and 0,01 m s^{-1}(LD1c and LD2c), respectively. The highest velocity is representative of the typical surface vertical upward velocity encountered in the LES LANG simulations.

A preliminary set of simulation was conducted to determine the baseline values of photo-acclimative parameters. One baseline is for square wave illumination (LD1 and LD2). The virtual phytoplankton was subjected to light dark alternation, with a flat illuminated period correspondent to different discrete value of irradiance intensities, from 1 to 1200 μEinst $m^{-2}s^{-1}$

The values of the photo-physiological properties correspondent to the different growth irradiance are those resulting during the last day of illumination. These values are considered to represent the typical values under a given square wave growth irradiance and set the first baseline.

The second baseline corresponds to the diurnal mean properties of phytoplankton subjected to sinusoidal illumination (SIN1 and SIN2). Various realistic peak irradiances have been used in order to investigate a wide range of mean irradiances perceived during a day. The length of the photo-period has been fixed to twelve hours for all the simulations.

The results of the second baseline (SIN1 and SIN2) will be also compared to the other baseline (LD1 and LD2), to clarify the impact of the sinusoidal irradiance in the IBM results.

In case of sinusoidal illumination, the timing of the rise and the fall become crucial parameters, especially if the fluctuations are slow. For example, rising in the water column during the first part of the day, when the irradiance is increasing by itself, produces different illuminations than rising in the second part of the day. The impact by this factor as been analyzed considering different timings for the first rise, but the influence on the mean properties of the last day of simulation was minimal.

It is important to note that for the fluctuating irradiance superimposed on the square wave, the surface and maximal irradiances considered were 300, 696 and 1200 μEinst $m^{-2}s^{-1}$, respectively. The second one corresponds to the mean irradiance of the only sinusoidal illumination considered for the SIN1a,b and c and SIN2a,b and c, and the third corresponds to the peak irradiance of the sinusoidal illumination.

The rationale was that of comparing fluctuating irradiances having the same mean irradiance but different maximum values with illumination having the same maximal irradiance but different mean values.

Three patterns under fluctuating irradiance were already found (section 1.2.2): the photo-physiological properties acclimate to the mean irradiance, to an irradiance lower that the mean, to an irradiance higher than the mean.

The simulations here discussed were run to better analyze those emergent features produced by the photo-physiological model.

We have one mean value for each SIN1a,b and c and SIN2a,b and c simulations; and three values for each LD1a,b and c and LD2a,b and c simulations, that will differ for the mean irradiance perceived during the hours of illumination.

The analysis was conducted on the mean diurnal photo-physiological properties and the carbon growth rates during the last day of simulation, when the response was found to be representative of an acclimated and reproducible state.

7.2 Results and Discussion

7.2.1 Photo-physiology and growth under periodically fluctuating irradiances

For the transparent water case, the mean daily $chla : C$ ratios were computed and plotted (fig. 7.1) as a function of the mean daily irradiance of the different mode of illumination.

The $chla : C$ LD1 values (continuous line in fig. 7.1) increases in the low light zone and

decrease in the high irradiance zones. The $chla : C$ SIN1 values follow the same pattern but the sinusoidal illumination produces higher values for sinusoidal irradiance with an higher peak irradiance (and lower if the peak irradiance is lower).

As shown in the previous section 4.3.4, the two baselines LD1 and SIN1 show similar averaged values, for what concerns the biochemical parameters.

The results of the Havelková-Doušová et al. (2004) study confirm the results obtained with the fluctuating illumination simulations. The fluctuating illuminated phytoplankton shows a $chla : C$ ratio higher than the $chla : C$ ratio found in the two square-wave and sinusoidal baselines. The phytoplankton grown under fluctuating irradiance have a $chla : C$ ratio always linked to the acclimation state of a lower non fluctuating illumination.

This pattern is most visible in SIN1a, b and c and in the higher mean irradiance LD1a, b and c, while the low irradiance LD1a, b and c are more similar to the values encountered with the same flat or sinusoidal photon dose. In this case the oscillation and the results are less clear. The $chla : C$ ratio of SIN1a, b and c and LD1a, b and c with the same mean irradiance is almost equal. It means that, for this case, under fluctuating irradiance the shape of the surface light signal is not important. Fluctuations, because of the continuous change in the direction of the modification of the light intensity, trigger the hysteresis effect and force phytoplankton to adapt to low light intensity.

The frequency of the fluctuations does not seem to be important, even if at low light intensity it is evident an emphasized response by the LD1c, that reproduce $chla : C$ values evidently higher than LD1b and LD1a. But this occurs at low mean light intensity, when, in general, the $chla : C$ ratio are more similar to the baselines.

In the case of more turbid waters (fig. 7.2), the effect of the fluctuating light is more evident, especially for the fastest fluctuations in the LD2c and SIN2c simulations. All the high mean irradiance fluctuating simulations show a lower light acclimated state. This trend in the slower velocity simulations is less evident and the low light acclimated state

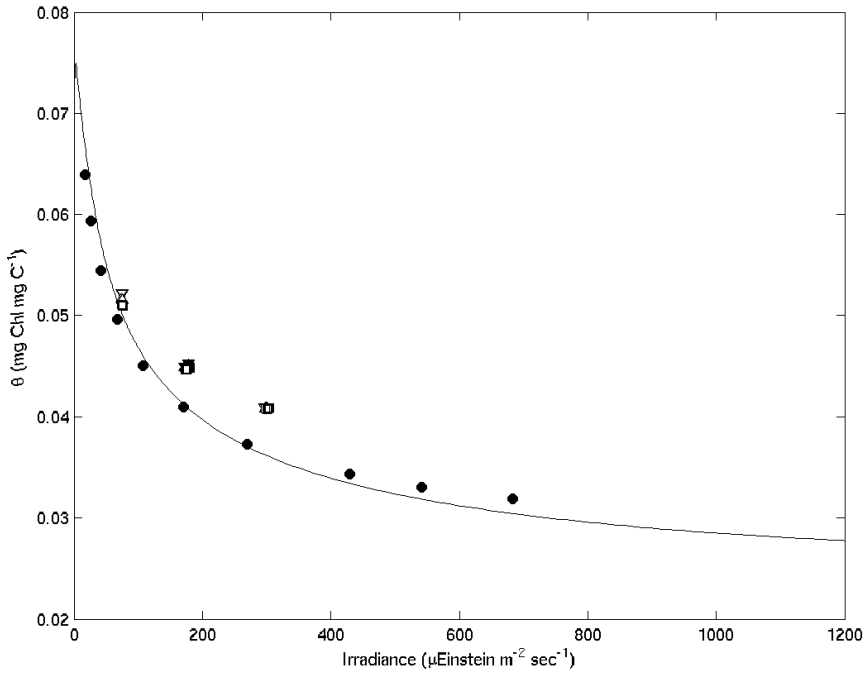

Figure 7.1: Averaged $chla : C$ ratio during the last day of simulations performed in the more transparent water case as a function of the growth irradiance, expressed as mean diurnal irradiance. Continuous line represents the square wave illumination cycle (LD1) and black full circles represents the sinusoidal illumination cycle (SIN1). The remaining open black symbols represent the fluctuating illumination derived by a symmetrical vertical velocity in the more turbid water case with a square wave surface irradiance of 300, 696 and 1200 µEinst $m^{-2}s^{-1}$ The squares represents a vertical velocity 0,001 m s^{-1} (LD1a), the triangles up a velocity of 0,005 m s^{-1} (LD1b) and the triangles down a velocity of 0,01 m s^{-1} (LD1c). The correspondent black full symbols represent the fluctuating illumination derived by the correspondent vertical velocity in the more turbid water case with a sinusoidal surface irradiance, with a peak irradiance of 1200 µEinst $m^{-2}s^{-1}$ (SIN1a, SIN1b, SIN1c). SIN1a, SIN1b and SIN1c values are hidden by the symbols of the LD1a, LD1b and LD1c with the same mean irradiance: it seems that they are very similar, between them and with the correspondent LD values.

increases its relevancy with the fluctuations velocity. It is noteworthy that the fluctuations are generally quicker than the previous case, because of the increased turbidity of the water column.

At low mean irradiance the pattern is inverted. LD2a and LD2b simulations have a $chla : C$ lower than the ratio found in phytoplankton grown under the same dose of photons, but in a square wave quality. LD2c has a biochemical composition similar to the square-wave illumination. A possible explanation is that the fluctuations produced with a low light intensity in a turbid water column produces prolonged dark period, that the square-wave grown phytoplankton does not experiences. During the dark period, the response of the model is governed only by the respiration rates and then the dark phases of the fluctuations block the tendency to increase the ratio at low irradiance.

It seems also that SIN2a, b and c are more low light adapted than the correspondent LD2a, b and c.

The differential rates of photoacclimation to upward or downward shifts in irradiance have been previously suggested to enable phytoplankton cells to better survive in a turbulent environment (Dusenberry, 2000).

In this dynamic reconstruction of the system, the increase in the light-harvesting efficiency, as already found with steady-state simulations by Dusenberry (2000) is confirmed. However, before concluding that this low light adjustments produce higher production rates, it is important to analyze the other responses under fluctuating irradiances and the effective costs of these adjustments.

For these reasons it is important to analyze the other photo-physiological responses and the carbon growth rates derived dynamically.

It is evident (fig. 7.3) that the square wave baseline (LD1), shows increasing damage with the increase in the irradiance, following a non-linear relationship. The non linearity is due to the interaction with the dynamics of the σ_{PSII}, whose increase at low irradiance

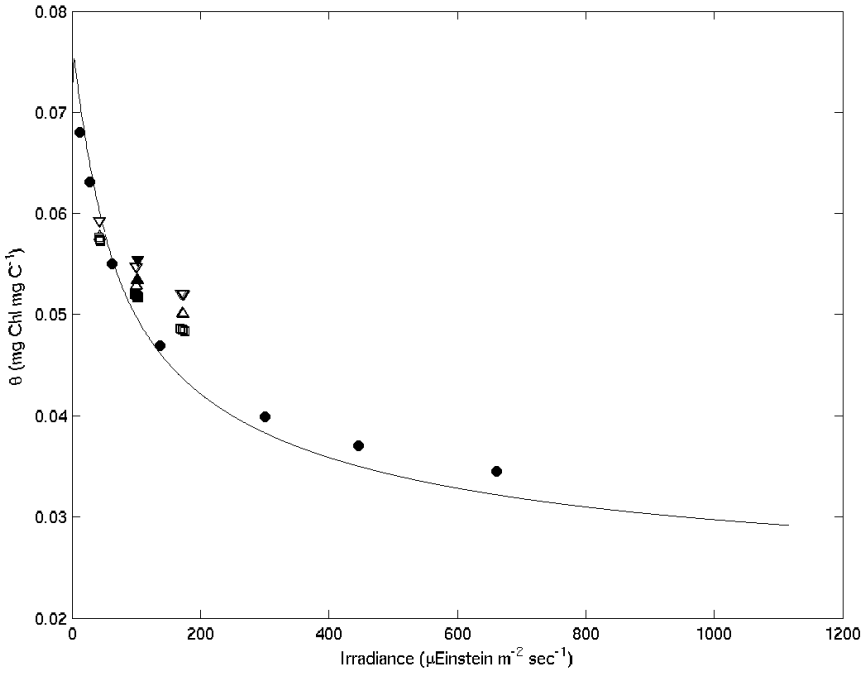

Figure 7.2: Averaged $chla : C$ ratio during the last day of simulations performed in the more turbid water case as a function of the growth irradiance, expressed as mean diurnal irradiance. The symbols represent the same illumination modes of fig. 7.1 but for LD2, LD2a, b, c, SIN2, SIN2a, b, c. The $chla$ concentration is ten times bigger than in the transparent water case.

is modulated by the parametrization of the packaging effect.

The sinusoidal illumination (SIN1) produces always higher damage, as compared to the square-wave irradiance. The memory of the highest irradiance perceived during sinusoidal simulation is evident.

The damage due to fluctuating irradiance is always bigger, than the damage that equal dose of irradiance supplied with other time courses of illumination; the quickest fluctuations produce the highest damage (LD1c and SIN1c). The memory of the highest irradiance is important, but the damage shown by LD1c with the highest mean irradiance and SIN1c are not comparable. The SIN1c and the LD1c with the highest mean irradiance perceive a total dose of photons that is different, but they experiences the same highest irradiance (1200 μEinst $m^{-2}s^{-1}$). However, the highest mean irradiance LD1c produces a 50% increased damage respect to the one produced by SIN2c: the dose of light that they receive is more important for determining the damage than the memory of the highest irradiance.

The increased σ_{PSII} connected with the higher $chl\,a : C$ ratio at fluctuating illumination is one of the reason of the damage encountered. In addition, the intrinsic nature of the inhibition, with the constant of damage and repair chosen, does not allow the phytoplankton to completely repair the damage received, during the time spent at lower irradiance.

In the case of more turbid water, the situation is different: the constants of damage and repair are faster. In fact the fitting to reproduce under realistic turbid turbulent scenario the photo-inhibition found in the P^{chl} *vs* E *in situ* curves produced fastest constants. For this reason, the memory of the highest irradiance perceived is less important and the SIN2 illumination produces a lower damage compared with the LD2 illumination. The damage due to the central part of the sinusoidal irradiance is quickly repaired after. It means that in this case, the memory of the lowest irradiance is more important.

It is important to note, however, that, even with those intrinsic characteristics, the fluctuating irradiance produces an higher damage in respect to the square-wave and sinusoidal

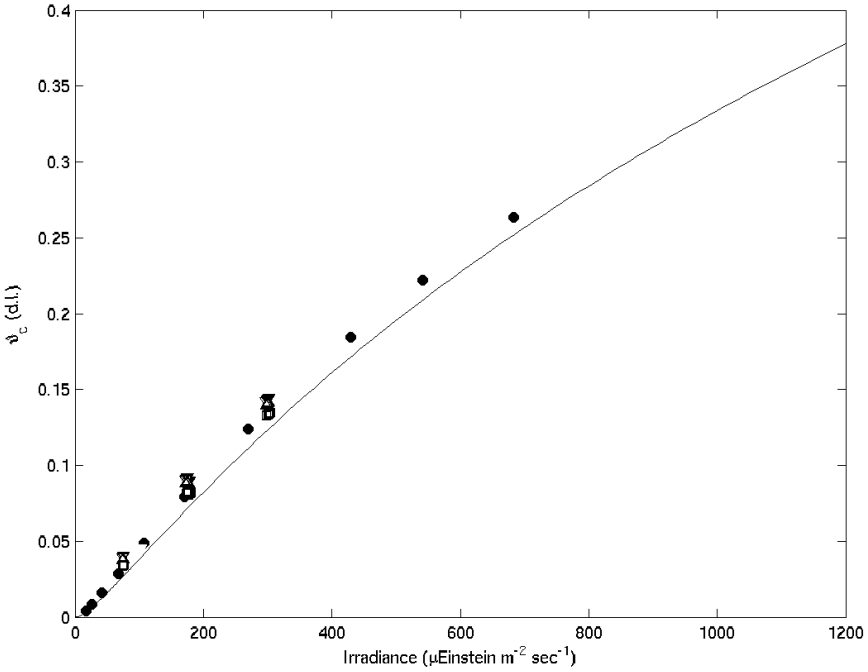

Figure 7.3: Average relative number of damaged reaction centers during the last illumination cycle performed in the more transparent water case as a function of the growth irradiance, expressed as mean diurnal irradiance. Also in this case the symbols of fig. 7.1 have been conserved.

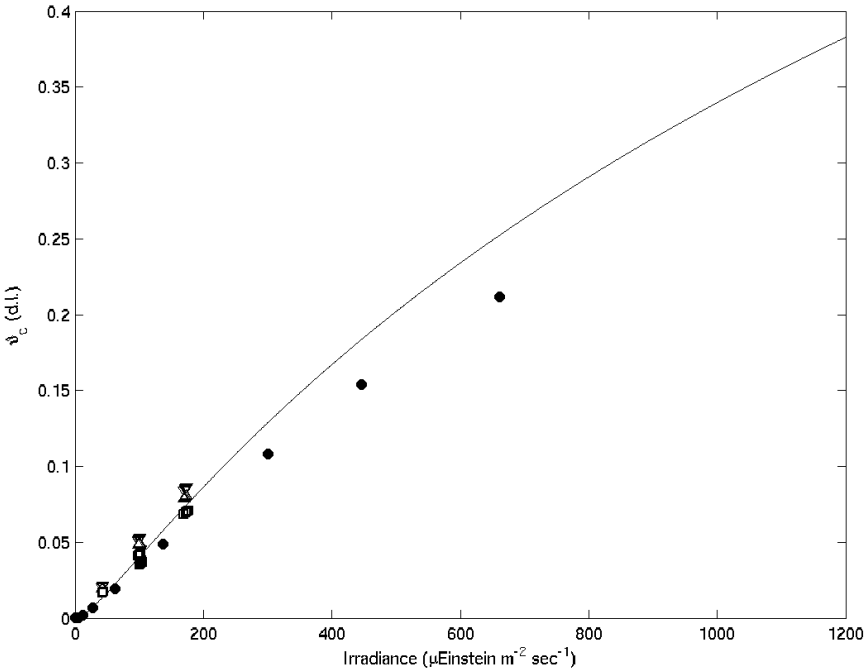

Figure 7.4: Average relative number of damaged reaction centers during the last illumination cycle performed in the more turbid water case as a function of the growth irradiance, expressed as mean diurnal irradiance. Also in this case the symbols used in the previous figures have been conserved and the *chl a* concentration is then times bigger than in fig. 7.3

regimes. This is totally due to the effect of the time-dependent increase in the σ_{PSII}. In fact, the intrinsic nature of the photo-inhibition, in this case, would be more favourable for the organisms under fluctuating irradiance, as evident from the previous analysis. Moreover, the interaction between the low light acclimated state for what concerns the pigment synthesis and the damage related to the increased cross section of the PSII produces an higher inhibition in respect to square wave or slower fluctuations.

It is important to clarify that the highest photo-inhibition found under fluctuating irradiance does not mean that in turbid mixed waters the phytoplankton are more damaged than in stable water columns. In fact, the previous analysis compares only the effect of the time variability of the illumination. It is obvious that being the damage dose-dependent, the effect of relief from photo-inhibition due to the easy escape from the upper inhibiting irradiance in a turbid environment is still evident, because escaping from the higher irradiance reduces the dose of photons received.

In figure 7.5 are reported the mean growth rates showed by the simulated phytoplankton of the more transparent water case as a function of the mean diurnal growth irradiance. It is evident that a variable illumination produces always, in the frame of the updated mechanistic model used, lower growth rates than the square-wave modality.

The simulated photo-acclimation produces the highest growth rates if the phytoplankton is fully adapted to the growth irradiance. Each perturbation to the tendency to reach the fully acclimated state with the growth irradiance decreases the averaged daily growth.

The SIN1 growth rates are lower in respect to the LD1, because the phytoplankton photosynthesize always at a rate that is not optimal for the irradiance perceived. In fact, during the low irradiance period of the sinusoidal regime, phytoplankton are not able to harvest the light as if they were grown at this low irradiance. The advantage that it can receive from the early morning increased light-harvesting efficiency, is not enough to compensate the disadvantage of the lower illumination during late morning and late

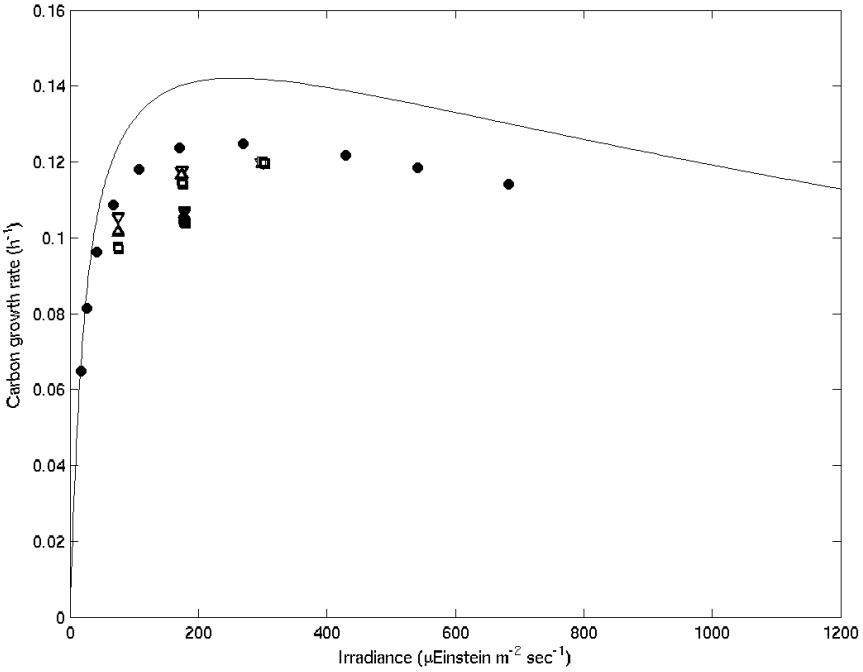

Figure 7.5: Averaged carbon growth rate during the last illumination cycle performed in the more transparent water case as a function of the growth irradiance, expressed as mean diurnal irradiance. The meaning of the symbols is the same than before.

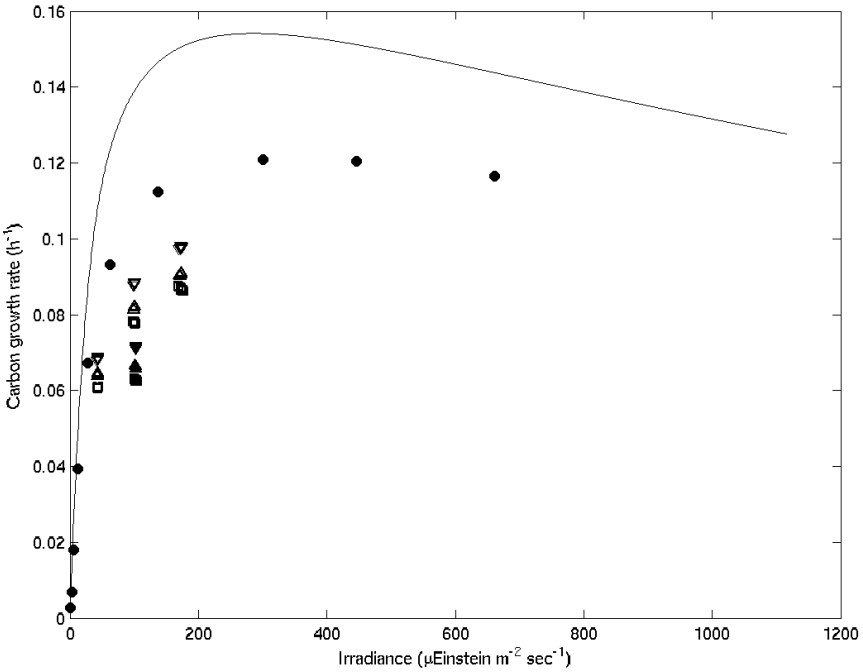

Figure 7.6: Averaged carbon growth rate during the last illumination cycle performed in the more turbid water case (*chla*concentration ten times bigger that in fig. 7.5) as a function of the growth irradiance, expressed as mean diurnal irradiance. The meaning of the symbols is the same than before.

afternoon. In addition, the second part of the day is affected by the photo-inhibition due to the midday intensity.

Also the fluctuating resulting growth rates are lower than the correspondent square-wave ones, even if increasing the mean growth irradiance seems to decrease this difference. Probably, fluctuating illumination with mean growth irradiance of 500μEinst $m^{-2}s^{-1}$, would be more similar to the correspondent square wave growth rates, but this mode of illumination does not exist in nature.

Havelková-Doušová et al. (2004) compared only the sinusoidal experimental growth rates, with the fluctuating one. Their experimental results show that cells grown under sinusoidal regime with superimposed fluctuations have growth rates comparable with the growth rates found under the highest total dose of photons supplied with simple sinusoidal illumination. In our transparent water case, the difference between the growth in these two cases (the SIN1 with the highest mean irradiance and SIN1a, b, c) is in the order of 28%. However, the highest mean irradiance LD1a, b, and c produces an averaged growth rates higher than the one produced by the square-wave irradiance at 1200 μEinst $m^{-2}s^{-1}$ Phytoplankton in LD1a, b and c experience as peak irradiance of 1200 μEinst $m^{-2}s^{-1}$ and, even if is subjected to the 25% of the total daily irradiance of 1200 μEinst $m^{-2}s^{-1}$ LD1, grow quicker.

Increasing the maximum irradiance perceived, it becomes more evident the advantage derived by relief from photo-inhibition. On the contrary, at low mean fluctuating irradiance, the increased light harvesting ability due to the time variability of irradiance is not enough to give phytoplankton an advantage. The continuous unbalance between irradiance perceived and acclimated state, decreases the net growth rates of this simulated phytoplankton.

The same pattern is evident, but with enlarged difference, in the turbid water case (fig. 7.6). It is important to note that, in this case, the range of the mean irradiance

under fluctuating illumination is limited. The turbidity of the water reduces the degree of freedom of the system, that never reaches high values. At high mean irradiance the disadvantage would be less evident (as happens for the highest mean irradiance LD1a, b and c). All the realistic fluctuating illumination reproduced in turbid waters determine an unbalancing of the light-harvesting component which becomes the dominating term.

It is important to note, however, that comparing LD1a with LD1b and LD1c, (and LD2a with LD2b and LD2c) the quickest fluctuations produce the highest growth rates, especially at the lowest mean irradiance LD1a, b and c. This pattern is confirmed also comparing SIN1a with SIN1b and SIN1c. Low frequency fluctuations produces a lower growth rates respect to the higher frequency fluctuations, but both produces growth rates always lower than the square-wave correspondent illumination case.

The increased growth rates in the quickest fluctuations compared with the slowest should be related to the higher light-harvesting component of the first, that at low mean irradiances is always determinant. This interpretation is supported by the similarity of the growth rates between LD1a, LD1b and LD1c with the highest mean irradiance. These three fluctuating regimes are, indeed, in a range of irradiance where the light-harvesting capacity is less determinant. Here the photo-inhibitory effect starts to be important and the disadvantage related to the increased σ_{PSII} decreases photosynthetic rate.

However, the increased growth rates under quicker fluctuations in respect to the ones performed under slower ones is due to the same compensatory effect already mentioned for the comparison between the LANGs and EKMs simulations. This point will be better analyzed in the next section, that will extend the previous results to the more realistic simulations presented in the previous chapter.

7.2.2 Extending to the Individual Based Model

In figures 7.7 and 7.8 have been reported the mean characteristics of the sinusoidal simulations presented in the previous section as a function of the mean growth irradiance, together with the the mean daily properties of the individual based simulations presented in the previous chapter (see table 6.4.2 in section 6.4.2).

The increased light harvesting capacity, due to the simulated mixing is confirmed in both water transparency cases, for the three representations of the mixing (fig. 7.7(a) and fig. 7.8(a)). This increased averaged harvesting capacity is accompanied by an increased average damage only in the water turbid case, where the mean values of the damage perceived by the individuals is higher than the damage of the corresponding sinusoidal regime (fig. 7.8(b)). In the more transparent water case, the difference is unimportant and the mean damage is comparable with the mean damage perceived under a sinusoidal irradiance that supply the same photon dose (fig. 7.7(b)).

Those results confirm the interpretation of the analysis based on the transilient matrix of the LANG2 simulation (fig. 6.16 discussed in section 6.4.2). The upward mixed individuals lose their advantage due to the increased light-harvesting efficiency, increasing the time necessary to reach the surface, because the increased cross section of the PSII related to the low and fluctuating illumination adaptation increases the damage rate (already fast) of the reaction centers.

The non-linear interaction of unbalanced photo-physiology and dynamic environment produces growth rates always lower than the growth rates obtained under the homologous sinusoidal illuminations. However, in the more transparent water case, those growth rates are more similar to those obtained under sinusoidal illumination in respect to the more turbid water case (figs. 7.7(c)and 7.8(c)).

In addition, they are similar to the growth rates performed under the maximal sinusoidal irradiance, that is the surface irradiance used in the IBM (fig. 7.7(c)).

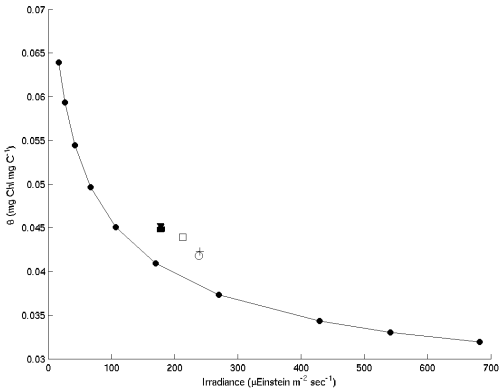

(a) $chla : C$ ratio

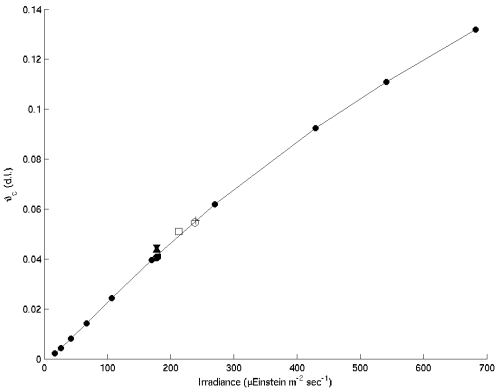

(b) Relative number of damaged reaction centers

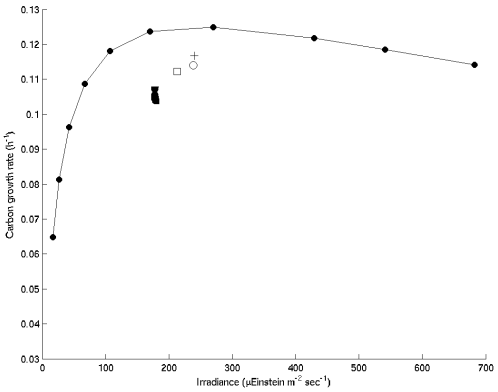

(c) Carbon growth rate

Figure 7.7: Averaged daily properties of the last day of simulations performed in the more transparent water case as a function of the growth irradiance, expressed as mean diurnal irradiance. The full circles represents different sinusoidal illumination cycle, united by a continuous line (SIN1). The colored squares represent the fluctuating illumination derived by a symmetrical vertical velocity of 0,001 m s^{-1} in the more transparent water case with a surface sinusoidal illumination cycle, with a peak irradiance of 1200 μEinst $m^{-2}s^{-1}$ (SIN1a) . Colored triangles up are for the fluctuating irradiance, but due to a vertical velocity of 0,005 m s^{-1} (SIN1b) and the colored triangles down to a vertical velocity of 0,01 m s^{-1}(SIN1c). The open square sign the mean OML correspondent properties of the LANG1 simulation as a function of the mean irradiance, the open circle is the same but for EKM1 and the cross represents RW1.

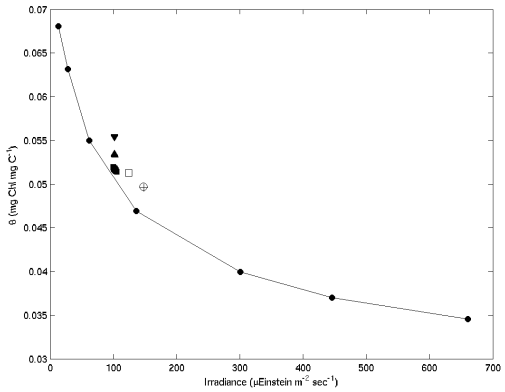

(a) $chla : C$ ratio

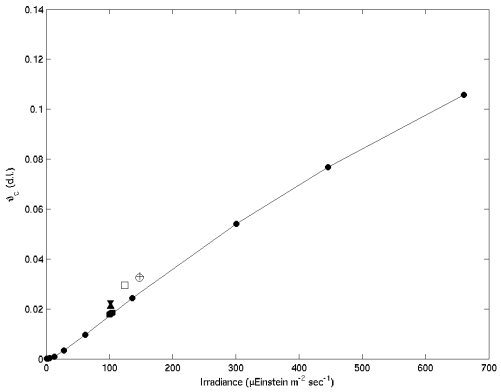

(b) Relative number of damaged reaction centers

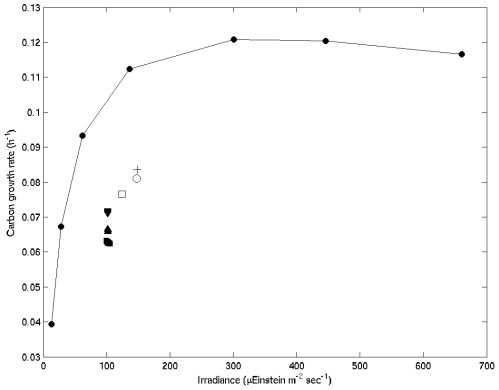

(c) Carbon growth rate

Figure 7.8: Averaged daily properties of the last day of simulations performed in the more turbid water case as a function of the growth irradiance, expressed as mean diurnal irradiance. The full circles represents different sinusoidal illumination cycle, united by a continuous line (SIN2). The colored squares represent the fluctuating illumination derived by a symmetrical vertical velocity of 0,001 m s^{-1} in the more turbid water case with a surface sinusoidal illumination cycle (SIN2a), with a peak irradiance of 1200 μEinst $m^{-2}s^{-1}$ Colored triangles up are for the fluctuating irradiance, but due to a vertical velocity of 0,005 m s^{-1} (SIN2b) and the colored triangles down to a vertical velocity of 0,01 m s^{-1}(SIN2c). The open square sign the mean OML correspondent properties of the LANG2 simulation as a function of the mean irradiance, the open circle is the same but for EKM2 and the cross represents RW2.

This in turn means that the physiological adaptation to a transparent water mixed environment gives the individuals immersed in highly turbulent mixed layer the ability to grow with rates comparable with surface population under stable and clear sky environment, that perceive a total daily photon flux three times higher. In the more turbid water case, the results are different. The physiological adaptation in a mixed and turbid environment gives the individuals the ability to grow with rates of a population that perceive the half of the total daily photon flux perceived under turbulent conditions.

In the first case, it is important to note that the rates in the surface population compared with the transparent water case were affected by photo-inhibition, while in the more turbid case the photo-inhibition effect was generally less evident and the general limiting factor was light harvesting.

In order to quantify the impact of the photo-physiological adaptations on the growth rates in all the theoretical conditions considered before, the static carbon growth rates correspondent to all the simulation presented in section 7.1, have been compared with the dynamic ones (respectively red and black symbols in fig. 7.9(a) and fig. 7.9(b)). In this way the patterns of the interaction between mixing, photo-physiological adaptation and growth rates, outlined in section 6.4.2, can be extended to more theoretical cases, that should be correlated to other realistic environmental conditions.

It is evident that in both the water case the static phytoplankton simulated under the baseline illuminations (LD1 and LD2 and SIN1 and SIN2), have a higher growth rate in respect to the dynamic one at the high mean irradiance supplied. On the contrary at low photon supply static phytoplankton grow slower.

In the static case, it is important only the mean irradiance perceived: it does not exists any significant difference related to the velocity of the fluctuations if is not considered the photo-acclimative response.

Photo-acclimative responses could increase the variability between the growth rates of

phytoplankton grown under irradiances with a different time spectrum of the amplitude but with the same photon flux. It was already concluded that they can also decrease the variability between the resulting growth rates under different time courses of the irradiance with different total photon flux perceived (comparison between LANGs and EKMs simulations in section 6.4.2).

In conclusion, two fundamental patterns are common. The first one derives comparing growth rates of oceanic mixed layers derived statically both from an environmental and from a photo-physiological point of view (red lines in figs.7.9(a) and 7.9(b)) to growth rates derived from a dynamic point of view of the illumination signal without considering the photo-acclimative responses (red symbols in the same figures). It is possible to say that bulk estimates of the OML phytoplankton growth always overestimate the ones derived with a lagrangian approach without considering photoacclimation.

The second pattern is obtained comparing the estimates derived by lagrangian light histories coupled with statically photo-physiological growth models (red symbols) with the complete dynamic reproduction of the system (black symbols).

It is evident that in turbid OML (fig. 7.9(b)) the static estimates always underestimate the growth rates. In the more transparent water case, it happens only at low mean irradiance regimes: at high mean irradiance they are, indeed, overestimated.

The photo-physiological adaptations considered decrease the growth rates at high irradiance via down-regulation of the pigment content and photo-inhibition, and increase them at low irradiance, for the opposite behaviour.

It is important to underline that the differences in the two cases are linked to the shapes of the fluctuations supplied and, of course, to the physiology prescribed to phytoplankton. However it is important to note, also, that the high irradiance mean regimes, where the static estimates could overestimate the growth rates, are impossible to be obtained in more turbid water, where the mean irradiances of phytoplankton moving in a sufficiently deep

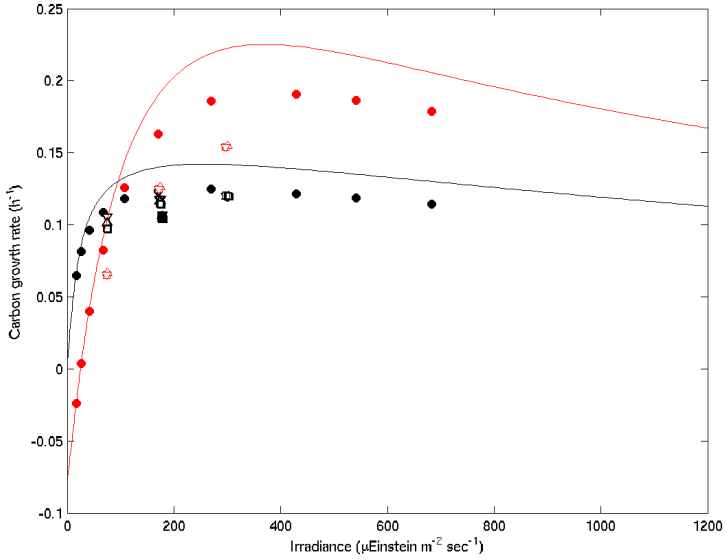

(a) Transparent water case

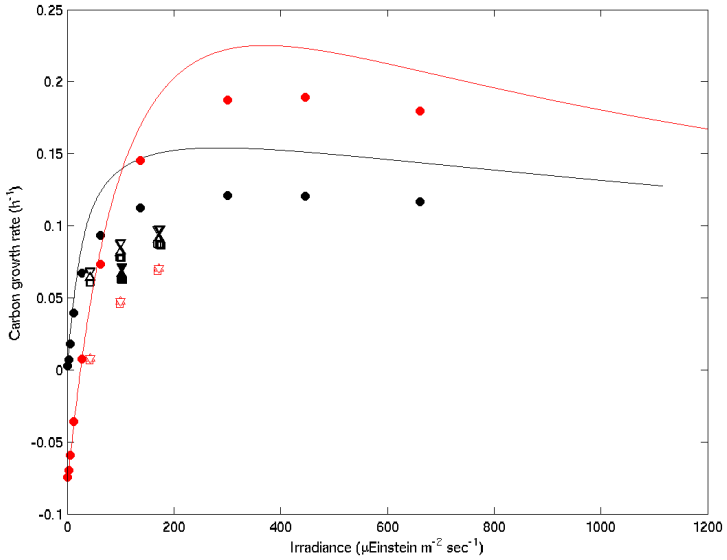

(b) Turbid water case

Figure 7.9: Mean carbon growth rates computed "statically" and "dynamically" as a function of the mean diurnal growth irradiance, in the two cases of transparency of the water. The symbols represents the same modes of illumination as for the figs.7.1 and 7.1. The homologous red symbols and lines corresponds to the "static" condition, while the black symbols and lines to the "dynamic" state.

mixed layer is always lower than in the more transparent case.

It seems evident that the non-linear overall effect of photo-physiological adjustments considered in these analysis reduce the range of the possible growth rates really performed by phytoplankton in realistic mixed environment.

The theoretical growth rates derived by the $P^{chl}vs$ E curve go through a wide growth rate range that is restricted to a smaller one of realistic growth rates that can be performed in the OML.

This takes place because of the three causes:

- the dynamical nature of irradiance,
- the realistic limit to the combination of time spectrum of the amplitude of the irradiance and its mean value,
- the non-linear nature of the realistic photo-physiological plasticity reproduced.

Part III

Discussion and Conclusions

Chapter 8

General Discussion

Phytoplankton photosynthesis in the ocean depends on light availability which decreases exponentially with depth. Mixing in the photic zone moves cells along that exponential gradient causing variations in the irradiance to which cells are exposed up to three orders of magnitude on time scale of hours. Because of the harmful effect of high irradiance and because of the decrease in the relative capturing efficiency of pigments, namely $chla$, with the increase of their concentration in the photosynthetic apparatus phytoplankton must continuously regulate the $chla$ content. There are several additional mechanisms, which were discussed in chapter 1, that concur in the response of phytoplankton to a varying light field. Though, the regulation of the optical and effective cross section of the photosynthetic apparatus via the change in relative pigment content is one of the most effective aspect studied. It is, in fact, one of the few responses for which mechanistic models have been produced. Many of the experiments on which the models are built do not allow to answer to a relevant question, namely, to what extent phytoplankton growth is improved or hampered in relationship to the light fluctuations that cells do experience in the mixed layer under a natural illumination cycle?

The present study addressed the above question with the aim of improving, on the

long run, our knowledge of the role of photacclimative responses in the natural selection of phytoplankton and on species competition and succession in the extant ocean.

The effort was carried out along three lines:

- To mplement a numerical model of mixing in the OML which could be considered as the best reconstruction of particle trajectories in the layer.
- To implement a numerical model of photoresponse which reflects at its best the observed response of phytoplanton at light variations.
- To analyze the responses of virtual phtoplankton in a virtual mixed layer and to obtain quantitative estimates of their impact

As for the modelling of mixed layer, I used three different models. A typical random walk, which I built, and a LES in two configurations, without and with the Langmuir circulation, whose code has been made available by senior colleagues of my Institute. The first configuration of the LES is somehow unrealistic because Langmuir Circulation is strictly associated with the presence of the waves. In addition, lacking the large scale eddies it produces diffusive fields that may well be represented by a random walk where the diffusion coefficient is properly assigned. In this sense, the first configuration of the LES and the Random Walk describe a very similar physics.

I then forced the LES with a moderate wind stress to have 3D flow fields and from then I derived, through a lagrangian approach, the properties of the turbulent field which I used also for parameterizing the Random Walk.

The LES with the Langmuir circulation doubled the mixing intensity on the mixed layer and produced a deepening up to 40 m of the turbulent mixing as compared to the no Langmuir case. In addition, via the application of the transilient turbulent theory, an increased downward mixing due to the typical feature of increased vertical downward velocities in the convergence zones of Langmuir cells was observed. The mixed layer simulated

without the parameterization for the Langmuir circulation has a more diffusive turbulence decreasing with depth. The pattern is similar to a spiral of Ekman with superimposed small scale chaotic motion. Both those models were used to transport virtual passively buoyant phytoplankters in the water column.

The three modalities for the simulation of the vertical displacements and so the light history of the individuals have been used by the IBM in two theoretical realistic conditions: a first case of oligotrophic and transparent water ($Z_{eu} \approx Z_m \approx 65$m in the no Langmuir case) has been compared with a more eutrophic and turbid case ($Z_{eu} \approx 35$ that is to say $Z_{eu} \approx 1/2\ Z_m$, in the same no Langmuir conditions). Both cases can occur in actively mixed oceanic layer in zone submitted to constant winds.

The time scale of the mixing was found to be around three hours, that is a short period if compared with the time scales for the biochemical modification (order of the days), while it is comparable with the time scale for the photo-inhibition processes (order of few hours). The interaction between those kinetics suggests the presence of non-linear terms, producing responses related to the time spectrum of the irradiance perceived and not simply to the total supply.

The photo-physiology of the individuals submitted to the three mixing modes has shown differences, above all between the individuals subjected to the coherent motion of the Langmuir circulation and the ones immersed in a more diffusive Mixed layer.

It is important to note that the differences that have been found between the random walk approach and the correspondent LES simulation are not significant. The mean irradiance perceived by the individuals moved with trajectories mimicked by the random walk was slightly higher as well as the averaged growth rates. In addition, also the mean photo-physiological properties of the individuals both in terms of distribution of probability and in terms of averaged values have evidenced no significant differences.

By contrast, the enhanced mixing, due to Langmuir circulation, increased the variance

between the light history of the individuals immersed in the OML, while the probability that an individual immersed in a more diffuse mixed layer would perceive a given average light intensity during a day was more related to the light profile in the water. This enhanced variability, encountered under Langmuir turbulence, produced individuals that on the average showed biochemical characteristics of a lower light intensity and a photo-inhibition that did not reach high values.

This *low light* adaptation, clearly related to the fluctuating irradiance in mixing conditions together with the lower light of the deep part of the layer, is a consequence of the biological hysteresis in the adaptation of the light-harvesting pigment content.

The absence of signals of high damage related to photo-inhibition, under Langmuir circulation, is due to the relief effect that the higher vertical velocities produce, because they give the individuals the possibility to quickly escape from the surface inhibiting irradiance. This feature of relief from photo-inhibition due to mixing, was already evidenced by the results of the empirical lagrangian model of phytoplankton photo-response of Nagai et al. (2003). The authors concluded that the mixing should increse by 7,4% the phytoplanktonic daily biomass accumulation respect to a more stable case immersed in a turbid (type 2 water) mixed layer subjected to diurnal warming and cooling. The growth enhancing effect of the increased $chla : C$ ratio in phytoplankton immersed in a turbulent mixed layer was proposed also by Dusenberry (2000) who used a steady state model.

However, this is the first attempt to quantify the interaction between the two photo-responses and their overall effect in a dynamical and mechanistic simulation of phytoplanktonic single cells.

As mentioned before, cells immersed in a mixed layer interested by Langmuir cells, showed a pigment content typical of lower light acclimated cells and more moderate photo-inhibition, in respect to cells immersed in a simply diffusive mixed layer.

However, the growth rates calculated with dynamical and mechanistic laws were more

similar between the two mixing cases, both in more transparent waters and in more turbid ones.

The photoacclimation is responsible of a compensatory effect that has increased the growth rates of individuals immersed in a deeper mixed layer up to almost the growth rates of cells immersed in a mixed layer that perceived a light supply increased for the 11%. In particular, a higher mean instantaneous growth rates of cells immersed in the first 40 meters (interested by the Langmuir cells), as compared to those of the first 40 meters of the mixed layer characterized only for diffusive turbulence, was found, in both transparent turbid waters.

By contrast, in the lower part of the water column, the Langmuir turbulent mixed layer showed a lower growth rates in respect to the Ekman case. In the Langmuir turbulence, the increased mixing advantages the growth in the upper part of the column, where cells with an higher light-harvesting efficiency (due to hysteresis and to the lower irradiance intensity perceived at greater depths) have been submitted to an high irradiance; while the increased downward velocities have transfered down in the water column individuals unable to harvest efficiently the irradiance field, because still photo-inhibited and photo-protected by the decrease in the $chla$ content.

This double pattern, on the average, favoures the cells immersed in the deeper and less illuminated Langmuir mixed layer, grown at rates comparable with the individuals immersed in a mixed layer where the mean light supply is higher.

The impact of the dynamic photo-acclimation has been quantified and has displayed differences between the turbid and the less turbid water case. In turbid water photo-acclimation increases by 88% the growth rates in the diffusive mixing condition considered and doubles the growth rates in the Langmuir turbulence. In less turbid waters, the dynamic of photacclimation increases the growth rates, in the part of the mixed layer with Langmuir circulation, by 30% and decreases it by 20% in mixed Layer that does not

reproduce the formation of the Lamgmuir cells.

This different pattern between the more transparent and the more turbid water case is due to the intrinsic nature of photo-acclimative plasticity. In fact, the photo-acclimative responses enhances the growth rates at low irradiance, via increase in the quantum yield of photosynthesis, while decreases it at high irradiance via down-regulation of the pigment content and dynamic photo-inhibition. This pattern is mirrored in the dynamic regime, where low mean irradiance dynamic regime has produced an advantage because of the photo-acclimative plasticity, while higher mean irradiance regime has produced a disadvantage.

The reduction of the photosynthetic performances at high irradiance, resulting from photacclimation, can be interpreted as an adaptation to reduce the risk of irreversible photodamage, which could eventually lead to cell death. Current views also suggest that photo-inhibition, generally considered just detrimental, can be seen as a way to sink out excessive and potentially irreversibly damaging irradiances (Adir et al., 2003).

It is also important to underline that time variation of irradiance and its intensity have, in nature, restricted degrees of freedom. High variability in the irradiance fields is generally related to low mean irradiances for phytoplankters in the mixed layer, while high mean irradiances are generally supplied in more stable and less variable oceanic environments. Photo-acclimation acts on the growth rates of phytoplankters decreasing the effective distance between the overall growth performances in the two extreme cases: the *hysteresis* effect related to mixing increases the performances in the first case, while the high-irradiance responses down-regulate them in the second case.

The results of this mechanistic reproduction of light-related responses should be extended to discuss the regulation of the acclimation to diurnal variation of the irradiance. In the model acclimation to variable illumination is governed by the same rules both if it is due to the diurnal cycle and if it is connected to changes in the depth in the water column

or to atmospheric events. It can be supposed the existence of a form of self-regulation to prevent acclimation to a predictable variation of irradiance if it is not advantageous to respond to this signal as if it was a signal of light modification due to unpredictable processes.

It has been previously suggested that photo-acclimation is not a physiological acclimation to light-dark cycle, and that the pigment pattern recognized in cultures grown under square wave irradiance was related to other modes of regulation (Post et al., 1984). The model reproduces the general features of acclimation of $C : chl\,a$ ratios to light-dark cycle via the interaction between the respiration rate and the transition between light and dark, with the decrease of the ratio triggered by the light-dark transition and its increase by the opposite transition. This response has been observed in cultures grown at square-wave irradiances as anticipating the real trigger (Post et al., 1984).

In sinusoidal illumination simulation the signal of the light-dark transition was anticipated by the gradual decrease of irradiance, while it was always related to the light signal in the dawn. The overall consequence on the mean daily pigment ratio was, though, minimal. The gradual and continuous acclimation to the sinusoidal illumination did not change the averaged biochemical characteristic of the virtual phytoplankton, which were similar to those grown under square-wave regime. The same rules of acclimation, that have produced via the hysteresis effect a significative modification of the biochemical properties, under quickly fluctuating irradiances, are not significant if the gradient of the illumination is slow like the diurnal modification due to the changes in the declination of the sun.

It seems much more important the signal of the light-dark and dark-light transition resetting the biochemistry of phytoplankton via nocturnal respiration that the pattern of illumination.

The effect of a sinusoidal illumination, however, even if does not modify significantly the biochemical characteristics of simulated phytoplankton, decreases its growth rates, respect

to the square wave grown, up to 2 % at high total daily supply.

This decrease is principally due to the saturating and inhibiting irradiances that under sinusoidal illumination the individuals can perceive. In fact, even if the raise of the quenching at high irradiances is not explicitly reproduced, the overall consequences of the acclimation considered in the model have produced a realistic midday depression in the photosynthetic performances, because of the decrease in the quantum yield via modification of the pigment content and because of the photo-inhibition.

Therefore, a model that treats equally the irradiance gradient, is able via the particular interaction of the kinetic of the acclimation and the rate of modification of the irradiance to reproduce reliable results under sinuosoidal illumination, without a direct inclusion of a self-regulator.

The decrease in the growth rate of simulations conducted under sinusoidal irradiances respect to the square-wave ones does not seem related to the costs of an acclimation which could be better regulated in case of an internal control, but to the midday depression, that the model via a decrease of the σ_{PSII} and via photo-inhibition reproduce.

Chapter 9

Conclusions

In the introduction three questions were proposed as relevant to the focus of the study. In the following I give a synthetic, though, preliminary answer to them.

> *Which are the typical scales of photoacclimation as compared to the scales of possible variations in the natural environment?*

Photo-acclimation spans over a wide range of scales, from the order of seconds to the order of days. Here I considered processes with the shorter scales as being at the steady-state, while regulation of modification of the photo-capture (order of days) and reversible damage of reaction centers due to the photo-oxidative power (order of few hours) were fully dynamic. The scales of variation of irradiance in the natural environment cover a similar range; the individuals immersed in the turbid OML can transit from the surface irradiance to the complete dark in less than one hour and viceversa. It is important to underline that the typical features of the Langmuir circulation can produce vertical downward velocity of the order of 5 cm s^{-1}, that are up to five times bigger than the upward quickest one. This kind of asymmetry is typical also of another process such convection.

It is noteworthy that quicker decrease of irradiance respect to the correspondent increase should partially reduce the hysteresis effect recognized under fluctuating irradiances.

However it is more important to notice that the variation that the natural environment causes and the concurrent non linear effect of the photo-acclimation narrows the range of realistic growth rates due to the simulated photo-physiology.

Which is the impact of mixing on the biomass accumulation of phytoplankton of known photophysiology?

The biomass accumulation predicted by the two realistic representation of an OML differs among the turbid and the more transparent case: The daily biomass accumulation shows a 80% increase from the turbid to the more transparent water subjected to the wind-driven diffusive mixing and an 85% increase in the OML interested by the Langmuir circulation.

In the two irradiance field cases the decrease quantified passing from the first kind of mixing to the Langmuir one is of almost 5% in the more transparent waters and of almost 10% in the more turbid waters. It is important to note that the decrease of the mean irradiance perceived by the individuals between the two kind of mixing is of the 11% in the more transparent waters ($Z_{eu} \approx Z_m \approx 65$m in the Ekman case) and of the 16 % in the other case ($Z_{eu} \approx 35$, that is to say $Z_{eu} \approx 1/2\, Z_m$ of the Ekman case).

What can be inferred from the above responses about key evolutionary constraints on phytoplankton?

The photo-acclimative responses considered in this study decrease the daily biomass accumulation by 70 % in fluctuating regimes with a large daily total supply and increase it by 148% in similar regimes under low daily total supply of irradiance.

Those large differences may be overestimated because the comparison was made with the ideal condition of already acclimated cells without computing the average integrated growth rate.

However, the first one may be interpreted as the need to warrant the survival rates of the individuals, when subjected to potentially damaging irradiances, which would be

the case of highly transparent waters. This hypothetical advantage of the photosynthetic down-regulation via prevention of damage is not demonstrated by this study, but it seems a reasonable hypothesis.

By contrast, dynamic photo-acclimation increases biomass daily accumulation, when the irradiance is not so intense or, better, under mixed and shaded environment.

In addition, it has been shown that the light-dark alternation has an important effect to reset the photo-acclimative diurnal responses in 12:12 photo-period; its modification under longer or shorter photo-period requests further investigation.

It has been, also, shown that the daily averaged biochemical properties under sinusoidal and square wave irradiance are almost reproducible without any internal self-regulator, together with the recognized midday depression of photosynthetic performances, also if the NPQ related depression is not dynamically directly included in the model.

The timing of the increase and decrease of the $C : chla$ ratio, in experimental conditions, seems to anticipate the trigger of the transition between light and dark respect to the simulated ones. This observed shift, not reproduced in the simulation, could be related to the metabolic modifications related to the division process. Indeed, in the implemented IBM, the division process is just a consequence of a continuous growth. In the real phytoplankters the division process produces discrete cell-cycle stages that probably changes its necessity and behaviour. The influence of this neglected process on the overall results of the simulation cannot be determined, however its influence determining the anticipation of the trigger for the biochemical photo-related adjustments can be hypothesized.

An IBM approach is even more suited to analyze the possible impact of such regulative mechanisms, i.e., the interaction between photo-responses and cell cycle, under realistic conditions to determines whether and to what extent they can improve the fitness of phytoplankton in the mixed layer.

Part IV

Supplementary Material

Appendix A

Source Codes

A.1 Photo-physiological Individual Based Model for Phytoplankton Moving in the Mixed Layer

Fortran codes for the IBM described in chapter 6

A.1.1 main.f90

```
!program main.f90 for the IBM with trajectories derived by the LES
      program main
      implicit none
      integer i,days(2),ntot,ntotideal,jchl,ichl,ntotreal,nstrati,t,k,&
               ba, si(1),dada,j,p,ra,nstrato,day,ka,ntota,ntotin,id,&
               itermorte,pu,tm,du,daysf,rest
       integer,allocatable,dimension (:,:) :: indprof,indiv
       integer,allocatable,dimension (:) :: ri
       real jul, Emax, lat, kw, kc,rappr,z,Nq1,N0,Next,deltat,Eo,&
            pi,psi,delta,tz,sb,o,nfot1,sigma01,tau1,kd1,kr1,ChlCiniz1,&
            nfot2,sigma02,tau2,kd2,kr2,ChlCiniz2,&
            nfot3,sigma03,tau3,kd3,kr3,ChlCiniz3,mortraterest(2),&
            mortrate
       real proftot2(200000,480), xtot2(200000,480),ytot2(200000,480),&
            E(1440),baba(200000),A(480,200000),cont(1:121)
       real, allocatable :: &
       ChlC0(:),ChlC1(:),ChlC(:,:),C0(:),C1(:),C(:,:),&
       NC0(:),NC1(:),sigma1(:),sigma0(:),inib0(:),inib1(:),&
       mamma0(:),mamma1(:),prof1(:),prof(:,:),&
       Ez1(:),Ez(:,:),Cu1(:),Cu(:,:),&
       chlmat(:,:),chl(:),ncellmat(:,:),ncell(:),kchlmat(:,:),kchl(:),&
       flag(:,:),ind(:),morte0(:),morte1(:),ind2(:,:),Pcm1(:),Pcm0(:)
!
         days(1)=10
         days(2)=2
         daysf=days(1)+days(2)
        ntota=20000 ! solo x dichiarazione matrici
        nstrati=121
        ntot=2400
        ntotin=ntot/3
!
        allocate(ChlC0(ntota),ChlC1(ntota),&
                 C0(ntota),C1(ntota),&
                 NC0(ntota),NC1(ntota),sigma1(ntota),&
                 inib0(ntota),inib1(ntota),sigma0(ntota),&
```

```
                mamma0(ntota),mamma1(ntota),&
                prof1(ntota),&!prof(ntota,g) ,&
                Ez1(ntota),&!Ez(ntota,g)       ,&
                Cu1(ntota),&!Cu(ntota,g)   ,&
                chl(nstrati),Pcm0(ntota),Pcm1(ntota),&
                ncell(nstrati),&
                kchl(nstrati) ,&
                flag(200000,daysf),indprof(ntota,daysf),ri(ntota),&
                ind(ntota),ind2(ntota,2),&
                morte0(ntota),morte1(ntota))

        open(332,file='NC.dat',access='append')
        open(333,file='ChlC.dat',access='append')

        open(334,file='C.dat',access='append')
        open(335,file='inib.dat',access='append')
        open(336,file='prof.dat',access='append')
        open(337,file='Ez.dat',access='append')
        open(338,file='Cu.dat',access='append')
        open(339,file='sigma.dat',access='append')
        open(444,file='chlmat.dat',access='append')
        open(445,file='ncellmat.dat',access='append')
        open(446,file='kchlmat.dat',access='append')
!
        open(666,file='ind.dat',access='append')
        open(667,file='ind2.dat',access='append')
!
!**********read x y and z of the LES trajectories from three external file
        open(11,file='../trajcassandra_120m/x_120.txt',action='read',status='old')
        read(11,*) A
        xtot2=transpose(A)
        close(11)
        open(12,file='../trajcassandra_120m/y_120.txt',action='read',status='old')
        read(12,*) A
        ytot2=transpose(A)
        close(12)
        open(13,file='../trajcassandra_120m/z_120.txt',action='read',status='old')
        read(13,*) A
        proftot2=120.-(transpose(A))
        close(11)

         i=1000
```

```
        j=400
           write(*,*)i,j,xtot2(i,j)
           write(*,*)i,j,ytot2(i,j)
           write(*,*)i,j,proftot2(i,j)
           write(*,*) 'inizio'
! create a vector for the light
       jul=31+28+15
       Emax=1500
       lat=40

       pi=4.0*atan(1.0)
       write(*,*) pi
       kw=0.027 !morel 1988
       kc=0.0518!morel 1988
       psi=2*pi*jul/365.

       do i=1,1440
          tz=2*pi*i/1440
          delta=0.39637-22.9133*cos(psi)+4.02543*sin(psi)-&
                0.3872*cos(2.*psi)+0.052*sin(2.*psi)
          sb=sin(lat*pi/180.)*sin(delta*pi/180.)-cos(lat*pi/180.)*&
             cos(delta*pi/180.)*cos(tz)
        if (sb.gt.0) then
                E(i)=Emax*sb
        else
                E(i)=0
        endif

       enddo
      ! ****** parameters for the transparent water case ******

        nfot1=0.1533e-4*1.08
        sigma01=1.6
        tau1=0.0058
        kd1=6*(1.e-7)
        kr1=kd1/0.00065
        ChlCiniz1=0.0421

       mortraterest(1)=0
       mortraterest(2)=.1

      !inizialization
```

```
inib0(1:ntot)=0.
ChlC0(1:ntotin)=ChlCiniz1
ChlC0(ntotin+1:2*ntotin)=ChlCiniz1
ChlC0(2*ntotin+1:3*ntotin)=ChlCiniz1
morte0(1:ntot)=0.

C0(1:ntot)=1.e-8
NC0(1:ntot)=0.2
sigma0(1:ntot)=sigma01
Pcm0(1:ntot)=ChlCiniz1*nfot1/tau1
rappr=2*1.e6
ntotideal=ntot*rappr
mamma0(1:ntot)=0.
flag(:,1)=1.

 nstrato=ntotin/120

 allocate(indiv(nstrato,nstrati-1))
 ra=1
 do k=1,3
 cont(1:121)=0
 do i=1,200000
 if (proftot2(i,480)>120.) then
 flag(i,1)=0
 elseif  (flag(i,1).ne.0) then
  j=floor(proftot2(i,1))+1
 if (cont(j).le.nstrato) then
 cont(j)=cont(j)+1
 indprof(ra,1)=i
 flag(i,1)=0
 ra=ra+1
 endif
 endif
 enddo
 enddo

 id=-12

do i=1,ntot
   ind(i)=i
   ind2(i,1)=i
   ind2(i,2)=1
```

```
           flag(indprof(i,1),1)=0
           prof1(i)=proftot2(indprof(i,1),1)
             write(778,*) prof1(i)
        enddo

        sigma1(:)=sigma0(:)
        Pcm1(:)=Pcm0(:)
         NC1(:)=NC0(:)
        inib1(:)=inib0(:)
        ChlC1(:)=ChlC0(:)
        C1(:)=C0(:)
        morte1(:)=morte0(:)
        deltat=180
        ntotreal=ntot
        ba=1
        write(*,*) 'ciclo'
!****if rest =1 spinup if rest = 2 realistic simulation
        do rest=1,2
        write(*,*),'rest',rest
        pause
        mortrate=mortraterest(rest)

        itermorte=nint((mortrate*(ntotreal)*(deltat/(60*60*24)))**-1)
        write(*,*)'itermorte',itermorte

! *****start do on the days
        do day=1,days(rest)
        write(*,*)'ntot',ntot
        write(*,*)'ntotreal',ntotreal

                              if (day.ne.1) then
                              flag(:,day)=1.
                              do i=1,ntot
                                   flag(indprof(i,day-1),day)=0
                              enddo
                              do i=1,200000
                                 if (proftot2(i,480)>120.) then
                                     flag(i,day)=0
                                 endif
                               enddo

                              do i=1,ntot
```

```
                        ka=indprof(i,day-1)
                        do j=1,200000
                        baba(j)=flag(j,day)*sqrt((xtot2(j,1)-&
                    xtot2(ka,480))**2+(ytot2(j,1)-ytot2(ka,480))**2+&
                    33*((proftot2(j,1)-proftot2(ka,480))**2))
                    enddo
                    dada=minloc(baba,DIM=1,MASK=baba.gt.0)
                    indprof(i,day)=dada
                    flag(dada,day)=0
                    enddo
                    endif
                    write(*,*)'day',day
                    write(*,*)'ntot',ntot
                tm=0
      t=0

! *****start integration with time ******************************
      do k=0,3600*24-deltat,deltat
            t=t+1
            tm=tm+1
            o=(3*t/1440)
            Eo=E(1+t*3-nint(o)*1440)
            chl(1:121)=0
            ncell(1:121)=0
! **********start selfshading effect*****************************
            do du=1,ntot
               if (ChlC1(du).ne.0) then
               jchl=floor(prof1(du))+1
               chl(jchl)=chl(jchl)+ChlC1(du)*C1(du)*rappr
               ncell(jchl)=ncell(jchl)+1
               endif
            enddo
            do du=1,nstrati
               kchl(du)=kc*(sum(chl(1:du)**0.428))!morel 1988
            enddo
!**********end selfshading effect************************
              call rperm(ri,ntot,id)
              pu=0
! **********start do on the individuals*****************************
            do p=1,ntot
               i=ri(p)
               prof1(i)=proftot2(indprof(i,day),t)
```

```
              ichl=floor(prof1(i))
              Ez1(i)=Eo*exp(-kw*prof1(i)-kchl(ichl))
!              Ez1(i)=207.93
! *************start if to see if the cell duplicates or normally reacts***************
              if ((mamma0(i).ne.1.).and.&
              (morte1(i).ne.1)) then
!*********call subroutine GMHM for the resolution of the photophysiology and growth
            call GMHM(nfot1,sigma0(i),tau1,kd1,kr1,ChlCiniz1,&
            Ez1(i),C0(i),ChlC0(i),inib0(i),C1(i),rest,&
            ChlC1(i),inib1(i),Cu1(i),mamma1(i),NC0(i),NC1(i),&
            sigma1(i),Pcm0(i),Pcm1(i))

              elseif(mamma1(i).eq.1.) then

                    ntot=ntot+1
                    if (ntot.gt.ntota) then
                 write(*,*)'error troppe cellule x matrici ora',ba
                             stop
                    endif

                    ntotreal=ntotreal+1
                    C1(ntot)=C1(i)/2.
                    NC1(ntot)=NC1(i)
                    sigma1(ntot)=sigma1(i)
                    Pcm1(ntot)=Pcm1(i)

                    inib1(ntot)=inib1(i)

                    ChlC1(ntot)=ChlC1(i)
                    mamma1(ntot)=2.
                    ind(ntot)=ind(i)
                    ind2(ntot,1)=i
                    ind2(ntot,2)=ba
                    C1(i)=C1(i)/2.
                    mamma1(i)=2.
                    morte1(i)=0.
                    do j=1,200000
                       baba(j)=flag(j,day)*sqrt((xtot2(j,t)-&
                       xtot2(indprof(i,day),t))**2+(ytot2(j,t)-&
                     ytot2(indprof(i,day),t))**2+33*((proftot2(j,t)-&
                       proftot2(indprof(i,day),t))**2))
                    enddo
```

```
                        dada=minloc(baba,DIM=1,MASK=baba.gt.0)
                        indprof(ntot,day)=dada
                        flag(dada,day)=0
                        prof1(ntot)=proftot2(dada,t)

!***************end if if to see if the cell duplicates or normally reacts**********
       morte1(i)=1
       mamma1(i)=5
       C1(i)=0
       NC1(i)=0
       sigma1(i)=0
       Pcm1(i)=0
        ChlC1(i)=0
       Cu1(i)=0
       inib1(i)=0
       Ez1(i)=0
       else
               write(*,*)'error mortemamma',&
               morte0(i),morte1(i),mamma0(i),mamma1(i)
               pause
       endif
                if ((itermorte.eq.0).and.&
            (pu.lt.(nint(mortrate*(ntotreal)*(deltat/(60*60*24))))))&
                then
                pu=pu+1
                ntotreal=ntotreal-1
                morte0(i)=1
                morte1(i)=1
                C1(i)=0
                NC1(i)=0
                sigma1(i)=0
                Pcm1(i)=0
                ChlC1(i)=0
                Cu1(i)=0
                inib1(i)=0
                Ez1(i)=0
                mamma1(i)=5
                elseif((itermorte.ne.0).and.(pu.eq.0)&
                .and.((mod(tm,itermorte).eq.0).and.(morte0(i).ne.1)))&
                then
                pu=pu+1
                ntotreal=ntotreal-1
```

```
                morte1(i)=1
                C1(i)=0
                NC1(i)=0
                sigma1(i)=0
                Pcm1(i)=0
                ChlC1(i)=0
                Cu1(i)=0
                inib1(i)=0
                Ez1(i)=0
                mamma1(i)=5
                itermorte=nint((mortrate*(ntotreal)*&
                (deltat/(60*60*24)))**-1)
                tm=0
                endif


           enddo
!**********end do on the individuals**********************************
! ********at time t X0=X1 to start new integration*************
            C0(:)=C1(:)
            NC0(:)=NC1(:)
            sigma0(:)=sigma1(:)
            Pcm0(:)=Pcm1(:)
            ChlC0(:)=ChlC1(:)
            inib0(:)=inib1(:)
            mamma0(:)=mamma1(:)
            morte0(:)=morte1(:)
!*******save the results each time step if it is the realistic simulation*******
                        if (rest.eq.2) then
       write(332,*) NC0
       write(333,*)ChlC0
       write(334,*)C0
       write(335,*)inib0
       write(336,*)prof1
       write(337,*)Ez1
       write(338,*)Cu1
       write(339,*)sigma1
       write(444,*)chl
       write(445,*)ncell
       write(446,*)kchl
                   endif
                   ba=ba+1
```

```
            enddo
! *****end integration with time*******************************
                write(*,*)'ntot',ntot
                write(*,*)'ntotreal',ntotreal
! end do on the days
       enddo
!end do for the restart
       enddo
! write two controls and close all the files of output
           write(666,*)ind
           write(667,*)ind2
        write(*,*)'fine ntot=',ntot
        close(332)
        close(333)
        close(334)
        close(335)
        close(336)
        close(337)
        close(338)
        close(339)
        close(444)
        close(445)
        close(446)
       end
```

A.1.2 GMHM.f90

```
!soubroutine GMHM wich solves the photophysiology and the growth of singles cells
       subroutine GMHM(nfot,sigma0,tau,kd,kr,ChlCiniz,sole,C0,ChlC0,&
               inibc0,C,rest,ChlC,inibc,Cu,mamma,NC0,NC,sigma,Pcm0,Pcm)
       implicit none
       real nfot,sigma,tau,kd,kr,sole,C0,ChlC0,NC0,C,ChlC,NC,Cu,dt,&
            alpha,ChlNm,Kn,N_cost,NCm,NCo,shap,Ccellmax,irr,E,&
            Pcm,Pqm,PS,Nam,Na,ChlCs,Cg,dNC,ChlCiniz,N,N0,&
            inibc0, inibc, dinibc,mamma,NCred,ChlCm,basres,S,sigma0,b,&
            iniba,inibb,k,Pcm0
!
       integer LD,rest
        k=kd/kr
       NCo=0.05
       N_cost=3.21
       dt=180
       N0=7*14.2
```

```
       Kn=0.1*14.2
       NCm=0.2
       NCred=0.1760
       ChlCm=0.072
       S=0.236
       sigma=sigma0
       b=0.627 ! bricaud JGR 1998
       alpha=(1-inibc0)*nfot*sigma !mgChl.a per umolphoton (m2g-1 chl.a)(gC umol-1 photon )
       if (sole.eq.0) then
              Pcm=Pcm0
       else
        Pcm=ChlCiniz*(1-inibc0)*nfot/tau!mg C mg C-1 sec-1
       endif
       shap=0.01
       ChlNm=0.389
       Ccellmax=20*1e-9 !mg C cell -1
!****intizialize the variables
       C=C0
       ChlC=ChlC0
       N=N0
       NC=NC0
       inibc=inibc0
      ! relative concentration of D1 destroyed protein
      ! inib=1 no inhibition!!!!
       E=sole+1e-3!% micro Einst m-2 sec -1
       Pqm=Pcm*((NC-NCo)/(NCm-NCo))! Maximum  photosynthetic rate sec-1
       ! considering N status and photoinibition
       PS=Pqm*(1-exp(-alpha*ChlC*E/Pqm))
       !carbon specific rate of photosynthesis (gC g-1C sec-1)
       ! considering photoinhibition
       Nam=Pcm*NCm*S
       !Maximum rate of N-assimilation (gN g-1C d-1)
       Na=Nam*((1-NC/NCm)/(1-NC/NCm+shap))*N/(N+Kn)
       !N-source assimilation(transport+incorporation) (gN g-1C sec-1)
       Cu=PS-(N_cost*Na)
       !C-specific growth rate is photosynthesis minus respiration
       !associated with N-assimilation) (gC g-1C sec-1)
       ChlCs=Na*ChlNm*(PS/(alpha*ChlC*E))-ChlC*Cu
!
!
           iniba=(1+sigma*E*tau+k*tau*(sigma*E)**2)**-1
           !centers steady state solution han2002
```

```
!
           inibb=iniba*sigma*E*tau
           !closed centers steady state solution han 2002
!
           dinibc=-kr*(inibc)+kd*sigma*E*inibb
           ! variation in the inactivated centers han 2002:
           ! variation of the relative concentration of D1 protein
           ! inhibition in strictly due to difference between
           ! protein recovered and protein destroyed by the light
!
         Cg=C*Cu
           !Increase in C biomass (mgC cell-1 sec-1)
           dNC=NC*Cu
           !Correction of NC with C increase (gN g-1C d-1)
!
! ***** rest-1 is to increase the carbon in the cell only
! ***** when it is the realistic simulation
        C=C0+(rest-1)*dt*Cg
        !C biomass (mgC cell-1)
!
      ChlC=min((ChlC0+dt*ChlCs),(ChlNm*NCm))
      !Chlorophyll:C (gChla g-1C)
!
        N=N0 !... -dt*Na*C*rappr
        !N source (nitrate and/or ammonium) concentration
        !(usually a variable) (ugN L-1)
!
      inibc=inibc+dinibc*dt
        ! mg proten D1 /mg protein D1 ... ad
!
      NC=NC0-dt*dNC+dt*Na
        !Cell N-quota N:C (gN g-1C)
!
      sigma=sigma0*(ChlC/ChlC0)**b
      !antenna size of the reaction centers
!*******if to set mamma=1 if cell have to duplicate in the main program
       if (C.gt.Ccellmax) then
          mamma=1.
       else
          mamma=3.
       endif
       end subroutine
```

A.2 Photo-physiology under Simulated Periodically Fluctuating Irradiances

Matlab code for the SIN2c simulation under periodically fluctuating irradiance described in chapter 7

A.2.1 sinusvel10.m

```
%create a vector for the sinusoidal light
      jul=31+28+15
      Emax=1500
      lat=40

      pi=4.0*atan(1.0)
      kw=0.027 %%morel 1988
      kc=0.0518%morel 1988
      psi=2*pi*jul/365.

      for i=1:1440
         tz=2*pi*i/1440;
         delta=0.39637-22.9133*cos(psi)+4.02543*sin(psi)-...
               0.3872*cos(2.*psi)+0.052*sin(2.*psi);
         sb=sin(lat*pi/180.)*sin(delta*pi/180.)-cos(lat*pi/180.)*...
            cos(delta*pi/180.)*cos(tz);
       if (sb>0)
               Esin(i)=Emax*sb;
       else
               Esin(i)=0;
       end

       end
      % parameters for the turbid water case ******
nfot=0.1333e-4
tau=0.0058
kd= 8*(1.e-7)
kr= kd/0.0006
ChlCiniz=0.0517
sigmainiz=1.449;%1.5040e6

  k=kd/kr
  NCo=0.05
  N_cost=3.21
  dt=180
```

```
  N0=7*14.2 % valore alto nuts replete
  Kn=0.1*14.2
  NCm=0.2
  NCred=0.1760
  ChlCm=0.072
  S=0.236
  b=0.627 % bricaud JGR 1998
  clear i
% start for on the hours
for ora =1:24
ora
%create vector for the 6 initial condition for the Chl:C ratio
for i=1:6
ChlC0v(i)=0.01*i;
end
clear i
%start for on the 6 initial condition for the Chl:C ratio
for ichlc=1:6
    ichlc
NC0=0.17;
N0=7.2*14.2;
ChlC0=ChlC0v(ichlc);
C0=15*1e-9;
np=20;
chl(1:121)=1.;
%calculate selfshading in the turbid water case
   for du=1:121
       kchl(du)=kc*(sum(chl(1:du).^0.428));
   end
%set the depth of the domain and the velocity of the patch in the domain
dominio=80;
as=1;
for i=1:10
vela(i)=0.002*10;
end
clear i

if suegiu==1
suegiu;
pause
itin=it+1
veli(1)=-vela(ivel)./(as+1)
```

```
veli(2)=as*vela(ivel)./(as+1)
prof0=dominio
else
it=(ora-1)*20;
itin=it+1;
prof0=0
veli(1)=as*vela(ivel)./(as+1);
veli(2)=-vela(ivel)./(as+1);
end

for ipr=3:2:1400
veli(ipr)=veli(1);
veli(ipr+1)=veli(2);
end
giro=1;
vel=veli(giro);
velm=(abs(veli(1))+abs(veli(2)))/2;
%initialize the variables
ChlC0=ChlC0v(ichlc);
sigma0=sigmainiz*(ChlC0/ChlCiniz)^b;
Pcm0=ChlCiniz*nfot/tau;
%start for to calculate the integration with time
for t=0:dt:60*60*24*18
it=it+1;
C=C0;
ChlC=ChlC0;
N=N0;
NC=NC0;
sigma=sigma0;
prof=prof0;
if prof<0
    sugiro(ichlc,ivel,suegiu+1,giro)=it;
vel;
prof=-prof;
  giro=giro+1;
vel=veli(giro);
end
if prof>80
prof=dominio*2-prof;
giro=giro+1;
vel=veli(giro);
giugiro(ichlc,ivel,suegiu+1,giro)=it;
```

```
end
ichl=ceil(prof)+1;
o=(3*it/1440);
Eo=Esin(1+it*3-floor(o)*1440);
Ez1=Eo*exp(-kw*prof-kchl(ichl));
E=Ez1+1e-3;%
if it==itin
iniba0=(1+sigma*E*tau+k*tau*(sigma*E)^2)^-1; %centers open steady state han2002
inibb0=iniba0*sigma*E*tau; %centers closed steady state han 2002
inibc0=1-(iniba0+inibb0)
end
inibc=inibc0;
 alpha=(1-inibc)*nfot*sigma; %mgChl.a per umolphoton (m2g-1 chl.a)(gC umol-1 photon )
 Pcm=Pcm0*isnan(Ez1/Ez1)+(1-isnan(Ez1/Ez1))*ChlCiniz*(1-inibc)*nfot/tau;
 %mg C mg C-1 sec-1
 shap=0.01;
 ChlNm=0.389;
 Ccellmax=20*1e-9; %mg C cell -1
 Pqm=Pcm*((NC-NCo)/(NCm-NCo));% Maximum  photosynthetic rate sec-1
 % considering N status and photoinibition
 PS=Pqm*(1-exp(-alpha*ChlC*E/Pqm));
 %carbon specific rate of photosynthesis (gC g-1C sec-1)
 % considering fotoinibition
 %Nam=Pcm*NCm
 Nam=Pcm*NCm*S;
 %Maximum rate of N-assimilation (gN g-1C d-1)
 %for GM1 and GM2, delete S from equation
 Na=Nam*((1-NC/NCm)/(1-NC/NCm+shap))*N/(N+Kn);
 %N-source assimilation(transport+incorporation) (gN g-1C sec-1)
 Cu=PS-(N_cost*Na);
 %C-specific growth rate is photosynthesis minus respiration
 %associated with N-assimilation) (gC g-1C sec-1)
 ChlCs=Na*ChlNm*(PS/(alpha*ChlC*E))-ChlC*Cu;
 iniba=(1+sigma*E*tau+k*tau*(sigma*E)^2)^-1; %centers open steady state han 2002
 inibb=iniba*sigma*E*tau; %centers closed steady state han 2002
 dinibc=-kr*(inibc)+kd*sigma*E*inibb;%variaton in the centers inhibited han 2002
 % variation of the relative concentration of D1 protein
 % inhibition in strictly due to difference between
 % protein recovered and protein destroyed by the light
 Cg=C*Cu;
 %Increase in C biomass (mgC cell-1 sec-1)
 dNC=NC*Cu;
```

```
 %Correction of NC with C increase (gN g-1C d-1)
 C=C0+dt*Cg;
 %C biomass (mgC cell-1)
 ChlC=min((ChlC0+dt*ChlCs),(ChlNm*NCm));
 %Chlorophyll:C (gChla g-1C)
 N=N0; %... -dt*Na*C*rappr
 %N source (nitrate and/or ammonium) concentration
 %(usually a variable) (ugN L-1)
 inibc=inibc0+dinibc*dt;
 % mg proten D1 /mg protein D1 ... ad
 NC=NC0-dt*dNC+dt*Na;
 %%Cell N-quota N:C (gN g-1C)

sigma=sigmainiz*(ChlC/ChlCiniz)^b;
C0=C;
NC0=NC;
ChlC0=ChlC;
inibc0=inibc;
sigma0=sigma;
Pcm0=Pcm;
prof0=prof+vel*dt;
%save the results in a threedimensional matrix:it is the time step of the simulation
%ichlc depends on the initial condition for chl:C
%ivel can be setted to change if the simulation for different velocities (SIN2a,b or c)
%is due contemporarly
Cv(it,ichlc,ivel)=C;
NCv(it,ichlc,ora,ivel)=NC;
ChlCv(it,ichlc,ora,ivel)=ChlC;
inibcv(it,ichlc,ora,ivel)=inibc;
sigmav(it,ichlc,ora,ivel)=sigma;
profv(it,ichlc,ora,ivel)=prof;
Ev(it,ichlc,ora,ivel)=E;
Cuv(it,ichlc,ora,ivel)=Cu;
rhochl1v(it,ichlc,ora,ivel)=Na*ChlNm*(PS/(alpha*ChlC*E));
rhochlc2v(it,ichlc,ora,ivel)=(PS/(alpha*ChlC*E));
PSv(it,ichlc,ora,ivel)=PS;
Pqmv(it,ichlc,ora,ivel)=Pqm;
Nav(it,ichlc,ora,ivel)=Na;
end
end
end
%save the results in a MATLAB output file
```

```
save sinusvel10
```

Bibliography

N. Adir, Hagit Z., S. Shochat, and O. Itzhak. Photoinhibition - a historical perspective. *Photosynthesis Research*, 76:343–370, 2003.

M. A. Altabet, M. J. Higginson, and D. W. Murray. The effect of millennial-scale changes in arabian sea denitrification on atmospheric co2. *Nature*, 415:159–162, 2002.

J. M. Anderson, Y. Park, and W. S. Chow. Unifying model for the photoinactivation of photosystem ii in vivo under steady-state photosynthesis. *Photosynthesis Research*, 56: 1–13, 1998.

T. Anning, H. L. MacIntyre, S. M. Pratt, P. J. Sammes, S. Gibb, and R. J. Geider. Photoacclimation in the marine diatom skeletonema costatum. *Limnol Oceanogr*, 45(8): 1807–1817, 2000.

D. E. Archer and K. Johnson. A model of the iron cycle in the ocean. *Global Biogeochemical Cycles*, 14:269–279, 2000.

L. Arin, C. Marrase, M. Maar, F. Peters, M. M. Sala, and M. Alcaraz. Combined effects of nutrients and small-scale turbulence in a microcosm experiment. I. Dynamics and size distribution of osmotrophic plankton. *Aquatic Microbial Ecology*, 29(1):51–61, 2002.

M. Babin, A. Morel, and B. Gentili. Remote sensing of sea surface Sun-induced fluorescence: consequences of natural variations in the optical characteristics of phytoplankton and the quantum yield of chlorophyll a fluorescence. *International Journal of Remote Sensing*, 17:2417–2448, 1996.

M. Baklouti, F. Diaz, C. Pinazo, V. Faure, and B. Queguiner. Investigation of mechanistic formulations depicting phytoplankton dynamics for models of marine pelagic ecosystems and description of a new model. *Progress in Oceanography*, 71:1–33, 2006a.

M. Baklouti, V. Faure, L. Pawlowski, and A. Sciandra. Investigation and sensitivity analysis of a mechnaistic phytoplankton model implemented in a new modular numerical tool (eco3m) dedicated to biogeochemical modelling. *Progress in Oceanography*, 71:34–58, 2006b.

S. L. Baldauf. The deep roots of eukaryotes. *Science*, 300:1703–1706, 2003.

T. T. Bannister and E. A. Laws. Modeling phytoplankton carbon metabolism. In P. G. Falkowski, editor, *Primary Productivity in the Sea*, pages 243–248. Plenum, New York, 1980.

R. Barrett, M. Berry, T. Chan, J. Demmel, J. Donato, J. Dongarra, V. Eijkhout, R. Pozo, C. Romine, and H. Van Der Vost. *Templates for the Solution of Linear Systems: Building Blocks for Iterative Methods*. SIAM, Philadelphia, 1994.

R. Bassi and S. Caffarri. Lhc proteins and the regulation of photosynthetic light harvesting function by xanthophylls. *Photosynthesis Research*, 64:243–256, 2000.

G. N. Baturin. Phosphorus cycle in the ocean. *Lithology and Mineral Resources*, 38: 101–119, 2003.

M. J. Behrenfeld, O. Prasil, Z. S. Kolber, M. Babin, and P. G. Falkowski. Compensatory changes in Photosystem II electron turnover rates protect photosynthesis from photoinhibition. *Photosynthesis Research*, 58(3):259–268, 1998.

M. J. Behrenfeld, O. Prasil, M. Babin, and F. Bruyant. In search of a physiological basis for covariations in light-limited and light-saturated photosynthesis. *Journal of Phycology*, 40(1):4–25, 2004.

D. Blasco. Observations on the diel migration of marine dinoflagellates off the Baja California coast. *Marine Biology*, 46(1):41–47, 1978.

A. Bricaud, A. Morel, M. Babin, K. Allali, and H. Claustre. Variations of light absorption by suspended particles with the chlorophyll a concentration in oceanic (Case 1) waters: analysis and implications for bio-optical models. *Journal of Geophysical Research*, 103 (C13):33,33–34,33, 1998.

W. S. Broecker and T. Peng. *Tracers in the sea*. Lamont-Doherty Geological Observatory, New York, 1982.

C. Brunet, R. Casotti, B. Aronne, and V. Vantrepotte. Measured photophysiological parameters used as tools to estimate vertical water movements in the coastal Mediterranean. *Journal of Plankton Research*, 25(11):1413–1425, 2003.

D. Campbell, V. Hurry, A. K. Clarke, P. Gustafsson, and G. Oquist. Chlorophyll Fluorescence Analysis of Cyanobacterial Photosynthesis and Acclimation. *Microbiol. Mol. Biol. Rev.*, 62(3):667–683, 1998.

C. Casper-Lindley and O. Björkman. Fluorescence quenching in four unicellular algae with different light-harvesting and xanthophyll-cycle pigments. *Photosynthesis Research*, 56 (3):277–289, 1998.

D. Cianelli, M. Ribera d'Alcala', V. Saggiomo, and E. Zambianchi. Coupling mixing and photophysiological response of antarctic plankton: a lagrangian approach. *Antarctic Science*, 16(2):133–142, 2004.

P. Claquin, J. C. Kromkamp, and V. Martin-Jezequel. Relationship between photosynthetic metabolism and cell cycle in a synchronized culture of the marine alga Cylindrotheca fusiformis (Bacillariophyceae). *European Journal of Phycology*, 39(1):33–41, 2004.

H. Claustre, A. Bricaud, M. Babin, F. Bruyant, L. Guillou, F. Le Gall, D. Marie, and F. Partensky. Diel variations in Prochlorococcus optical properties. *Limnol. Oceanogr*, 47(6):1637–1647, 2002.

A. D. D. Craik and S. Leibovich. A rational model for Langmuir circulations. *Journal of Fluid Mechanics*, 73:401–426, 1976.

J. J. Cullen and M. R. Lewis. The kinetics of algal photoadaptation in the context of vertical mixing. *J. Plankton Res*, 10(5):1039–1063, 1988.

J. J. Cullen and G. J. MacIntyre. Behavior, physiology and the niche of depth-regulating phytoplankton. In D. M. Anderson, A. D. Cembella, and G. M. Hallegraeff, editors, *Physiological ecology of Harmful Algal Blooms*. Springer-Verlag, Heidelburg, 1998.

J. J. Cullen, P. J. S. Franks, D. M. Karl, and A. Longhurst. Physical influences on marine ecosystem dynamics. In Allan R. Robinson, McCarthy James J., and Rothschild Brian J., editors, *The Sea*, volume 12 of *The Sea*, pages 297–336. John Wiley and Sons, New York, 2002.

C. De Boor. *A Practical Guide to Splines*. Springer, 2002.

C. de Boyer Montégut, G. Madec, A. S. Fischer, A. Lazar, and D. Iudicone. A global mixed layer depth climatology based on individual profiles. *Journal of Geophysical Research*, 68(2), 2004.

B. Demmig-Adams and W. W. Adams. Photoprotection and Other Responses of Plants to High Light Stress. *Annual Review of Plant Physiology and Plant Molecular Biology*, 43(1):599–626, 1992.

K. L. Denman and J. Marra. Modelling the time dependent photoadaptation of phytoplankton to fluctuating light. *Elsevier Oceanography Series*, 42:341–359, 1986.

J. D. Dodge and B. Hart-Jones. The Vertical and Seasonal Distribution of Dinoflagellates in the North Sea II. Blyth 1973-1974 and Whitby 1975. *Bot. Mar*, 20:307–311, 1977.

J. F. Dower and K. L. Denman. Small-scale physical processes and plankton biology. In J.H. Steele, S.A. Thorpe, and K.K. Turekian, editors, *Encyclopedia of Ocean Sciences*, pages 2834–2839. Academic Press, London, 2001.

P. Duarte and J. G. Ferreira. Dynamic modelling of photosynthesis in marine and estuarine ecosystems. *Environmental Modeling and Assessment*, 2(1):83–93, 1997.

Z. Dubinsky, P. G. Falkowski, and K. Wyman. Light Harvesting and Utilization by Phytoplankton. *Plant Cell Physiol.*, 27(7):1335–1349, 1986.

J. A. Dusenberry. Steady-state single cell model simulations of photoacclimation in a vertically mixed layer: implications for biological tracer studies and primary productivity. *Journal of Marine Systems*, 24:201–220, 2000.

J. A. Dusenberry, R. J. Olson, and S. W. Chisholm. Frequency Distributions of Phytoplankton Single-Cell Fluorescence and Vertical Mixing in the Surface Ocean. *Limnology and Oceanography*, 44(2):431–435, 1999.

E. Ebert, U. Schumann, and R. Stull. Nonlocal turbulent mixing in the convective boundary layer evaluated from large-eddy simulation. *Journal of the Atmospheric Sciences*, 46:2178–2207, 1989.

P. H. C. Eilers and J. C. H. Peeters. Dynamic behaviour of a model for photosynthesis and photoinhibition. *Ecological Modelling*, 69(1):113–133, 1993.

V. W. Ekman. On the influence of the earth's rotation on ocean-currents. *Arkiv Fur Matematic, Astronomi och Fysik*, 2(11):1–53, 1905.

J. Escoubas, M. Lomas, J. LaRoche, and P. G. Falkowski. Light intensity regulation of cab gene transcription is signaled by the redox state of the plastoquinone pool. *Proc. Natl. Acad. Sci. USA*, 92:10237–10241, 1995.

P. G. Falkowski. Light-shade adaptation and vertical mixing of marine phytoplankton: a comparative field study. *J. Mar. Res*, 41:215–237, 1983.

P. G. Falkowski and J. LaRoche. Acclimation to spectral irradiance in algae. *Journal of Phycology*, 27:8–14, 1991.

P. G. Falkowski and T. G. Owens. Light-shade adaptation two strategies in marine phytoplankton. *Plant Physiology*, 66:592–595, 1980.

P. G. Falkowski and J. A. Raven. *Aquatic Photosyntesis*. Blacwell Science, Oxford, 1997.

P. G. Falkowski and C. D. Wirick. A simulation model of the effects of vertical mixing on primary productivity. *Marine Biology*, 65(1):69–75, 1981.

P. G. Falkowski, R. T. Barber, and V. Smetacek. Biogeochemical controls and feedbacks on ocean primary production. *Science*, 281:200–206, 1998.

D. Farmer and C. McNeil. Photoadaptation in a convective layer-Observations. *Deep Sea Research Part II: Topical Studies in Oceanography*, 46(11):2433–2446, 1999.

B. Faugeras, O. Bernard, A. Sciandra, and M. Levy. A mechanistic modelling and data assimilation approach to estimate the carbon/chlorophyll and carbon/nitrogen ratios in a coupled hydrodynamical-biological model. *Nonlinear Processes in Geophysics*, 11(4): 515–533, 2004.

T. Fisher, R. Shurtz-Swirski, S. Gepstein, and Z. Dubinsky. Changes in the Levels of Ribulose-l,5-bisphosphate Carboxylase/Oxygenase (Rubisco) in Tetraedron minimum (Chlorophyta) during Light and Shade Adaptation. *Plant Cell Physiol.*, 30(2):221–228, 1989.

I. A. Flameling and J. Kromkamp. Photoacclimation of scenedesmus protuberans (chlorophyceae) to fluctuating irradiances simulating vertical mixing. *Journal of Plankton Research*, 19:1011–1024, 1997.

K. J Flynn, M. J. R. Fasham, and C. R. Hipkin. Modelling the interaction between ammonium and nitrate uptake in marine phytoplankton,. *Philosophical Transactions of the Royal Society*, 352:1625–1645, 1997.

K. J. Flynn, H. L. Marshall, and R. J. Geider. A comparison of two n-irradiance interaction models of phytoplankton growth. *Limnology and Oceanography*, 46(7):1794–1802, 2001.

P. J. S. Franks and J. Marra. A simple new formulation for phytoplankton photoresponse and an application in a wind-driven mixed-layer model. *Marine Ecology Progress Series*, 111(1):143–153, 1994.

E. Garcia-Mendoza, H. C. P. Matthijs, H. Schubert, and L. R. Mur. Non-photochemical quenching of chlorophyll fluorescence in chlorella fusca acclimated to constant and dynamic light conditions. *Photosynthesis Research*, 74(3):303–315, 2002.

R. W. Garwood. An ocean mixed layer model capable of simulating cyclic states. *J. Phys. Oceanogr.*, 7:455–468, 1977.

R. J. Geider, H. L. MacIntyre, and T. M. Kana. A dynamic model of photoadaptation in phytoplankton. *Limnol. Oceanogr.*, 41:1–15, 1996.

R. J. Geider, H. L. MacIntyre, and T. M. Kana. A dynamic model of phytoplankton growth and acclimation: Responses of the balanced growth rate and chlorophyll a: Carbon ratio to light, nutrient limitation and temperature. *Mar. Ecol. Prog. Ser.*, 148:187–200, 1997.

R. J. Geider, H. L. MacIntyre, L. M. Graziano, R. McKay, and L. Michael. Responses of the photosynthetic apparatus of dunaliella tertiolecta (chlorophyceae) to nitrogen and phosphorus limitation. *European Journal of Phycology*, 33(4):315–332, 1998a.

R. J. Geider, H. L. MacIntyre, and T. M. Kana. A dynamic regulatory model of phytoplanktonic acclimation to light, nutrients, and temperature. *Limnol. Oceanogr.*, 43: 679–694, 1998b.

I. Grouneva, T. Jakob, C. Wilhelm, and R. Goss. Influence of ascorbate and pH on the activity of the diatom xanthophyll cycle-enzyme diadinoxanthin de-epoxidase. *Physiologia Plantarum*, 126:205–211, 2006.

G. Guglielmi, J. Lavaud, B. Rousseau, A. L. Etienne, J. Houmard, and A. V. Ruban. The light-harvesting antenna of the diatom Phaeodactylum tricornutum. *FEBS Journal*, 272 (17):4339, 2005.

B. P. Han. A Mechanistic Model of Algal Photoinhibition Induced by Photodamage to Photosystem-II. *Journal of Theoretical Biology*, 214(4):519–527, 2002.

B. P. Han, M. Virtanen, J. Koponen, and M. Straskraba. Effect of photoinhibition on algal photosynthesis: a dynamic model. *J. Plankton Res.*, 22(5):865–885, 2000.

F. H. Harlow and J. E. Welch. Numerical calculation of time-dependent viscous incompressible flow. *Phys. Fluids*, 8(12):2182–2189, 1965.

G. R. Hasle. Phototactic vertical migration in marine dinoflagellates. *Oikos*, 2(2):162–175, 1950.

H. Havelková-Doušová, O. Prášil, and M.J. Behrenfeld. Photoacclimation of Dunaliella tertiolecta (Chlorophyceae) Under Fluctuating Irradiance. *Photosynthetica*, 42(2):273–281, 2004.

R. Herzig and Z. Dubinsky. Effect of photoacclimation on the energy partitioning between cyclic and non-cyclic photophosphorylation. *New Phytologis*, 123(4):665–672, 1993.

Y. Huot. *Sun-Induced Fluorescence of Phytoplankton in the Ocean: Linking Physiology and Remote Sensing*. PhD thesis, Dalhousie University, Halifax, Nova Scotia, December 2004.

G. E. Hutchinson. The paradox of the plankton. *The American Naturalist*, 95:137–145, 1961.

B. W. Ibelings, B. M. A. Kroon, and L. R. Mur. Acclimation of Photosystem II in a Cyanobacterium and a Eukaryotic Green Alga to High and Fluctuating Photosynthetic Photon Flux Densities, Simulating Light Regimes Induced by Mixing in Lakes. *New Phytologist*, 128(3):407–424, 1994.

M. Jansen, V. Gaba, B. M. Greenberg, A. K. Mattoo, and M. Edelman. Low threshold levels of ultraviolet-B in a background of photosynthetically active radiation trigger rapid degradation of the D 2 protein of photosystem-II. *Plant journal*, 9(5):693–699, 1996.

E. G. Jørgensen. The adaptation of plankton algae IV. Light adaptation in different algal species. *Physiologia Plantarum*, 22:1307–1315, 1969.

E.G. Jørgensen. Chlorophyll Content and Rate of Photosynthesis in Relation to Cell Size of the Diatom Cyclotella Meneghiniana. *Physiologia Plantarum*, 17(1004):136–145, 1964.

D. Kaftan, T. Meszaros, J. Whitmarsh, and L. Nedbal. Characterization of Photosystem II Activity and Heterogeneity during the Cell Cycle of the Green Alga Scenedesmus quadricauda. *Plant Physiology*, 120(2):433–442, 1999.

D. Kamykowski, H. Yamazaki, and G. S. Janowitz. A lagrangian model of phytoplankton photosynthetic response in the upper mixed layer. *J. Plankton Res.*, 16(8):1059–1069, January 1, 1994 1994.

L.H. Kantha and C.A. Clayson. *Small Scale Processes in Geophysical Fluid Flows.* Academic Press, 2000.

L.H. Kantha and C.A. Clayson. An improved mixed layer model for geophysical applications. *Journal of Geophysical Research*, 99(C12):25235–25266, 1994.

L. Karp-Boss, E. Boss, and P. A. Jumars. Nutrient fluxes to planktonic osmotrophs in the presence of fluid motion. *Oceanography and Marine Biology Annual Review*, 34:71–107, 1996.

D. A. Kiefer and B. G. Mitchell. A Simple, Steady State Description of Phytoplankton Grwoth Based on Absorption Cross Section and Quantum Efficiency. *Limnology and Oceanography*, 28(4):770–776, 1983.

B. Kok. On the inhibition of photosynthesis by intense light. *Biochim Biophys Acta*, 21 (2):234–44, 1956.

A. N. Kolmogorov. The local structure of turbulence. *Dokl. Akad. Nauk SSSR*, 30:301–305, 1941.

T. Kondo, C. A. Strayer, R. D. Kulkarni, W. Taylor, M. Ishiura, S. S. Golden, and C. H. Johnson. Circadian Rhythms in Prokaryotes: Luciferase as a Reporter of Circadian Gene Expression in Cyanobacteria. *Proceedings of the National Academy of Sciences*, 90(12): 5672–5676, 1993.

E. B. Kraus and J. S. Turner. A one-dimensional model of the seasonal thermocline, ii, the general theory and its consequences. *Tellus*, 19:98–105, 1967a.

E. B. Kraus and J. S. Turner. *A One-dimensional Model of the Seasonal Thermocline.* Woods Hole Oceanographic Institution, 1967b.

J. Kromkamp and M. Limbeek. Effect of short-term variation in irradiance on light harvesting and photosynthesis of the marine diatom Skeletonema costatum: a laboratory study simulating vertical mixing. *JGM. Journal of general microbiology*, 139:2277–2284, 1993.

R. Kroning and J. Bruijesten. On the theory of heat and mass transfer from a sphere in a flowing medium at low values of reynolds number. *Applied Science Researches*, A(2): 439–446, 1951.

J. C. Lagarias, J. A. Reeds, M. H. Wright, and P. E. Wright. Convergence Properties of the Nelder–Mead Simplex Method in Low Dimensions. *SIAM Journal of Optimization*, 9(1):112–147, 1998.

I. Langmuir. Surface motion of water induced by wind. *Science*, 87:119–123, 1938.

W. G Large, J. C McWilliams, and S. C Doney. Oceanic vertical mixing: a review and a model with a nonlocal boundary layer parameterization. *Reviews of Geophysics*, 32(4): 363–404, 1994.

J. Lavaud, B. Rousseau, H. J. van Gorkom, and A. L. Etienne. Influence of the Diadinoxanthin Pool Size on Photoprotection in the Marine Planktonic Diatom Phaeodactylum tricornutum. *Plant Physiol.*, 129(3):1398–1406, 2002.

J. Lavaud, B. Rousseau, and A. L. Etienne. General features of photoprotection by energy dissipation in planktonic diatoms (bacillariophyceae). *Journal of Phycology*, 40:130–137, 2004.

E. A Laws, D. G. Redalje, D. M. Karl, and M. S. Chalup. A theoretical and experimental examination of the predictions of two recent models of phytoplankton growth. *Journal of Theoretical Biology*, 105(3):469–491, 1983.

B. P. Leonard and S. Mokhtari. Beyond first order upwinding: the ULTRA-SHARP alternative for nonoscillatory steady-state simulation of convection. *Int. J. Numer. Methods Eng*, 30(2):141–154, 1990.

B.P Leonard. Elliptic Systems: Finite-Difference Method IV. In W. J. Minkowycz, editor, *Handbook of Numerical Heat Transfer*. Wiley & Sons: New York, 1988.

M. R. Lewis, J. J. Cullen, and T. Platt. Relationships between vertical mixing and photoadaptation of phytoplankton: Similarity criteria. *Marine Ecology Progress Series*, 15 (1–2):141–149, 1984a.

M. R. Lewis, E. P. W. Horne, J. J. Cullen, N. S. Oakey, and T. Platt. Turbulent motions may control phytoplankton photosynthesis in the upper ocean. *Nature*, 311:49–50, 1984b.

M. Li and C. Garrett. Cell merging and the jet/downwelling ratio in Langmuir circulation. *Journal of Marine Research*, 51(4):737–769, 1993.

M. Li, C. Garrett, and E. Skyllingstad. A regime diagram for classifying turbulent large eddies in the upper ocean. *Deep-Sea Res. I*, 52:259–278, 2005.

S. P Long, S. Humpries, and Paul G. Falkowski. Photoinhibition of photosynthesis in nature. *Annu. Rev. Plant Physiol. Plant Mol. Biol.*, 45:633–662, 1994.

H. L. MacIntyre and R. J. Geider. Regulation of rubisco activity and its potential effect on photosynthesis during mixing in a turbid estuary. *Marine Ecology Progress Series*, 144:247–264, 1996.

H. L. MacIntyre, T. D. Sharkey, and R. J. Geider. Activation and deactivation of ribulose-1,5-bisphosphate carboxylase/oxygenase (rubisco) in three marine microalgae. *Photosynthesis Research*, 51:93–106, 1997.

H. L. MacIntyre, T. M. Kana, T. Anning, and R. J. Geider. Photoacclimation of photosynthesis irradiance response curves and photosynthetic pigments in microalgae and cyanobacteria. *Journal of Phycology*, 38(1):17–38, 2002.

K. H. Mann and J. R. N. Lazier. *Dynamics of marine ecosystems*. Blackwell Science, 2nd edition, 1996.

R. Margalef. Life-forms of phytoplankton as survival alternatives in an unstable environment. *Oceanologica Acta*, 1:493–509, 1978.

P. Mariani. *Effects of Small Scale Motion on Plankton*. PhD thesis, Università degli studi di Napoli "Federico II", 2004.

J. Marra. Effect of short-term variations in light intensity on photosynthesis of a marine phytoplankter: A laboratory simulation study. *Marine Biology*, 46(3):191—202, 1978a.

J. Marra. Phytoplankton photosynthetic response to vertical movement in a mixed layer. *Marine Biology*, 46(3):203–208, 1978b.

H. L. Marshall, R. J. Geider, and K. J. Flynn. A mechanistic model of photoinhibition. *New Phytologist*, 145(2):347–359, 2000.

J. C. McWilliams, P. P. Sullivan, and C. H. O. H. Moeng. Langmuir turbulence in the ocean. *Journal of Fluid Mechanics*, 334:1–30, 1997.

G. L. Mellor and P. A. Durbin. The structure and dynamics of the ocean surface mixed layer. *J. Phys. Oceanogr*, 5(71):8–728, 1975.

G. L. Mellor and T. Yamada. Development of a turbulence closure for geophysical fluid problems. *Rev. Geophys.*, 20:851–875, 1982.

G. L. Mellor and T. Yamada. A hierarchy of turbulence closure models for planetary boundary layers. *Journal of the Atmospheric Sciences*, 31(1791):1806, 1974.

L. Michaelis and M. L. Menten. Die Kinetik der Invertinwirkung. *Biochemische Zeitschrift*, 49:333–369, 1913.

C. M. Moore, D. J. Suggett, A. E. Hickman, Y. N. Kim, J. F. Tweddle, J. Sharples, R. J. Geider, and P. M. Holligan. Phytoplankton photoacclimation and photoadaptation in response to environmental gradients in a shelf sea. *Limnol. Oceanogr.*, 51(2):936–949, 2006.

A. Morel. Optical modeling of the upper ocean in relation to its biogenous matter content (case I waters). *Journal of Geophysical Research*, 93(C9):10,749–768,10, 1988.

P. Müller, X. P. Li, and K. K. Niyogi. Non-photochemical quenching. a response to excess light energy. *Plant Physiology*, 125:1558–1566, 2001.

W. H. Munk and J. A. Riley. Absorbtion of nutrients by acquatic plants. *Journal of Marine Researches*, 11:215–240, 1952.

J. Myers. Culture conditions and development of the photosynthetic mechanism. III. influence oflight intensity on the cellular characteristics of *Chlorella. J. Gen. Physiol.*, 29: 419–427, 1946a.

J. Myers. Culture conditions and development of the photosynthetic mechanism. IV. influence oflight intensity on the photosynthetic characteristics of *Chlorella. J. Gen. Physiol.*, 29:429–440, 1946b.

T. Nagai, H. Yamazaki, and D. Kamikowski. A lagrangian photoresponse model coupled with 2nd-order turbulence closure. *Marine Ecology Progress Series*, 265:17–30., 2003.

P. J. Neale and P. J. Richerson. Photoinhibition and the diurnal variation of phytoplankton photosynthesis. 1. Development of a photosynthesis-irradiance model from studies of in situ responses. *Journal of Plankton Research*, 9(1):167–193, 1987.

J. A. Nelder and R. Mead. A simplex method for function minimization. *Computer Journal*, 7(4):308–313, 1965.

I. Ohad, N. Keren, H. Zer, H. Gong, T. S. Mor, A. Gal, S. Tal, and Y. Eisenberg-Domovich. Light induced degradation of the photochemical reaction center II-D1 protein in vivo: an integrative approach. *Photoinhibition of Photosynthesis: from the Molecular Mechanisms to the Field*, pages 161–177, 1994.

R. J. Olson, S. W. Chisholm, E. R. Zettler, and J. A. Dusenberry. Advances in oceanographythrough flow cytometry. In S. Demers, editor, *Individual Cell and Particle Analysis in Oceanography*. Springer-Verlag, 1991.

C. Pahl-Wostl and D.M. Imboden. DYPHORA–a dynamic model for the rate of photosynthesis of algae. *J. Plankton Res.*, 12(6):1207–1221, 1990.

Y. I. I. Park, W. S. Chow, C. B. Osmond, and J. M. Anderson. Electron transport to oxygen mitigates against the photoinactivation of Photosystem II in vivo. *Photosynthesis Research*, 50(1):23–32, 1996.

W. J. Pasciak and J. Gavis. Transport limitation of nutrient uptake in phytoplankton. *Limnology and Oceanography*, 19(6):881–888, 1974.

L. Pawlowski, O. Bernard, E. Le Floc'h, and A. Sciandra. Qualitative behaviour of a phytoplankton growth model in a photobioreactor. In *Proceedings of the 15th IFAC World Congress*, Barcelona, Spain, 2002.

M. J. Perry, M. C. Talbot, and R. S. Alberte. Photoadaption in marine phytoplankton: Response of the photosynthetic unit. *Marine Biology*, 62(2):91–101, 1981.

T. Pfannschmidt, A. Nilsson, and J. F. Allen. Photosynthetic control of chloroplast gene expression. *Nature*, 397:625–628, 1999.

O. M. Phillips. *The Dynamics of the Upper Ocean*. Cambridge University Press, 1977.

J. Piera. *Signal processing of microstructure profiles: integrating turbulent spatial scales in aquatic ecological modeling*. PhD thesis, Universidad de Girona, 2002.

T. Platt, C. L. Gallegos, and W. G. Harrison. Photoinhibition of photosynthesis in natural assemblages of marine phytoplankton. *J. Mar. Res*, 38(4):687–701, 1980.

A. F. Post, Z. Dubinski, K. Wyman, and P. G. Falkowski. Kinetics of light-intensity adaptation in a marine planktonic diatom. *Mar. Biol.*, 83:231–238, 1984.

J. F. Price and M. A. Sundermeyer. Stratified Ekman layers. *Journal of Geophysical Research*, 104(C9):20467–20494, 1999.

J. F. Price, R. A. Weller, and R. Pinkel. Diurnal cycling: Observations and models of the upper ocean response to diurnal heating, cooling, and wind mixing. *J. Geophys. Res.*, 91:8411–8427, 1986.

E. M. Purcell. Life at low reynolds number. *American Journal of Physics*, 45:3–11, 1977. B006 - Physics and our world: A symposium in honor of Victor F. Weiskopf.

A. Quigg and J. Beardall. Protein turnover in relation to maintenance metabolism at low photon flux in two marine microalgae. *Plant Cell and Environment*, 26(5):693–703, 2003.

M. Ragni. *Circadian patterns in key physiological processes of the marine diatom Phaeodactilum tricornutum*. PhD thesis, Open University, London, 2005.

O. Ragueneau, P. Treguer, A. Leynaert, R. F. Anderson, M. A. Brzezinski, D. J. DeMaster, R. C. Dugdale, J. Dymond, G. Fischer, R. Francois, C. Heinze, E. Maier-Reimer, V. Martin-Jezequel, and B. Nelson, D. M.and Queguiner. A review of the si cycle in the modern ocean: recent progress and missing gaps in the application of biogenic opal as a paleoproductivity proxy. *Global and Planetary Change*, 26:317–365, 2000.

J. A. Raven. Chloroplasts of eukaryotic micro-organisms., 1980.

J. A. Raven. A cost-benefit analysis of photon absorption by photosynthetic unicells. *New Phytologist*, 98(4):593–625, 1984.

J. A. Raven and J. Beardall. The lower limit of photon fluence rate for phototrophic growth: the significance of'slippage' reactions. *Plant, Cell and Environment*, 5:117–124, 1982.

J. A. Raven, M. C. W. Evans, and R. E. Korb. The role of trace metals in photosynthetic electron transport in O 2-evolving organisms. *Photosynthesis Research*, 60(2):111–150, 1999.

K. Richardson, J. Beardall, and J. A. Raven. Adaptation of unicellular algae to irradiance: an analysis of strategies. *New Phytologist*, 93:157–191, 1983.

D. M. Riper, T. G. Owens, and P. G. Falkowski. Chl turnover in skeletonema costatum, a marine plankton diatom. *Plant Physiology*, 64:49–54, 1979.

O. N. Ross and J. Sharples. Recipe for 1-d lagrangian particle-tracking models in space-varying diffusivity. *Limnology and Oceanography Methods*, 2:289–302, 2004.

A. V. Ruban, J. Lavaud, B. Rousseau, G. Guglielmi, P. Horton, and A. L. Etienne. The super-excess energy dissipation in diatom algae: comparative analysis with higher plants. *Photosynthesis Research*, 82:165–175, 2004.

P. Sagaut. *Large Eddy Simulation for incompressible flows. An introduction.* Springer-Verlag, Berlin,, 2001.

E. Sakshaug, A. Bricaud, Y. Dandonneau, P. G. Falkowski, D. A. Kiefer, L. Legendre, A. Morel, J. Parslow, and M. Takahashi. Parameters of photosynthesis: definitions, theory and interpretation of results. *Journal of Plankton Research*, 19:1637–1670, 1997.

L. P. Sanford and S. M. Crawford. Mass Transfer versus Kinetic Control of Uptake across Solid-Water Boundaries. *Limnology and Oceanography*, 45(5):1180–1186, 2000.

A. Sciandra, J. Gostan, Y. Collos, C. Descolas-Gros, C. Leboulanger, V. Martin-Jezequel, M. Denis, D. Lefevre, C. Copin-Montegut, and B. Avril. Growth-Compensating Phenomena in Continuous Cultures of Dunaliella tertiolecta Limited Simultaneously by Light and Nitrate. *Limnology and Oceanography*, 42(6):1325–1339, 1997.

B. Shuter. A model of physiological adaptation in unicellular algae. *J Theor Biol*, 78(4): 519–52, 1979.

R. Simo. Production of atmospheric sulfur by oceanic plankton: biogeochemical, ecological and evolutionary links. *TRENDS in Ecology and Evolution*, 16:287–294, 2001.

E. D. Skillingstad, W. D. Smyth, J. N. Moum, and H. Wijesekera. Upper-ocean turbulence during a westerly wind burst: a comparison of large-eddy simulation results and microstructure measurements. *J. Phys. Oceanog.*, 29:5–28, 1999.

J. Smagorinsky. General circulation experiments with the primitive equations. *Monthly Weather Review*, 91(3):99–165, 1963.

W. Smyth and J. Moum. Ocean turbulence, 2000.

E. Steemann Nielsen and E. G. Jørgensen. The adaptation of plankton algae I. General Part . *Physiologia Plantarum*, 21:401–413, 1968.

Robert F. Strzepek and Paul J. Harrison. Photosynthetic architecture differs in coastal and oceanic diatoms. *Nature*, 431:689–692, 2004.

R. B. Stull. Review of non-local mixing in turbulent atmospheres: Transilient turbulence theory. *Boundary-Layer Meteorology*, 62(1):21–96, 1993.

R. B. Stull. Transilient turbulence theory. Part I: The concept of eddy-mixing across finite distances. *J. Atmos. Sci*, 41:3351–3367, 1984.

H. U. Sverdrup. On conditions for the vernal blooming of phytoplankton. *J. Cons. Int. Explor. Mer.*, 18:287–295, 1953.

H. Tennekes and J. L. Lumley. *A first course in turbulence*. MIT Press Cambridge, Mass, 1972.

D. J. Thomson. Criteria for the selection of stochastic models of particle trajectories in the turbulent atmosphere. *Journal Fluid Mechanics*, 180:529–556, 1987.

S. A. Thorpe. Small-scale processes in the upper ocean boundary layer. *Nature*, 318: 519–522, 1985.

M. A. van Leeuwe, B. van Sikkelerus, W. W. C. Gieskes, and J. Stefels. Taxon-specific differences in photoacclimation to fluctuating irradiance in an Antarctic diatom and a green flagellate. *Marine Ecology Progress Series*, 288:9–19, 2005.

I. Vass, S. Styring, T. Hundal, A. Koivuniemi, E. Aro, and B. Andersson. Reversible and Irreversible Intermediates during Photoinhibition of Photosystem II: Stable Reduced Q SUB A/SUB Species Promote Chlorophyll Triplet Formation. *Proceedings of the National Academy of Sciences*, 89(4):1408–1412, 1992.

D. Vaulot, R. J. Olson, and S. W. Chisholm. Light and dark control of the cell cycle in two marine phytoplankton species. *Exp Cell Res*, 167(1):38–52, 1986.

D. Vaulot, R. J. Olson, S. Merkel, and S. W. Chisholm. Cell-cycle response to nutrient starvation in two phytoplankton species, Thalassiosira weissflogii and Hymenomonas carterae. *Marine Biology*, 95(4):625–630, 1987.

W. F. Vincent, N. Bertrand, and J. J. Frenette. Photoadaptation to intermittent light across the St. Lawrence Estuary freshwater–saltwater transition zone. *Mar. Ecol. Prog. Ser*, 110:283–292, 1994.

A.W. Visser. Using random walk models to simulate the vertical distribution of particles in a turbulent water column. *Marine Ecology Progress Series*, 158:275–281, 1997.

H. Wagner, T. Jakob, and C. Wilhelm. Balancing the energy flow from captured light to biomass under fluctuating light conditions. *New Phytologist*, 169:95–108, 2006.

R. G. Walters. Towards an understanding of photosynthetic acclimation. *Journal of Experimental Botany*, 56(411):435–447, 2005. Light Stress in Plants: Mechanisms and Interactions Special Issue.

D. J. C. Wang, J. C. McWilliams, and W. G. Large. Large-eddy simulation of the diurnal cicle of deep equatorial turbulence. *J. Phys. Oceanog.*, 28:129–148, 1998.

J. D. Woods and R. Onken. Diurnal variation and primary production in the ocean–Preliminary results of a Lagrangian ensemble model. *Journal of Plankton Research*, 4 (3):735–756, 1982.

H. Yamazaki and D. Kamykowski. The vertical trajectories of motile phytoplankton in a wind-mixed water column. *Deep Sea Research Part I: Oceanographic Research Papers*, 38(2):219–241, 1991.

H. Yamazaki, G. Sugihara, G. J. Kirkpatrick, and D. Kamykowski. Is the photosynthetic process nonlinear? *Journal of Plankton Research*, 15(11):1297–1308, 1993.

H. Yamazaki, D. L. Mackas, and K. L. Denman. Coupling small-scale physical processes with biology. *The Sea*, 12:51–112, 2002.

O. Zikanov, D. N. Slinn, and M. R. Dhanak. Large-eddy simulations of the wind-induced turbulent Ekman layer. *Journal of Fluid Mechanics*, 495:343–368, 2003.

A. Zingone and T. Wyatt. Harmful algal blooms: keys to the understanding of phytoplankton ecology. In A. R. Robinson, J. McCarthy, and B. J. Rothschild, editors, *The Sea. The Global Coastal Ocean; Multiscale Interdisciplinary Processes*. Harvard University Press, Harvard, 2004.